Robert W. Field

Spectra and Dynamics of Small Molecules

Alexander von Humboldt Lectures



Lecture Notes in Physics

Volume 900

Founding Editors

- W. Beiglböck
- J. Ehlers
- К. Нерр
- H. Weidenmüller

Editorial Board

- B.-G. Englert, Singapore, Singapore
- P. Hänggi, Augsburg, Germany
- M. Hjorth-Jensen, Oslo, Norway
- R.A.L. Jones, Sheffield, UK
- M. Lewenstein, Barcelona, Spain
- H. von Löhneysen, Karlsruhe, Germany
- J.-M. Raimond, Paris, France
- A. Rubio, Donostia, San Sebastian, Spain
- S. Theisen, Potsdam, Germany
- D. Vollhardt, Augsburg, Germany
- J.D. Wells, Geneva, Switzerland
- G.P. Zank, Huntsville, USA

The Lecture Notes in Physics

The series Lecture Notes in Physics (LNP), founded in 1969, reports new developments in physics research and teaching-quickly and informally, but with a high quality and the explicit aim to summarize and communicate current knowledge in an accessible way. Books published in this series are conceived as bridging material between advanced graduate textbooks and the forefront of research and to serve three purposes:

- to be a compact and modern up-to-date source of reference on a well-defined topic
- to serve as an accessible introduction to the field to postgraduate students and nonspecialist researchers from related areas
- to be a source of advanced teaching material for specialized seminars, courses and schools

Both monographs and multi-author volumes will be considered for publication. Edited volumes should, however, consist of a very limited number of contributions only. Proceedings will not be considered for LNP.

Volumes published in LNP are disseminated both in print and in electronic formats, the electronic archive being available at springerlink.com. The series content is indexed, abstracted and referenced by many abstracting and information services, bibliographic networks, subscription agencies, library networks, and consortia.

Proposals should be sent to a member of the Editorial Board, or directly to the managing editor at Springer:

Christian Caron Springer Heidelberg Physics Editorial Department I Tiergartenstrasse 17 69121 Heidelberg/Germany christian.caron@springer.com

More information about this series at http://www.springer.com/series/5304

Spectra and Dynamics of Small Molecules

Alexander von Humboldt Lectures



Robert W. Field Department of Chemistry Massachusetts Institute of Technology Cambridge Massachusetts USA

ISSN 0075-8450 ISSN 1616-6361 (electronic) Lecture Notes in Physics ISBN 978-3-319-15957-7 ISBN 978-3-319-15958-4 (eBook) DOI 10.1007/978-3-319-15958-4

Library of Congress Control Number: 2015938105

Springer Cham Heidelberg New York Dordrecht London © Springer International Publishing Switzerland 2015

This work is subject to copyright. All rights are reserved by the Publisher, whether the whole or part of the material is concerned, specifically the rights of translation, reprinting, reuse of illustrations, recitation, broadcasting, reproduction on microfilms or in any other physical way, and transmission or information storage and retrieval, electronic adaptation, computer software, or by similar or dissimilar methodology now known or hereafter developed.

The use of general descriptive names, registered names, trademarks, service marks, etc. in this publication does not imply, even in the absence of a specific statement, that such names are exempt from the relevant protective laws and regulations and therefore free for general use.

The publisher, the authors and the editors are safe to assume that the advice and information in this book are believed to be true and accurate at the date of publication. Neither the publisher nor the authors or the editors give a warranty, express or implied, with respect to the material contained herein or for any errors or omissions that may have been made.

Printed on acid-free paper

Springer International Publishing AG Switzerland is part of Springer Science+Business Media (www.springer.com)

Preface

I am a card-carrying, small-molecule spectroscopist. I like simple models and the possibility of certainty that an analysis is correct.

When I was a graduate student in William Klemperer's laboratory, I received a precious gift: I became a molecular spectroscopist. In my 40 years at MIT, my students, postdocs, and collaborators kept me focused on the crucial question: "what makes *this* experiment interesting?" Often, they provided both question and answer. I have been energized and educated by their questions, ideas, and ah-hah moments. Always, they had me saying brilliant things I did not know that I knew. But a mirror never knows the beauty it reflects. I dedicate this book to William Klemperer and *my* special sub-group of *his* scientific descendants.

Frequency-domain experimentalists observe transition frequencies and intensities. Wavefunctions are not directly observable. The challenges of spectroscopy are: (a) assign the observed transitions; (b) fit the directly sampled energy levels to a quantum mechanical model; (c) make predictions about other spectra; and most importantly, (d) capture the dynamics and dynamical mechanisms that are encoded in the spectrum. The effective Hamiltonian, **H**^{eff}, is an essential tool for meeting all four of these challenges without license to take a peek at the wavefunction (especially its nodal structure, which is tantamount to assignment, and its time evolution, which reveals mechanism). This short book is an express user's guide for beginners who know neither the basics nor the elegant simplicity and intuitionguiding power of the models that lie beyond archival molecular constants. It is not a textbook. It is neither rigorous nor logical. My goal in writing this book is to provide a set of ideas, tools, and challenges that will ignite the ability of beginning students to see what is intuitive and memorable in molecular spectra.

The lecture format permits strong opinions, personal choices of topics, and intentionally incomplete examples. My idea is to provoke my readers to explore other examples, to create freehand figures that are qualitatively but not quantitatively correct, and to practice using tools and concepts that are derived from my idiosyncratic point of view rather than from a balanced and scholarly treatment. I have attempted to make connections between disparate topics without being burdened by lengthy justification. I have presented several of my favorite topics. My dream

vi Preface

is that mastery of the main topics in these eight chapters/lectures will serve the student as preparation for productive years as a spectroscopist, and will be at least as enlightening as a semester-long sojourn in a course based on a carefully integrated formal textbook.

The vast majority of citations in this book are to relevant sections of *The Spectra* and *Dynamics of Diatomic Molecules* [1], and to a long paper devoted to my favorite topic, effective Hamiltonians [2]. This excess of self-citation is one of the special privileges accruing to an author of lecture notes rather than a textbook.

I thank the Alexander von Humboldt Foundation for the Humboldt Research Award that gave me the opportunity to spend several months as a member of Gerard Meijer's Molecular Physics Department at the Fritz Haber Institute of the Max Planck Society in Berlin. I especially thank Gerard Meijer for inviting me into his laboratory while it was crackling with excitement, creativity, and experimental virtuosity.

I am thrilled that this book will be published as the harbinger of a new Springer book series entitled "Alexander von Humboldt Lectures," the purpose of which is to make the lectures presented by Humboldt Awardees and Humboldt Professors available to students who were unable to attend them in person. Bretislav Friedrich had the idea for this series and I thank him for talking me into putting my lectures into book form.

This book owes its existence to Peter Giunta's ingenuity, artistry, and efficiency. The text for each lecture was written longhand in Berlin and FAXed to Peter at MIT in Cambridge on the day before the lecture. Peter created a LaTeX draft, which I would proofread, mark up, and send back to Peter. Before each lecture I was able to hand out a set of notes to the class!

Cambridge, MA, USA

Robert W. Field

References

- H. Lefebvre-Brion, R.W. Field, The Spectra and Dynamics of Diatomic Molecules (Elsevier, Boston, 2004)
- R.W. Field, J. Baraban, S.H. Lipoff, A.R. Beck, Effective Hamiltonians, in *Handbook of High-Resolution Spectroscopies*, ed. by M. Quack, F. Merkt (Wiley, Oxford, 2010)

Contents

1	Intro	Introduction		
	1.1	Rotation: The Rigid Rotor	1	
	1.2	Vibration: The Harmonic Oscillator	2	
	1.3	Electronic Structure: The Particle in a Box and the		
		Hydrogen Atom	3	
	1.4	Transition Selection and Propensity Rules: ΔJ ,		
		Franck–Condon, and ΔS	4	
	1.5	Rotational Branches, Vibrational Bands, and Electronic		
		Transitions	5	
	1.6	Some Sum Rules	8	
	1.7	Eigenstates are Stationary	10	
	Refer	rences	11	
2	Hier	archy of Terms in the Effective Hamiltonian	13	
_	2.1	Adiabatic and Diabatic Representations	13	
	2.1	2.1.1 Introduction	13	
		2.1.2 Adiabatic vs. Diabatic Representations	14	
	2.2	H ^{spin-orbit}	16	
	2.3	H ^{ROT} , the Rotational Operator	17	
	2.4	Hund's Cases.	18	
		2.4.1 H ⁽⁰⁾ vs. H ⁽¹⁾	22	
	2.5	Two Basis Sets for the 2 × 2 "Two-Level" Problem	22	
	2.6	Some Reasons for Patterns	23	
	2.7	Straight Line Plots	24	
	2.8	Stacked Plots	25	
	2.9	Angular Momenta: A Brief Summary	29	
	2.10	Where Have We Been and Where are We Going?	30	
	References			
3	Speci	troscopic Perturbations: Homogeneous and Heterogeneous	33	
		What Is a Perturbation?	33	
	3.2	Level Shifts and Intensity Borrowing	41	
	- · -	== : := =====		

viii Contents

	3.3	Two Qualitatively Distinct Classes of Perturbation:		
		Homogeneous and Heterogeneous		
	3.4	Franck-Condon Factors		
	3.5	Which Franck-Condon Factors Should I Use?		
	3.6	Intensity Borrowed from a <i>Nearby</i> Bright State		
	3.7	Intensity Borrowed from an Energetically Remote Bright State		
	3.8	Intensity Interference Effects		
	Refe	rences		
4	The	Effective Hamiltonian for Diatomic Molecules		
•	4.1	Introduction		
	4.1	Main Topics of This Lecture		
	4.2	·		
		4.2.1 R-Dependence		
		4.2.2 How Do We Account for Interactions with		
		Energetically Remote States?		
	4.2	4.2.3 Van Vleck Transformation		
	4.3	R-Dependence Is Encoded in v, J Dependence		
		4.3.1 Transition Moments: $\mu(R) \to M_{v',v''}$		
		4.3.2 Centrifugal Distortion, D_e		
		4.3.3 Vibration-Rotation Interaction, α_e : A Small Surprise		
	4.4	Van Vleck Transformation for Non- $^{1}\Sigma^{+}$ States		
		4.4.1 Centrifugal Distortion		
		4.4.2 The Van Vleck Transformation		
		4.4.3 Example of Centrifugal Distortion in a ${}^{3}\Pi$ State		
		4.4.4 Λ-Doubling		
	4.5	Summary		
	Refe	rences		
5	Rota	ation of Polyatomic Molecules		
	5.1	Introduction		
	5.2	Rotational Energy Levels of Rigid Polyatomic Rotors		
	3.2	5.2.1 Symmetric Top		
		5.2.2 Asymmetric Top		
	5.3	Correlation Diagrams: WHY?		
	3.3	5.3.1 Prolate-Oblate Top Correlation Diagram		
		5.3.2 Assignments of Rotational Transitions		
	5.4	Vibrational Dependence of Rotational Constants		
		rences		
6	_	ntum Beats		
	6.1	Introduction		
	6.2	Time-Dependent Schrödinger Equation (TDSE)		
	6.3	"Bright" and "Dark" States		
	6.4	Dynamics		
	6.5	Quantum Beats		
		6.5.1 Simple Two-Level Quantum Beats		
		6.5.2 Two-Level Treatment of OB with Complex Energies		

Contents ix

		6.5.3	What Does a Quantum Beat Signal Look Like?	103	
		6.5.4	Population Quantum Beats	104	
		6.5.5	Level-Crossing vs. Anticrossing	110	
	Refer	ences		110	
7	The l		re Hamiltonian for Polyatomic Molecule Vibration	113	
	7.1		ffective Vibrational Hamiltonian for Polyatomic		
			cules	113	
	7.2	Harmo	onic Oscillator	114	
		7.2.1	Matrix Elements of P and Q	114	
		7.2.2	Dimensionless Forms: $\hat{\mathbf{H}}$, $\hat{\mathbf{Q}}$, $\hat{\mathbf{P}}$	114	
	7.3	Polyat	tomic Molecules	118	
		7.3.1	Basis Set as Product of $3N - 6$ Harmonic		
			Oscillator Eigenstates	118	
		7.3.2	Oscillator Eigenstates		
			in the $\psi_{v_1,v_2,,3N-6}^{(0)}$ Basis Set	119	
		7.3.3	Breakdown of Non-Degenerate Perturbation Theory	120	
		7.3.4	Polyads	121	
		7.3.5	Patterns for Spectral Assignment and		
			Mechanisms of Intramolecular Vibrational		
			Redistribution (IVR) and Unimolecular Isomerization	123	
	7.4	Polya	ds in the Acetylene Electronic Ground State (S ₀)	124	
	Refer	•		127	
8	Intro	moloon	llar Dynamics: Representations, Visualizations,		
o			iisms	129	
	8.1		the "Pluck" at $t = 0$ to the Time-Evolving State	130	
	8.2		bation Theory	130	
	8.3		ne: A Hindered Rotor. A Fully Worked Out Example	132	
	8.4		luck: $\Psi(Q, t = 0)$	139	
	8.5		t) Contains too Much Information	140	
	0.5	8.5.1		141	
		8.5.2	Motion in State Space	143	
	8.6		anism	145	
				153	
	References 1				

List of Figures

Form of R and P rotational branches
Energy level pattern of four J_a atomic-ion components
A reduced term value plot of $E(J) - BJ(J+1)$ vs. J for a ${}^3\Sigma^+$ state in case (b)
Term value stacked plot
Raw spectrum stacked plot
Raw spectrum stacked plot for mostly core-nonpenetrating Rydberg states of CaF.
Reduced term-value plots
A perturbation diagram
A comparison of the SiO H ¹ Σ (0,0) (top) and (1,0) (bottom) bands
Pattern of level shifts at a level-crossing
Intensity borrowing
Schematic illustration of intensity interference effects
Exact and approximate block-diagonalization of ${\bf H}$ Λ -doubling in a ${}^1\Pi$ state
Rotation of a mass point in a plane at constant distance, r, from the coordinate origin
Energy level patterns for prolate and oblate symmetric tops
Prolate-oblate correlation diagram
Eigenstates excited by a short excitation pulse from a single common eigenstate
Bright and dark States
A level diagram for transitions between the <i>e</i> and <i>g</i> states, which have different potential energy surfaces
Pump/probe scheme for photodissociation of ICN

xii List of Figures

Fig. 6.5	Wavepacket transit through an ionic∼covalent potential	
	energy curve crossing in NaI	95
Fig. 6.6	Clocking of the photodissociation of NaI (and NaBr)	
	as the nuclear wavepacket repeatedly traverses the	
	ionic/covalent curve crossing	96
Fig. 6.7	A two-level quantum beating system with 100 %	
	modulation depth	100
Fig. 6.8	A bright singlet state perturbed by an accidentally	
	degenerate dark triplet state	104
Fig. 6.9	Reduced Term Value Plot	105
Fig. 6.10	Quantum beats detected in fluorescence to a	
	lower-lying triplet state	106
Fig. 6.11	Polarized Excitation with Linearly Polarized Radiation	109
Fig. 8.1	Internal rotation of -CH ₃ in toluene	133
Fig. 8.2	A part of a sixfold hindered rotor potential	134
Fig. 8.3	Various Measures of Intrapolyad Dynamics	147
Fig. 8.4	Contributions of Specific Resonance Terms to	
-	Intrapolyad Dynamics	150

Chapter 1 Introduction

This is a book about the spectra and dynamics of small molecules in the gas phase. It is emphatically not a textbook. Despite their size, small molecules *at high excitation* are capable of behaving badly. They do not follow the simple energy level and transition intensity patterns codified in textbooks. Sometimes the transgressions are subtle and sometimes they are catastrophic. For me, the deviations from standard patterns are much more beautiful and instructive than the patterns themselves.

This book is based on my belief that it should be possible to convey, to beginning students, the excitement and vitality of the study of small molecules by focusing on the bad behavior of molecules that one inevitably encounters when one ventures beyond the acquisition of archival molecular constants. Any attempt to cleanse spectra of pattern-defying behavior risks throwing the baby out with the bathwater.

In order to recognize a broken pattern, it is necessary to know something about the nature and origin of the standard patterns.

1.1 Rotation: The Rigid Rotor

The freely rotating, rigid rotor is the starting point for representing and understanding the rotation of diatomic molecules, and, by not so simple extensions, the rotation of *all* molecules. The rigid rotor provides the energy level pattern that we expect will be encoded in the spectrum,

$$E(J)/hc = F(J) = BJ(J+1)$$

[h is Planck's constant, c is the speed of light, F is the symbol conventionally used to represent rotational energy (in cm⁻¹ units), B is the rotational constant, and J is the rotational quantum number]. The rigid rotor model also relates the

1

© Springer International Publishing Switzerland 2015 R.W. Field, *Spectra and Dynamics of Small Molecules*, Lecture Notes in Physics 900, DOI 10.1007/978-3-319-15958-4_1 2 1 Introduction

experimentally measured quantity, B, to the geometric structure of the molecule,

$$B(\text{cm}^{-1}) = (\hbar^2)(1/hc)(1/2\mu R^2) = 16.85673 [\mu(\text{amu}) R(\text{Å})^2]^{-1}$$

[\hbar is $h/2\pi$, $\mu = \frac{m_1 m_2}{(m_1 + m_2)}$ is the reduced mass, and μR^2 is the moment of inertia]. For a diatomic molecule, the geometric structure contained in B is the internuclear distance, R.

For real molecules, the value of B depends weakly on the vibrational and rotational quantum numbers and strongly on the electronic state. J can be either integer or half-integer. The rotational *constant* is not really constant! The v, J, and isotopologue dependencies of B are dealt with by the use of additional molecular constants, often treated merely as fitting parameters. When a molecule has nonzero total electron spin, S, or non-zero projection of the total electron orbital angular momentum on the internuclear axis, Λ , the rotational structure of multiplet electronic states, $^{2S+1}\Lambda_{\Omega}$, is more complicated. 2S+1 is the "spin multiplicity", $\Omega=\Lambda+\Sigma$ is the projection of ${\bf J}$ on the internuclear axis, and Σ is the projection of ${\bf S}$ on the internuclear axis. Nevertheless, the $B^{\rm eff}J(J+1)$ pattern of energy levels associated with *effective* rotational constants forms a foundation for assembling the rotational levels into recognizable and interpretable patterns.

1.2 Vibration: The Harmonic Oscillator

The harmonic oscillator is the starting point for representing and understanding the vibrations of *all* molecules. A diatomic molecule has only one vibrational normal mode. The energy levels of a harmonic oscillator are

$$E(v)/hc = G(v) = \omega_e(v + 1/2),$$

where G is the symbol generally used to represent vibrational energy levels, ω_e is the vibrational constant (in cm⁻¹ units), the subscript $_e$ denotes "equilibrium" and is an inseparable part of the notation for the vibrational constant, and v is the always-integer vibrational quantum number. The harmonic oscillator force constant, k,

$$E = \frac{1}{2}k(R - R_e)^2$$

is expressed in terms of ω_e (in cm⁻¹ units) and μ (in g·mole⁻¹) is

$$k/J \cdot m^{-2} = 5.89183 \times 10^{-5} (\omega_e/cm^{-1})^2 (\mu/g \cdot mole^{-1})$$

or

$$k/\text{cm}^{-1} \cdot \text{Å}^{-2} = 2.96602 \times 10^{18} (\omega_e/\text{cm}^{-1})^2 (\mu/\text{g} \cdot \text{mole}^{-1}).$$

[Note that $k/J \cdot m^{-2} = k/N \cdot m^{-1}$.] Note that, for all v of a harmonic oscillator, the $G(v+1)-G(v) \equiv \Delta G(v+1/2)$ energy level spacing is independent of v. For real molecules, the vibrational level structure is "anharmonic", and this anharmonicity is represented by a proliferation of molecular constants. For an N-atom, nonlinear, polyatomic molecule, there are 3N-6 vibrational "normal modes," each of which has its own harmonic vibrational frequency, ω_{ei} , and the vibrational energy levels and state labels are, respectively,

$$G(v_1, v_2, \dots v_{3N-6}) = \sum_{i=1}^{3N-6} \omega_{ei}(v_i + 1/2).$$

Even when the vibrational energy level pattern is distorted by anharmonicity and other large and local effects that arise from accidental degeneracy of two or more harmonic oscillator vibrational energy levels, the harmonic pattern of equally spaced vibrational levels within each normal mode is the primary basis for establishing the quantum number assignments of the subset of all vibrational energy levels that are observed in a spectrum.

1.3 Electronic Structure: The Particle in a Box and the Hydrogen Atom

It is much more difficult to generalize about standard patterns of electronic states than about the standard patterns for rotational and vibrational states. There are two classes of electronic states, *valence* states and *Rydberg* states. A valence state of a molecule is based on bonding, nonbonding, and antibonding Molecular Orbitals constructed from Linear Combinations of valence Atomic Orbitals (LCAO-MO). Valence state orbitals resemble particle in a box orbitals in two vague ways: (a) their energies are determined by the spatial extent of the AOs from which they are constructed, the larger the spatial extent (delocalization), the lower the energy (stabilization by delocalization); (b) since the E(n+1) - E(n) energy spacings of particle in a box states increase as the quantum number, n, increases (n-1) is the number of nodes), one never sees a series consisting of more than a few orbitally-related valence states, because the higher-n orbitals (more nodes) are either increasingly antibonding (dissociation) or their orbital energy lies above the ionization limit. Qualitative information (energy, shape, and vibrational frequencies) about molecular valence states is best obtained from LCAO-MO models [1–3].

The energy level structure of molecular Rydberg electronic states (the v=0 level of each Rydberg state) is very closely related to that of the Hydrogen atom. The energy levels of the Hydrogen atom are

$$E_{n\ell}/hc = T_{n\ell} = IE - Z^2 \Re/n^2.$$

4 1 Introduction

(T is the symbol generally used to specify electronic energy, IE is the ionization energy, IE is the integer charge of the bare nucleus, the zero of energy is the energy of the lowest electronic state, the IE is located at $n=\infty$, which is where the Rydberg series converges), where n is the principal quantum number, n is integer, ℓ is the orbital angular momentum quantum number, and \Re is the Rydberg constant ($\Re=109,737\,\mathrm{cm}^{-1}$). Uniquely for Hydrogen and hydrogenic atomic-ions (He⁺, Li²⁺, Be³⁺, ...), the energy levels are located at integer values of n and the energies are independent of ℓ . Along a molecular Rydberg series, the v=0 energy levels are located at

$$E_{n^{\star}\ell\lambda}/hc = T_{n^{\star}\ell\lambda,0} = \mathrm{IE}_0 - \Re/n^{\star 2},$$

where IE₀ is the energy of the v=0 level of the electronic state of the molecular ion, to which the Rydberg series converges as $n\to\infty$, n^\star is the effective principal quantum number, $n^\star\equiv n-\delta_{\ell\lambda}$, and $\delta_{\ell\lambda}$ is the *quantum defect* of the ℓ , λ -Rydberg series. The quantum defects of molecular Rydberg series depend strongly on ℓ and on the projection of ℓ on the molecule-fixed (near)-symmetry axis (e.g. λ for a linear molecule). Successive levels in a Rydberg series are located at n^\star , $n^\star+1$, $n^\star+2$, ... and are spaced as

$$E(n^* + 0.5) - E(n^* - 0.5) \equiv \Delta E(n^*)/hc = 2\Re/n^{*3}$$
.

These *integer steps* of n^* define readily observable patterns that are often used to pick out and assign series of Rydberg electronic states and, by extrapolation, to determine the ionization energy of the molecule.

Rydberg series come in two very distinct flavors: low- ℓ series have characteristically large and positive quantum defects because they are strongly *core-penetrating*; high- ℓ series are *core-nonpenetrating* and have characteristically small quantum defects because the orbital angular momentum centrifugal barrier, $\ell(\ell+1)/(m_e r^2)$, keeps the Rydberg electron outside of the ion-core.

1.4 Transition Selection and Propensity Rules: ΔJ , Franck-Condon, and ΔS

One never observes energy levels directly. The energy levels are encoded in the spectrum as *transitions* between pairs of energy levels governed by selection and propensity rules. There are *rigorous transition selection rules* for electric dipole allowed transitions, based on rigorously good quantum numbers, such as J and parity: $\Delta J = 0, \pm 1$, parity $+ \leftrightarrow -$. There are strong but *approximate transition selection rules*, based on approximately good quantum numbers, such as the total electron spin (S) and the respective projections of the orbital, spin, and total angular momenta onto the internuclear axis in a linear molecule $(\Lambda, \Sigma, \text{ and } \Omega)$:

 $\Delta S=0, \Delta\Lambda=\Delta\Omega=0, \pm 1, \Delta\Sigma=0$. The goodness of S is broken by *spin-orbit* interactions. The goodness of the projection quantum numbers is broken by terms in the rotational Hamiltonian (S-uncoupling, $-B\mathbf{J}^{\pm}\mathbf{S}^{\mp}$, and L-uncoupling, $-B\mathbf{J}^{\pm}\mathbf{L}^{\mp}$) and by spin-orbit. Finally, there are *transition propensity rules* that are based on the size of an overlap integral, for example between initial and final vibrational $\chi_v^e(R)$ (Δv =anything) or Rydberg orbital $\phi_{\ell\lambda}^{n\star}(r)$ (Δn^{\star} = anything) wavefunctions,

$$\int_{0}^{\infty} dR \chi_{v'}^{e'}(R) \chi_{v''}^{e''}(R) \text{ or } \int_{0}^{\infty} dr \phi_{\ell'\lambda'}^{n^{\star\prime}}(r) \phi_{\ell''\lambda''}^{n^{\star\prime\prime}}(r).$$

There is usually a simple classical mechanical reason for large versus small values of the overlap integrals upon which transition propensity rules are based. [Spectroscopic convention requires that the upper and lower energy states be labeled by ' and ", respectively.]

The Franck-Condon factor for a transition between the v' vibrational level of the e' electronic state and the v'' vibrational level of the e'' electronic state is the square of the vibrational overlap integral,

$$q_{v',v''}^{e',e''} = \left[\int_{0}^{\infty} dR \chi_{v'}^{e'}(R) \chi_{v''}^{e''}(R) \right]^{2}.$$

The classical mechanical basis for Franck–Condon factors is that, in a sudden transition between the e' and e'' electronic states, the nuclear coordinates and momenta cannot change. This suddenness is a consequence of the *Born–Oppenheimer approximation*: electrons move much faster than nuclei. Large Franck–Condon factors arise for *vertical transitions* between a turning point of the e', v' state and a turning point of the e'', v'' state. Turning points are special classically, because the nuclear velocity goes to zero at the turning point, thus considerable probability accumulates near the turning point.

1.5 Rotational Branches, Vibrational Bands, and Electronic Transitions

Pure rotation transitions occur in the microwave region and are made allowed by a nonzero value of the electric dipole moment. The selection rules are $\Delta J=0,\pm 1$ and parity $+\leftrightarrow-$. For a diatomic molecule, the $\Delta J=\pm 1$ transitions $1\leftrightarrow0$, $2\leftrightarrow1$, and $3\leftrightarrow2$ occur respectively at 2B, 4B, and 6B. For a molecule in an orbitally degenerate state, such as a ${}^1\Pi$ state, there can be $\Delta J=0$ transitions (between Λ -doublet components), which generally occur at much lower frequency than $\Delta J=\pm 1$ transitions. The frequencies of $J=1\leftrightarrow0$ pure rotation transitions depend weakly on vibrational level, because the B-values are weakly v-dependent. Thus, for a molecule with significant vibrational excitation, there can be a cluster

6 1 Introduction

of pure rotation transitions in each $J \leftrightarrow J \pm 1$ 2B, 4B, 6B, ...2JB region, one for each significantly populated vibrational level. However, we do not think of this sequence of pure rotation transitions as forming a "rotational branch." The reason for this is technical (the limited tuning range of microwave oscillators) rather than fundamental.

Vibration-rotation transitions occur in the infrared region and are made allowed by the internuclear distance dependence of the electric dipole moment, $\left(\frac{\partial \mu}{\partial R}\right)_{R=R_e} \neq 0$. Each $v' \leftrightarrow v''$ vibrational band has R(J'=J''+1) and P(J'=J''-1) rotational branches (Fig. 1.1). Q branches (J'=J'') are electric

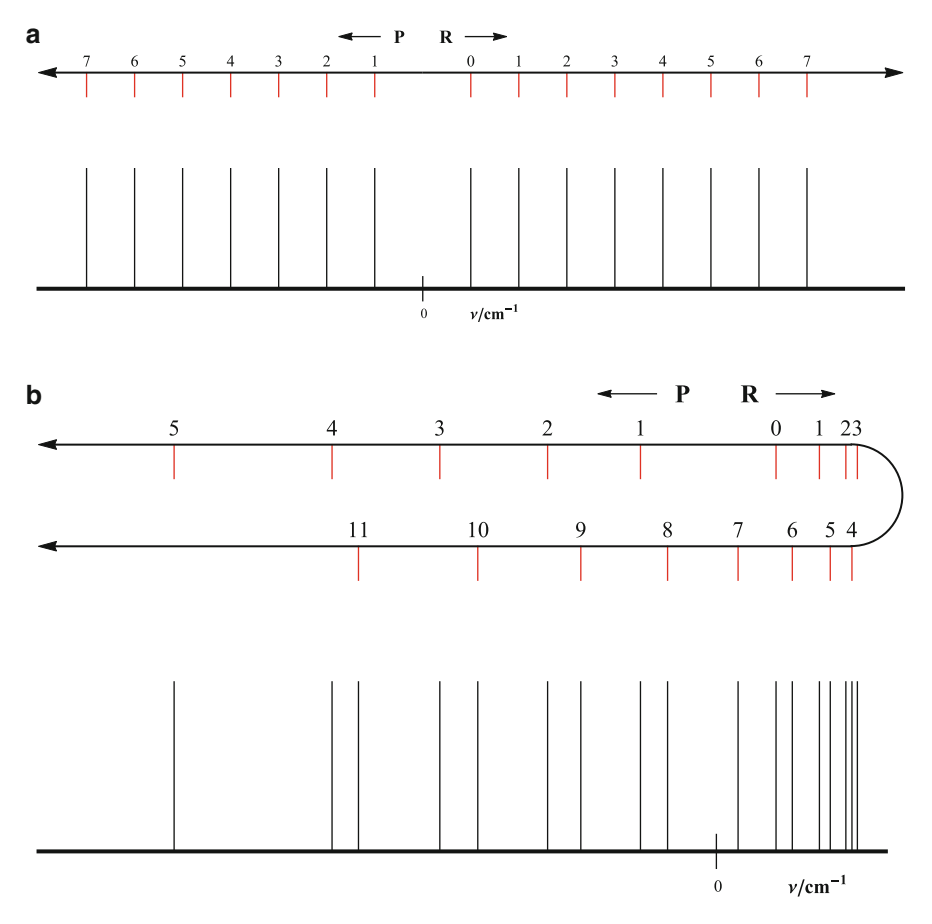


Fig. 1.1 Form of R and P rotational branches. (a) $B' = B'' = 1.0 \text{ cm}^{-1}$, no bandhead, typical of a vibration-rotation band. There is an easily recognized zero-gap. (b) $B' = 0.88 \text{ cm}^{-1}$, $B'' = 1.12 \text{ cm}^{-1}$, $\Delta B = -0.24 \text{ cm}^{-1}$, bandhead in R branch at $J'_H = \frac{B' + B''}{-2\Delta B} = 4.17$. Note that lines from the returning part of the *R* branch overlap with the low-J lines of the *R* branch, fall into the zero-gap, and overlap with the *P* branch. It becomes difficult to see the zero-gap or to assign lines by counting lines from the R(0) and P(1) lines. I thank David Grimes for creating this figure

dipole forbidden (except when $\Lambda \neq 0$) for vibration-rotation transitions of diatomic molecules. The R branch lines in a v' - v'' vibration-rotation band occur at

$$R(J'')_{v',v''} = \omega_e(v'-v'') + B'(J''+1)(J''+2) - B''J''(J''+1)$$

$$= \omega_e(v'-v'') + J''^2(B'-B'') + J''(3B'-B'') + 2B'$$

$$\approx \omega_e(v'-v'') + J''^2(\Delta B) + J''(2B) + 2B'',$$

where $\Delta B \equiv B' - B''$. The P branch lines occur at

$$P(J'')_{v',v''} = \omega_e(v' - v'') + B'(J'' - 1)(J'') - B''J''(J'' + 1)$$

$$= \omega_e(v' - v'') + J''^2(B' - B'') + J''(-B' - B'')$$

$$\approx \omega_e(v' - v'') + J''^2(\Delta B) - J''(2B).$$

The Q branch lines occur at

$$Q(J'')_{v',v''} = \omega_e(v'-v'') + J''(J''+1)\Delta B.$$

The R and P branches are described by a very small quadratic-in-J'' term, large linear-in-J" terms of opposite signs, and a constant term. Note that the coefficient of the quadratic-in-J'' term is ΔB , which is much smaller than the coefficient of the linear-in-J'' term, 2B. Ignoring the quadratic term, the R branch lines are separated by intervals of +2B, run toward higher energy (blue), and the first R line is R(0) at $\omega_e(v'-v'')+2B'$. The P branch lines are separated by intervals of -2B and the first P line is P(1) at $\omega_e(v'-v'')-2B'$. R(0)-P(1)=4B is known as the "zero-gap," which is a distinctive feature that usually permits absolute assignment of the rotational lines in a vibration-rotation band. When the zero-gap is obscured by overlap with transitions from another vibrational or isotopologue band, it becomes necessary to use *rotational combination differences* to establish secure absolute rotational assignments:

lower state combination difference
$$\Delta_2 F''(J'') = R(J''-1) - P(J''+1)$$

$$= B''[4J''+2]$$
 upper state combination difference
$$\Delta_2 F'(J') = R(J'') - P(J'')$$

$$= B'[4J'+2].$$

8 1 Introduction

It is necessary to find an identical set of rotational combination differences from a *vibrationally linked* pair of bands (for example 1–0 and 2–0 bands for v''=0 or 2–0 and 2–1 for v'=0 in order make secure rotational assignments.

Electronic-vibration-rotation bands occur in the Visible and Ultraviolet regions. They are made allowed by a nonzero electric dipole electronic transition moment. For example, N_2 does not have allowed pure rotation or rotation-vibration transitions, but it does have allowed electronic transitions (in the Vacuum Ultraviolet region). Each e'-e'' electronic transition is a band system that consists of many v'-v'' vibration-rotation bands. The relative intensities of a progression of vibrational bands observed in absorption [(v',v'') for $v'=0,1,2,\ldots]$ or emission [(v',v'') for $v''=0,1,2,\ldots]$ are given by Franck–Condon factors. There are R, Q, and P rotational branches. However, unlike the simple situation for rotation-vibration bands where $|B'-B''| \ll B$, the $J^2(B'-B'')$ term in R(J''), Q(J''), and P(J'') cannot be ignored. A *bandhead* will form in either the R or P branch, which always causes the zero-gap region to be obscured. Instead of having rotational lines with approximately equal spacings of 2B, the lines in one branch will form an extremum

$$\frac{dR}{dJ} = 0 = 2J''(B' - B'') + (3B' - B'')$$

$$J''_{\text{head},R} = -\frac{3B' - B''}{2(B' - B'')}$$

$$\frac{dP}{dJ} = 0 = 2J''(B' - B'') - (B' + B'')$$

$$J''_{\text{head},P} = +\frac{B' + B''}{2(B' - B'')}.$$

If B' > B'', the bandhead occurs in the P branch and the band is said to be *blue degraded*. If B' < B'' (the more usual situation), the bandhead occurs in the R branch and the band is *red degraded*. When a bandhead occurs, it is difficult to resolve and sequentially number the rotational lines near the head, because the zerogap region is filled with lines from the returning part of the head-forming branch. It is always necessary to use vibrationally-linked rotational combination differences to rotationally assign each vibrational band in an electronic transition. *There is no safe shortcut*.

1.6 Some Sum Rules

The intensities of transitions are determined by a product of three molecule-specific factors and a bunch of fundamental constants and transition frequency factors. These three molecule-specific factors, electronic oscillator strength $(f_{e',e''})$, vibrational

1.6 Some Sum Rules 9

Franck-Condon factor $\left(q_{v',v''}^{e',e''}\right)$, and rotational linestrength factor $\left(S_{J',J''}^{\lambda',\lambda''}\right)$, are "normalized" by intuitively satisfying sum rules. Many textbooks fail to mention these sum rules.

The sum rule for rotational linestrength factors (known as Hönl-London factors for diatomic molecules) may be understood by the answer to the following question. In the absence of local effects due to the interaction between different electronic states, would you expect the radiative lifetime for every J', M' component of an e', v' excited electronic-vibration level to be equal? The answer is ves! Another closely related question is, would you expect the sum over the intensities of all absorption transitions, from a single J'', M'' component of the e'', v'' electronicvibration level to all J', M' components of one e', v' level, to be independent of J'', M''? The answer is also yes! If the radiation used to excite the absorption transition is unpolarized and isotropic (equal intensity in all propagation directions). then one expects that the total absorption intensity is also independent of M''. There are a variety of normalization conventions for rotational linestrength factors. The unwary user is advised to evaluate sums over all transitions from a given e', J' or e'', J'' level. This sum should be independent of J and should be a simple integer that is related to the spin (2S+1), $\pm \Lambda$ orbital $[(2-\delta_{0,\Lambda})]$, and spatial (2J+1)degeneracies [4–7].

The sum rule for vibrational intensity (Franck-Condon) factors is

$$\sum_{v', \text{continuum}} q_{v',v''} = \sum_{v'', \text{continuum}} q_{v',v''} = 1,$$

where the Franck–Condon factor, $q_{v',v''}$, is the square of the vibrational overlap integral. This sum rule arises from the fact that all bound vibrational states, plus the vibrational continuum, form a *complete* set of functions in terms of which any arbitrary function, defined over the same domain, may be expanded. This sum rule is computationally and intuitively important. The Franck–Condon factor for the v', v'' vibrational band tells us what fraction of the total vibrational transition intensity from a given initial level resides in a particular band.

There is an intuitively appealing sum rule for the strengths of electronic transitions. The *oscillator strength* [5, 8], $f_{e',e''}$, is a measure of the strength of the $e' \leftarrow e''$ transition relative to that of the strongest possible one-electron transition from the electronic ground state, which would have an oscillator strength equal to the number of electrons that could participate in that transition. For example, the Na 2 P(2p) \leftarrow 2 S(2s) transition has an f value slightly smaller than 1. The sum of f-values for all transitions from the Na 2 S(2s) ground state to all Na 2 P(np) excited states is 1. For Mg, which has a 1 S(2s 2) ground state, the oscillator strength sum to all 1 P(2snp) states is 2, because the 1 S(2s 2) state of Mg has two 2s electrons and either one can be excited to an np orbital. The f value for an upward transition is positive, and that for a downward transition is negative. This means that, starting from the Na 2 P(2p) state, the f-value sum for all upward transitions (to 2 S(ns) and 2 D(nd) states) is going to be slightly smaller than 2, because the oscillator strength

10 1 Introduction

sum for all upward and downward transitions out of the Na ²P(2p) state must be 1. The oscillator strength sum rule provides insight into the maximum possible transition strength from a given initial state and how much transition strength is left over for all other transitions out of that state. Similar oscillator strength sum rules apply to molecules.

For electronic-vibration-rotation transitions we have a product of three linestrength factors, each of which follows an a priori known sum rule. These sum rules are valuable both for building insight and for discovering the normalization scheme implicitly built into a linestrength formula that you did not derive for yourself.

1.7 Eigenstates are Stationary

Our instinctive classical mechanical view of a molecule is of something that embodies a hierarchy of motions: electron motions are fast, vibrational motions are slower, and rotational motions are the slowest. But this dynamical view is *inconsistent* with both experimental reality (the frequency-domain spectrum prominently displays transitions between discrete energy levels) and the computational reality of the time-independent Schrödinger equation, $\mathbf{H}\psi_n = E_n\psi_n$. ψ_n is an eigenfunction of the time independent Hamiltonian, \mathbf{H} , where each ψ_n is associated with an energy eigenvalue, E_n . The $\{\psi_n\}$ are both *not moving* and *not directly observable*!

It is very strange that what we can observe in a frequency domain experiment, energy levels and transition intensities, tells us nothing about intramolecular electronic-vibrational-rotational motions (what is moving, how fast, and what are the amplitudes of motion?) and nothing about the quantum mechanical wavefunction that is supposed to tell us everything that is knowable about each non-moving quantum mechanical state of the molecule. This *quantum weirdness* is part of what makes spectroscopy beautiful and mysterious.

The energy level and intensity patterns that we observe in a spectrum encode both dynamics and the set of wavefunctions, $\{\psi_n\}$. When we assign the energy levels in a spectrum and fit them to an electronic-vibrational-rotational model, we determine the numerical values of the important terms in the molecular Hamiltonian. Each term in this Hamiltonian is the product of an abstract quantum mechanical operator and an empirically determined molecular constant. This is not the exact Hamiltonian. It is an effective Hamiltonian, \mathbf{H}^{eff} , which is merely a convenient fit model. But it is very special because we get from it the complete set of experimentally relevant $\{\psi_n\}$. We do not measure the $\{\psi_n\}$. We measure the molecular constants. The $\{\psi_n\}$ are determined from the combination of a model and the molecular constants.

But it is even better than this! We get the intramolecular motions demanded by our intuition when we combine the time-dependent Schrödinger equation,

$$\mathbf{H}\Psi = i\hbar \frac{\partial \Psi}{\partial t},$$

References 11

with physically realistic plucks of the quantum mechanical system. These plucks create a $\Psi(t=0)$ state at t=0,

$$\Psi(0) = \sum_{n} c_n \psi_n,$$

which is not a single eigenstate of the \mathbf{H}^{eff} . The time-evolving form of this state, $\Psi(t)$, is a superposition of several eigenfunctions, ψ_n , that belong to different eigenenergies, E_n ,

$$\Psi(t) = \sum_{n} c_n \psi_n e^{-iE_n t/\hbar}.$$

The probability density, $\Psi^*\Psi$, that is associated with this $\Psi(t)$ moves. It does everything expected of a rigid rotor, a harmonic oscillator, and an electron in planetary orbit around a positive ion. Each eigenstate is stationary, but the totality of the energy levels encodes motion.

References

- 1. A.D. Walsh, J. Chem. Soc. (London), 2260-2288 (1953)
- 2. J.P. Lowe, K. Peterson, Quantum Chemistry, 3rd edn. (Elsevier, Amsterdam, 2006)
- 3. R.J. Gillespie, I. Hargittai, The VSEPR Model of Molecular Geometry (Dover, Boston, 2012)
- E.E. Whiting, A. Schadee, J.B. Tatum, J.T. Hougen, R.W. Nicholls, J. Mol. Spectrosc. 80, 249– 256 (1980)
- 5. R.C. Hilborn, Am. J. Phys. 50, 982-986 (1982)
- 6. J.T. Hougen, *The Calculation of Rotational Energy Levels and Rotational Line Intensities in Diatomic Molecules*. NBS Monograph, vol. 115 (U.S. National Bureau of Standards, 1970)
- 7. P.F. Bernath, Spectra of Atoms and Molecules, 2nd edn. (Oxford University Press, Oxford, 2005)
- 8. H. Lefebvre-Brion, R.W. Field, *The Spectra and Dynamics of Diatomic Molecules* (Elsevier, Amsterdam, 2004)

Chapter 2

Hierarchy of Terms in the Effective Hamiltonian

This lecture is an introduction to effective Hamiltonians, transition selection rules, Hund's coupling cases, pattern-forming rotational quantum numbers, and straight line plots. The goal is to create a fit model: \mathbf{H}^{eff} . This \mathbf{H}^{eff} must have the following desirable characteristics: (a) the \mathbf{H}^{eff} gives a good fit to both frequencies and relative intensities of measured transitions; (b) the \mathbf{H}^{eff} is capable of dealing with nontextbook spectra: perturbations [1], extra lines and intensity anomalies, for which there exist \mathbf{no} directly applicable analytic formulas (Hund's cases); (c) the \mathbf{H}^{eff} permits reduction of spectra to "deperturbed" molecular constants, which provide a basis for extrapolation to other spectra, explanation of other anomalies (e.g. R, P intensity ratios in a fluorescence progression), and a compact, cause-and-effect generator of "dynamics". This is what I often refer to as going "Beyond Molecular Constants"; (d) the \mathbf{H}^{eff} provides a framework for comparison to theoretical calculations. Be careful, experimentalists and theorists often use the same name for different quantities (empirical fit vs. full deperturbation); and (e) there are three important terms in the \mathbf{H}^{eff} :

$$\mathbf{H}^{\text{eff}} = \mathbf{H}^{\text{electronic}}(R) + \mathbf{H}^{\text{spin-orbit}} + \mathbf{H}^{\text{rotation}}.$$

2.1 Adiabatic and Diabatic Representations

2.1.1 Introduction

There is no such thing as a textbook spectrum. In order to be able to make sense of a spectrum, one needs some simple ideas rather than a collection of all-purpose algebraic formulas. These ideas include *transition selection rules* and expected energy level patterns. An *effective Hamiltonian*, **H**^{eff}, generates the energy level patterns [2]. One should never mistake the effective Hamiltonian for the exact

Hamiltonian. The **H**^{eff} is much simpler and more useful. It forces the spectroscopist to make decisions about the expected relative magnitudes of the distinct physical effects represented by each of the additive terms in the Hamiltonian. The dreaded Hund's coupling cases [3] arise from different orderings of the magnitudes of electronic, rotational, and spin—orbit terms. Hund's cases are useful because they tell you what energy level pattern you should expect to find in the spectrum. Each Hund's case corresponds to a different rotational pattern-forming quantum number and an explicit identification of a term that tries to disrupt that pattern.

Where do potential energy curves come from? What makes it possible to think of the solutions of the Schrödinger equation for a molecule as a product of an electronic wavefunction and a vibrational wavefunction? We label molecular energy levels with electronic and vibrational quantum numbers rather than some simple scheme in which the electronic-vibration eigenstates are numbered in energy order. The goal of this separation of molecular structure into electronic and vibrational parts is to enable insight, intuition, and simplification.

2.1.2 Adiabatic vs. Diabatic Representations

There are two quite different approaches to the electronic-vibrational structure of molecules: **adiabatic** and **diabatic** [4]. The former is mathematically rigorous and the latter is often more intuitively appealing. The one that a spectroscopist chooses to use to understand and represent a spectrum depends on the nature of the pathology expressed in the spectrum. When there is no pathology (the mythical textbook spectrum), the choice of adiabatic vs. diabatic approach is purely a matter of taste.

Because electrons "move much faster" than nuclei, it is reasonable to use the "clamped nuclei" = Born-Oppenheimer = adiabatic representation. At each nuclear geometry, we solve the electronic Schrödinger equation

$$\mathbf{H}^{\text{electronic}}(R) = \mathbf{H}^{\text{el}(0)}(R) + \sum_{i} \sum_{i < j} \frac{e^2}{4\pi \varepsilon_0 r_{ij}(R)},$$

where geometry, R, is a parameter rather than a variable. The $1/r_{ij}$ term is segregated outside of $\mathbf{H}^{\text{el}(0)}$ because it contains, among many other important effects, the interactions between same-symmetry electronic states that are responsible for avoided crossings. This equation is solved on a grid of values of R. The solutions, $\psi_k^{\text{el}}(r;R)$, $E_k(R)$, are electronic wavefunctions that are functions of electron $\{r_i\}$ coordinates and parametrically dependent on nuclear coordinates $\{R_I\}$. We think of the $E_k(R)$ as a potential energy curve (diatomic molecules) or surface (polyatomic molecules) for the k-th electronic state. The vibrational wavefunctions, $\chi_v^k(R)$, and energy levels E_{v_k} are obtained by solving a nuclear motion Schrödinger equation for motion on the k-th potential energy surface, completely neglecting effects due to all other potential energy surfaces. This is a crucial approximation: the **Born-Oppenheimer** approximation [4].

For a diatomic molecule, adiabatic potential energy curves for electronic states of the same symmetry cannot cross [5]. They must avoid crossing. As a result, adiabatic curves often have peculiar shapes. This is a sign of something pathological. At an avoided crossing, the electronic wavefunction can change rapidly with internuclear distance, R. As a result, derivatives with respect to nuclear coordinates, R, of the $\psi_k^{\rm el}(r;R)\chi_v^k(R)$ electronic-nuclear product wavefunction give rise to non-zero off-diagonal k,v;k',v' matrix elements between different electronic-vibrational states. These inter-electronic state interactions, often called "kinetic energy couplings", are caused by the neglected $\frac{\partial}{\partial R_I}$ and $\frac{\partial}{\partial R_I}\frac{\partial}{\partial R_J}$ terms operating on the electronic wavefunctions.

The idea that the electronic wavefunction might be strongly dependent on nuclear geometry offends intuition. A state is a state, or is it? The idea that electronic structure is roughly independent of nuclear geometry is embodied in the *diabatic* representation. Diabatic potential curves cross. They have "normal looking" shapes.

In the diabatic picture only part of \mathbf{H}^{el} is diagonalized. The part that is excluded is the part that causes avoided crossings. The big computational problem is that it is not possible to identify and isolate a particular term in \mathbf{H}^{el} that causes interactions between adiabatic electronic states of the same symmetry. The diabatic representation is intuitively appealing (a state is a state) but mathematically troublesome. If we had diabatic electronic states, $\{\psi_k^{\text{el}, \text{diab}}\}$, it would be possible to compute the set of vibrational wavefunctions and energy levels of each diabatic electronic state. But now inter-electronic interactions are neglected. It is necessary to add these interactions, in the form of factored interaction terms

$$H_{iv_i,jv_k}^{\text{el}} = \langle \psi_i, v_i | \mathbf{H}^{\text{el}} | \psi_j, v_j \rangle$$

$$= {}_r \langle \psi_i | \mathbf{H}^{\text{el}} | \psi_j \rangle_{r} {}_R \langle v_i | v_j \rangle_{R}}$$

$$= H_{ii}^{\text{el}} \langle v_i | v_j \rangle.$$

It turns out, to a very good approximation, that

$$H_{ij}^{\text{el}} = \frac{\min\left[V_i^{\text{ad}}(R) - V_j^{\text{ad}}(R)\right]}{2}$$

(one-half the energy of closest approach of the two adiabatic curves) and the $H_{ij}^{\rm el}(R)$ function is sampled at the R-value of this closest approach.

Whether the adiabatic or diabatic repesentation is more computationally convenient depends on the size of the would-be neglected interaction terms relative to the vibrational level spacings in the adiabatic or diabatic potential energy curves.

Whether one works in the adiabatic or diabatic representation, the key to getting started in modeling the energy levels observed in a spectrum is to obtain a complete electronic-vibrational basis set. In principle, we need

$$\left\{\psi_i^{\text{el}}(R)\right\}, \left\{E_i^{\text{el}}(R)\right\}, \left\{\chi_{v_i}(R)\right\}, \left\{E_{v_i}^{\text{vib}}\right\}$$

but in practice we need only a few $\psi_i^{\text{el}}(R)$ over a small range of R and only the χ_{v_i} , $E_{v_i}^{\text{vib}}$ that are relevant to the region of the observed spectrum.

The selection rules for Helectronic are:

- Δ (all angular momentum and symmetry quantum numbers) = 0
- $\langle \psi_i^{\text{el}} | \mathbf{H}^{\text{electronic}} | \psi_j^{\text{el}} \rangle = 0$ if ψ_i and ψ_j differ by more than two spin–orbitals.

A *spin-orbital* is a one-electron wavefunction that is labeled by body-frame orbital (λ) and spin (σ) quantum numbers: e.g. a p ($\ell = 1$) orbital gives six spin-orbitals: $1\alpha, 1\beta, -1\alpha, -1\beta, 0\alpha, 0\beta$.

For each $\Lambda - S$ electronic state (i) we get a potential energy curve, $V_{e_i}(R)$, either from theory or derived, via Rydberg-Klein-Rees (RKR-LeRoy), from experimental molecular constants [1, 6]. [See http://leroy.uwaterloo.ca/programs.html for RKR1 and LEVEL [7].] Every spectroscopist should know how to use these programs.

Input to RKR: two "dumb" power series:

G(v) and B(v) describe the v-dependence of vibrational energy levels and rotational constants as power series in v + 1/2, where the coefficients of each $(v + 1/2)^m [J(J+1)]^n$ term are "Dunham constants."

$$G(v) = \sum_{m=0}^{m_{\text{max}}} Y_{mn=0}(v+1/2)^m \quad \{Y_{00}, \omega_e, \omega_e x_e, \omega_e y_e, \dots\}$$

$$B(v) = \sum_{m=0}^{m'_{\text{max}}} Y_{mn=1}(v+1/2)^m \quad \{B_e, \alpha_e, \gamma_e, \dots\}$$

$$E_{vJ} = \sum_{m=0}^{m} Y_{mn}(v+1/2)^m [J(J+1)]^n \quad \text{Dunham expansion [8, 9]}.$$

These are insight-free (dumb) representations of experimental data.

The Y_{mn} are dumb because they are a one-size-fits-all representation of experimental measurements. There is no intuitive or insightful model behind the Y_{mn} .

2.2 H^{spin-orbit} [10]

The spin-orbit term in \mathbf{H}^{eff} is widely misunderstood. Part of the mystery surrounding $\mathbf{H}^{\text{spin-orbit}}$ is due to its unnecessarily mysterious association with "relativistic" effects.

$$\mathbf{H}^{\text{spin-orbit}} = \sum_{i,\text{electrons}} a(r_i) \boldsymbol{\ell}_i \cdot \mathbf{s}_i \cong A\mathbf{L} \cdot \mathbf{S}$$
 (a one-electron operator)

 $a(r_i)$ is a radial function, $\sim 1/r_i^3$, heavily weighted in the near-nucleus region. The angular momentum operators, ℓ_i and \mathbf{s}_i , are atomic one-electron operators, and are the primary reason for the simplicity and usefulness of the spin–orbit operator.

Matrix elements of HSO follow the rigorous selection rules:

$$\Delta \Lambda = 0, \pm 1$$

$$\Delta S = 0, \pm 1$$

$$\Delta \Sigma = -\Delta \Lambda$$

$$\Delta \Omega = 0$$

$$\Delta \text{parity} = 0$$

$$\Sigma^{+} \leftrightarrow \Sigma^{-}$$

 $\Delta(\text{spin-orbitals}) = 0, \pm 1 \text{ (change in occupied spin-orbitals)}^{\dagger}$

 Λ is the projection of electronic orbital angular momentum on the internuclear axis. S is the total electron spin. Σ is the projection of S on the internuclear axis. $\Omega = \Sigma + \Lambda$ is the projection of the total electron angular momentum (orbital and spin) onto the internuclear axis. Since the rotational angular momentum, R, of a diatomic molecule is, by definition, perpendicular to the internuclear axis, Ω is also the projection of I on the internuclear axis. The I symmetry species expresses the effect of reflection (I of the electronic wavefunction for a I state through a plane containing the internuclear axis.

Note that the selection rules for the frequently used AL·S *operator replacement* for \mathbf{H}^{SO} are (misleadingly) more restrictive than those for the $a\ell_i \cdot s_i$ form of \mathbf{H}^{SO} .

The molecular spin-orbit interaction constant is closely related to atomic spin-orbit constants. It gets large for heavy atoms. It gets small as $n^{\star -3}$, where n^{\star} is the effective principal quantum number for Rydberg states.

$$[IP - E_{n^*} \equiv \Re/n^{*2}]$$
 where \Re is the Rydberg constant, 109,737 cm⁻¹.

2.3 H^{ROT}, the Rotational Operator [11]

 $\mathbf{H}^{\mathrm{ROT}}$ contains the rotational angular momentum, \mathbf{R} , and an integral over the internuclear distance, R,

$$\mathbf{H}^{\text{ROT}} = B_{ij}\mathbf{R}^2 = B_{ij}[\mathbf{J} - \mathbf{L} - \mathbf{S}]^2,$$

[†] If spin–orbitals are labeled 1, 2, 3, 4, ... then ψ_{1234} differs by one spin–orbital from ψ_{1235} or ψ_{1534} .

where B_{ij} is an integral of the "rotational constant" operator, B(R), over the vibrational wavefunctions of the v_i and v_j states,

$$B_{ij} \equiv \frac{\hbar^2}{2\mu} \langle v_i | R^{-2} | v_j \rangle.$$

If the units of \mathbf{H}^{ROT} are energy (Joules), the units of B_{ij} are cm⁻¹, the angular momentum operator, \mathbf{R}^2/\hbar^2 , is converted into a unitless function of quantum numbers, then

$$B_{ij}/\text{cm}^{-1} = \frac{16.85762908}{\mu/g \cdot \text{mol}^{-1}} \langle v_i | R^{-2} / \text{Å}^{-2} | v_j \rangle.$$

It is possible to arrange the angular momenta in several convenient ways. The one that I prefer is most appropriate for the Hund's case (a) basis set, $|^{2S+1}\Lambda_{\Omega}\rangle = |n\Lambda S\Sigma\rangle |\Omega JM\rangle$ where $\Omega = \Lambda + \Sigma$.

The top line of the expression for ${\bf R}^2$ consists exclusively of terms that have diagonal matrix elements

$$\hbar^2 \left\{ [J(J+1) - \Omega^2] + L_\perp^2 + [S(S+1) - \Sigma^2] \right\}.$$

Because matrix elements of $\vec{\bf L}$ cannot be universally expressed for a non-spherical object, we replace the expectation value of ${\bf L}^2-{\bf L}_z^2$ by the usually ignored fit-parameter, L_\perp^2 .

The second line of the expression for \mathbf{R}^2 consists of terms that have non-zero off-diagonal matrix elements between Hund's case (a) basis functions. The $|^{2S+1}\Lambda_{\Omega}\rangle$ basis-functions are eigenfunctions of all of the operators in the first line.

2.4 Hund's Cases[3]

Everyone except spectroscopists hates them. Spectroscopists need them because they tell what kind of patterns will be found among the energy levels. This enables spectra to be "assigned". We are assured of being able to assign rigorously good

[†] Orbit-spin is not the same as spin-orbit.

2.4 Hund's Cases 19

quantum numbers (operators that commute with the exact **H**), but the really difficult and important task is assignment of non-rigorously good quantum numbers. These non-rigorous quantum numbers are the basis for patterns in the spectrum that aid assignment of eigenstates and understanding of the dynamics encoded in these eigenstates.

There are three important terms in the molecular \mathbf{H}^{eff} .

- 1. \mathbf{H}^{el} (lifts the degeneracy of the states that arise from a single electronic configuration)
- 2. The spin-orbit term, \mathbf{H}^{SO} (diagonal in Ω), (lifts the degeneracy of the Ω -components of one ΛS state and mixes different ΛS states). For example, ${}^{3}\Pi$ is split into $\Omega = 0, 1, 2$ components and ${}^{3}\Pi_{1}$ can interact with ${}^{1}\Pi_{1}$.

$$\begin{split} E^{\mathrm{SO}} &= \left\langle n\Lambda S\Sigma | \mathbf{H}^{\mathrm{SO}} | n\Lambda S\Sigma \right\rangle \\ \Omega &= \Lambda + \Sigma \\ &\quad \text{and} \\ &\quad \left\langle n\Lambda = 1, S = 0, \Sigma = 0 | \mathbf{H}^{\mathrm{SO}} | n'\Lambda = 1, S = 1, \Sigma = 0 \right\rangle \neq 0 \end{split}$$

3. \mathbf{H}^{ROT} (destroys Ω via the $B\mathbf{J}_{\pm}\mathbf{S}_{\mp}$ and $B\mathbf{J}_{\pm}\mathbf{L}_{\mp}$ spin- and L-uncoupling terms)

These three terms in the \mathbf{H}^{eff} are at war [12]. The relative orders of magnitude of differences between their expectation values guide us in the application of perturbation theory to this problem (see the discussion of perturbation theory in Chap. 3.1). They determine what we put into $\mathbf{H}^{(0)}$ and what acts as a perturbation and must be put into $\mathbf{H}^{(1)}$. We will see that this choice of how to partition \mathbf{H}^{eff} terms into $\mathbf{H}^{(0)}$ vs. $\mathbf{H}^{(1)}$ amounts to a choice of basis set.

- $\mathbf{H}^{(\mathrm{el})} > \mathbf{H}^{(\mathrm{SO})} > \mathbf{H}^{(\mathrm{ROT})}$ case (a) J is pattern-forming: $E(J) = \frac{\mathrm{case}\;(\mathrm{a})}{B_{\Omega}J(J+1)}$ [the pattern is J(J+1)] Ω is good $B_{\Omega} = B + (B^2/A)\frac{2(\Omega-\Lambda)}{\Lambda}$
- $\bullet \quad H^{(\text{SO})} > H^{(\text{el})} > H^{(\text{ROT})} \qquad \qquad \underline{\text{case (c)}}$

J is rotational pattern forming,

 Ω is good. The atom-in-molecule quantum numbers $J_a = L_a + S_a$ might also be good. J_a is the total atomic angular momentum of one open-shell atom, appropriate for ligand field theory.

For example, in $Ce^{2+}O^{2-}$ the $Ce^{2+}fs$ configuration gives rise to $14 \times 2 = 28$ components: ${}^{3}\Phi$, ${}^{1}\Phi$, ${}^{3}\Delta$, ${}^{1}\Delta$, ${}^{3}\Pi$, ${}^{1}\Pi$, ${}^{3}\Sigma^{+}$, ${}^{1}\Sigma^{+}$.

These Λ -S state labels are the conventional but stupid way to look at the states and energy levels. Instead, $f\left(j=\frac{7}{2} \text{ and } \frac{5}{2}\right)$ couples to $s\left(j=\frac{1}{2}\right)$ to make $J_a=4,3,3,2$ components with the same energy level pattern as in a free Ce²⁺ atom [13] (see Fig. 2.1).

These four J_a atomic-ion components see the O^{2-} ligand as a point charge that splits each of them into $2J_a + 1$ components according to Ω_a , the projection of J_a on the internuclear axis. As a result, the pattern of four levels is replicated

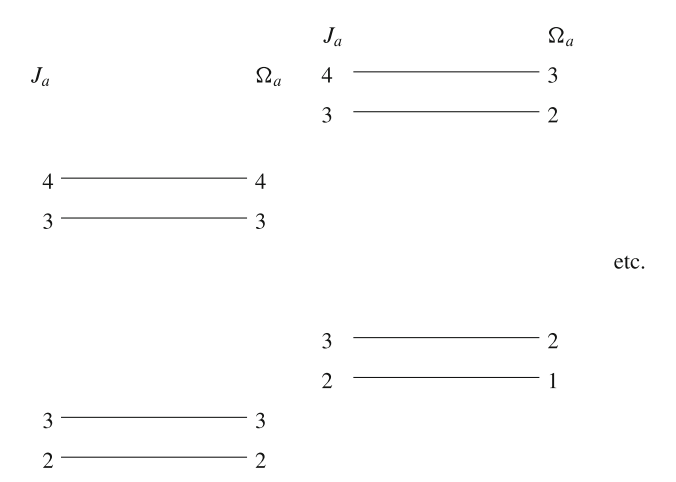


Fig. 2.1 The energy level pattern of four J_a atomic-ion components is replicated as \mathbf{J}_a goes from parallel to the internuclear axis ($\Omega_a = J_a$) toward perpendicular to the internuclear axis ($\Omega_a = 0$)

Fig. 2.2 The energy levels of a ${}^3\Sigma^+$ state. N is pattern-forming [BN(N+1)] and the three J components of each N value exhibit a splitting pattern much smaller than 2BN

and each replica is displaced by an energy related to the strength of the ligand field. This is an example of an unconventional energy level pattern that can be understood by choosing the physically appropriate basis set.

•
$$\mathbf{H}^{(\text{el})} > \mathbf{H}^{(\text{rot})} > \mathbf{H}^{(\text{SO})}$$
 $\underline{\text{case (b)}}$ D^{\dagger} is rotational pattern-forming Ω , Σ are not good. J is good.

 Σ -states are almost always in case (b) because their spin-orbit splitting is necessarily zero. The energy levels of a ${}^3\Sigma^+$ state are easy to understand when N is regarded as rotationally pattern forming (Fig. 2.2).

 $^{^{\}dagger}N$ is the total angular momentum exclusive of spin, N = J - S.

2.4 Hund's Cases 21

Consider N = 2. There are three spin components: $J = 1(F_3)$, $J = 2(F_2)$, and $J = 3(F_1)$. J can be rigorously determined via selection rules. If N is "good", we can replace N in BN(N + 1) by the appropriate value of J.

Rotational Energy
$$F_1 \ N = J - 1 \ B(J - 1)(J) = B[J(J + 1) - 2J]$$

$$F_2 \ N = J \qquad BJ(J + 1) = BJ(J + 1)$$

$$F_3 \ N = J + 1 \ B(J + 1)(J + 2) = B[J(J + 1) + 2(J + 1)]$$

So if we make "reduced term value" plots of all rotational energy levels as E(J) - BJ(J+1) vs. J, we obtain three curves from which F_1, F_2, F_3 assignments, hence N assignments can be established by inspection.

•
$$\mathbf{H}^{(\mathrm{rot})} > \mathbf{H}^{(\mathrm{el})} > \mathbf{H}^{(\mathrm{SO})}$$
 case (d)
 $R = N - \mathcal{L}$ is rotational pattern-forming,
 $E(R) = BR(R+1) = B[N(N+1) - 2\mathcal{L}N + \mathcal{L}^2 - \mathcal{L}].$
In the case (d) limit, a reduced term value plot of $E(N) - BN(N+1)$ vs. N may be used to determine \mathcal{L} . \mathcal{L} is the projection of ℓ on \mathbf{R} .

Rydberg States. The Rydberg electron can be weakly coupled to the ion-core. When this occurs, the rotation-vibration levels of the ion-core form the dominant case (d) patterns that guide assignment of the spectra [14].

 ℓ is good. \mathcal{L} , the projection of ℓ on **R** (*not* on the z-axis!), is good.

•
$$\mathbf{H}^{(\mathrm{SO})} > \mathbf{H}^{(\mathrm{ROT})} > \mathbf{H}^{(\mathrm{el})}$$
 case (e)

Rydberg States
$$\begin{cases} j \text{ is good (the total angular momentum} } \\ 0 \text{ of the Rydberg electron)} \\ J^{+} \text{ is good (the total angular momentum of the ion-core)} \end{cases}$$

 J^+ is rotational pattern-forming ($J^+ = J - j$). The pattern is $B^+ J^+ (J^+ + 1)$. Usually a large $\mathbf{H}^{(SO)}$ is associated with the ion-core, not with the Rydberg electron (the expectation value of \mathbf{H}^{SO} for the Rydberg electron scales as $n^{\star - 3}$, where n^{\star} is the effective principal quantum number).

• $\mathbf{H}^{(\text{ROT})} > \mathbf{H}^{(\text{SO})} > \mathbf{H}^{(\text{el})}$ is usually ignored because it is impossible to make $\mathbf{H}^{(\text{el})}$ small while maintaining $\mathbf{H}^{(\text{SO})}$ as larger (except for Rydberg states built on an ion-core with a large, n^* -independent spin-orbit splitting), because both scale as n^{*-3} .

(Hund's coupling cases correspond to these three terms arranged in 3! = 6 orders.)

2.4.1 $H^{(0)}$ vs. $H^{(1)}$

Recall perturbation theory [15]: the energy of the n-th level is given by

$$E_n = E_n^{(0)} + E_n^{(1)} + E_n^{(2)} = H_{nn}^{(0)} + H_{nn}^{(1)} + \sum_{m} \left| \frac{\left| H_{nm}^{(1)} \right|^2}{E_n^{(0)} - E_m^{(0)}} \right| \quad (\text{' means } n \neq m)$$

Note that a large energy denominator keeps the basis set "good" but a large value of $\left|H_{nm}^{(1)}\right|$ makes the basis "bad".

If $\mathbf{H}^{(\text{rot})}$ and $\mathbf{H}^{(\text{SO})}$ are at war, one choice of basis gives large energy denominators from $\mathbf{H}^{(\text{SO})}$ and small off-diagonal matrix elements as numerators from $\mathbf{H}^{(\text{ROT})}$. The other choice of basis gives large energy denominators from $\mathbf{H}^{(\text{ROT})}$ and small numerators from $\mathbf{H}^{(\text{SO})}$. One is free to chose either basis set, but the one for which the $\left\{E_n^{(0)}\right\}$ more closely resembles the observed pattern of eigen-energies is more convenient to use.

2.5 Two Basis Sets for the 2 x 2 "Two-Level" Problem

This example illustrates how the good and evil roles of opposing factors can be interchanged. Normally we think of zero-order energy level differences that appear along the diagonal of an $\mathbf{H}^{\mathrm{eff}}$, such as the spin-orbit $A\Lambda\Sigma$ term, as good because they preserve the simple case (a) level pattern. The non-diagonal $-BJ_{\pm}L_{\mp}$ L-uncoupling term is evil because, at sufficiently high- $J\left[J>\frac{A\Lambda}{B}\right]$ it vanquishes $A\Lambda\Sigma$ and forces the level pattern to follow case (d). In case (d), what remains of the influence of \mathbf{H}^{SO} resides off-diagonal between same-J, same-parity, different-N basis states. The simplest illustration of this role-reversal between \mathbf{H}^{SO} and $\mathbf{H}^{\mathrm{ROT}}$ is the two-level problem.

The $\mathbf{H}^{(\text{eff})}$ for the 2 × 2 problem is usually expressed as

$$E_{1}^{(0)} = \overline{E} + \Delta/2 \qquad \overline{E} = \frac{E_{1}^{(0)} + E_{2}^{(0)}}{2}$$

$$E_{2}^{(0)} = \overline{E} - \Delta/2 \qquad \Delta = E_{1}^{(0)} - E_{2}^{(0)}$$

$$\mathbf{H}_{12}^{(1)} = \langle 1 | \mathbf{H}^{(1)} | 2 \rangle = V_{12}$$

$$\mathbf{H} = \begin{pmatrix} \overline{E} & 0 \\ 0 & \overline{E} \end{pmatrix} + \begin{pmatrix} \Delta/2 & V_{12} \\ V_{12} & -\Delta/2 \end{pmatrix}.$$

The Δ term tries to keep the basis "good" and the V_{12} term opposes Δ . The eigenvalues are $E_{\pm} = \overline{E} \pm [(\Delta/2)^2 + V_{12}^2]^{1/2}$. This basis is more convenient when

 $|\Delta| \gg |V_{12}|$. Now consider a change of basis set:

$$|a\rangle = 2^{-1/2}[|1\rangle + |2\rangle]$$

$$|b\rangle = 2^{-1/2}[|1\rangle - |2\rangle]$$

$$\langle a|\mathbf{H}|a\rangle = \frac{1}{2}[H_{11} + H_{22} + 2V_{12}] = \overline{E} + V_{12}$$

$$\langle b|\mathbf{H}|b\rangle = \frac{1}{2}[H_{11} + H_{22} - 2V_{12}] = \overline{E} - V_{12}$$

$$\langle a|\mathbf{H}|b\rangle = \langle b|\mathbf{H}|a\rangle = \frac{1}{2}[H_{11} - H_{22} + V_{12} - V_{12}] = \Delta/2$$

The transformed $\mathbf{H}^{(eff)}$ is

$$\tilde{\mathbf{H}} = \begin{pmatrix} \overline{E} & 0 \\ 0 & \overline{E} \end{pmatrix} + \begin{pmatrix} V_{12} & \Delta/2 \\ \Delta/2 - V_{12} \end{pmatrix}$$

The V_{12} term tries to keep the basis good while the Δ term opposes V_{12} . This basis is more convenient when $|V_{12}| \gg |\Delta|$. Notice that $\Delta/2$ and V_{12} have exchanged roles [16]!

2.6 Some Reasons for Patterns

It is usually clear in advance which Hund's case will be most appropriate (because we know how $\mathbf{H}^{(SO)}$ and $\mathbf{H}^{(el)}$ scale with $n^{\star -3}$).

 Σ -states are always case (b) except at lowest N. Why? [The spin–spin term lifts the degeneracy of same-J, different- Ω states.] There is no force that tells S the location of the body axis. Each N is 2S+1 degenerate: the fine structure components J=N-S (F_{2S+1}) to N+S (F_1) and all 2S+1 spin-components have the same total parity, which is $(-1)^N$ for Σ^+ states and $(-1)^{N+1}$ for Σ^- states. (F_i is a special notation for the labeling of spin components [17].) J and parity are always good.

Rydberg states generally have two flavors:

- 1. *core-non-penetrating*, ℓ is good because the Rydberg electron is a passive passenger, thus ion-core quantum numbers are pattern-forming;
- 2. core-penetrating, ℓ is bad, ℓ and s couple to the ion-core quantum numbers to make N and J. For example Rydberg states of the HfF molecule have half-integer rotational pattern-forming quantum numbers (even though ion-core is $^1\Sigma^+$) [18]. The half-integer quantum numbers imply that the Rydberg electron still has strong enough $\mathbf{H}^{(SO)}$ that $\mathbf{H}^{(SO)} > \mathbf{H}^{(rot)}$.

2.7 Straight Line Plots

Consider $a^2\Pi$ state. It is really four states $(^2\Pi_{3/2e}, ^2\Pi_{3/2f}, ^2\Pi_{1/2e}, ^2\Pi_{1/2f})$, treated as one. Will the pattern-forming rotational quantum number be integer or half integer?

case (a) case (b)

$$J$$
, half integer N , integer

$$E(1/2) = \frac{3}{4}B \qquad E(0) = 0B$$

$$E(3/2) = \frac{15}{4}B \qquad 3B \qquad E(1) = 2B$$

$$E(5/2) = \frac{35}{4}B \qquad E(2) = 6B$$

The consecutive level spacing pattern $3B, 5B, \ldots$ (energy levels linear in J(J+1)) is easily distinguished from $2B, 4B, 6B, \ldots$ (energy levels linear in N(N+1)).

Consider a case (b) $^3\Sigma^+$ State (no spin-orbit) parity $(-1)^N$

J is rigorously good (revealed by selection rules) but N is pattern-forming (revealed by pattern).

$$J = N + 1$$
 goes as $B(J - 1)J$ F_1
 $J = N$ goes as $BJ(J + 1)$ F_2
 $J = N - 1$ goes as $B(J + 1)(J + 2)$ F_3

From a "stacked plot" of spectra recorded by excitation from consecutive J'' values [14], we know J. So we can make a *reduced term value plot* that displays the correct value of N. The reduced term value is [19]

$$E(J) - \overline{B}J(J+1) = -2\overline{B}J = -2\overline{B}(N+1) \qquad F_1$$

$$E(J) - \overline{B}J(J+1) = 0 \qquad \qquad F_2$$

$$E(J) - \overline{B}J(J+1) = 2\overline{B}(J+1) = 2\overline{B}N. \qquad F_3$$

When we plot the reduced term values of a ${}^3\Sigma^+$ state vs. J [not J(J+1) nor N nor N(N+1)!], we get three straight-line plots with slopes $-2\overline{B}$, 0, and $+2\overline{B}$. These patterns enable assignment of N (Fig. 2.3).

2.8 Stacked Plots 25

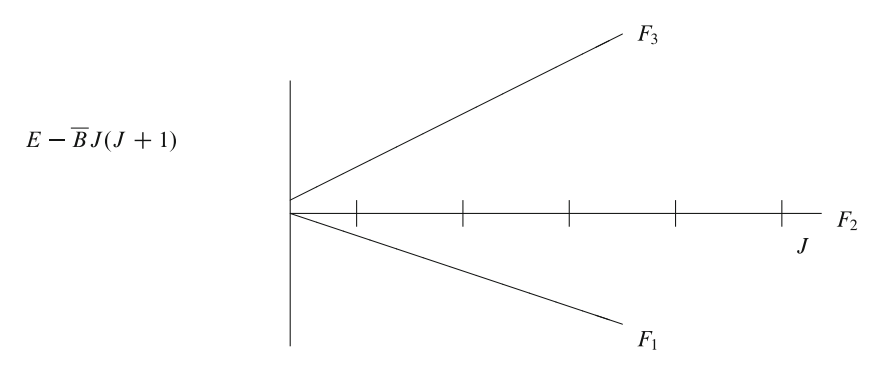


Fig. 2.3 A reduced term value plot of E(J) - BJ(J+1) vs. J for a $^3\Sigma^+$ state in case (b). J is always a rigorously good quantum number, so J can always be determined from the spectrum. The reduced term value plot is based on known quantities E(J) and J and is used to determine a non-rigorously good but pattern-forming quantum number, N

2.8 Stacked Plots

What is the difference between rigorous and pattern-forming quantum numbers? A rigorous quantum number is related to the eigenvalue of an operator that commutes with the exact molecular Hamiltonian, for example J (J^2) and parity \pm are rigorously good quantum numbers for an isolated molecule at zero external magnetic and electric fields. It is always possible (but not always trivial) to determine the *rigorously good quantum numbers* of every eigenstate. Methods include Optical Optical Double Resonance (OODR) via a J- and parity-assigned intermediate state. From each J, + intermediate state, the second transition can only terminate in (J-1)-, J-, and (J+1)-final states. J-assignments are secured via lower-state rotational combination differences, as illustrated by Fig. 2.4, or by polarization diagnostics [20].

Complete specification of an eigenstate often requires the use of *approximately good quantum numbers* as labels in addition to the rigorously good quantum numbers, as illustrated in Figs. 2.5 and 2.6.

These additional labels are often eigenvalues of an operator that does not commute with the exact Hamiltonian, for example $\mathbf{N} = \mathbf{J} - \mathbf{S}$. However, in the limit that some term in the exact Hamiltonian can be neglected (e.g. the effects of \mathbf{H}^{SO} can be negligible at high-J relative to the effects of the $-B\mathbf{J} \cdot \mathbf{S}$ spin-uncoupling term from \mathbf{H}^{ROT}). When this occurs, N (\mathbf{N}^2) becomes pattern-forming, and it is possible to use the BN(N+1) pattern in the spectrum to determine the value of the N quantum number. At high enough J, N becomes pattern-forming

$$\overline{B}N(N+1) = \overline{B}(J-S)(J-S)(J-S+1) = \overline{B}[J(J+1)-2JS+S^2-S]$$

where $S \equiv J - N$, S changes in steps of 1 in the interval, $[-S \le S \le S]$ and is the projection of S on N. \overline{B} is the approximately known rotational constant (for Rydberg

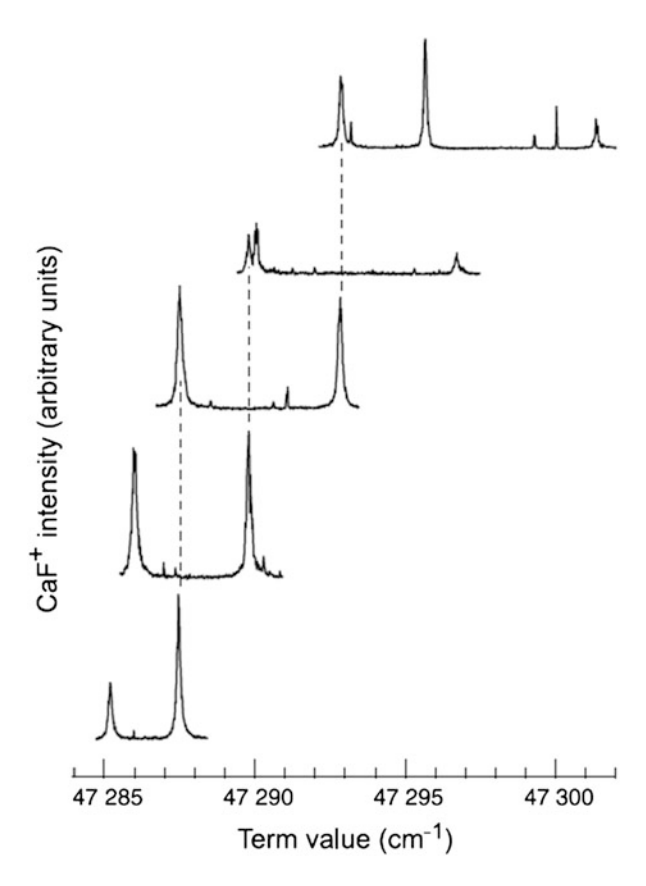


Fig. 2.4 Term value stacked plot. A consecutive-N' series of optical-optical double resonance spectra [Rydberg $\leftarrow D^2\Sigma^+$, $D^2\Sigma^+ \leftarrow X^2\Sigma^+$] of CaF is plotted vs. the absolute energy of the upper Rydberg level. Each Rydberg $\leftarrow D^2\Sigma^+$ spectrum is shifted by the absolutely known term value of the intermediate N' level, which is the term value of the X(v'', N'') initial level plus the transition frequency of the laser that pumps the D-X transition. Transitions connected by a *vertical dashed line* terminate in the same upper N-level. The value of this N quantum number is determined by the D-state rotational combination difference, R(N-1)-P(N+1) [14]. Reproduced with permission from Fig. 4 in J.J. Kay, D.S. Byun, J.O. Clevenger, V.S. Petrovic, R. Seiler, J.R. Barchi, A.J. Merer, and R.W. Field, Can. J. Chem. 82, 791–803 (2004). Copyright 2004, Canadian Science Publishing or its licensors

states it is the rotational constant of the molecular ion-core, for triplet states it is the effective rotational constant of the F_2 (J=N) spin-component. A reduced term value plot of

$$E^{\text{ROT}}(J) - \overline{B}J(J+1) = \overline{B}[-2JS + S^2 - S] \text{ vs. } J$$

has slope $-2\overline{B}S$, from which S and then N are determined.

2.8 Stacked Plots 27

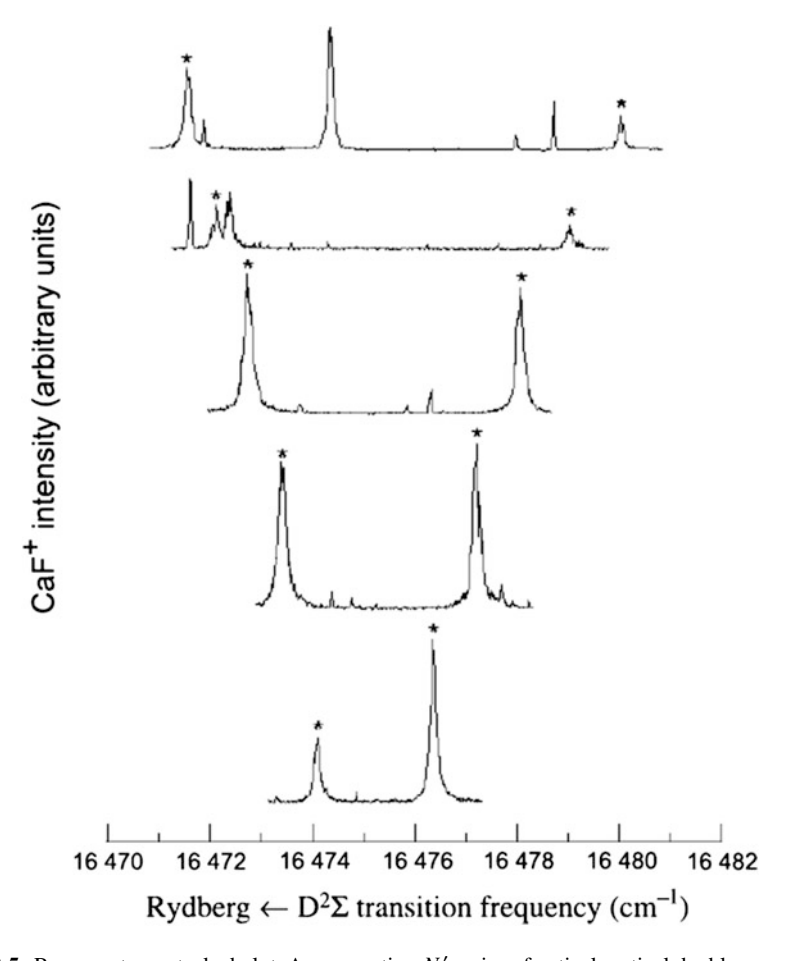


Fig. 2.5 Raw spectrum stacked plot. A consecutive-N' series of optical-optical double resonance spectra of CaF is plotted vs. the frequency of the Rydberg $\leftarrow D^2\Sigma^+$ laser. There is no spectrum-to-spectrum shift to remove the effect of different term value for each intermediate level. This sort of stacked plot reveals the energy level pattern associated with each rotational branch. It is this sort of information that displays the pattern-forming rotational quantum numbers rather than the rigorously conserved rotational quantum numbers. Once a branch pattern is observed, attention is focused on what is the difference between the absolutely known rigorous quantum number and the approximately conserved pattern-forming quantum number. This sort of determination need be done only once for each branch in order to make a plot of the reduced term value, $E^{\text{obs}}(N, \text{parity}) - BN(N+1)$ vs. N [14]. Reproduced with permission from Fig. 5 in J.J. Kay, D.S. Byun, J.O. Clevenger, V.S. Petrovic, R. Seiler, J.R. Barchi, A.J. Merer, and R.W. Field, Can. J. Chem. 82, 791–803 (2004). Copyright 2004, Canadian Science Publishing or its licensors

To summarize, J is determined by a Term Value Stacked Plot (Fig. 2.4) [14] or by R,P vs Q polarization diagnostics [21]. Then, for the organization of transitions into branches as shown on a Raw Spectrum Stacked Plot (Figs. 2.5 and 2.6), one

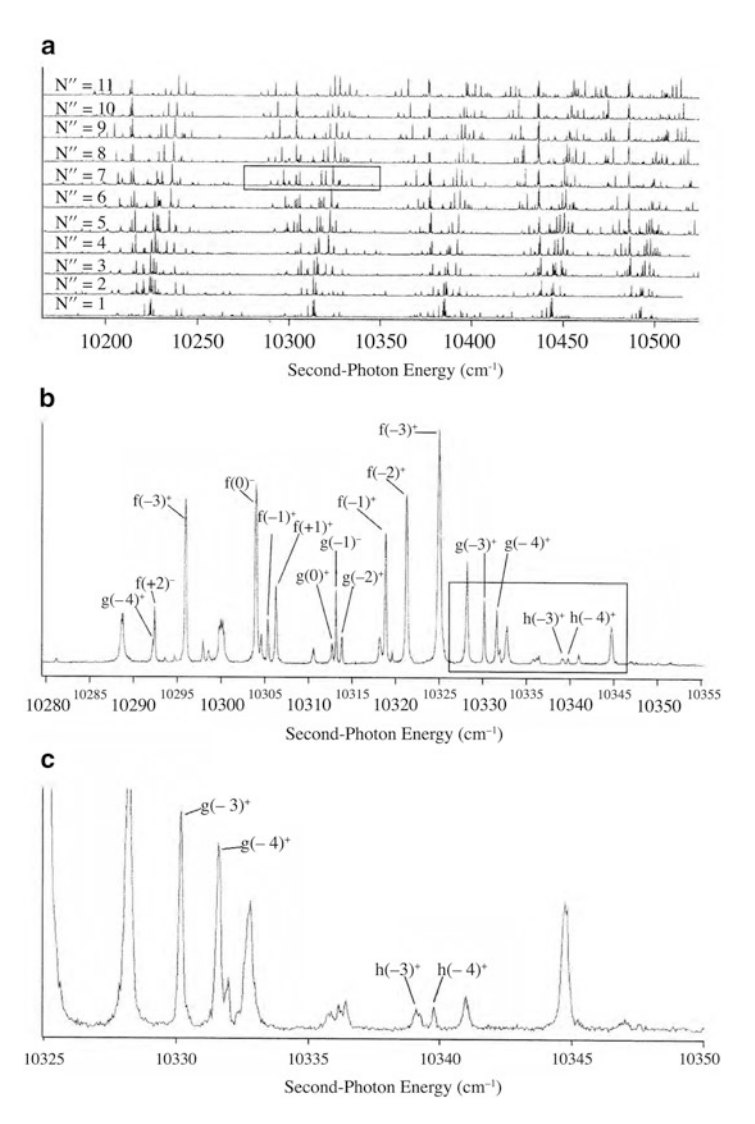


Fig. 2.6 Raw spectrum stacked plot for mostly core-nonpenetrating Rydberg states of CaF. The importance of pattern-forming quantum numbers is illustrated by this three-part figure. The spectral patterns shown in Figs. 2.4 and 2.5 are quite simple, because they involve transitions into core-penetrating Rydberg states. Nonpenetrating states are vastly more numerous and require assignment of *two* nonrigorous but pattern-forming quantum numbers, ℓ and N^+ , where ℓ is the nearly good orbital angular momentum quantum number of the Rydberg electron and N^+ is the nearly good rotational quantum number of the ion-core. It turns out that in CaF the $F'^2\Sigma^+$ intermediate state is prolific in providing transitions to core-nonpenetrating states. Part (a) shows raw stacked plots, from which the observed transitions are organized into many rotational branches. Part (b) shows the detail of the boxed part of the N''=7 spectrum. Each peak is labeled by its upper state ℓ and $\ell_R=N-N^+$ quantum numbers. ℓ ranges from 3 (f) to 5 (h) and ℓ_R ranges from $+\ell$ to $-\ell$. Part (c) shows even finer detail for the boxed region of the spectrum in part (b) [21]. Reproduced with permission from Fig. 1 in J.J. Kay, S.L. Coy, V.S. Petrovic, B.M. Wong, and R.W. Field, *J. Chem. Phys.* 128, 194301/1–20 (2008). Copyright 2008, AIP Publishing LLC

uses the reduced term value plot to determine N for at least one transition in each rotational branch. This determines J - N for all of the lines in that branch.

For Rydberg states (Fig. 2.6) at effective principal quantum number $n^* > 10$, rotational branches from transitions into many Rydberg states are closely spaced, perhaps even entangled. OODR is needed to simplify the spectrum and stacked plots make most J and \mathcal{L} (the projection of the orbital angular momentum of the Rydberg electron, ℓ , on the ion-core rotational angular momentum, \mathbf{N}^+ or \mathbf{J}^+) assignments automatic.

2.9 Angular Momenta: A Brief Summary

An angular momentum operator, A, is defined by the commutation rule

$$[\mathbf{A}_i, \mathbf{A}_j] = i\hbar \sum_k \varepsilon_{ijk} \mathbf{A}_k$$

$$\varepsilon_{ijk} = +1 \text{ if } (i, j, k) \to (x, y, z) \text{ in cyclic order}$$

$$-1 \text{ if } (i, j, k) \to (x, y, z) \text{ in anticyclic order}$$

$$0 \text{ if one component is repeated}$$

The angular momentum $|A\alpha M_A\rangle$ are simultaneously eigenfunctions of \mathbf{A}^2 , \mathbf{A}_z , and \mathbf{A}_Z .

$$\mathbf{A}_{z} |A\alpha M_{A}\rangle = \hbar\alpha |A\alpha M_{A}\rangle$$

$$\mathbf{A}_{\pm} |A\alpha M_{A}\rangle = \hbar[A(A+1) - \alpha(\alpha \pm 1)]^{1/2} |A\alpha \pm 1M_{A}\rangle^{\dagger}$$

$$\mathbf{A}_{\pm} = \mathbf{A}_{x} \pm i\mathbf{A}_{y}$$

$$\mathbf{A}^{2} |A\alpha M_{A}\rangle = \hbar^{2}A(A+1) |A\alpha M_{\alpha}\rangle.$$

We are mostly concerned with *body*-fixed angular momentum components (denoted by lower-case x, y, z)

$$(\mathbf{L}, \Lambda), (\mathbf{S}, \Sigma), (\mathbf{J}, \Omega), \quad \mathbf{N} = \mathbf{J} - \mathbf{S}, \mathbf{F} = \mathbf{J} + \mathbf{I}.$$

[†]There is a special complication that arises for the body-fixed components of angular momenta that contain the rotation of the body frame (\mathbf{J} , $\mathbf{N} = \mathbf{J} - \mathbf{S}$, but not \mathbf{L} or \mathbf{S}). For these angular momenta, the body-fixed components follow "reversed angular momentum commutation rules", $[\mathbf{A}_i, \mathbf{A}_j] = -\sum_k \varepsilon_{ijk} \mathbf{A}_k$, and the roles of \mathbf{A}_+ and \mathbf{A}_- are exchanged.

$$\mathbf{L}_{z} | n \Lambda S \Sigma \rangle = \hbar \Lambda | n \Lambda S \Sigma \rangle$$

$$\mathbf{S}_{z} | n \Lambda S \Sigma \rangle = \hbar \Sigma | n \Lambda S \Sigma \rangle$$

$$\mathbf{J}_{z} | n \Lambda S \Sigma \rangle = \hbar (\Lambda + \Sigma) | n \Lambda S \Sigma \rangle.$$

The Stark (electric field) and Zeeman (magnetic field) effects and electronic transition intensities are related to *laboratory*-fixed components of angular momenta (denoted by upper case X, Y, Z)

$$\mathbf{J}_{Z} |\Omega JM\rangle = \hbar M |\Omega JM\rangle.$$

Just as all of the matrix elements of the magnitude and components of an angular momentum operator, A, may be derived from the commutation rule definition of A, other operators, B, may be classified relative to A by the commutation rule:

$$[A_i, B_j] = i\hbar \sum_k \epsilon_{ijk} B_k.$$

This reduced form of the Wigner–Eckart Theorem guides evaluation of matrix elements of **B** in the $|A\alpha M_A\rangle$ basis set [22].

2.10 Where Have We Been and Where are We Going?

This lecture has been an unconventional introduction to finding the appropriate $\mathbf{H}^{(\mathrm{eff})}$ model. Once we find it, all we need to do is adjust the parameters (molecular constants) that define the $\mathbf{H}^{(\mathrm{eff})}$ to get a good least-squares fit to all of the energy levels. The important trick is to build a simple but physical model that includes all of the terms in the $\mathbf{H}^{(\mathrm{eff})}$ that affect the observed pattern of energy levels and transition intensities. Once we have a spectroscopically well determined $\mathbf{H}^{(\mathrm{eff})}$, we can compute a very large range of spectroscopic and dynamical effects. We have much more than an archival table of molecular constants. This is what I mean by going "beyond the molecular constants".

References

- 1. H. Lefebvre-Brion, R.W. Field, *The Spectra and Dynamics of Diatomic Molecules*, Sect. 2.1 (Elsevier, Amsterdam, 2004)
- R.W. Field, J. Baraban, S.H. Lipoff, A.R. Beck, Effective Hamiltonians in Handbook of High-Resolution Spectroscopies, ed. by M. Quack, F. Merkt (Wiley, New York, 2010)
- 3. H. Lefebvre-Brion, R.W. Field, *The Spectra and Dynamics of Diatomic Molecules*, Sect. 3.2 (Elsevier, Amsterdam, 2004)

References 31

4. H. Lefebvre-Brion, R.W. Field, *The Spectra and Dynamics of Diatomic Molecules*, Sect. 3.1 (Elsevier, Amsterdam, 2004)

- 5. J. von Neumann, E.P. Wigner, Z. Phys. **40**, 742 (1927)
- 6. H. Lefebvre-Brion, R.W. Field, *The Spectra and Dynamics of Diatomic Molecules*, Sect. 5.1.3 (Elsevier, Amsterdam, 2004)
- 7. R.J. LeRoy, http://leroy.uwaterloo.ca/programs.html (RKR1 and LEVEL)
- 8. J.L. Dunham, Phys. Rev. 41, 721 (1932)
- 9. Ch.H. Townes, A.L. Schawlow, Microwave Spectroscopy (Dover, New York, 2012), pp. 9-13
- H. Lefebvre-Brion, R.W. Field, The Spectra and Dynamics of Diatomic Molecules (Elsevier, Amsterdam, 2004), pp. 181–191
- 11. H. Lefebvre-Brion, R.W. Field, *The Spectra and Dynamics of Diatomic Molecules* (Elsevier, Amsterdam, 2004), pp. 107–110
- 12. H. Lefebvre-Brion, R.W. Field, *The Spectra and Dynamics of Diatomic Molecules* (Elsevier, Amsterdam, 2004), p. 100
- R.W. Field, Berichte der Bunsengesellschaft für Physikalische Chemie 86, 771–779 (1982);
 C. Linton, M. Dulick, R.W. Field, P. Carette, P.C. Leyland, R.F. Barrow, J. Mol. Spectrosc. 102, 441–497 (1983)
- J.J. Kay, D.S. Byun, J.O. Clevenger, X. Jiang, V.S. Petrović, R. Seiler, J.R. Barchi, A.J. Merer, R.W. Field, Can. J. Chem. 82, 791–803 (2004)
- C. Cohen-Tannoudji, B. Diu, F. Laloë, Quantum Mechanics, Chap. 11 (Wiley, New York, 1977), pp. 1095–1108
- 16. H. Lefebvre-Brion, R.W. Field, *The Spectra and Dynamics of Diatomic Molecules* (Elsevier, Amsterdam, 2004), p. 121
- 17. H. Lefebvre-Brion, R.W. Field, *The Spectra and Dynamics of Diatomic Molecules* (Elsevier, Amsterdam, 2004), p. 131
- K.C. Cossel, D.N. Gresh, L.C. Sinclair, T. Coffey, L.V. Skripnikov, A.N. Petrov, N.S. Mosyagin, A.V. Titov, R.W. Field, E.R. Meyer, E.A. Cornell, J. Ye, Chem. Phys. Lett. 546, 1–10 (2012)
- 19. H. Lefebvre-Brion, R.W. Field, *The Spectra and Dynamics of Diatomic Molecules*, Fig. 3.18 (Elsevier, Amsterdam, 2004), p. 215
- 20. V.S. Petrovic, R.W. Field, J. Chem. Phys. 128, 014301/1-014301/8 (2008)
- 21. J.J. Kay, S.L. Coy, V.S. Petrović, R.W. Field, J. Chem. Phys. 128, 194301/1–20 (2008)
- C. Cohen-Tannoudji, B. Liu, F. Laloë, Quantum Mechanics (Wiley, New York, 1977), pp. 1049–1055

Chapter 3 Spectroscopic Perturbations: Homogeneous and Heterogeneous

A spectroscopic perturbation is a local disruption of the expected "textbook" pattern of energy levels and transition intensities. It results when degeneracy accidentally occurs between two or more "pure" same-J, same-parity states, which are capable of interacting with each other via some usually harmless term in the effective Hamiltonian. Perturbations between same- Ω states are called *homogeneous* (because the interaction matrix element is independent of J) and those where $\Delta\Omega=1$ are called *heterogeneous* (because the interaction matrix element is proportional to J) [1, 2]. Level shifts, extra lines, intensity borrowing, and interference-related intensity anomalies occur at perturbations. Near a perturbation an enormous amount of information becomes available about "dark states," which are normally excluded from direct observation by transition selection rules. When a dark state becomes observable via perturbation by a "bright state", which Franck–Condon factors are relevant, those of the bright state or the dark state? Interference effects can provide a unique signature of the presence of an unexpected perturber as well as reveal the relative signs of two off-diagonal matrix elements.

3.1 What Is a Perturbation? [3]

Sometimes nature appears to be unkind. The regular patterns of spectra seem to be capriciously disrupted. These disruptions, called *perturbations* (the German word, *Störungen*, seems more appropriate), actually contain crucial information about both structure (otherwise unobservable states) and dynamics (rate and mechanism of energy flow between the normally static and therefore boring isolated states).

A perturbation is a disruption of the regular frequency and intensity patterns one expects to find in a spectrum.

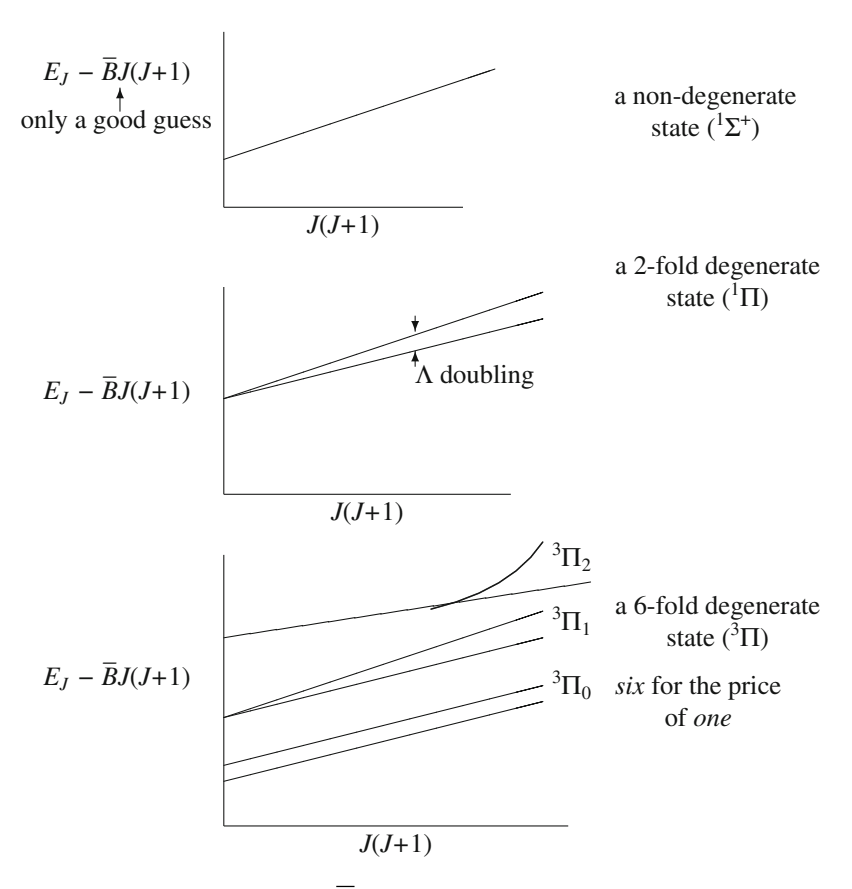


Fig. 3.1 "Reduced term-value" plots. \overline{B} is a best guess for the actual B-value. By subtracting $\overline{B}J(J+1)$ from the observed term value, E_J , one is able to display the term energy curves on an expanded energy axis. This subtraction does not distort the energy differences between potentially interacting states because the same energy is subtracted from same-J levels

The frequency pattern is best viewed in a "reduced term-value" plot [4]. This reduction permits magnification of the energy scale (vertical axis) in order to see small stuff (Fig. 3.1).

A Rydberg complex can be even more complicated: nd consists of $^2\Delta$, $^2\Pi$, and $^2\Sigma^+$ states, ten components altogether.

A perturbation looks like this (Fig. 3.2):

The regular series of strong lines at low-J belongs to the bright state, but near J_x , one regular series of lines ends abruptly and a new one starts, as if out of nowhere.

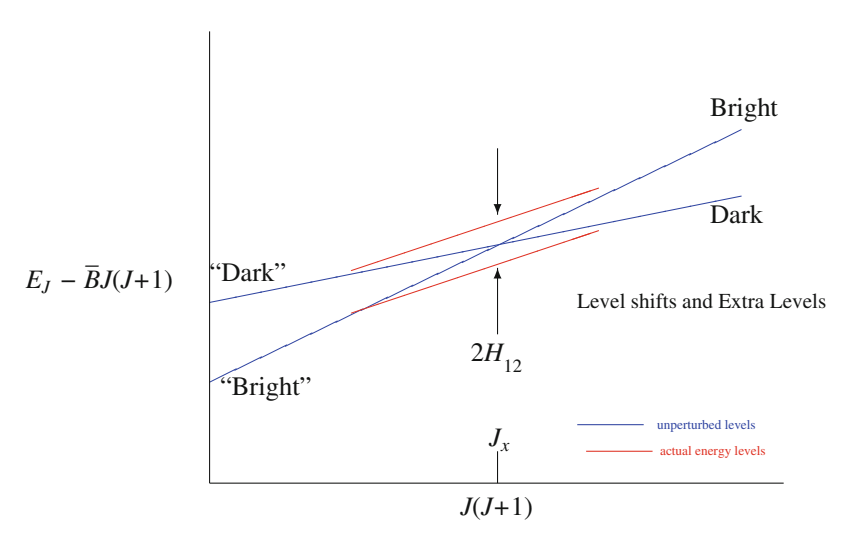


Fig. 3.2 A perturbation diagram. This reduced term value plot shows a bright state $(E_0^{\text{bright}} < E_0^{\text{dark}}, B^{\text{bright}} > B^{\text{dark}})$ being crossed from below by a dark state. The J-value of exact degeneracy is J_x . The interaction matrix element is H_{12} and, at J_x , the two interacting states differ in energy by $2H_{12}$. The selection rule for perturbations is $\Delta J = 0$, so all that matters is the vertical energy difference between the unperturbed ($dark\ curve$) and the resultant actual ($light\ curve$) energy levels

We understand a *perturbation* using **perturbation theory** [5–7]. Perturbation theory is essential for a spectroscopist. The equations of **non-degenerate perturbation theory** are:

$$\mathbf{H} = \mathbf{H}^{(0)} + \mathbf{H}^{(1)}$$

$$E_n = E_n^{(0)} + H_{nn}^{(1)} + \sum_{m \neq n}' \frac{\left| H_{nm}^{(1)} \right|^2}{E_n^{(0)} - E_m^{(0)}} \text{(the ' implies } m \neq n\text{)}$$

$$|n\rangle = |n\rangle^{(0)} + \sum_m' \frac{H_{mn}^{(1)}}{E_n^{(0)} - E_m^{(0)}} |m\rangle^{(0)}.$$

You need **degenerate perturbation theory** when

$$\left| \frac{H_{nm}^{(1)}}{E_n^{(0)} - E_m^{(0)}} \right| > 1 \text{ for some values of } m.$$

Consider two unperturbed electronic-vibrational energy levels, $|e_1, v_{e_1}\rangle$ and $|e_2, v_{e_2}\rangle$.

$$E_{e_1,v_{e_1}}^{(0)}(J) = E_{e_1,v_{e_1}} + B_{e_1,v_{e_1}}J(J+1)$$

$$E_{e_2,v_{e_2}}^{(0)}(J) = E_{e_2,v_{e_2}} + B_{e_2,v_{e_2}}J(J+1)$$

$$\Delta_{12} \equiv E_{e_1,v_{e_1}} - E_{e_2,v_{e_2}}, \overline{E}_{12} = \frac{1}{2} \left[E_{e_1,v_{e_1}} + E_{e_2,v_{e_2}} \right]$$
$$\delta B_{12} = B_{e_1,v_{e_1}} - B_{e_2,v_{e_2}}, \overline{B} = \frac{1}{2} \left[B_{e_1,v_{e_1}} + B_{e_2,v_{e_2}} \right]$$

and the rigorous selection rule, $\Delta J = 0$.

The 2×2 H^{eff} for these two states is

$$\begin{split} \mathbf{H}(J) &= \begin{pmatrix} \overline{E}_{12} + \overline{B}_{12}J(J+1) & 0 \\ 0 & \overline{E}_{12} + \overline{B}_{12}J(J+1) \end{pmatrix} \\ &+ \begin{pmatrix} \frac{\Delta_{12}}{2} + \frac{\delta B_{12}}{2}J(J+1) & V_{12} \\ V_{12} & -\frac{\Delta_{12}}{2} - \frac{\delta B_{12}}{2}J(J+1) \end{pmatrix}. \end{split}$$

 V_{12} is the interaction term that makes life interesting. The eigenvalues and eigenvectors are, by perturbation theory:

$$\begin{split} E_{\pm}(J) &= \left[\overline{E}_{12} + \overline{B}J(J+1)\right] \pm \left[\frac{\Delta_{12}}{2} + \frac{\delta B_{12}}{2}J(J+1)\right] \pm \frac{V_{12}^2}{\Delta_{12} + \delta B_{12}J(J+1)} \\ |+\rangle &= |e_1, v_{e_1}\rangle + \frac{V_{12}}{\Delta + \delta B_{12}J(J+1)} |e_2, v_{e_2}\rangle \\ |-\rangle &= |e_2, v_{e_2}\rangle - \frac{V_{12}}{\Delta + \delta B_{12}J(J+1)} |e_1, v_{e_1}\rangle \end{split}$$

or, by exact solution of the secular equation:

$$0 = \begin{vmatrix} \frac{\Delta_{12}}{2} + \frac{\delta B_{12}}{2} J(J+1) - E & V_{12} \\ V_{12} & -\frac{\Delta_{12}}{2} - \frac{\delta B_{12}}{2} J(J+1) - E \end{vmatrix}$$

$$E_{\pm}(J) = \left[\overline{E}_{12} + \overline{B}J(J+1)\right] \pm \left[\frac{\Delta_{12}}{2} + \frac{\delta B_{12}}{2}J(J+1)\right]$$
$$\pm \left[\left(\frac{\Delta_{12}}{2} + \frac{\delta B_{12}}{2}J(J+1)\right)^2 + V_{12}^2\right]^{1/2}$$

$$\begin{split} |\pm\rangle &= 2^{-1/2} \left[\left(1 \pm \frac{\Delta_{12} + \delta B_{12} J(J+1)}{E_+(J) - E_-(J)} \right)^{1/2} |e_1, v_{e_1}\rangle \right. \\ & \pm \left(1 \mp \frac{\Delta_{12} + \delta B_{12} J(J+1)}{E_+(J) - E_-(J)} \right)^{1/2} |e_2, v_{e_2}\rangle \right]. \end{split}$$

Note that these formulas for the eigenvectors are obviously correct in the *two limits*, $V_{12} = 0$ and $V_{12} = \infty$.

If $\Delta_{12} > 0$ and $\delta B_{12} < 0$, then the zero-order states will cross at J_x when

$$\Delta_{12} + \delta B_{12} J_x (J_x + 1) = 0$$

$$J_x (J_x + 1) = -\Delta_{12} / \delta B_{12}$$

$$J_x = \left[-\Delta_{12} / \delta B_{12} \right]^{1/2} - \frac{1}{2}.$$

At J_x , the two perturbed energy levels are separated by $2V_{12}$ and the two states are 50:50 mixed

$$E_{+}(J_{x}) - E_{-}(J_{x}) = 2V_{12}$$

 $|\pm\rangle = 2^{-1/2} [|e_{1}v_{e_{1}}\rangle \pm |e_{2}v_{e_{2}}\rangle].$

Let's step back from the equations for a moment.

When there are more than two simultaneously interacting states, we can deal with this by defining a larger than 2×2 effective Hamiltonian matrix [8]. We use a nonlinear least squares fit (because there are no analytic formulas) of the parameters $\left\{E_i^{(0)}, B_i^{(0)}, H_{i,j}^{(1)}, \text{ etc.}\right\}$ that define the \mathbf{H}^{eff} so that the observed energy levels are fitted to measurement accuracy. The molecular constants we obtain are said to be "deperturbed". All effects of the perturbation are accounted for. The energy levels (and the associated eigenvectors) describe what is seen (and an extrapolation to what could in principle be seen) in the spectrum.

Figure 3.3 shows the spectrum of a perturbation-free v=0 level and a massively perturbed v=1 level. These two spectra look profoundly different, even though the v=0 and 1 levels belong to the same electronic state (SiO $H^1\Sigma^+$).

If $E_1^{(0)} > E_2^{(0)}$: **Level Shifts**. This kind of up-shift followed by down-shift (or vice-versa) discontinuity in the energy level patterns is the unmistakeable signature of a perturbation (Fig. 3.4).

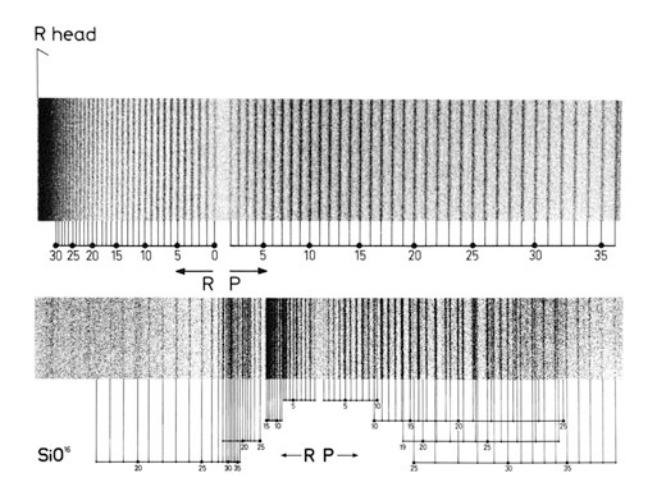


Fig. 3.3 A comparison of the SiO $H^1\Sigma$ (0,0) (top) and (1,0) (bottom) bands. The (0,0) band at 1,435 Å is perturbation-free, but perturbations in the v=1 level of the $H^1\Sigma$ state cause the (1,0) band at 1,413 Å to be shattered. (Courtesy I. Renhorn [9].) Reproduced with permission of Ingmar Renhorn. Reproduced from Fig. 2.1 in H. Lefebvre-Brion and R.W. Field, *The Spectra and Dynamics of Diatomic Molecules*, Elsevier (2004)

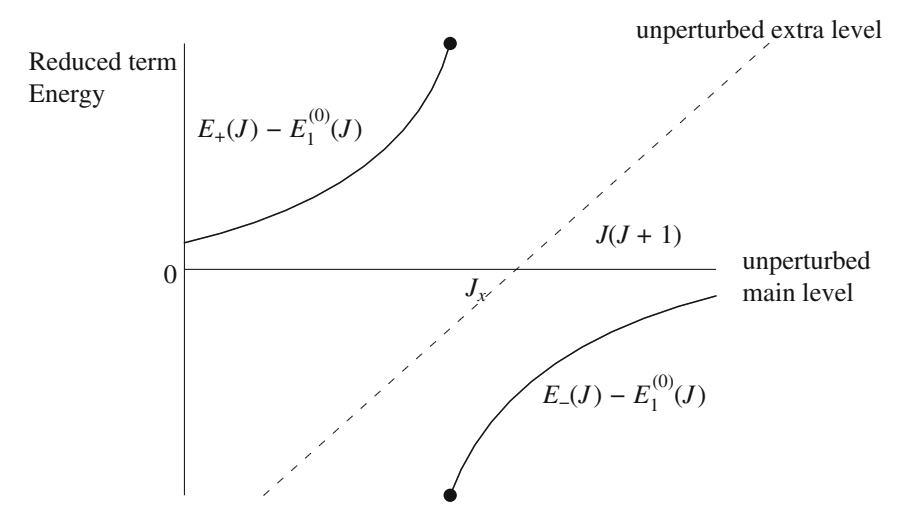


Fig. 3.4 The $E_1^{(0)}$ "main" level is crossed from below by the $E_2^{(0)}$ level as J increases. The intersection between $E_1^{(0)}(J)$ and $E_2^{(0)}(J)$ occurs at J_x . The dashed line is the reduced energy of the "extra" level, $E_2^{(0)}(J) - E_1^{(0)}(J)$, the horizontal solid line is the reduced energy of the "main" level, $E_1^{(0)}(J) - E_1^{(0)}(J)$, and the two curved solid lines are the reduced energy of the perturbed main level at $J \leq J_x$, $E_+(J) - E_1^{(0)}(J)$, and at $J \geq J_x$, $E_-(J) - E_1^{(0)}(J)$. The dots on the two solid curves suggest that two transitions (main and extra line) are observed at each J near J_x . The level shifts shown in this figure are accompanied by intensity borrowing illustrated in Fig. 3.5

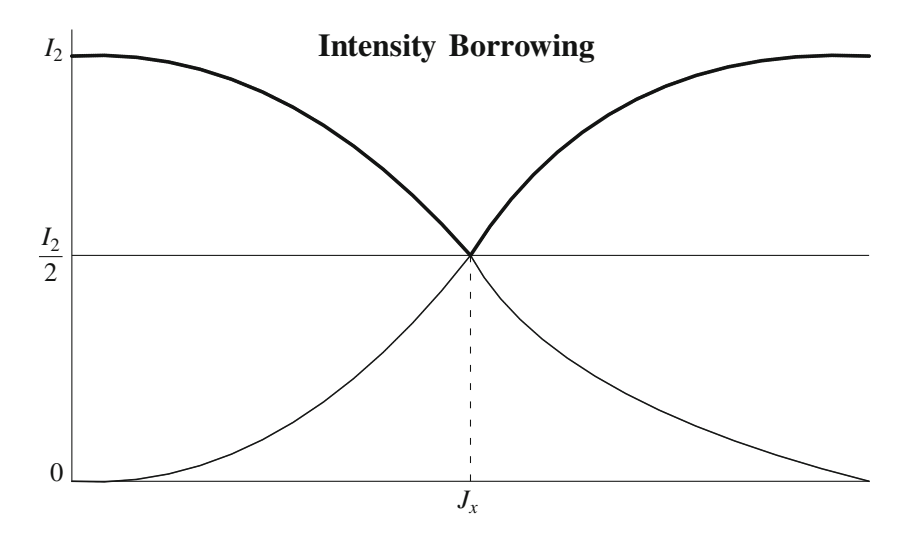


Fig. 3.5 Intensity borrowing. When two zero-order states cross through degeneracy at $J=J_x$, one zero-order state is said to be "bright" and the other "dark". Brightness and darkness are not absolute terms, they apply to the specific energy level from which the two states are observed. For example, if the initial state is e_0 , v_0 , then the zero-order state 1 is dark if $\mu_{e_1v_1,e_0v_0}=0$ and state 2 is bright if $\mu_{e_2v_2,e_0v_0}\neq 0$. The intensities of transitions into the predominantly bright $(I(J)>I_2/2)$ and dark $(I(J)<I_2/2)$ states are shown as heavy and light lines, respectively. Note that the transitions into the predominantly bright state form two series of lines separated by a large energy gap $(2H_{12})$ at J_x

The three part Fig. 3.6 below illustrates various cases of level shift and intensity borrowing *in the presence of intensity interference*:

```
top state 2 is bright, state 1 is dark middle \mu_{10} = \mu_{20} (node in I at J_x) bottom 2\mu_{10} = \mu_{20} (node shifted from J_x)
```

What can you say about the effect of the sign of the quantity $V_{12}\mu_{10}\mu_{20}$? This is an important question because it seems to violate the expectation that you can never determine the sign of an off-diagonal matrix element because the sign has no observable consequences. However, the sign of a product of two or more off-diagonal matrix elements is observable. Why? How? Notice that the intensity node occurs in the E_- rather than the E_+ series of levels in the middle section of Fig. 3.6.

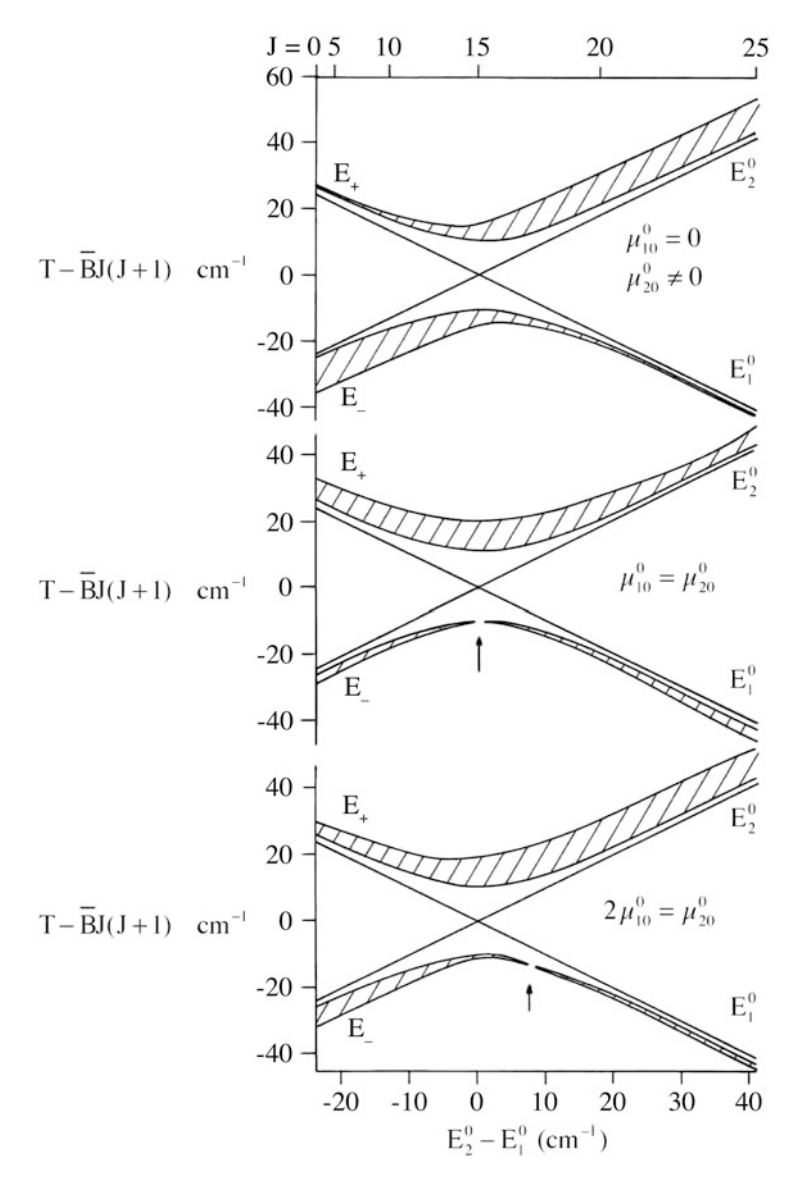


Fig. 3.6 Schematic illustration of intensity interference effects, which can be counter-intuitive. The *straight lines* are the basis function (i.e., deperturbed) reduced term values, $E_1^0 - \overline{B}J(J+1)$, where $\overline{B} = (B_1^0 + B_2^0)/2$. The level crossing occurs at J = 15 ($B_1^0 = 0.9$ cm⁻¹, $B_2^0 = 1.1$ cm⁻¹, $H_{12} = 10$ cm⁻¹). The inner edges and widths of the *solid curves* depict, respectively, the energies of the perturbed levels, E_+ and E_- [reduced by $\overline{B}J(J+1)$], and the intensities of the transitions into E_+ and E_- . The *top frame* illustrates simple intensity borrowing, $\mu_{10}^0 = 0$. The *middle frame* shows the vanishing of intensity at the crossing point (J = 15), $E_1^0 = E_2^0$, when $\mu_{10}^0 = \mu_{20}^0$. The *bottom frame* exemplifies the general case, $\mu_{10}^0 \neq \mu_{20}^0 \neq 0$ (here $2\mu_{10}^0 = \mu_{20}^0$), where the intensity vanishing point is at ($J \simeq 17.3$). [From Dressler (1970) [10].] Reproduced with permission of Kurt Dressler (October 8, 2014). Reproduced from Fig. 6.7 in H. Lefebvre-Brion and R.W. Field, *The Spectra and Dynamics of Diatomic Molecules*, Elsevier (2004)

3.2 Level Shifts and Intensity Borrowing [11]

It is evident from the formulas for the perturbed energy levels and eigenvectors that there will be two prominent phenomena at J-values near J_x , level shifts and intensity borrowing.

Level Shifts. If
$$E_1^{(0)}(J) > E_2^{(0)}(J)$$

Using degenerate perturbation theory, we obtain

$$E_{+} - E_{1}^{(0)} = + \left[\left(\Delta_{12}/2 + \frac{\delta B_{12}}{2} J(J+1) \right)^{2} + V_{12}^{2} \right]^{1/2}$$

or, simplified to non-degenerate perturbation theory, we obtain

$$\approx \frac{V_{12}^2}{\Delta_{12} + \delta B_{12} J(J+1)}$$

$$E_{-} - E_2^{(0)} = -\left[\left(\Delta_{12}/2 + \frac{\delta B_{12}}{2} J(J+1) \right)^2 + V_{12}^2 \right]^{1/2}.$$

Intensity Borrowing. Suppose that basis state $|1\rangle$ is bright and basis state $|2\rangle$ is dark in the particular experiment under consideration.

This means, in transitions from state $|0\rangle$

$$\mu_{10} = \langle 1|\mu|0\rangle \neq 0$$
 bright $\mu_{20} = \langle 2|\mu|0\rangle = 0$ dark

[Brightness/darkness is not absolute. It depends on the nature of state $|0\rangle$. For example, $|0\rangle$ and $|1\rangle$ are singlet states and $|2\rangle$ is a triplet state.]

$$I_{+} \approx I_{1} \left[1 - \frac{V_{12}^{2}}{(\Delta_{12} + \delta B_{12}J(J+1))^{2}} \right]$$
 small loss of intensity from "main"
$$I_{-} \approx I_{1} \left[\frac{V_{12}^{2}}{(\Delta_{12} + \delta BJ(J+1))^{2}} \right]$$
 borrowing of intensity in "extra" line

There are two intuitive and useful rules for perturbations:

- 1. Level shifts are equal in magnitude and opposite in direction;
- 2. Intensity is conserved, $I_1 = I_+ + I_-$ (when states 1 and 2 are both bright $I_1(J) + I_2(J) = I_+(J) + I_-(J)$);
- 3. Minimum of $E_+(J) E_-(J)$ occurs at $J = J_x$ and is equal to $2V_{12}$.

There is a special situation at J_x :

$$E_1^{(0)}(J_x) = E_2^{(0)}(J_x)$$

 $I_+(J_x) = I_-(J_x)$ (not true if states 1 and 2 are *both* bright),

which means that it is possible to know, at the center of a perturbation (i.e. at J_x), based on extrapolation of the energy and intensity of the bright state from J=0 to J_x , what is the energy and intensity of the transition into the extra level.

3.3 Two Qualitatively Distinct Classes of Perturbation: Homogeneous and Heterogeneous [1, 2]

Homogeneous	Heterogeneous
(Spin-orbit, inter-electronic)	$(BJ_{\pm}L_{\mp} \text{ and } BJ_{\pm}S_{\mp})$
$\Delta\Omega = 0$	$\Delta\Omega = \pm 1$
V_{12} is independent of J	$V_{12} \propto [J(J+1) - \Omega(\Omega \pm 1)]^{1/2} \approx (J+1/2)$
$(\Omega \text{ is eigenvalue of } \mathbf{J}_z)$	

The analytic formulas for heterogeneous perturbations are slightly different from those for homogeneous perturbations. One key difference is that, at $J\gg J_x$, the effects of the perturbation on the energy levels and transition intensities never vanish because both the matrix element squared (numerator) and energy difference (denominator) are both $\propto J(J+1)$. Consider this a fine point.

3.4 Franck-Condon Factors [12, 13]

The intensities for transitions between the vibrational levels of two electronic states are governed by Franck–Condon factors

$$I_{e_1,v_{e_1},e_2,v_{e_2}} \propto q_{v_{e_1},v_{e_2}} \equiv \langle v_{e_1}|v_{e_2}\rangle^2$$

Franck-Condon factors (always positive) are the *square* of a vibrational overlap integral (which can be either positive or negative). They are calculated using Robert LeRoy's "Level" program, based on RKR potential curves calculated from experimentally measured vibrational G(v) and rotational B(v) functions, using Robert LeRoy's "RKR1" program [12].

3.5 Which Franck-Condon Factors Should I Use?

What Franck-Condon factor must be used to calculate the intensity of a perturbed vibrational band?

The perturbed states are mixtures of two (or more) vibration-electronic states. So how do we think of the vibrational wavefunction: *mixed* or *schizophrenic*?

mixed:
$$|ev_{\text{mixed}}\rangle = \alpha |v_{e_1}\rangle + \beta |v_{e_2}\rangle$$

schizophrenic: $|ev_{\text{mixed}}\rangle = \alpha |e_1\rangle |v_{e_1}\rangle + \beta |e_2\rangle |v_{e_2}\rangle$

where α and $\beta = [1 - \alpha^2]^{1/2}$ are the mixing coefficients for the $|e_i\rangle |v_{e_i}\rangle$ basis states in the eigenstates.

The correct choice, schizophrenic, is based on the fact that v_{e_1} vibrational character is always associated with e_1 electronic character. This is a consequence of the Born–Oppenheimer approximation [14, 15], from which we obtain the concept of electronic potential energy surfaces and wavefunctions written as a product of an electronic times a vibrational factor.

$$|e_i v_{e_i}\rangle = |e_i\rangle |v_{e_i}\rangle$$
.

There is no perturbation term that is capable of mixing the vibrational levels belonging to the e_i and e_j electronic states, in the manner

$$|ev_{\text{mixed}}\rangle = |e_i\rangle [\alpha |v_{e_i}\rangle + \beta |v_{e_i}\rangle].$$

It is a very common and tempting error to think of mixed vibrational states without their *essential* electronic cofactor. *Schizophrenic* is an appropriate metaphor because the $|v_{e_i}\rangle$ vibrational wavefunction carries its $|e_i\rangle$ electronic character whereas the $|v_{e_i}\rangle$ wavefunction is inseparable from its $|e_i\rangle$ electronic character.

The intensity of a transition into a mixed state (including the possibility that both e_1 and e_2 are "bright") is [16]

$$\begin{split} I_{ev_{\text{mixed}},e_0,v_{e_0}} & \propto |\alpha \ \langle e_0v_{e_0}|\pmb{\mu}|e_1v_{e_1}\rangle + \beta \ \langle e_0v_{e_0}|\pmb{\mu}|e_2v_{e_2}\rangle|^2 \\ & = |\alpha\mu_{e_0,e_1} \ \langle v_{e_0}|v_{e_1}\rangle + \beta\mu_{e_0,e_2} \ \langle v_{e_0}|v_{e_2}\rangle|^2 \\ & = \alpha^2\mu_{e_0,e_1}^2 q_{v_{e_0},v_{e_1}} + \beta^2\mu_{e_0,e_2}^2 q_{v_{e_0},v_{e_2}} \\ & + 2\alpha\beta\mu_{e_0,e_1}\mu_{e_0,e_2} \ \langle v_{e_0}|v_{e_1}\rangle \ \langle v_{e_0}|v_{e_2}\rangle \\ & \alpha^2 = 1 - \beta^2. \end{split}$$

Notice that the first two terms (the α^2 and β^2 terms) are always positive, but the third term (the $\alpha\beta$ term) can be either positive or negative, resulting in either constructive or destructive interference [17]. (Be sure you can prove that the third term can

never be so large and negative that it causes $I_{ev_{\text{mixed}},e_0v_{e_0}} < 0$. A negative transition probability would be silly. Why? It would be a reliable indicator that error has crept in!) The third term is a quantum mechanical interference effect that is of great diagnostic importance in the spectroscopy of perturbed states.

3.6 Intensity Borrowed from a Nearby Bright State

Suppose we have a dark electronic state, e_2 , that borrows its intensity from one nearby vibrational level, v_{e_1} , of the bright electronic state, e_1 . What is the Franck–Condon factor for emission to the v_{e_0} vibrational levels?

 e_2 is dark, β^2 is the fractional bright state character in the dark state, $\beta^2 < 1/2$ (the $e_2v_{e_2}$ state has a small amount of $e_1v_{e_1}$ bright character)

$$I_{e,v_{
m mixed},e_0,v_{e_0}} \propto eta^2 \mu_{e_1,e_0}^2 q_{v_{e_1},v_{e_0}}$$
 The bright state Franck–Condon factor

3.7 Intensity Borrowed from an *Energetically Remote* Bright State

Now suppose that the dark state borrows all of its intensity from all of the vibrational levels of one energetically remote bright perturbing electronic state.

Completeness tells us how to express the dark vibrational state, $|v_{e_2}\rangle$, as a superposition of bright vibrational states, $|v_{e_1}\rangle$

$$|v_{e_2}\rangle = \sum_{v_{e_1}} |v_{e_1}\rangle \langle v_{e_1}|v_{e_2}\rangle.$$

The mixing coefficient of every bright vibrational state in the dark vibrational state is included here, based on the usually good approximation that the interaction matrix element may always be expressed as the product of a constant electronic factor and a vibrational overlap integral

$$\langle e_1, v_{e_1} | \mathbf{H} | e_2, v_{e_2} \rangle = H_{e_1, e_2} \langle v_{e_1} | v_{e_2} \rangle$$
.

For the dark, predominantly $|e_2\rangle |v_{e_2}\rangle$ state, interacting with a bright remote perturber

$$|\text{mixed}\rangle = |e_2\rangle |v_{e_2}\rangle + H_{e_1,e_2} |e_1\rangle \sum_{v_{e_1}} \left[|v_{e_1}\rangle \frac{\langle v_{e_1} | v_{e_2}\rangle}{E_{v_{e_2}}^{(0)} - E_{v_{e_1}}^{(0)}} \right],$$

which is useful for calculating the intensity of the transition to $|e_0v_{e_0}\rangle = |e_0\rangle |v_{e_0}\rangle$

$$\langle e_0 | \langle v_{e_0} | \boldsymbol{\mu} | \text{mixed} \rangle = \mu_{e_0, e_2}^{0} \langle v_{e_0} | v_{e_2} \rangle + H_{e_1, e_2} \mu_{e_0, e_1} \sum_{v_{e_1}} \langle v_{e_0} | v_{e_1} \rangle \frac{\langle v_{e_1} | v_{e_2} \rangle}{E_{v_{e_2}}^{(0)} - E_{v_{e_1}}^{(0)}}.$$

$$(e_2 \text{ is dark})$$

Here is the key trick: if the remote state is so remote that $E_{v_2}^{(0)} - E_{v_{e_1}}^{(0)}$ does not depend significantly on v_{e_1} , then we replace the energy denominator by the constant term $\Delta E_{21}^{(0)}$.

$$\left\langle e_0 | \left\langle v_{e_0} | \boldsymbol{\mu} | \mathrm{mixed} \right\rangle = \frac{H_{e_1,e_2}}{\Delta E_{21}^{(0)}} \mu_{e_0,e_1} \sum_{v_{e_1}} \left\langle v_{e_0} | v_{e_1} \right\rangle \left\langle v_{e_1} | v_{e_2} \right\rangle.$$

Next, we use completeness in reverse

$$\sum_{v_{e_1}} \langle v_{e_0} | v_{e_1} \rangle \langle v_{e_1} | v_{e_2} \rangle = \langle v_{e_0} | v_{e_2} \rangle !$$

Thus

$$I_{\mathrm{mixed},v_{e_0}} \propto \left(rac{\mathbf{H}_{e_1,e_2}\mu_{e_0,e_1}}{\Delta E_{21}^{(0)}}
ight)^2 q_{v_{e_0},v_{e_2}}.$$
 The dark state Franck—Condon factor

Even though all of the transition strength is borrowed from the remote bright perturber, e_1 , the Franck–Condon factor is that of the dark state, e_2 ! This is the opposite of what happens for a single, locally perturbing vibrational level of a bright state.

3.8 Intensity Interference Effects [17]

Consider a state that consists of a mixture of two bright electronic-vibrational states, $|e_1, v_{e_1}\rangle$ and $|e_2, v_{e_2}\rangle$. The intensity distribution along a vibrational progression of fluorescence transitions into the e_0 , v_{e_0} levels is not simply described by a weighted sum of Franck–Condon factors.

$$\alpha^2 \mu_{e_0,e_1}^2 q_{v_{e_0},v_{e_1}} + \beta^2 \mu_{e_0,e_2}^2 q_{v_{e_0},v_{e_2}}.$$

There is also an interference term

$$2\alpha\beta\mu_{e_0,e_1}\mu_{e_0,e_2}\langle v_{e_0}|v_{e_1}\rangle\langle v_{e_0}|v_{e_2}\rangle$$
.

This term can make the observed intensity either larger or smaller than expected based on the naive weighted sum of Franck–Condon factors. There are many kinds of interference effects, and they are *always* of diagnostic value. One of my favorites, the anomalous ratio of R(J-1):P(J+1) rotational line intensities for fluorescence out of one member of a pair of states mixed by a heterogeneous $(\Delta\Omega=\pm1)$ interaction, is beyond the scope of the present lecture. So think about this on your own!

References

- 1. J.T. Hougen, Monograph, vol. 115 (National Bureau of Standards, Washington, 1970)
- H. Lefebvre-Brion, R.W. Field, The Spectra and Dynamics of Diatomic Molecules (Elsevier, Amsterdam, 2004), p. 98
- 3. H. Lefebvre-Brion, R.W. Field, *The Spectra and Dynamics of Diatomic Molecules*, Sect. 2.1 (Elsevier, Amsterdam, 2004)
- H. Lefebvre-Brion, R.W. Field, The Spectra and Dynamics of Diatomic Molecules (Elsevier, Amsterdam, 2004), pp. 117–119
- C. Cohen-Tannoudji, B. Liu, F. Laloë, Quantum Mechanics (Wiley, New York, 1977), pp. 1095–1104
- D.A. McQuarrie, Quantum Chemistry (University Science, Sausalito, California, 2008), pp. 396–404
- P.F. Bernath, Spectra of Atoms and Molecules, 2nd edn. (Oxford University Press, Oxford, 2005), pp. 94–96
- 8. R.W. Field, J. Baraban, S.H. Lipoff, A.R. Beck, Effective Hamiltonians, in *Handbook of High-Resolution Spectroscopies*, ed. by M. Quack, F. Merkt (Wiley, New York, 2010)
- 9. H. Lefebvre-Brion, R.W. Field, *The Spectra and Dynamics of Diatomic Molecules*, Fig. 2.1 (Elsevier, Amsterdam, 2004)
- H. Lefebvre-Brion, R.W. Field, The Spectra and Dynamics of Diatomic Molecules, Fig. 6.7 (Elsevier, Amsterdam, 2004)
- 11. H. Lefebvre-Brion, R.W. Field, *The Spectra and Dynamics of Diatomic Molecules*, Sect. 6.2 (Elsevier, Amsterdam, 2004)
- 12. R.J. LeRoy, http://leroy.uwaterloo.ca/programs.html (RKR1 and LEVEL)
- 13. P.F. Bernath, *Spectra of Atoms and Molecules*, 2nd edn. (Oxford University Press, Oxford, 2005), pp. 328–332
- 14. H. Lefebvre-Brion, R.W. Field, *The Spectra and Dynamics of Diatomic Molecules*, Sect. 3.1 (Elsevier, Amsterdam, 2004)
- 15. P.F. Bernath, *Spectra of Atoms and Molecules*, 2nd edn. (Oxford University Press, Oxford, 2005), pp. 97–99
- H. Lefebvre-Brion, R.W. Field, The Spectra and Dynamics of Diatomic Molecules, Sect. 6.2 (Elsevier, Amsterdam, 2004)
- 17. H. Lefebvre-Brion, R.W. Field, *The Spectra and Dynamics of Diatomic Molecules*, Sect. 6.3 (Elsevier, Amsterdam, 2004)

Chapter 4 The Effective Hamiltonian for Diatomic Molecules

The \mathbf{H}^{eff} is not the exact Hamiltonian [1]. It is a *fit-model* that is constructed so that it captures all of the appropriate quantum number dependences. It is necessary to convert an infinite dimension and internuclear distance-dependent Hamiltonian into a finite dimension matrix model in which the R-dependence is encoded in the v, J dependence of the observed energy levels and transition intensities [2]. The Van Vleck transformation [3] folds effects of all remote perturbers into the finite dimension fit model. Examples treated include: transition moments, centrifugal distortion in ${}^{1}\Sigma^{+}$ states, vibration-rotation interaction (α_{e}), centrifugal distortion in ³Π states, and Λ-doubling. Spectroscopists need a fit model to account for all details of their spectrum, which include (a) transition frequencies, (b) relative intensities of transitions, (c) ability to extrapolate beyond the observed region of the spectrum, (d) elimination of assignment ambiguities, (e) provide an explanation of surprising v, J dependences of certain molecular constants, (f) revealing hidden inter-relationships between observed quantities, (g) extraction of information from intensity interference effects [4], (h) determination of internuclear distance, R, dependences when only v, J-dependences can be measured [2], (i) evaluation of statistically rigorous sensitivities of the fit parameters to the actually observed data set, and (j) provide a basis for a decision about whether an outlier line is due to a blunder or a perturbation.

4.1 Introduction

The exact **H** is an infinite dimension matrix because the molecule possesses an infinite number of rotation-vibration-electronic states. It is impossible to find the exact eigenvalues and eigenvectors of an infinite dimension secular determinant. So we must somehow reduce the dimension of **H** to include only the tiny fraction of state space directly sampled by our experiment. The method by which this

is done is called the "Van Vleck Transformation" (also known as the "Contact Transformation") [3]. It is a souped-up version of second order non-degenerate perturbation theory. It is more beautiful than it appears at first sight. It can have the flexibility to deal with any situation that nature provides. Most importantly, our \mathbf{H}^{eff} is expressed in terms of the absolute minimum number of adjustable parameters [1].

We observe transitions between energy levels. We do not observe all energy levels. And we do not directly observe the internuclear distance dependence of any property. Information about other electronic states and R-dependences is encoded in the v, J dependence of energy levels (and the relative intensities of transitions). How do we obtain this missing information?

Alternatively, we want to build a *fit model* that is capable of fitting our observations to measurement accuracy. This is an effective Hamiltonian, \mathbf{H}^{eff} . It is not the exact Hamiltonian. And, once the data is fitted, it is far more accurate than anything our ab initio theorist friends can compute (Fig. 4.1).

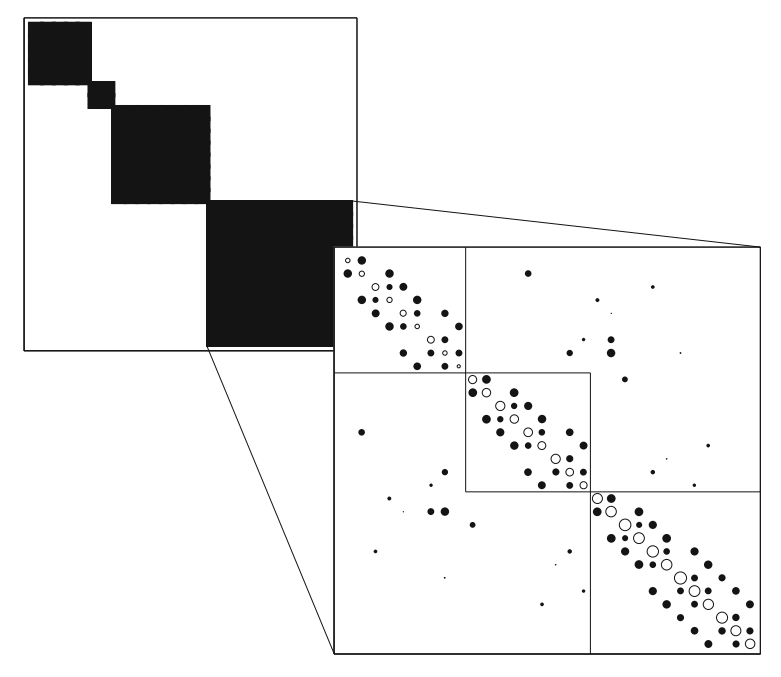


Fig. 4.1 The *upper left panel* shows the exact block-diagonalization of **H**^{exact} according to a set of operators that commute with the exact Hamiltonian. The *lower right panel* shows an expanded view of the lower right symmetry block. Non-zero matrix elements are indicated with *dots*, sized according to magnitude. Zero order energies (on-diagonal matrix elements) are marked with *open circles*, and are scaled differently than the off-diagonal elements [1]. Reproduced with permission from Fig. 1 in R.W. Field, J.H. Baraban, S.H. Lipoff, and A.H. Beck, "Effective Hamiltonians," in *Handbook of High-resolution Spectroscopy*, M. Quack and F. Merkt (editors), John Wiley & Sons (2011). Copyright 2011, John Wiley & Sons, Inc.

4.2 Main Topics of This Lecture

This lecture is based on three important ideas.

4.2.1 R-Dependence [2]

All terms in the molecular Hamiltonian are either explicitly (e.g. the B(R) rotational "constant" operator) or implicitly (via the Born–Oppenheimer approximation, the electronic Schrödinger equation is solved at each point on a grid of nuclear coordinates) dependent on internuclear distance, R. These R-dependences are encoded in the vibration-rotation energy levels.

The first step is to do a power series expansion of each term in the Hamiltonian (keeping only the first two terms)

$$\mathbf{H}(R) = \mathbf{H}(R_0) + \left. \frac{\partial \mathbf{H}}{\partial R} \right|_{R=R_0} (R - R_0)$$

where R_0 is a conveniently chosen reference geometry (usually R_e for the electronic state under consideration) and recognize that $(R - R_e)$ is the displacement from equilibrium. If we make a harmonic oscillator approximation, we know both selection rules $(R^1 \leftrightarrow \Delta v = \pm 1)$ and explicit values of all non-zero $\langle v | (R - R_e) | v \pm 1 \rangle$ matrix elements.

$$R - R_e \equiv \mathbf{Q} = \left[\frac{\hbar}{2\pi c\mu\omega}\right]^{1/2} \hat{\mathbf{Q}} = \left[\frac{\hbar}{4\pi c\mu\omega}\right]^{1/2} (\mathbf{a} + \mathbf{a}^{\dagger})$$
$$\langle v - 1|\mathbf{a}|v\rangle = v^{1/2}$$
$$\langle v + 1|\mathbf{a}^{\dagger}|v\rangle = (v+1)^{1/2}$$

where ω is in cm⁻¹ units, $\hat{\mathbf{Q}}$ is the dimensionless displacement coordinate, and \mathbf{a} and \mathbf{a}^{\dagger} are annihilation and creation operators (more on these in later lectures).

4.2.2 How Do We Account for Interactions with Energetically Remote States?

We try to use *second-order non-degenerate* **perturbation theory**[5, 6] to account for the neglect of interactions with all energetically remote states. These include different vibrational levels of the same electronic state (this is where the

R-dependence is taken into account) and the rotation-vibration levels of all other energetically remote electronic states. The second-order energy shifts are

$$E_{e_1,v_{e_1},J}^{(2)} = \sum_{e_n,v_{e_n}} \frac{\left| H_{e_1,v_{e_1},J;e_n,v_{e_n},J}^{(1)} \right|^2}{E_{e_1,v_{e_1},J}^{(0)} - E_{e_n,v_{e_n},J}^{(0)}}.$$

We also have the first order (diagonal in $\mathbf{H}^{(1)}$) energy terms

$$E_{e_1,v_{e_1},J}^{(1)} = H_{e_1,v_{e_1},J;e_1,v_{e_1},J}^{(1)}$$

and first order corrections to the wavefunctions

$$|e_1, v_{e_1}, J\rangle = |e_1, v_{e_1}, J\rangle^{(0)} + \sum_{e_n, v_{e_n}} \frac{H_{e_1, v_{e_1}, J; e_n, v_{e_n}, J}^{(1)}}{E_{e_1, v_{e_1}, J}^{(0)} - E_{e_n, v_{e_n}, J}^{(0)}} |e_n, v_{e_n}, J\rangle^{(0)}.$$

This approach does not work when there are a few quasi-degenerate "perturber" levels for which the convergence criterion for second-order perturbation theory

$$\left| \frac{\mathbf{H}_{ij}^{(1)}}{\Delta E_{ij}^{(0)}} \right| \gtrsim 1$$

is not met. These quasi-degenerate perturber levels must be included in an enlarged \mathbf{H}^{eff} matrix [1].

But non-degenerate perturbation theory also fails to work when the state of interest consists of several fine-structure levels, such as the six $(\Omega, \text{ parity: } \Omega = 2, 1, 0, \text{ parity } = \pm)$ components of a ${}^3\Pi$ state or the $(2\ell+1)(2s+1)$ components of an $n\ell$ Rydberg complex. We need a special modification of 2nd order perturbation theory. This is called the "Van Vleck transformation", or the "Contact Transformation."

4.2.3 Van Vleck Transformation [3]

The **Van Vleck transformation** has the effect of folding interactions with all remote rovibronic states (denoted by ϕ , S, Λ , Ω' , $v_{S,\Lambda}$) into the effective Hamiltonian for

the electronic state of interest, α , which has 2S + 1 Ω -components,

$$H_{\Omega v,\Omega''v}^{\mathrm{eff}-\alpha} = \sum_{\phi,S,\Lambda,\Omega',v_{S,\Lambda}} \frac{H_{\alpha \Omega v;\phi,\Omega',v_{S,\Lambda}} H_{\phi \Omega' v_{S,\Lambda};\alpha \Omega''v}}{\frac{1}{2} \left\lceil E_{\alpha \Omega v}^{(0)} + E_{\alpha \Omega''v}^{(0)} \right\rceil - E_{\phi \Omega' v_{S,\Lambda}}^{(0)}}.$$

Note that, unlike second-order perturbation theory, the Van Vleck transformation adds corrections to both diagonal and *off-diagonal* elements of $\mathbf{H}^{\mathrm{eff}}$. This looks horrible, but it is the spectroscopist's best friend. *One crucial point*: each of these corrections to each element of the finite dimension $\mathbf{H}^{\mathrm{eff}}$ is formally an infinite sum over *all* remote states [1]. But actually, you need only a sum over all of the symmetries of remote electronic states that are allowed to interact with the α -type state. A relatively small number of second-order parameters (one for each symmetry) provides full flexibility in the $\mathbf{H}^{\mathrm{eff}}$. Of course, one seldom evaluates these infinite sums ab initio; one determines their values by fitting the observed spectrum.

4.3 *R*-Dependence Is Encoded in v, J Dependence [2]

Replace *R***-dependent terms** in the internuclear dependence of the operators that correspond to observable properties by the *v*, *J* dependence of the actually observed quantities.

4.3.1 Transition Moments: $\mu(R) \to M_{v',v''}$

According to the Born–Oppenheimer approximation [7, 8], the $e_i v_{e_i}$, $e_j v_{e_j}$ matrix elements of any R-dependent operator may be evaluated in two steps. First, at fixed-R, integrate over the electronic coordinates. For the $\mu(R)$ example, integration over the electronic coordinates (denoted by r adjacent to each bra and ket)

$$\langle e_i v_{e_i} | \boldsymbol{\mu}(R) | e_j v_{e_j} \rangle_r = \langle v_{e_i} | M_{e_i, e_j}(R) | v_{e_j} \rangle$$

where $M_{e_i,e_j}(R)$ is an electronic transition moment function. Integration over the nuclear coordinates (denoted by $_R$ adjacent to each bra and ket)

$${}_{R}\langle v_{e_i}|M_{e_i,e_j}(R)|v_{e_j}\rangle_{R}=M^{e_i,e_j}_{v_{e_i},v_{e_j}}.$$

The set of $M_{v_{e_i},v_{e_j}}^{e_i,e_j}$ encodes all R-dependence of $\mu(R)$ in the e_i,e_j electronic subspace.

4.3.2 Centrifugal Distortion, D_e [9]

Centrifugal distortion comes from the *R*-dependence of the rotational "constant" operator. We want to expand B(R), in cm⁻¹ units, as a power series in $\mathbf{Q} \equiv R - R_e$, $B(R) = \frac{\hbar^2}{4\pi c \mu} R^{-2}$

$$\frac{1}{R^2} = \frac{1}{(Q + R_e)^2} = \frac{1}{R_e^2} \left(\frac{Q}{R_e} + 1\right)^{-2}$$

$$= \frac{1}{R_e^2} \left[1 - 2\left(\frac{Q}{R_e}\right) + 3\left(\frac{Q}{R_e}\right)^2 - 4\left(\frac{Q}{R_e}\right)^3 + \dots \right]$$

$$B(R) = B_e \left[1 - 2\left(\frac{Q}{R_e}\right) + 3\left(\frac{Q}{R_e}\right)^2 - \dots \right]$$

$$B_e = \frac{\hbar}{4\pi c \mu} R_e^{-2} \Longrightarrow R_e = \left[\frac{4\pi c \mu}{\hbar} B_e \right]^{-1/2}$$

$$Q = \left[\frac{\hbar}{4\pi c \mu \omega} \right]^{1/2} (\mathbf{a} + \mathbf{a}^{\dagger})$$

$$\frac{Q}{R_e} = \left[\frac{\hbar}{4\pi c \mu \omega} \right]^{1/2} \left[\frac{4\pi c \mu B_e}{\hbar} \right]^{1/2} (\mathbf{a} + \mathbf{a}^{\dagger}) = \left[\frac{B_e}{\omega_e} \right]^{1/2} (\mathbf{a} + \mathbf{a}^{\dagger}).[10]$$

$$\mathbf{H}^{ROT} = hcB_e \left[1 - 2\left(\frac{B_e}{\omega_e}\right)^{1/2} (\mathbf{a} + \mathbf{a}^{\dagger}) + 3\left(\frac{B_e}{\omega_e}\right) (\mathbf{a} + \mathbf{a}^{\dagger})^2 \dots \right] J(J+1)$$

 $B_e/\omega_e \approx 10^{-3}$ is a good order-sorting parameter.

$$\mathbf{H}^{(0)} = hcB_e J(J+1)$$

$$\mathbf{H}^{(1)} = hcB_e \left[-2 \left(\frac{B_e}{\omega_e} \right)^{1/2} (\mathbf{a} + \mathbf{a}^{\dagger}) + 3 \left(\frac{B_e}{\omega_e} \right) (\mathbf{a} + \mathbf{a}^{\dagger})^2 \right] J(J+1)$$

$$E_J = E_J^{(0)} + E_J^{(1)} + E_J^{(2)}$$

$$E_J^{(0)} = hcB_e J(J+1).$$

For $E_{v,J}^{(1)}$ we are only looking for *diagonal* elements of $\mathbf{H}^{(1)}$

$$E_{J,v}^{(1)} = 3hc(B_e^2/\omega_e)J(J+1)\langle v|(\mathbf{a}\mathbf{a}^{\dagger} + \mathbf{a}^{\dagger}\mathbf{a})|v\rangle$$

= $3hc(B_e^2/\omega_e)J(J+1)2(v+1/2)$
= $6hc(B_e^2/\omega_e)(v+1/2)J(J+1)$.

Now, from the usual (truncated) Dunham expansion for B_v ,

$$B_v = B_e - \alpha_e(v + 1/2)$$

we obtain

$$\alpha_e = -6hc(B_e^2/\omega_e) < 0.$$

This implies that B_v increases as v increases. We know that this is wrong! More on this soon. The final step is to evaluate the second-order perturbation sum for $E_{J,v}^{(2)}$.

$$\begin{split} E_{J,v}^{(2)} &= \sum_{v' \neq v} \frac{\left(H_{v,v'}^{(1)}\right)^2}{E_v^{(0)} - E_{v'}^{(0)}} = \frac{\left(H_{v,v+1}^{(1)}\right)^2}{E_v^{(0)} - E_{v+1}^{(0)}} + \frac{\left(H_{v,v-1}^{(1)}\right)^2}{E_v^{(0)} - E_{v-1}^{(0)}} \\ &= [hcB_eJ(J+1)]^2 \frac{4(B_e/\omega_e)}{hc\omega_e} \left[\frac{v+1}{-1} + \frac{v}{1}\right] \\ &= \frac{4(hc)^2 B_e^3}{hc\omega_e^2} [J(J+1)]^2 (-1). \end{split}$$

We identify the coefficient of $[J(J+1)]^2$ with D_e

$$E_{J,v}^{(2)} = -hcD_e[J(J+1)]^2$$

thus

$$D_e \equiv \frac{4B_e^3}{\omega_e^2} \qquad \text{(in cm}^{-1} \text{ units)}.$$

This is the famous "Kratzer relation", valid in the harmonic oscillator limit (which is always appropriate at low-v) [11]. Inclusion of additional terms like

$$hcB_e\left(3\frac{B_e}{\omega_e}\right)(\mathbf{a}^2+\mathbf{a}^{\dagger 2})J(J+1)$$

in $\mathbf{H}^{(1)}$ gives higher-order corrections to D_v , e.g. the value of β_e in

$$D_v = D_e - \beta_e(v + 1/2).$$

This exercise seems to suggest that inclusion of centrifugal distortion may be implemented simply by replacing B_v wherever it appears in \mathbf{H}^{ROT} by

$$[B_v - D_v J(J+1)].$$

It turns out that this is *not correct* for non- $^{1}\Sigma^{+}$ electronic states. The correct treatment of centrifugal distortion will be presented when the Van Vleck transformation is introduced.

4.3.3 Vibration-Rotation Interaction, α_e : A Small Surprise

We found, in the harmonic oscillator limit, that α_e has the empirically incorrect sign

$$\alpha_{e,\text{harmonic}} = -6hc(B_e^2/\omega_e).$$

Now we go back and introduce the missing anharmonic correction term, which fixes an instructive flaw in our logic

$$V(\mathbf{Q}) = hc\omega_e(v + 1/2) - b\mathbf{Q}^3. \qquad (b > 0)$$

This sign of b is correct for causing the potential energy function, $V(\mathbf{Q})$, to become harder than harmonic at $\mathbf{Q} < 0$ and softer than harmonic when $\mathbf{Q} > 0$, which is what we expect for a molecule that must dissociate at $\mathbf{Q} > 0$

$$\mathbf{Q}^{3} = \left[\frac{\hbar}{4\pi c\mu\omega_{e}}\right]^{3/2} (\mathbf{a} + \mathbf{a}^{\dagger})^{3}$$
$$(\mathbf{a} + \mathbf{a}^{\dagger})^{3} = \mathbf{a}^{3} + \mathbf{a}^{\dagger 3} + \mathbf{a}^{2}\mathbf{a}^{\dagger} + \mathbf{a}\mathbf{a}^{\dagger}\mathbf{a} + \mathbf{a}^{\dagger}\mathbf{a}^{2} + \mathbf{a}^{\dagger 2}\mathbf{a} + \mathbf{a}^{\dagger}\mathbf{a}\mathbf{a}^{\dagger} + \mathbf{a}\mathbf{a}^{\dagger 2}$$
$$\mathbf{N} \equiv \mathbf{a}^{\dagger}\mathbf{a}.$$

A little algebra

$$(\mathbf{a} + \mathbf{a}^{\dagger})^3 = \mathbf{a}^3 + \mathbf{a}^{\dagger 3} + 3(\mathbf{N} + 1)\mathbf{a} + 3\mathbf{N}\mathbf{a}^{\dagger}.$$

Thus

$$\mathbf{H}^{(1)} = -3b \left[\frac{\hbar}{4\pi c \mu \omega_e} \right]^{3/2} \left[(v+1)\mathbf{a}^\dagger + v\mathbf{a} \right] - b \left[\frac{\hbar}{4\pi c \mu \omega_e} \right]^{3/2} \left[\mathbf{a}^{\dagger 3} + \mathbf{a}^3 \right]$$
 keep these ignore these
$$b' \equiv b \left[\frac{\hbar}{4\pi c \mu \omega_e} \right]^{3/2}.$$

[†]We ignore the $[\mathbf{a}^{\dagger 3} + \mathbf{a}^{3}]$ terms here because they follow $\Delta v = \pm 3$ selection rules, thus they cannot result in interference via cross-terms with the $\Delta v = \pm 1$ matrix elements from the

We have a term from $-b'\mathbf{Q}^3$ in $\mathbf{H}^{(1)}$ that has $\Delta v = \pm 1$ selection rules. Recall that we also had a term from $\mathbf{H}^{\mathrm{ROT}}$, $hcB_eJ(J+1)[-2(B_e/\omega_e)^{1/2}(\mathbf{a}+\mathbf{a}^{\dagger})]$ that has $\Delta v = \pm 1$ selection rules. We must add the two kinds of terms in $\mathbf{H}^{(1)}$ that have the same selection rule before computing $E^{(2)}$ by squaring the off-diagonal matrix elements. This is a very important point!

$$\begin{split} \mathbf{H}^{(1)} &= -2hcB_e^{3/2}\omega_e^{-1/2}J(J+1)(\mathbf{a}+\mathbf{a}^\dagger) - 3b'[(v+1)\mathbf{a}^\dagger + v\mathbf{a}] \\ H_{v,v+1}^{(1)} &= -2hcB_e^{3/2}\omega_e^{-1/2}J(J+1)(v+1)^{1/2} - 3b'(v+1)^{3/2} \\ H_{v,v-1}^{(1)} &= -2hcB_e^{3/2}\omega_e^{-1/2}J(J+1)v^{1/2} - 3b'v^{3/2} \\ &\frac{\left(H_{v,v+1}^{(1)}\right)^2}{-hc\omega_e} = \frac{12(hc)B_e^{3/2}\omega_e^{-1/2}J(J+1)b'(v+1)^2}{-hc\omega_e} + \underset{\text{incorrect } v, J}{\text{squared terms with the } \\ \frac{\left(H_{v,v-1}^{(1)}\right)^2}{+hc\omega_e} = \frac{12(hc)B_e^{3/2}\omega_e^{-1/2}J(J+1)b'(v^2)}{+hc\omega_e} + \underset{\text{dependence}}{\text{squared terms with wrong } v, J \\ &E_{v,J}^{(2)} = -12(B_e/\omega_e)^{3/2}b'J(J+1)2(v+1/2) \end{split}$$

Note that this term is negative and usually large enough to overpower the harmonic term

$$+6hc(B_e^2/\omega_e)$$
 $\left| -24(B_e/\omega_e)^{3/2}b' \right|$ anharmonic term

This derivation illustrates the value of the $\mathbf{a}, \mathbf{a}^{\dagger}$ operators in better displaying the terms in \mathbf{H} that share the same Δv selection rule. These same- Δv terms give rise to interference effects in $E_{J,v}^{(2)}$.

4.4 Van Vleck Transformation for Non- $^{1}\Sigma$ + States

Worked examples for ${}^3\Pi$ state. A diagrammatic method is described by which second-order corrections to the rotational and spin-orbit parameters of a ${}^3\Pi$ state are evaluated.

 $hcB_eJ(J+1)[-2(\beta_e/\omega_e)^{1/2}(\mathbf{a}+\mathbf{a}^\dagger)]$ term in $\mathbf{H}^{\mathrm{ROT}}$. There are $\Delta v=\pm 3$ cross terms from the $-4\left(\frac{Q}{R_e}\right)^3$ term in the expansion of B(R), but the sum of these cross terms has a $J(J+1)(v+1/2)^2$ quantum number dependence, which means that they act as a correction to the γ_e term in $B_v=B_e-\alpha_e(v+1/2)+\gamma_e(v+1/2)^2$.

4.4.1 Centrifugal Distortion

Centrifugal distortion is not simply accounted for by "replace BJ(J+1) by [B-DJ(J+1)]J(J+1)."

When the energy level formula for a single (non-degenerate) electronic state is corrected for effects of energetically remote perturbing states [including remote vibrational levels of *the same* electronic state that are brought in by the R-dependence of molecular "constants", such as B(R)] it is possible to use ordinary non-degenerate second-order perturbation theory. However, when the electronic state in question consists of several related spin- and parity-components, the effective Hamiltonian for that state must be treated by quasi-degenerate perturbation theory. In simple language, a small dimension \mathbf{H}^{eff} must be diagonalized. For example, for a ${}^3\Pi$ state, the \mathbf{H}^{eff} for rotation is

$$\mathbf{H}^{\text{ROT}} = B(R)[(\mathbf{J}^2 - \mathbf{J}_z^2) + \mathbf{L}_{\perp}^2 + (\mathbf{S}^2 - \mathbf{S}_z^2) - (\mathbf{J}^+ \mathbf{L}^- + \mathbf{J}^- \mathbf{L}^+) - (\mathbf{J}^+ \mathbf{S}^- + \mathbf{J}^- \mathbf{S}^+) + (\mathbf{L}^+ \mathbf{S}^- + \mathbf{L}^- \mathbf{S}^+)]$$

(Matrix elements of L^2 cannot be evaluated for a non-spherical object, thus $L^2 - L_z^2$ is replaced by L_\perp^2 , which is diagonal in Hund's case (a) and ignored.)

$$\mathbf{H}^{SO} = \sum_{i} \mathbf{a}_{i} \left[\ell_{iz} s_{iz} + \frac{1}{2} \left(\ell_{i}^{+} s_{i}^{-} + \ell_{i}^{-} s_{i}^{+} \right) \right],$$

which may be replaced by the familiar $A\mathbf{L}_z\mathbf{S}_z$ for $\Delta S=0$, $\Delta\Lambda=0$ matrix elements. (The full form of \mathbf{H}^{SO} must be used for all $\Delta S\neq 0$ matrix elements.)

$$\mathbf{H}(^{3}\Pi) = {}^{3}\Pi_{1} \begin{pmatrix} E_{\Pi} + B_{\Pi}[J(J+1) - 4 + 2 - 1] + A_{\Pi} & -B_{\Pi}[J(J+1) - 2]^{1/2}[2]^{1/2} & 0 \\ -B_{\Pi}[J(J+1) - 2]^{1/2}[2]^{1/2} & E_{\Pi} + B_{\Pi}[J(J+1) - 1 + 2 - 0] & -B_{\Pi}[J(J+1)]^{1/2}[2]^{1/2} \\ 0 & -B_{\Pi}[J(J+1)]^{1/2}[2]^{1/2} & E_{\Pi} + B_{\Pi}[J(J+1) - 0 + 2 - 1] - A_{\Pi} \end{pmatrix}.$$

 E_{Π} , B_{Π} , and A_{Π} are respectively the energy, rotational constant, and spin-orbit constant for the ${}^{3}\Pi$ multiplet state.

It is not sufficient to correct this $\mathbf{H}^{\mathrm{eff}}$ for the effects of remote perturbing states merely along the diagonal, as in the standard recipe of second-order non-degenerate perturbation theory. It is also not sufficient to replace B_{Π} wherever it occurs, both on- and off-diagonal, by $[B_{\Pi} - D_{\Pi}J(J+1)]$. The Van Vleck transformation provides a simple procedure for correcting the $\mathbf{H}^{\mathrm{eff}}$ to include all remote perturbers. One particularly beautiful thing about the Van Vleck Transformation is that *each* added correction term is implicitly a sum over *all* remote perturber electronic-vibration levels of a specified symmetry. This gives a generally applicable fit model without excessive flexibility (exactly the *minimum* number of adjustable fit parameters). However, it does this at the cost of compromising the microscopic (mechanical, Born–Oppenheimer) meaning of all of the fit parameters [12].

Computational theorists often do not understand the contaminated meaning of molecular parameters obtained from an \mathbf{H}^{eff} fit.

4.4.2 The Van Vleck Transformation [3]

The Van Vleck transformation specifies correction terms according to their location in the \mathbf{H}^{eff} matrix. I find a simple "railroad diagram" helpful and instructive. The four steps for constructing this railroad diagram follow.

4.4.2.1 List of Initial and Final States

Specify the initial and final state locations in the matrix elements of \mathbf{H}^{eff} , for example

initial state final state

$${}^{3}\Pi_{2}, \pm, v {}^{3}\Pi_{2}, \pm, v {}^{3}\Pi_{1}, \pm, v {}^{3}\Pi_{1}, \pm, v {}^{3}\Pi_{2}, \pm, v {}^{3}\Pi_{0}, \pm, v {}^{3}\Pi_{1}, \pm, v {}^{3}\Pi_{1}, \pm, v {}^{3}\Pi_{1}, \pm, v {}^{3}\Pi_{0}, \pm, v {}^{3}\Pi_{0$$

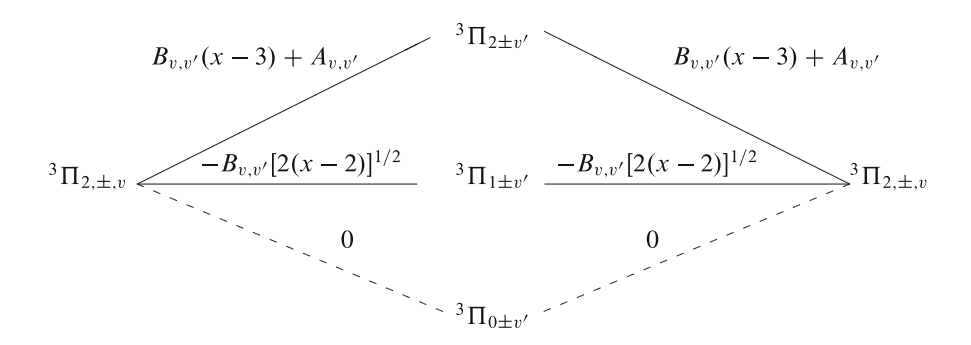
The \pm symbols represent the rigorously good parity quantum number. Usually $\mathbf{H}^{\mathrm{eff}}$ is real and symmetric, so it is not necessary to evaluate both

$$\begin{array}{ll} \text{initial} & \text{final} \\ {}^3\Pi_2 \pm & {}^3\Pi_1 \pm \\ & \textit{and} \\ \\ {}^3\Pi_1 \pm & {}^3\Pi_2 \pm . \end{array}$$

4.4.2.2 List of Relevant Intermediate States

4.4.2.3 Railroad Diagrams [1]

Draw connecting lines between the initial and intermediate states and between the intermediate and final states. Write, above each of the connecting lines, the value of the non-zero matrix element (from \mathbf{H}^{ROT} and \mathbf{H}^{SO}) between each connected pair of states $[x \equiv J(J+1)]$:



For example,

$$\langle {}^{3}\Pi_{2,\pm,v}|\mathbf{H}^{\text{ROT}}|{}^{3}\Pi_{2,\pm,v'}\rangle = B_{v,v'}[J(J+1) - \Omega^{2} + S(S+1) - \Sigma^{2}]$$

= $B_{v,v'}[J(J+1) - 4 + 2 - 1] = B_{v,v'}[x - 3]$

and

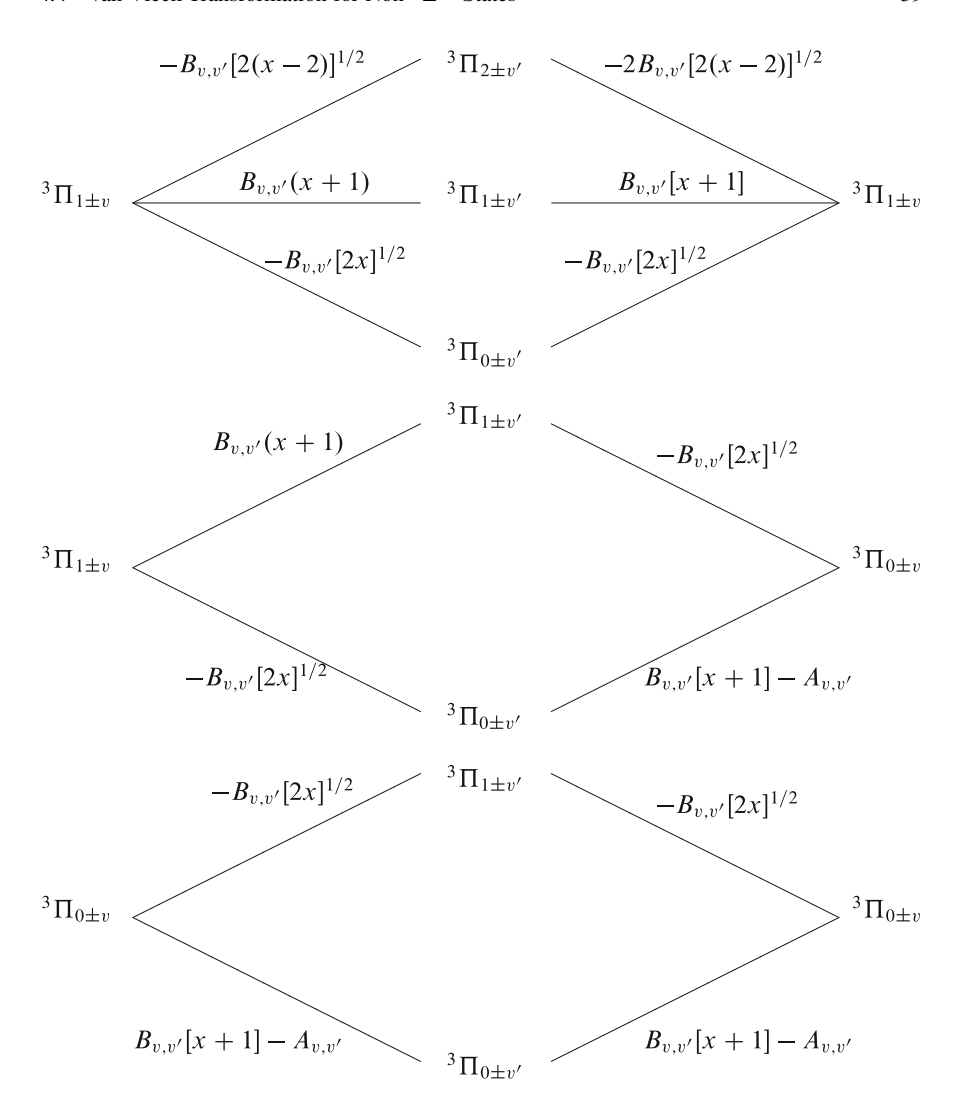
$$\langle {}^{3}\Pi_{2,\pm,v} | \mathbf{H}^{\mathrm{SO}} | {}^{3}\Pi_{2,\pm,v'} \rangle = A_{v,v'} \Lambda \Sigma = A_{v,v'}(1)(1) = A_{v,v'}.$$

$$-B_{v,v'}(x-3) + A_{v,v'} \qquad {}^{3}\Pi_{2\pm v'} \qquad -B_{v,v'}[2(x-2)]^{1/2}$$

$$-B_{v,v'}[2(x-2)]^{1/2} {}^{3}\Pi_{1\pm v'} \qquad B_{v,v'}[x+1] \qquad {}^{3}\Pi_{1\pm v}$$

$$-B_{v,v'}[2x]^{1/2} \qquad {}^{3}\Pi_{1\pm v} \qquad -B_{v,v'}[2x]^{1/2} \qquad {}^{3}\Pi_{0\pm v}$$

$${}^{3}\Pi_{2\pm v} \qquad -B_{v,v'}[2(x-2)]^{1/2} \qquad {}^{3}\Pi_{1\pm v'} \qquad -B_{v,v'}[2x]^{1/2} \qquad {}^{3}\Pi_{0\pm v}$$



4.4.2.4 Harvest the Information in Each Railroad Diagram

The next step is to multiply the pairs of matrix elements, insert the appropriate energy denominator, and evaluate the summation as specified by the Van Vleck

equation in Sect. 4.2.3:

$$H_{^3\Pi_2,^3\Pi_2} = \sum_{v'} \left[\frac{B_{v,v'}^2[(x-3)^2 + 2(x-2)] + A_{v,v'}^2 + 2B_{v,v'}A_{v,v'}(x-3)}{hc\omega(v-v')} \right]$$

$$= \sum_{v'} \frac{B_{v,v'}^2(x^2 - 4x + 5) + A_{v,v'}^2 + B_{v,v'}A_{v,v'}2(x-3)}{hc\omega(v-v')}.$$
Note that $D \equiv -\sum_{v' \neq v} \frac{B_{v,v'}^2}{hc\omega(v-v')}$ (this is the actual microscopic definition of the centrifugal distortion constant)
$$A_0 \equiv \sum_{v' \neq v} \frac{A_{v,v'}^2}{hc\omega(v-v')}.$$

4.4.3 Example of Centrifugal Distortion in a ${}^{3}\Pi$ State[9]

Here are all of the centrifugal distortion contributions to the effective Hamiltonian for a ${}^3\Pi$ state:

$$\left\langle {}^{3}\Pi_{0,\pm,v}|\tilde{\mathbf{H}}|^{3}\Pi_{0,\pm,v}\right\rangle = -D_{v}[x^{2} + 4x + 1]$$

$$\left\langle {}^{3}\Pi_{1,\pm,v}|\tilde{\mathbf{H}}|^{3}\Pi_{1,\pm,v}\right\rangle = -D_{v}[x^{2} + 6x - 3]$$

$$\left\langle {}^{3}\Pi_{2,\pm,v}|\tilde{\mathbf{H}}|^{3}\Pi_{2,\pm,v}\right\rangle = -D_{v}[x^{2} - 4x + 5]$$

$$\left\langle {}^{3}\Pi_{0,\pm,v}|\tilde{\mathbf{H}}|^{3}\Pi_{1,\pm,v}\right\rangle = +D_{v}[2(x + 1)(2x)^{1/2}]$$

$$\left\langle {}^{3}\Pi_{0,\pm,v}|\tilde{\mathbf{H}}|^{3}\Pi_{2,\pm,v}\right\rangle = -D_{v}[4x(x - 2)]^{1/2}$$

$$\left\langle {}^{3}\Pi_{1,\pm,v}|\tilde{\mathbf{H}}|^{3}\Pi_{2,\pm,v}\right\rangle = +D_{v}[2(x - 1)(2x - 4)^{1/2}]$$

$$x = J(J + 1).$$

The tilde over ${\bf H}$ is an indication that the ${\bf H}^{\rm eff}$ has been subjected to the Van Vleck transformation.

Note that the centrifugal distortion contributions that correspond to $\Delta\Omega = \text{even}$ are negative and those for $\Delta\Omega = \text{odd}$ are positive. $\Delta\Omega = 0$ terms are of order J^4 , $\Delta\Omega = 1$ terms are of order J^3 , and $\Delta\Omega = 2$ terms are of order J^2 . Even

though B_v does not appear in the $\Delta\Omega=2$ matrix element, D_v does appear in the $\Delta\Omega=2$ location. A lot of surprises! Failure to use exactly this form of the centrifugal distortion matrix would give a poor fit and would result in a requirement for many additional (spurious) fit parameters.

4.4.4 Λ -Doubling [13]

 Λ -doubling is the J-dependent splitting between + and - parity components of same-J, same- Ω levels of a $\Lambda \neq 0$ state.

4.4.4.1 Elimination of Nonsense

It is very tempting (and many have succumbed) to think of the Λ -doubling in a $^1\Pi$ state as a contribution of the electron to the moment of inertia. If the π -orbital lies along the \vec{J} axis, then the electron makes a negligible contribution to the B-value, precisely because it lies close to the rotation axis. If the π -orbital lies in the plane perpendicular to the \vec{J} axis, then the electron in this π -orbital makes the maximum possible contribution to the B-value. This makes lovely sense of the Λ -doubling in $^1\Pi$ states:

$$E(J, \pm) = E_{\Pi} + (B_{\Pi} \pm q_{\Pi})J(J+1).$$

But this is nonsense! Λ -doubling has absolutely nothing to do with electron inertial effects. Sometimes the Λ -doublet component that is even with respect to reflection in a plane $\perp \vec{J}$ lies at higher energy and sometimes it lies at lower energy than the component that is odd with respect to a plane $\perp \vec{J}$. Almost all Λ -doubling terms in the \mathbf{H}^{eff} arise from interaction with Σ -states! No, this is not "electron slippage."

4.4.4.2 Relationship Between Parity and e/f-Symmetry [14, 15]

Parity and e/f-symmetry are two ways of dealing with the *same* rigorous symmetry. Both (\pm) and $\binom{e}{f}$ symmetry labels are used because each provides insight. The rotational levels of a $^1\Sigma^+$ state have parity $(-1)^J$ but all J levels belong to e-symmetry. The Λ -doubling in a $^1\Pi$ state follows a J-alternating pattern, + above - for one value of J and - above + for J+1. The e/f-symmetry factors out the $(-1)^J$ rotational alternation of \pm -parity. As a result, the energy order of e/f components remains constant over a range of J-values. e/f symmetry also provides a simplified picture for rotational branches. Since the selection rule for all electric dipole allowed transitions is $+\leftrightarrow -$, all $\Delta J=\pm 1$ (R and P branch) transitions are $e\leftrightarrow e$ or $f\leftrightarrow f$, whereas all $\Delta J=0$ (Q branch) transitions are $e\leftrightarrow e$

or $f \leftrightarrow e$. Here are some simple examples: (a) a $^1\sum^+ -^1\sum^+$ transition consists exclusively of R and P branches because there are no f-symmetry rotational levels in a $^1\sum^+$ state; (b) a $^1\sum^- -^1\sum^+$ transition [which is electric dipole forbidden and only becomes allowed via an L-uncoupling $(-BL_\pm J_\mp)$ interaction of a $^1\sum$ state with a $^1\Pi$ state] consists exclusively of Q branches, because the $^1\sum^+$ state consists exclusively of e-symmetry levels and the $^1\Sigma^-$ state consists exclusively of f-symmetry levels; (c) each e-symmetry upper level in a $^1\Pi - ^1\Sigma^+$ transition can be sampled via R(J-1) and P(J+1) transitions whereas each f-symmetry level can only be sampled via one Q(J) transition, which often leads to difficulties in assignment (without lower state combination differences) of Q branch transitions; (d) all spectroscopic perturbations are between same-J, same-parity, same-e/f symmetry levels.

4.4.4.3 The Central Role of Σ -States

The reason that Σ -states are the sole source of Λ -doubling is easy to understand for odd-multiplicity molecules (odd-multiplicity = even number of electrons). *Odd-multiplicity* Σ -states have only one Ω -component with $\Omega=0$. All J-levels of this component have e-symmetry for ${}^1\Sigma^+$, ${}^3\Sigma^-$, and ${}^5\Sigma^+$ states and f-symmetry for ${}^1\Sigma^-$, ${}^3\Sigma^+$, and ${}^5\Sigma^-$ states [14, 15]. As a result, only one e/f component of a non-sigma state uniquely interacts with the only $\Omega=0$ e/f-symmetry component of the sigma state, resulting in an energy difference between the e- and f-symmetry $\Omega=0$ components of the non- Σ state. The situation is more complicated for even-multiplicity systems. In that case, the Σ -state ($\Lambda=0$) acts to connect $\Omega>0$ and $\Omega<0$ components of Σ and Π states. For example, the matrix elements between a ${}^2\Pi_{1/2}$ and a ${}^2\Sigma^+$ state have the unique $\Omega=0$ -crossing property (i.e. there are matrix elements between $\Omega=+1/2$ and $\Omega=-1/2$ basis states)

$$\begin{vmatrix} 2\Pi_{1/2} \frac{e}{f} \end{pmatrix} = 2^{-1/2} \left[|^{2}\Pi_{+1/2}\rangle \pm |^{2}\Pi_{-1/2}\rangle \right]$$

$$\begin{vmatrix} 2\Sigma^{+} \frac{e}{f} \end{pmatrix} = 2^{-1/2} \left[|^{2}\Sigma^{+}_{+1/2}\rangle \pm |^{2}\Sigma^{+}_{-1/2}\rangle \right]$$

$$\mathbf{H} = \frac{1}{2} \sum_{i} \mathbf{a}_{i} \left[\ell_{i}^{+} s_{i}^{-} + \ell_{i}^{-} s_{i}^{+} \right] - B \left[\mathbf{J}^{+} \mathbf{L}^{-} + \mathbf{J}^{-} \mathbf{L}^{+} \right]$$

$$\langle ^{2}\Pi_{1/2} \frac{e}{f} |\mathbf{H}|^{2} \Sigma^{+} \frac{e}{f} \rangle = \frac{1}{2} \left[\langle ^{2}\Pi_{+1/2} |\mathbf{H}|^{2} \Sigma^{+}_{+1/2}\rangle + \langle ^{2}\Pi_{-1/2} |\mathbf{H}|^{2} \Sigma^{+}_{-1/2}\rangle \right]$$

$$\pm \langle ^{2}\Pi_{+1/2} |\mathbf{H}|^{2} \Sigma^{+}_{-1/2}\rangle \pm \langle ^{2}\Pi_{-1/2} |\mathbf{H}|^{2} \Sigma^{+}_{+1/2}\rangle \right]$$

$$= \frac{1}{2} [\alpha + \alpha \mp \beta x^{1/2} \mp \beta x^{1/2}] = \alpha \mp \beta x^{1/2}$$

(note that the $\Omega=1/2,-1/2$ and $\Omega=-1/2,1/2$ matrix elements have opposite signs) where

$$\alpha = \langle +\pi\beta | a\ell^{+} \mathbf{s}^{-} | \sigma\alpha \rangle = \langle \pi | a\ell^{+} | \sigma \rangle$$
$$\beta = \langle v_{\Pi} | B(R) | v_{\Sigma} \rangle \langle \pi | \mathbf{L}^{+} | \sigma \rangle.$$

This unique Ω =0-crossing property is possessed exclusively by $|\Omega| = 1/2$ even-multiplicity Π states in interaction with even-multiplicity Σ -states.

4.4.4.4 General Λ-Doubling Hamiltonian, H^{LD} [16]

A definitive treatment of Λ -doubling in Π states is given by Brown and Merer [16]. For ${}^{2S+1}\Pi$ -states in the e/f basis set

$$\begin{vmatrix} 2S+1 & \Pi, J, \Omega & e \\ f & d \end{vmatrix} = 2^{-1/2} \left[|\Lambda = 1, S, \Sigma, J, \Omega\rangle \pm |\Lambda = -1, S, -\Sigma, J, -\Omega\rangle \right]$$

The (parity-dependent) Lambda-Doubling part of $\mathbf{H}^{\mathrm{eff}}$ is

$$\begin{split} \left< \Lambda &= \mp 1, \Sigma \pm 2, J, \Omega | \mathbf{H}^{\text{LD}} | \Lambda = \pm 1, \Sigma, J, \Omega \right> = \frac{1}{2} (o + p + q) x \\ & [\{ S(S+1) - \Sigma(\Sigma \pm 1) \} \{ S(S+1) - (\Sigma \pm 1)(\Sigma \pm 2) \}]^{1/2} \\ \left< \Lambda &= \mp 1, \Sigma \pm 1, J, \Omega \mp 1 | \mathbf{H}^{\text{LD}} | \Lambda = \pm 1, \Sigma, J, \Omega \right> - \frac{1}{2} (p + 2q) x \\ & [\{ S(S+1) - \Sigma(\Sigma \pm 1) \} \{ J(J+1) - \Omega(\Omega \mp 1) \}]^{1/2} \\ \left< \Lambda &= \mp 1, \Sigma, J, \Omega \mp 2 | \mathbf{H}^{\text{LD}} | \Lambda = \pm 1, \Sigma, J, \Omega \right> = \frac{1}{2} q x \\ & [\{ J(J+1) - \Omega(\Omega \mp 1) \} \{ J(J+1) - (\Omega \mp 1)(\Omega \mp 2) \}]^{1/2}, \end{split}$$

where x = J(J + 1).

The Λ -doubling is described by the o, p, q parameters, which respectively arise from $[\mathbf{H}^{\mathrm{SO}} + B(\mathbf{L}^+\mathbf{S}^- + \mathbf{L}^-\mathbf{S}^+)]^2$, $[\mathbf{H}^{\mathrm{SO}} + B(\mathbf{L}^+\mathbf{S}^- + \mathbf{L}^-\mathbf{S}^+)] \otimes [-B(\mathbf{J}^+\mathbf{L}^- + \mathbf{J}^-\mathbf{L}^+)]$ and $[-B(\mathbf{J}^+\mathbf{L}^- + \mathbf{J}^-\mathbf{L}^+)]^2$ matrix element product terms in $E^{(2)}$. Brown and Merer derive and discuss \mathbf{H}^{LD} matrices for ${}^2\Pi, {}^3\Pi, {}^4\Pi$, and ${}^5\Pi$ states.

4.4.4.5 Worked Examples

$\left({}^{3}\Pi_{1f}^{e} |\mathbf{H}|^{3}\Pi_{1f}^{e} \right)$, a Diagonal Contribution

Insert the definitions of e/f basis states:

$$\begin{vmatrix} 2S+1 & \Pi, J, \Omega \frac{e}{f} \end{vmatrix} = 2^{-1/2} \left[|\Lambda = +1, S = 1, \Sigma = 0, J, \Omega = +1 \right)$$

$$\pm |-1, 1, 0, J, -1\rangle \right]$$

$$\left\langle {}^{3}\Pi_{1} \frac{e}{f} | \mathbf{H}^{\mathrm{LD}} | {}^{3}\Pi_{1} \frac{e}{f} \right\rangle = \frac{1}{2} \left[\left\langle +1, 1, 0, J, +1 \left| \mathbf{H}^{\mathrm{LD}} \right| +1, 1, 0, J, +1 \right\rangle$$

$$+ \left\langle -1, 1, 0, J, -1 \left| \mathbf{H}^{\mathrm{LD}} \right| -1, 1, 0, J, -1 \right\rangle$$

$$\pm 2 \left\langle +1, 1, 0, J, +1 \left| \mathbf{H}^{\mathrm{LD}} \right| -1, 1, 0, J, -1 \right\rangle \right]$$

$$= \frac{1}{2} \left[0 + 0 \pm 2 \left\langle \mp 1, 1, 0, J, \mp 1 \middle| \mathbf{H}^{\mathrm{LD}} \middle| \pm 1, 1, 0, J, \pm 1 \right\rangle \right]$$

$$= \pm \frac{1}{2} q \left[\left\{ J(J+1) - 0 \right\}^{1/2} \left\{ J(J+1) - 0 \right\}^{1/2} \right]$$

$$= \pm \frac{1}{2} q J(J+1)$$

$\left\langle {}^{3}\Pi_{1}{}^{e}_{f}|\mathbf{H}|^{3}\Pi_{0}{}^{e}_{f}\right\rangle$, an Off-Diagonal Contribution

This term contributes to the Λ -doubling in ${}^3\Pi_1$ with the same J-dependence as the direct diagonal $\left\langle {}^3\Pi_1 {}^e_f | \mathbf{H}^{\mathrm{LD}} | {}^3\Pi_1 {}^e_f \right\rangle$ term.

$$\left\langle {}^{3}\Pi_{1} \frac{e}{f} | \mathbf{H}^{\mathrm{LD}} | {}^{3}\Pi_{0} \frac{e}{f} \right\rangle = \frac{1}{2} \left[\left\langle +1, 1, 0, J, +1 | \mathbf{H}^{\mathrm{LD}} | +1, 1, -1, J, 0 \right\rangle$$

$$+ \left\langle -1, 1, 0, J, -1 | \mathbf{H}^{\mathrm{LD}} | -1, 1, 1, J, 0 \right\rangle$$

$$\pm \left\langle +1, 1, 0, J, +1 | \mathbf{H}^{\mathrm{LD}} | -1, 1, 1, J, 0 \right\rangle$$

$$\pm \left\langle -1, 1, 0, J, -1 | \mathbf{H}^{\mathrm{LD}} | +1, 1, -1, J, 0 \right\rangle \right]$$

$$= \frac{1}{2} \left[0 + 0 \pm 2 \left\langle +1, 1, 0, J, +1 | \mathbf{H}^{\mathrm{LD}} | -1, 1, 1, J, 0 \right\rangle \right]$$

$$= \mp \frac{1}{2} (p + 2q) \left[\left\{ 2 - 0 \right\} \left\{ J(J+1) - 0 \right\} \right]^{1/2}$$

$$= \mp 2^{-1/2} (p + 2q) \left[J(J+1) \right]^{1/2}$$

For a
$${}^{3}\Pi$$
 state, $E^{(0)}\left({}^{3}\Pi_{1}\right) - E^{(0)}\left({}^{3}\Pi_{0}\right) = A,$
$$\left({}^{3}\Pi_{1}, J|\mathbf{H}|^{3}\Pi_{0}, J\right) = -B[2J(J+1)]^{1/2}.$$

thus the contribution to Λ -doubling in ${}^3\Pi_1$ via the $\left\langle {}^3\Pi_1, {}^e_f | \mathbf{H}^{LD} | {}^3\Pi_0, {}^e_f \right\rangle$ term is

$$E(^{3}\Pi_{1e}) - E(^{3}\Pi_{1f}) = \frac{\left[-B + \frac{1}{2}(p+2q)\right]^{2}(2x)}{A} - \frac{\left[-B - \frac{1}{2}(p+2q)\right]^{2}(2x)}{A}$$
$$= \frac{-2B(p+2q)(2x)}{A}$$
$$x = J(J+1)$$

Λ-Doubling in a ${}^{1}\Pi$ State Due to an Energetically Remote ${}^{3}\Sigma^{+}$ State

This situation is not discussed in the Brown and Merer paper [16] because it arises from a higher than second-order interaction path

$$^{1}\Pi \xrightarrow{\mathbf{H}^{SO}} {^{3}\Sigma_{1}^{+}} \xrightarrow{\mathbf{H}^{ROT}} {^{3}\Sigma_{0^{-}}^{+}} \xrightarrow{\mathbf{H}^{ROT}} {^{3}\Sigma_{1}^{+}} \xrightarrow{\mathbf{H}^{SO}} {^{1}\Pi}.$$

However, the two $\mathbf{H}^{\mathrm{ROT}}$ steps in the interaction path cause the ${}^{3}\Sigma^{+}$ state to reach case (b) limiting behavior, where N is the rotational pattern-forming quantum number. The rotational energy levels go as BN(N+1), even though J (and not N) is a rigorously good quantum number. To an excellent approximation, the e-symmetry levels are pure ${}^{3}\Sigma^{+}_{1}$ states, which have energies BJ(J+1) where N=J (the F_{2} spin-component) and the two f-symmetry components for each value of J are 50:50 mixtures of ${}^{3}\Sigma^{+}_{1}$ and ${}^{3}\Sigma^{+}_{0}$ characters (the F_{1} and F_{3} spin-components have, respectively, N=J+1 and N=J-1 characters)

$$\begin{vmatrix} {}^{3}\Sigma^{+}, J, \frac{F_{1}}{F_{3}}, f \end{vmatrix} = \frac{1}{2} \left[\begin{vmatrix} {}^{3}\Sigma_{1}^{+} \end{pmatrix} + \begin{vmatrix} {}^{3}\Sigma_{-1}^{+} \end{pmatrix} \right] \pm 2^{-1/2} \begin{vmatrix} {}^{3}\Sigma_{0-}^{+} \end{pmatrix}$$

with

$$E_{\Sigma}^{(0)}(J, f, F_1) = E_{\Sigma}^{(0)} + B_{\Sigma}[J(J+1) - 2J]$$

$$E_{\Sigma}^{(0)}(J, f, F_3) = E_{\Sigma}^{(0)} + B_{\Sigma}[J(J+1) + 2(J+1)]$$

$$E_{\Sigma}^{(0)}(J, e, F_2) = E_{\Sigma}^{(0)} + B_{\Sigma}J(J+1)$$

and

$$E_{\Pi}^{(0)}\left(J, \frac{e}{f}\right) = E_{\Pi}^{(0)} + B_{\Pi}J(J+1)$$
$$\Delta_{\Pi\Sigma} \equiv E_{\Pi}^{(0)} - E_{\Sigma}^{(0)}.$$

If one treats the spin–orbit ($\Delta\Omega=0$) interaction between the ${}^1\Pi$ and ${}^3\Sigma^+$ states by second-order non-degenerate perturbation theory, the level shift of the ${}^1\Pi$ f-symmetry component caused by the ${}^3\Sigma^+$ state is larger than that for the e-symmetry component (Fig. 4.2).

$$E_{\Pi}^{\text{LD}} = E_{\Pi e} - E_{\Pi f} = \frac{\left(\mathbf{H}^{\text{SO}}\right)^{2}}{\Delta_{\Pi \Sigma}} - \frac{\frac{1}{2}\left(\mathbf{H}^{\text{SO}}\right)^{2}}{\Delta_{\Pi \Sigma} - 2B_{\Sigma}(J+1)} - \frac{\frac{1}{2}\left(\mathbf{H}^{\text{SO}}\right)^{2}}{\Delta_{\Pi \Sigma} + 2B_{\Sigma}(J)}$$

$$= \frac{1}{2}\left(\mathbf{H}^{\text{SO}}\right)^{2} \left\{ \left[\frac{1}{\Delta_{\Pi \Sigma}} - \frac{1}{\Delta_{\Pi \Sigma} - 2B_{\Sigma}(J+1)} \right] + \left[\frac{1}{\Delta_{\Pi \Sigma}} - \frac{1}{\Delta_{\Pi \Sigma} + 2B_{\Sigma}(J)} \right] \right\}$$

$$I_{\Pi}$$

$$J_{e}$$

$$J_{f}$$

Fig. 4.2 Λ-doubling in a $^1\Pi$ state caused by a lower-lying $^3\Sigma^+$ state. The energy separation between the $^1\Pi$ and $^3\Sigma^+$ states is $\Delta_{\Pi\Sigma}(J)$

 $Jf(F_1) B_{\Sigma}(J-1)J$

4.5 Summary 67

$$\begin{split} &=\frac{1}{2}\left(\mathbf{H}^{\mathrm{SO}}\right)^{2}\left\{\frac{\Delta_{\Pi\Sigma}-(2B_{\Sigma}(J+1)-\Delta_{\Pi\Sigma})}{\Delta_{\Pi\Sigma}[\Delta_{\Pi\Sigma}-2B_{\Sigma}(J+1)]}+\frac{\Delta_{\Pi\Sigma}+2B_{\Sigma}J-\Delta_{\Pi\Sigma}}{\Delta_{\Pi\Sigma}[\Delta_{\Pi\Sigma}-2B_{\Sigma}(J)]}\right\}\\ &=\frac{B_{\Sigma}\left(\mathbf{H}^{\mathrm{SO}}\right)^{2}}{\Delta_{\Pi\Sigma}}\left\{\frac{-(J+1)}{\Delta_{\Pi\Sigma}-2B(J+1)}+\frac{J}{\Delta_{\Pi\Sigma}+2B(J)}\right\}\\ &=\frac{B_{\Sigma}\left(\mathbf{H}^{\mathrm{SO}}\right)^{2}}{\Delta_{\Pi\Sigma}}\left\{\frac{-4B_{\Sigma}J(J+1)-\Delta_{\Pi\Sigma}}{\Delta_{\Pi\Sigma}^{2}-4B_{\Sigma}^{2}J(J+1)-2B_{\Sigma}\Delta_{\Pi\Sigma}}\right\}\\ &\approx\frac{B_{\Sigma}\left(\mathbf{H}^{\mathrm{SO}}\right)^{2}}{\Delta_{\Pi\Sigma}^{3}}\left[4B_{\Sigma}J(J+1)+\Delta_{\Pi\Sigma}\right] \end{split}$$

4.5 Summary

The infinite dimension exact \mathbf{H} is reduced to a finite dimension $\mathbf{H}^{\mathrm{eff}}$ fit model. The $\mathbf{H}^{\mathrm{eff}}$ is a parametrically parsimonious replacement for the exact \mathbf{H} [1]. It is designed to reproduce all spectroscopic measurements to experimental accuracy. It is usually capable of extrapolation to energy levels and molecular properties that are not directly experimentally sampled in the data set that is actually fitted. One caution is that the parameters in the experimentally determined $\mathbf{H}^{\mathrm{eff}}$ are not necessarily physically or numerically equivalent to the parameters *of the same name* that are determined by a high-level ab initio computation.

Three main topics are discussed:

- (a) The internuclear distance dependences of molecular properties are indirectly determined from the v, J dependence of energy levels in combination with a power series expansion of R-dependent operators, where $R = \mathbf{Q} + R_e$ [2]. \mathbf{Q} is the displacement from equilibrium and is the natural variable of harmonic oscillator basis functions. All matrix elements and vibrational selection rules of integer powers of \mathbf{Q} are trivially obtained by replacing \mathbf{Q} by the creation-annihilation operators, \mathbf{a} and \mathbf{a}^{\dagger} [10].
- (b) Interactions of the states of interest with energetically remote states are dealt with by non-degenerate perturbation theory [5, 6], second-order for the energies $[E_{vJ} = E_{vJ}^{(0)} + E_{vJ}^{(1)} + E_{vJ}^{(2)}]$ and first-order for the wavefunctions

$$\left[|vJ\rangle = |vJ\rangle^{(0)} + \sum_{e_n, v_{e_n}, J} a_{e_n, v_{e_n}, J} |e_n, v_{e_n}, J\rangle^{(0)} \right].$$

This procedure cannot work when the states of interest are quasi-degenerate and the effects of energetically remote states must involve corrections to the off-diagonal matrix elements among the quasi-degenerate states of interest.

(c) The Van Vleck Transformation [3] provides the needed corrections to the \mathbf{H}^{eff} .

Examples treated include effects that arise from the R-dependence of the "rotational constant" operator, B(R). These include centrifugal distortion, D_e , and the value of the vibration-rotation interaction parameter, α_e [2]. A key point is that matrix elements between the v and v' basis states that correspond to the same value of Δv must be summed first and then squared. The interference between the $\Delta v = \pm 1$ matrix elements of the \mathbf{Q}^1 term in the expansion of B(R) and the $b\mathbf{Q}^3$ anharmonic term give a value of α_e with the correct (empirically observed) sign. Λ -doubling arises from spin-orbit and $-B\mathbf{J}^{\pm}\mathbf{L}^{\mp} + B\mathbf{L}^{\pm}\mathbf{S}^{\mp}$ interactions between $|\Lambda| > 0$ states and Σ -states [13, 16]. The o, p, q Λ -doubling parameters are defined and briefly discussed. The information in this lecture sets the stage for treatment of centrifugal distortion and rotation-vibration interactions in polyatomic molecules, where the A, B, C rotational constant operators are expressed as a power-series expansion of displacements from equilibrium for all 3N-6 vibrational normal modes (N is the number of atoms).

References

- R.W. Field, J. Baraban, S.H. Lipoff, A.R. Beck, Effective Hamiltonians, in *Handbook of High-Resolution Spectroscopies*, ed. by M. Quack, F. Merkt (Wiley, New York, 2010)
- H. Lefebvre-Brion, R.W. Field, The Spectra and Dynamics of Diatomic Molecules, Sect. 4.2 (Elsevier, Amsterdam, 2004)
- 3. H. Lefebvre-Brion, R.W. Field, *The Spectra and Dynamics of Diatomic Molecules*, Sect. 5.6 (Elsevier, Amsterdam, 2004)
- 4. H. Lefebvre-Brion, R.W. Field, *The Spectra and Dynamics of Diatomic Molecules*, Sect. 6.3 (Elsevier, Amsterdam, 2004)
- C. Cohen-Tannoudji, B. Diu, F. Laloë, Quantum Mechanics, Chap. 11 (Wiley, New York, 1977), pp. 1095–1108
- P.F. Bernath, Spectra of Atoms and Molecules, 2nd edn. (Oxford University Press, Oxford, 2005), pp. 94–96
- 7. H. Lefebvre-Brion, R.W. Field, *The Spectra and Dynamics of Diatomic Molecules*, Sect. 3.1 (Elsevier, Amsterdam, 2004)
- 8. P.F. Bernath, *Spectra of Atoms and Molecules*, 2nd edn. (Oxford University Press, Oxford, 2005), pp. 97–99
- H. Lefebvre-Brion, R.W. Field, The Spectra and Dynamics of Diatomic Molecules (Elsevier, Amsterdam, 2004), pp. 241–243
- H. Lefebvre-Brion, R.W. Field, The Spectra and Dynamics of Diatomic Molecules (Elsevier, Amsterdam, 2004), pp. 690–691
- H. Lefebvre-Brion, R.W. Field, The Spectra and Dynamics of Diatomic Molecules (Elsevier, Amsterdam, 2004), pp. 65–66
- R.N. Zare, A.L. Schmeltekopf, W.J. Harrop, D.L. Albritton, J. Mol. Spectrosc. 46, 37–66 (1973)
- 13. H. Lefebvre-Brion, R.W. Field, *The Spectra and Dynamics of Diatomic Molecules*, Sect. 5.5 (Elsevier, Amsterdam, 2004)
- 14. H. Lefebvre-Brion, R.W. Field, *The Spectra and Dynamics of Diatomic Molecules*, Sect. 3.2.2 (Elsevier, Amsterdam, 2004)
- J.M. Brown, J.T Hougen, K.P., Huber, J.W.C. Johns, I. Kopp, H. Lefebvre-Brion, A.J. Merer, D.A. Ramsay, J. Rostas, R.N. Zare, J. Mol. Spectrosc. 55, 500 (1975)
- 16. J.M. Brown, A.J. Merer, J. Mol. Spectrosc. **74**, 488 (1979)

Chapter 5 Rotation of Polyatomic Molecules

The effective Hamiltonian, rotational energies, transition selection rules, and notation for the rotational energy levels of an asymmetric top are derived and discussed [1, 2]. The effective Hamiltonian is factored into four sub-blocks by the Wang transformation. Depending on whether the transition moment lies along the body-fixed a, b, or c axis, one obtains easily-remembered transition selection rules. A diatomic molecule has one rotational constant, B, whereas a nonlinear polyatomic molecule has three rotational constants, A, B, and C, each of which is proportional to the reciprocal of one of the three principal axis moments of inertia, I_A, I_B, and I_C. Derivatives of each of these reciprocal moments of inertia with respect to each of the 3N-6 normal mode displacements, give vibration-rotation interaction and centrifugal distortion constants analogously to their perturbation theoretic derivation for a diatomic molecule.

5.1 Introduction

Rotation is the common feature of all gas phase molecular spectra:

Pure *Rotation*: Microwave*Rotation*-Vibration: Infrared

• Rotation-Vibration-Electronic: Visible and UV

We need to know how to go from spectrum to quantum number assignment to parameters in a fit model to symmetry information about properties of the molecule beyond rotation (for example, what is the body frame orientation of the permanent electric dipole moment? What are the vibrational or vibration-electronic symmetry species of the initial and final states?).

The notation used to label rotational energy levels, J_{K_a,K_c} , and transitions between rotational levels, e.g. ${}^pQ(6_{25})_b$ means J''=6, $K_a''=2$, $K_c''=5$, J'=6, $K_a'=1$, and $K_c'=6$ (*b*-type transition, transition moment along the body frame *b*-axis).

The information covered in this lecture is treated more rigorously and completely in Chap. 6 of *Spectra of Atoms and Molecules* by Peter F. Bernath, Oxford, 1995. Videos of my lectures #22–#24 appear on MIT's Open CourseWare (OCW) web site:

http://ocw.mit.edu/courses/chemistry/5-80-small-molecule-spectroscopy-and-dynamics-fall-2008/

It all begins with the Hamiltonian

$$H = T + V$$

for a *free rotor*, the potential energy $V(\phi, \theta) = 0$

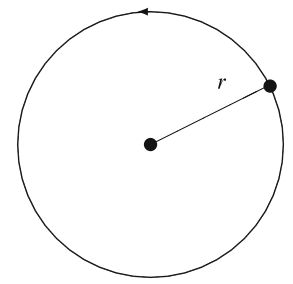
kinetic energy: $\mathbf{T} = \frac{1}{2}mv^2$

For rotation of a mass point in a plane (Fig. 5.1)

$$v = \omega r$$
 $p \equiv mv = mr\omega$ linear momentum
 $\ell \equiv I\omega$ angular momentum, I is moment of inertia (μr^2)
 $T = \frac{1}{2}mv^2 = \frac{p^2}{2m} = \frac{\ell^2}{2I}$ what is the algebraic form of I ?
$$\frac{(mr\omega)^2}{2m} = \frac{(I\omega)^2}{2I}$$

$$\frac{mr^2\omega^2}{2} = \frac{I\omega^2}{2}$$
 $I = mr^2$.

Fig. 5.1 Rotation of a mass point in a plane at constant distance, r, from the coordinate origin



5.1 Introduction 71

Now we need to generalize this to a rigid body consisting of point masses, m_{α} , located at \vec{r}_{α} in a coordinate system with origin at the center of mass. **This is not trivial!** We need to generalize I to matrix form:

$$\begin{pmatrix} \ell_x \\ \ell_y \\ \ell_z \end{pmatrix} = \begin{pmatrix} I_{xx} & I_{xy} & I_{xz} \\ I_{yy} & & \\ & I_{zz} \end{pmatrix} \begin{pmatrix} \omega_x \\ \omega_y \\ \omega_z \end{pmatrix}$$

diagonal elements of I: $I_{xx} = \sum_{\alpha} m_{\alpha} (y_{\alpha} + z_{\alpha})^2$ "moments of inertia"

off-diagonal elements of I: $I_{xy} \equiv -\sum_{\alpha} m_{\alpha} x_{\alpha} y_{\alpha}$ "products of inertia"

(all of this is derived in Bernath's book) [1]

$$\mathbf{T}^{\text{rot}} = \frac{1}{2} \vec{\boldsymbol{\omega}}^{\dagger} \mathbf{I} \vec{\boldsymbol{\omega}} = \frac{1}{2} (\omega_x \omega_y \omega_z) \left(\mathbf{I} \right) \begin{pmatrix} \omega_x \\ \omega_y \\ \omega_z \end{pmatrix},$$

which is a scalar quantity.

Now this form of T^{rot} is not very useful. We want to put it into the form

$$\mathbf{T}^{rot} = \vec{\boldsymbol{\ell}}^{\,\dagger} \frac{1}{\textbf{T}} \vec{\boldsymbol{\ell}}$$

because we know how to handle quantum mechanical angular momentum matrix elements: ℓ^2 , $\ell_{\pm} = \ell_x \pm i \ell_y$, and ℓ_z .

But how do we think about the reciprocal of a matrix? Or any function of a matrix?

I is real and symmetric. It can be diagonalized by a unitary transformation, $\mathbf{T}^{-1} = \mathbf{T}^{\dagger}$ († means conjugate transpose)

$$\tilde{\mathbf{I}} = \mathbf{T}\mathbf{I}\mathbf{T}^{\dagger} = \begin{pmatrix} I_a & 0 & 0 \\ 0 & I_b & 0 \\ 0 & 0 & I_c \end{pmatrix}$$

where I_a , I_b , and I_c are eigenvalues of **I** and a, b, c are orthogonal components of the "principal axis system". The labels a, b, c are assigned so that

$$I_a < I_b < I_c$$
.

It is usually possible to diagonalize **I** by inspection or (if there is a rotation symmetry axis, C_n) by solving a 2×2 (quadratic) problem. I am not going to write anything here about how to go from the molecular geometry to **I** and finally to $\tilde{\mathbf{I}}$.

If we have the eigenvalues of a matrix, we can do whatever mathematical operations we want on the matrix by performing that operation on the eigenvalues of that matrix, and then applying the inverse of the diagonalizing transformation to the diagonal matrix, $f(\mathbf{TIT}^{\dagger})$,

$$f(\mathbf{I}) = \mathbf{T}^{\dagger} f(\mathbf{T} \mathbf{I} \mathbf{T}^{\dagger}) \mathbf{T}.$$

For example

$$\mathbf{I}^{-1} = \mathbf{T}^{\dagger} \begin{pmatrix} 1/I_a & 0 & 0 \\ 0 & 1/I_b & 0 \\ 0 & 0 & 1/I_c \end{pmatrix} \mathbf{T}.$$

Let's use this result to get $\hat{\mathbf{H}}^{\text{rot}}$ into the desired form, expressed in terms of J_a , J_b , and J_c rather than ω_a , ω_b , and ω_c .

$$\hat{T}^{\text{rot}} = \frac{1}{2}\vec{\omega}^{\dagger}\mathbf{I}\vec{\omega}$$
but $\vec{J} = \mathbf{I}\vec{\omega}$

$$\vec{\omega} = \frac{1}{\mathbf{I}}\vec{J}$$

$$\hat{T}^{\text{rot}} = \frac{1}{2}\vec{J}^{\dagger}\frac{1}{\mathbf{I}}\mathbf{I}\frac{1}{\mathbf{I}}\vec{J} = \frac{1}{2}\vec{J}^{\dagger}\frac{1}{\mathbf{I}}\vec{J}$$

$$f(\mathbf{I}) = \mathbf{T}^{\dagger}f(\mathbf{T}\mathbf{I}\mathbf{T}^{\dagger})\mathbf{T}$$

$$\frac{1}{\mathbf{I}} = \mathbf{T}^{\dagger}\begin{pmatrix} 1/I_{a} & 0 & 0\\ 0 & 1/I_{b} & 0\\ 0 & 0 & 1/I_{c} \end{pmatrix}\mathbf{T}$$

$$\hat{T}^{\text{rot}} = \frac{1}{2}\vec{J}^{\dagger}\mathbf{T}^{\dagger}\begin{pmatrix} 1/I_{a} & 0 & 0\\ 0 & 1/I_{b} & 0\\ 0 & 0 & 1/I_{c} \end{pmatrix}\mathbf{T}\vec{J}$$

$$\mathbf{T}\vec{J} = \vec{\tilde{J}} = \begin{pmatrix} J_{a}\\ J_{b}\\ J_{c} \end{pmatrix}$$

$$\vec{J}^{\dagger}\mathbf{T}^{\dagger} = \vec{\tilde{J}}^{\dagger} = (J_{a} J_{b} J_{c}).$$

5.1 Introduction 73

We have the desired result

$$\tilde{\mathbf{T}}^{\text{rot}} = \frac{1}{2} \vec{\tilde{J}}^{\dagger} \tilde{\mathbf{I}}^{-1} \vec{\tilde{J}} = \frac{1}{2} \begin{pmatrix} J_a & J_b & J_c \end{pmatrix} \begin{pmatrix} 1/I_a & 0 & 0 \\ 0 & 1/I_b & 0 \\ 0 & 0 & 1/I_c \end{pmatrix} \begin{pmatrix} J_a \\ J_b \\ J_c \end{pmatrix} \\
= \frac{J_a^2}{2I_a} + \frac{J_b^2}{2I_b} + \frac{J_c^2}{2I_c}.$$

Thus, when we replace $\vec{\tilde{\omega}}$ in the kinetic energy expression by $\vec{\tilde{J}}$, we have

$$T^{\text{rot}} = \frac{J_a^2}{2I_a} + \frac{J_b^2}{2I_b} + \frac{J_c^2}{2I_c} = AJ_a^2 + BJ_b^2 + CJ_c^2$$

where A, B, C are rotational constants

$$A \geq B \geq C$$
,

and we are off to the races! It does not really matter how we got to this point. This gives us the \mathbf{H}^{ROT} from which we derive everything we need to know about the rotational levels of a non-linear polyatomic molecule.

We want to work out the rotational energy levels, being aware of the non-commutation of J_a , J_b , J_c .

These J_i operators are components of an angular momentum [see Sect. 2.8] and must follow the commutation rule definition of an angular momentum [this is for a "reversed angular momentum", which is a counter-intuitive situation that arises for components of a body-frame angular momentum that generates the rotation of the body] [3]

$$[\mathbf{J}_i,\mathbf{J}_j]=-i\hbar\sum_k arepsilon_{ijk}\mathbf{J}_k$$
 (the minus sign is required for a "reversed" angular momentum, which is appropriate for body frame rotational angular momentum components.)

$$\varepsilon_{ijk} = +1$$
 ijk are abc in cyclic order
= -1 ijk are abc in anticyclic order
= 0 if any 2 indices are repeated.

This commutation rule provides the most general and powerful path to derivation of all angular momentum matrix elements, but we will not follow that path in this lecture.

It is necessary to assert that \mathbf{J}^2 and any one of J_a , J_b , or J_c are members of a complete set of mutually commuting operators and that we can define a complete, orthonormal, angular momentum basis set that has the properties

$$\mathbf{J}^{2} |JK_{a}M\rangle = \hbar^{2}J(J+1)|JK_{a}M\rangle$$

$$\mathbf{J}_{a} |JK_{a}M\rangle = \hbar K_{a} |JK_{a}M\rangle$$

$$\mathbf{J}_{\pm} = \mathbf{J}_{b} \pm i \mathbf{J}_{c}$$

$$\mathbf{J}_{\pm} |JK_{a}M\rangle = \hbar [J(J+1) - K_{a}(K_{a} \mp 1)]^{1/2} |JK_{a} \mp 1M\rangle$$

$$(\mathbf{J}_{+} \text{ becomes a "lowering" operator despite its + subscript)}$$

$$\mathbf{J}_{Z} |JK_{a}M\rangle = \hbar M |JK_{a}M\rangle$$
(Capital letters are used to denote laboratory-fixed components.)

We like to use complete basis sets that are eigenfunctions of frequently encountered operators, because this allows us to evaluate matrix elements without ever explicitly evaluating an integral. For example

$$|\psi_m\rangle = \sum_{J,K} a_{JK} |JKM\rangle$$

$$\mathbf{J}^2 |\psi_m\rangle = \sum_{J,K} \hbar^2 J(J+1) a_{JK} |JKM\rangle$$

where $|\psi_m\rangle$ is any angular momentum state, which can be expressed as a linear combination of $|JKM\rangle$ states.

5.2 Rotational Energy Levels of Rigid Polyatomic Rotors

5.2.1 Symmetric Top

$$\mathbf{H} = A\mathbf{J}_a^2 + B\mathbf{J}_b^2 + C\mathbf{J}_c^2$$

prolate top:
$$B = C$$
 (cigar)
oblate top: $A = B$ (frisbee)

$$\begin{split} \mathbf{H}_{\text{prolate}} &= A \mathbf{J}_a^2 + B (\mathbf{J}_b^2 + \mathbf{J}_c^2) \qquad (B = C) \\ \mathbf{J}^2 &= \mathbf{J}_a^2 + \mathbf{J}_b^2 + \mathbf{J}_c^2 \\ \mathbf{J}_b^2 + \mathbf{J}_c^2 &= \mathbf{J}^2 - \mathbf{J}_a^2 \\ \mathbf{H}_{\text{prolate}} &= A \mathbf{J}_a^2 + B (\mathbf{J}^2 - \mathbf{J}_a^2) = (A - B) \mathbf{J}_a^2 + B \mathbf{J}^2 \\ E_{JK_a}^{\text{prolate}} &= \left\langle J' K_a' M \left| \mathbf{H}_{\text{prolate}} \right| J K_a M \right\rangle = \delta_{J'J} \delta_{K_a' K_a} \hbar^2 [(A - B) K_a^2 + B J (J + 1)] \end{split}$$

Similarly, for oblate top

$$E_{JK_c}^{\text{oblate}} = \hbar^2 [(C - B)K_c^2 + BJ(J + 1)].$$

Notice that the coefficient of K_a^2 is A-B>0 for prolate top, and of K_c^2 is C-B<0 for oblate top. The signs of A-B and C-B are determined by the convention $A\geq B\geq C$.

The lowest allowed value of J is K_a for a prolate top and K_c for an oblate top. There is no way that the magnitude of an angular momentum can be smaller than one of its projections.

The energy levels have the following patterns (Fig. 5.2):

Since K_a (prolate top) and K_c (oblate top) can be positive or negative, every |K| > 0 level is **doubly degenerate**. The actual eigenstates have definite parity and have the symmetrized forms

$$|J|K|\pm\rangle = 2^{-1/2}[|JK\rangle \pm |J-K\rangle].$$

The K-doubling is analogous to Λ -doubling in a diatomic molecule and the degeneracy of K > 0 levels is lifted by interactions with non-degenerate K = 0 states (by various mechanisms).

It is possible to prove that every molecule with a C_n n > 2 rotational symmetry axis (or an S_4 improper rotation axis) is a symmetric top with a permanent electric dipole moment exclusively along the symmetry axis.

Most molecules are not symmetric tops, but we use a linear combination of the symmetric top basis states to describe their energy levels and eigenstates.

5.2.2 Asymmetric Top

$$A \neq B \neq C$$

We use a clever trick to manipulate the \mathbf{H}^{rot} into a convenient form:

$$\mathbf{H}^{\text{rot}} = A\mathbf{J}_a^2 + B\mathbf{J}_b^2 + C\mathbf{J}_c^2.$$

For a "near prolate" top we do some simple operator algebra

$$B\mathbf{J}_{b}^{2} + C\mathbf{J}_{c}^{2} = \frac{(B+C)}{2}(\mathbf{J}_{b}^{2} + \mathbf{J}_{c}^{2}) + \frac{(B-C)}{2}(\mathbf{J}_{b}^{2} + \mathbf{J}_{c}^{2})$$

$$\mathbf{J}_{b}^{2} + \mathbf{J}_{c}^{2} = \mathbf{J}^{2} - \mathbf{J}_{a}^{2}$$

$$\mathbf{J}_{\pm} = \mathbf{J}_{b} \pm i\mathbf{J}_{c}$$

$$\mathbf{J}_{+}^{2} = \mathbf{J}_{b}^{2} - \mathbf{J}_{c}^{2} + i\mathbf{J}_{b}\mathbf{J}_{c} + i\mathbf{J}_{c}\mathbf{J}_{b}$$

$$\mathbf{J}_{-}^{2} = \mathbf{J}_{b}^{2} - \mathbf{J}_{c}^{2} - i\mathbf{J}_{b}\mathbf{J}_{c} - i\mathbf{J}_{c}\mathbf{J}_{b}$$

$$\mathbf{J}_{+}^{2} + \mathbf{J}_{-}^{2} = 2(\mathbf{J}_{b}^{2} - \mathbf{J}_{c}^{2}).$$

Thus

$$B\mathbf{J}_{b}^{2} + C\mathbf{J}_{c}^{2} = \frac{B+C}{2}(\mathbf{J}^{2} - \mathbf{J}_{a}^{2}) + \frac{B-C}{4}(\mathbf{J}_{+}^{2} + \mathbf{J}_{-}^{2})$$

$$\mathbf{H}^{\text{rot-prolate}} = \frac{B+C}{2}\mathbf{J}^{2} + \left(A - \frac{B+C}{2}\right)\mathbf{J}_{a}^{2} + \frac{B-C}{4}(\mathbf{J}_{+}^{2} + \mathbf{J}_{-}^{2})$$

$$\frac{B+C}{2} \equiv \overline{B}.$$

Notice that all of the matrix elements of the operators in this Hamiltonian are easily evaluated in the prolate symmetric top basis set.

But there is one non-trivial problem: the selection rules for \mathbf{J}_{+}^{2} and \mathbf{J}_{-}^{2} are respectively $\Delta K_{a}=-2$ and +2. Therefore we have some non-zero off-diagonal terms in $\mathbf{H}^{\mathrm{rot-prolate}}$ and we are eventually going to have to diagonalize this Hamiltonian matrix.

The form of the oblate asymmetric top Hamiltonian is similar

$$\mathbf{H}^{\text{rot-oblate}} = \frac{A+B}{2}\mathbf{J}^2 + \left(C - \frac{A+B}{2}\right)\mathbf{J}_c^2 + \left(\frac{A-B}{4}\right)(\mathbf{J}_+^2 + \mathbf{J}_-^2)$$
$$\frac{A+B}{2} \equiv \overline{B}.$$

Notice that if B = C for prolate or A = B for oblate, both asymmetric top Hamiltonians become identical to the corresponding symmetric top Hamiltonian.

Now we are going to simplify the asymmetric top Hamiltonian by a trick, called the *Wang Transformation*. This transformation "block-diagonalizes" the Hamiltonian according to two characteristics:

- Parity is rigorously conserved.
- The only non-zero matrix elements for both $\mathbf{H}^{\text{rot-prolate}}$ and $\mathbf{H}^{\text{rot-oblate}}$ have a $\Delta K = \pm 2$ selection rule. This separates the even-K and the odd-K states into two separate non-communicating groups. Overall, there are four

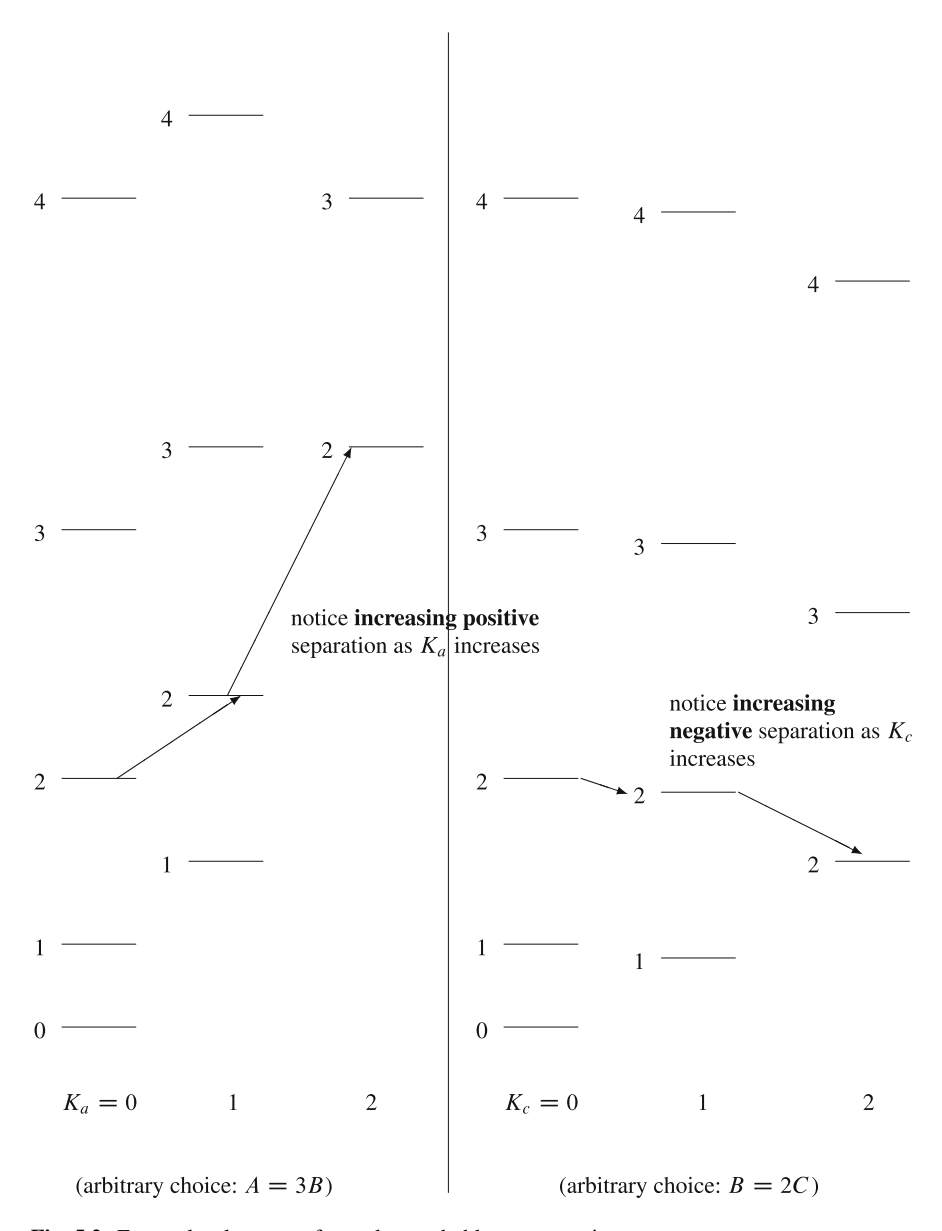


Fig. 5.2 Energy level patterns for prolate and oblate symmetric tops

non-communicating groups. These are often labeled by the even/odd-ness of K_a and K_c : ee, eo, oe, and oo.

We start with $\mathbf{H}^{\mathrm{ROT}}$ in a signed-K basis (not yet symmetrized into the parity basis) and perform a similarity transformation by this strange-looking matrix.

$$\mathbf{X} = \mathbf{X}^{-1} = 2^{-1/2} \begin{pmatrix} -1 & & & 1 \\ & \ddots & & & \ddots \\ & & -1 & 0 & 1 \\ & & 0 & 2^{1/2} & 0 \\ & & 1 & 0 & 1 \\ & & \ddots & & & \ddots \\ 1 & & & & 1 \end{pmatrix}$$

$$K =$$
 $J \ J - 1 \ \cdots \ 0 \ \cdots \ -J$
So, for $J = 2$

$$\mathbf{X} \begin{pmatrix} |J=2, K=2\rangle = |22\rangle \\ |21\rangle \\ |20\rangle \\ |2-1\rangle \\ |2-2\rangle \end{pmatrix} = \begin{pmatrix} 2^{-1/2}[-|22\rangle + |2-2\rangle] \\ 2^{-1/2}[-|21\rangle + |2-1\rangle] \\ |20\rangle \\ 2^{-1/2}[|21\rangle + |2-1\rangle] \\ 2^{-1/2}[|22\rangle + |2-2\rangle] \end{pmatrix}.$$

You obtain a transformed HROT that has structure

The lines between the zeroes symbolize non-zero entries that you must calculate. This transformed \mathbf{H}^{ROT} can be rearranged into block diagonal form

$$\begin{pmatrix} \boxed{\text{even } K \text{ even parity}} & 0 & 0 & 0 \\ 0 & \boxed{\text{odd } K \text{ even parity}} & 0 & 0 \\ 0 & 0 & \boxed{\text{even } K \text{ odd parity}} & 0 \\ 0 & 0 & \boxed{\text{odd } K \text{ odd parity}} \end{pmatrix}.$$

This form of **H**^{ROT} suggests correctly that there are four symmetry species for asymmetric top basis functions. Note that this symmetry classification of the rotational wavefunctions has nothing at all to do with the point group of the molecule. Even a molecule that has only the identity symmetry operation still has rotational levels belonging to four distinct symmetry species. *This will prove useful!*

It will also become a little more intuitive when we use the prolate-oblate correlation diagram to reveal the qualitative pattern of the eigen-energies and the $K_p K_o$ notation for labeling rotational energy levels. This is the most important point in this entire lecture!

5.3 Correlation Diagrams: WHY?

Correlation diagrams are a good way of capturing the qualitative pattern of energy levels that would have been revealed by laborious application of second-order perturbation theory. They combine the trivially obtainable patterns for simpler problems (symmetric prolate and symmetric oblate tops) with rigorous symmetry selection rules and **NOTHING ELSE**! (Fig. 5.3)

5.3.1 Prolate-Oblate Top Correlation Diagram

Recall that prolate tops have a term $(A - \overline{B})K_a^2$ which is large and positive while oblate tops have a term $(C - \overline{B})K_c^2$ which is small and negative. Consider, for example, only J = 4.

Crudely, depending on the value of $\frac{A-B}{A-C}$ (0 for oblate, 1 for prolate) you can draw a vertical line through the energy levels in Fig. 5.3 and get a good estimate of the expected energy level pattern. Actually Ray's asymmetry parameter

$$\kappa \equiv \frac{2B - A - C}{A - C}$$

is better ($\kappa = -1$ for prolate and $\kappa = +1$ for oblate). Some facts

- We draw the connecting lines in this particular pattern by obeying the "non-crossing rule." Since all of these levels belong to the same value of the rigorously conserved quantum number, J, there can be no level crossings, only avoided crossings. Levels of opposite parity with the same J can cross, but the pattern in the above diagram is the only pattern of connections that leaves no orphan levels. Every asymmetric top eigenstate must connect to a prolate top eigenstate in the limit B = C and to an oblate top eigenstate in the limit A = B. WE USE BOTH THE PROLATE AND OBLATE TOP K-values to label each state uniquely.
- J_{K_a,K_c} state labels are very *instructive*. Near the prolate limit, K_a gives the approximate projection of J on the a-axis. For each K_a there are two possible K_c values and they serve merely as indices. They do NOT tell anything about the projection of J on the c-axis. Near the oblate limit, K_c gives the projection of J on the c-axis and K_a is merely an index.

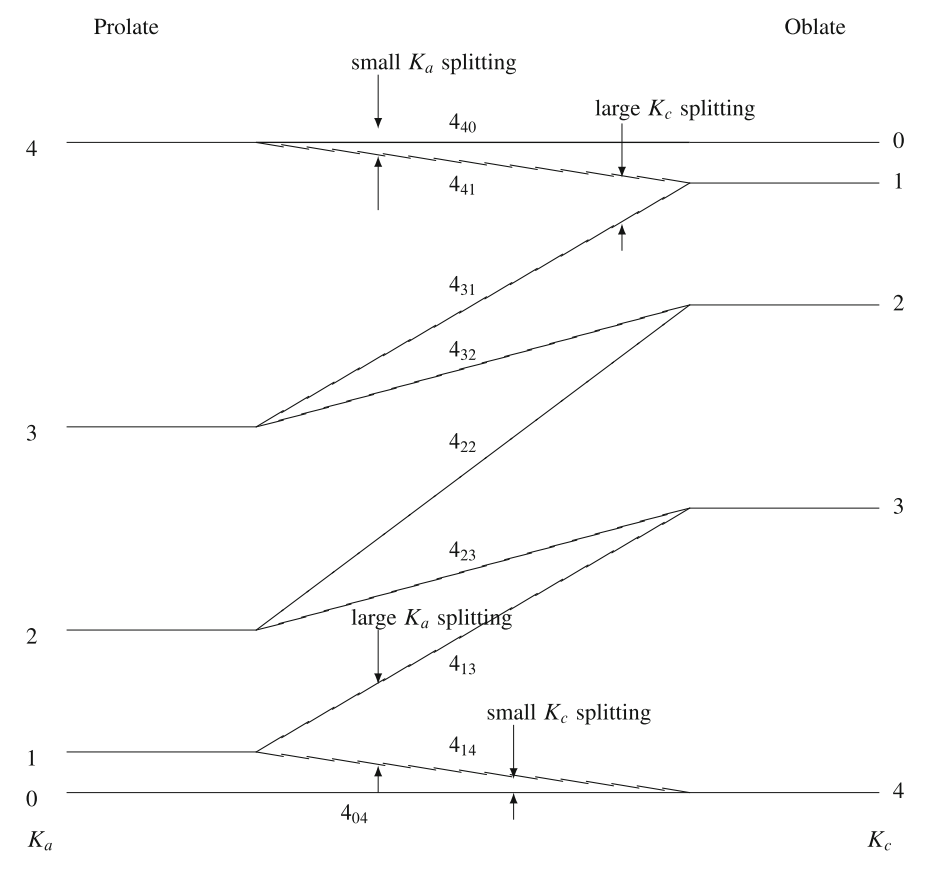


Fig. 5.3 Prolate–Oblate correlation diagram. This figure is a simplified version of Fig. 4.1 from Townes and Schawlow [4]

• For each value of J there are 2J + 1 energy levels. They may be divided into four groups of definite symmetry [the number of levels in each group is given in the two columns of the table below]: e is for even, o for odd, the first letter is for K_a , the second letter for K_c .

even
$$J$$
 odd J
ee $J/2 + 1$ $(J - 1)/2$
oo $J/2$ $(J + 1)/2$
eo $J/2$ $(J + 1)/2$
oe $J/2$ $(J + 1)/2$

• The energy separation between the two members of each $K \neq 0$ (K-doubling or "asymmetry splitting") is largest for K = 1. This is a simple consequence of the

 $\Delta K = \pm 2$ selection rule for \mathbf{J}_{+}^{2} and \mathbf{J}_{-}^{2} . The *K*-doubling in K = 1 is evaluated as follows:

$$2^{-1/2} [\langle JK_a = 1 | \pm \langle JK_a = -1 |] \times \left| \frac{B - C}{4} (\mathbf{J}_+^2 + \mathbf{J}_-^2) \right| 2^{-1/2} [|JK_a = 1\rangle$$

$$\pm |JK_a = -1\rangle]$$

$$= \frac{1}{2} \frac{B - C}{4} [\langle JK_a = 1 | \mathbf{J}_-^2 | JK_a = -1\rangle$$

$$\pm \langle JK_a = -1 | \mathbf{J}_+^2 | JK_a = +1\rangle]$$

$$= \frac{1}{2} \frac{B - C}{4} \{2[J(J+1)]^{1/2} [J(J+1)]^{1/2}\}$$

$$= \frac{(B - C)J(J+1)}{4}.$$

- The K-doubling is largest for a given J in $K_a = 1$ for a near prolate top with $J_{1,J-1}$ always above J_{1J} . The K-doubling is also largest for $K_c = 1$ in an oblate top, with J_{J1} always above $J_{J-1,1}$.
- There are two kinds of levels, those with $K_a + K_c = J$ and $K_a + K_c = J + 1$. The sign of the K-doubling of near prolate levels is always $J_{K_a,J-K_a}$ above $J_{K,J-K+1}$ (because of the negative sign of the coefficient of \mathbf{J}_c^2 in the oblate limit). The sign of the K-doubling of near oblate levels is always J_{J-K_c+1,K_c} above J_{J-K_c,K_c} (because of the sign of the coefficient of \mathbf{J}_a^2 in the prolate limit).
- The asymmetry splitting is largest when $K \ll J$.

5.3.2 Assignments of Rotational Transitions

There are many qualitative conclusions that may be drawn from the correlation diagram. These are based on the $A \geq B \geq C$ (or $I_a \leq I_b \leq I_c$) relative magnitudes of the rotational constants. These qualitative patterns are often the basis for symmetry assignments or for a warning that a perturbation by an accidentally close-lying level that belongs to a different electronic-vibrational state is occurring. But how do we determine the J_{K_a,K_c} assignments of observed energy levels? From the selection rules for electric dipole allowed transitions! These selection rules are very simple and are closely related to the selection rules for electronic transitions in diatomic molecules.

Recall: A $\Delta\Omega=0$ transition is called a *parallel transition*. The transition moment is along the internuclear axis, which we call "z" or "a" (Ω is analogous to K). $\Delta\Omega=0$ transitions have weak or absent Q branches ($\Delta J=0$).

A $\Delta\Omega=\pm 1$ transition is called a *perpendicular transition*. The transition moment is perpendicular to the internuclear axis. $\Delta\Omega=\pm 1$ transitions have strong Q branches.

We generalize to asymmetric tops by making a logically simple but elegant extension. If the permanent electric dipole moment is along one of the a, b, or c axes, then we say that the corresponding projection quantum number changes by an even number (zero is even) and the other projection quantum number(s) change by an odd number (one is an odd number). So here is the magic decoder:

a-type transitions:
$$\Delta K_a = \text{even}$$
, $\Delta K_c = \text{odd}$ (weak Q transitions in prolate limit, strong Q in near oblate limit)

b-type transitions:
$$\Delta K_a = \text{odd}$$
, $\Delta K_c = \text{odd}$ (strong Q branches)

c-type transitions:
$$\Delta K_a = \text{odd}$$
, $\Delta K_c = \text{even}$ (weak Q in near oblate, strong Q in near prolate)

This is easy to remember!

Sometimes the permanent dipole moment has projections on more than one of the a, b, or c axes. Then one has "mixed-type" transitions, the relative amplitudes of which tell us the relative magnitudes of the body-fixed permanent dipole moment along each of the a, b, or c axes. [In special cases there can be interferences between the transition amplitudes associated with two of the non-zero dipole moment projections. The sign of the interference effect gives the relative signs of the two dipole moment components.]

Examples of a, b and c-type transitions.

$$\begin{array}{c} \text{a-type Q: $4_{14} \rightarrow 4_{13}$ Weak or absent} \\ \text{$R: $4_{14} \rightarrow 5_{15}$} \\ \text{$P: $4_{14} \rightarrow 3_{13}$} \end{array} \\ \begin{array}{c} \text{b-type Q: $4_{14} \rightarrow 4_{23}$} \\ 4_{04} \rightarrow 4_{13} \end{array} \right\} \text{ Strong} \\ \text{$R: $4_{14} \rightarrow 5_{23}$, $4_{14} \rightarrow 5_{05}$} \\ 4_{04} \rightarrow 5_{15} \\ \text{$P: $4_{14} \rightarrow 3_{03}$} \\ 4_{14} \rightarrow 3_{21} \\ 4_{04} \rightarrow 3_{13} \end{array} \\ \begin{array}{c} \text{c-type Q: $4_{14} \rightarrow 4_{04}$} \\ 4_{14} \rightarrow 4_{22} \\ \text{$R: $4_{14} \rightarrow 5_{24}$} \\ 4_{04} \rightarrow 5_{14} \\ \text{$P: $4_{14} \rightarrow 3_{04}$} \\ 4_{04} \rightarrow 3_{12} \end{array} \right\} \text{ Weak}$$

Notation:
$$^{\Delta K_{p \text{ or } o}} \Delta J(J_{K_a,K_c})_a \text{ or } b \text{ or } c$$
.

For example, the $4_{14} \rightarrow 5_{24}$ transition is denoted as ${}^{r}R(4_{14})_{c}$.

[Be careful. The above example violates the strict convention in molecular spectroscopy: specify upper state (not initial state!) first. This notation for rotational transitions is more appropriate to describe vibration-rotation or electronic-vibration-rotation transitions. In a vibrational or an electronic-vibrational band, there is always a large energy difference between the upper state (all vibrational and rotational quantum numbers expressed with a single prime) and the lower state (all quantum numbers expressed with a double prime). Regardless of whether the transition is observed in absorption or emission, the name of the rotational transition is the same, and the notation specifies $\Delta K = K' - K''$, $\Delta J = J' - J''$, the lower state rotational quantum numbers $J''_{K''_a, K''_c}$ and the a, b, or c electric dipole component type of the transition.]

5.4 Vibrational Dependence of Rotational Constants

For an N-atom molecule there are 3N-6 vibrational normal modes. For a diatomic molecule (which can have only one normal mode) we used perturbation theory to compute the expected values of the centrifugal distortion constant, D, and the vibration-rotation interaction constant, α . We noticed that the value of α is determined by both $\Delta v = \pm 1$ off-diagonal matrix elements of $\frac{dB(R)}{dQ}\hat{Q}$ and the $-b\hat{Q}^3$ cubic anharmonicity term in the potential, V(Q). If we neglect $-b\hat{Q}^3$, then we get the wrong sign for $\alpha_e!$ B(R) is very large near the (hard) inner turning point $(1/R^2$ blows up) and small near the (soft) outer turning point. As v increases the wavefunction amplitude accumulates near the outer turning point. As a result, the softer turning point wins in the vibrational average of B(R). We want to use this sort of insight to be able to predict the α constants for a polyatomic molecule.

Bad news! For a polyatomic molecule there are three rotational constants, A, B, and C, and there are contributions to D and α from each of the three rotational constants for each of the 3N-6 normal modes. That will be an enormous amount of perturbation theory (the perturbation theory is do-able, but not by normal sane humans!). A computer is trained to compute derivatives of $1/I_a$, $1/I_b$, and $1/I_c$ with respect to each of the vibrational normal modes. Then the crank is turned and we get α_i^A , α_i^B , and α_i^C where i specifies which normal mode. Similarly, the contributions of each of the normal modes to the various centrifugal distortion constants can be computed.

The classic paper is "Simplification of the Molecular Vibration-Rotation Hamiltonian," by J.K.G. Watson [5].

References

- P.F. Bernath, Spectra of Atoms and Molecules, Chap. 6, 2nd edn. (Oxford University Press, Oxford, 2005)
- R.W. Field, Videos of lectures #22–24, Chemistry 5.80, in Small Molecule Spectroscopy and Dynamics. http://ocw.mit.edu/courses/chemistry/5-80-small-molecule-spectroscopy-anddynamics-fall-2008/ (2008)
- 3. J.M. Brown, B.J. Howard, Mol. Phys. 31, 1517 (1976); 32, 1197 (1977)
- 4. C.H. Townes, A.L. Schawlow, Microwave Spectros (Dover, New York, 2012)
- 5. J.K. Watson, Mol. Phys. 15, 479 (1968)

Chapter 6 Quantum Beats

A short pulse of radiation can excite transitions into two or more near-degenerate eigenstates from a common initial eigenstate, provided that the pulse duration is sufficiently short so that its uncertainty-broadened energy width "covers" several non-degenerate eigenstates. This produces a coherent superposition of several eigenstates, and, depending on the detection scheme, results in a sinusoidally oscillating and exponentially decaying signal, usually fluorescence. The oscillations are at the frequencies of the level spacings between most of the pairs of coherently excited eigenstates [1–4]. It is pedagogically useful to make a distinction between polarization quantum beats [5–7] and population [8–10] quantum beats. The key concept is "bright state" and "dark state". Brightness and darkness are not universal qualities, they are dependent on the nature of the excitation and detection schemes. Quantum beats provide a very high-resolution measure of the level structure, which is obtainable with a very crude, low-resolution pulsed laser [4, 6, 9]. Stark [7] and Zeeman [6] quantum beats are usually of the "polarization" type, whereas zero-field [9, 10] and field-tuned [6, 7] spectroscopic perturbations usually yield quantum beats of the "population" type.

6.1 Introduction

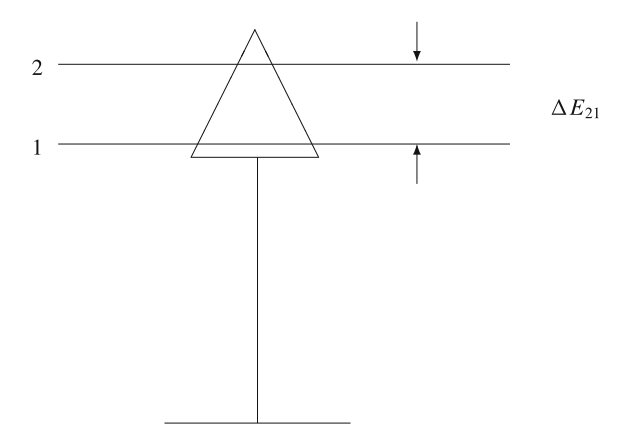
A short pulse of electromagnetic radiation creates a coherent superposition of several eigenstates. These eigenstates are excited from a single common eigenstate (Fig. 6.1).

There are two requirements for the observation of quantum beats [1]:

(a) the excitation pulse must be sufficiently short, of duration τ , so that $\Delta E_{21} \lesssim \frac{h}{\pi \tau}$. Thus the uncertainty width of the pulse covers the pair of eigenstates spaced by ΔE .

86 Guantum Beats

Fig. 6.1 Eigenstates excited by a short excitation pulse from a single common eigenstate



(b) The detection scheme must be capable of detecting a signal from both level 1 and level 2.

The coherent superposition state gives a sinusoidally oscillating and exponentially decaying signal. The oscillations are called **Quantum Beats**.

There are two basic flavors of Quantum Beats:

- POLARIZATION BEATS [5–7]
- POPULATION BEATS [8–10]

The outline of this lecture:

- (a) A reminder of the Time Dependent Schrödinger Equation (TDSE) and the behavior of its solutions for a *time-independent* **H** [11].
- (b) "Bright" and "Dark" States $\Psi(t)$ for a 2-state coherence [1] $P(x,t) = \Psi^*(x,t)\Psi(x,t)$ probability density [12] $A(t) = \int dx \Psi^*(x,0)\Psi(x,t)$ autocorrelation function [13] A Zewail-like wavepacket experiment [21, 23]
- (c) Quantum Beats

The two-level problem: from basis states (ϕ_0, ϕ_1) to eigenstates (ψ_+, ψ_-)

Two non-decaying states

Inclusion of decay [14]

Inclusion of detectability of each eigenstate

Population Quantum Beats [8]

Polarization Quantum Beats [5]

Zeeman Quantum Beats [6]

Stark Quantum Beats [7]

What can we measure?

6.2 Time-Dependent Schrödinger Equation (TDSE)

We consider only a time-independent H [11]. The TDSE is

$$i\hbar\frac{\partial\Psi}{\partial t}=\mathbf{H}\Psi.$$

The following discussion is a bit of a fraud because we will imagine experiments where a non-eigenstate is suddenly produced by some pulsed process. If we expand Ψ at t=0 as a linear combination of eigenfunctions of **H**

$$\Psi(0) = \sum_{j} a_{j} \psi_{j}$$

with eigen-energies E_i , then the solution to the TDSE is

$$\Psi(t) = \sum_{j} a_{j} \psi_{j} e^{-iE_{jt}/\hbar}.$$

The fact that this $\Psi(t)$ satisfies the TDSE is verified by

$$i\hbar \frac{\partial \Psi}{\partial t} = i\hbar \sum_{j} \left(\frac{-iE_{j}}{\hbar}\right) a_{j} \psi_{j} e^{-iE_{jt}/\hbar}$$
$$= \sum_{j} E_{j} a_{j} \psi_{j} e^{-iE_{jt}/\hbar}$$

and

$$\mathbf{H}\Psi(t) = \sum_{j} a_{j} e^{-iE_{jt}/\hbar} \mathbf{H} \psi_{j} = \sum_{j} a_{j} e^{-iE_{jt}/\hbar} E_{j} \psi_{j},$$

so Ψ satisfies the TDSE.

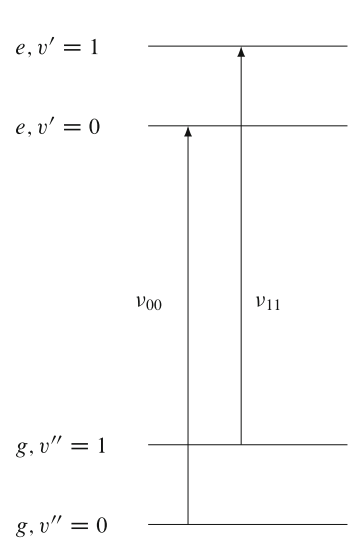
We know, if we have solved the time-independent Schrödinger equation, how to write a solution of the TDSE. This means, if we know $\Psi(0)$ we can trivially get $\Psi(t)$.

6.3 "Bright" and "Dark" States

Bright and Dark are properties of the specific experimental setup [15]. They are not universal properties of a given ψ_j . For example, suppose we have an experiment where we excite, from the v''=0 level of the electronic ground state, g, to an excited state, e (Fig. 6.2).

88 6 Quantum Beats

Fig. 6.2 Bright and dark states



If the molecular constants for the g and e states are nearly identical, then there is a Franck–Condon propensity rule, $\Delta v = 0$. State e, v' = 0 is bright for excitation from g, v'' = 0 with detection of fluorescence at $v_{00} \approx v_{11}$. State e, v' = 1 is dark for excitation from g, v'' = 0, but it would be bright for excitation from g, v'' = 1.

Now for a more interesting case. The g-state and e-state have quite different molecular constants. The Franck–Condon factors for excitation and fluorescence are not diagonal. But suppose only g, v''=0 is thermally populated. Then we have a level diagram (Fig. 6.3).

There are many vibrational levels of the e state that can be populated from the g,v''=0 state. So it seems like all of the e levels are bright. But this is not necessarily true! We can use a monochromator to select fluorescence from a specific e,v' level to a specific g,v'' level. If the resolution of the monochromator is sufficient and we are lucky that there is no accidental overlap of the $v_{ev',gv''}$ transition frequency with that of an emission transition from a different e,v' level, then only the selected e,v' level is bright. The rest are dark, with respect to this specific experimental setup [10].

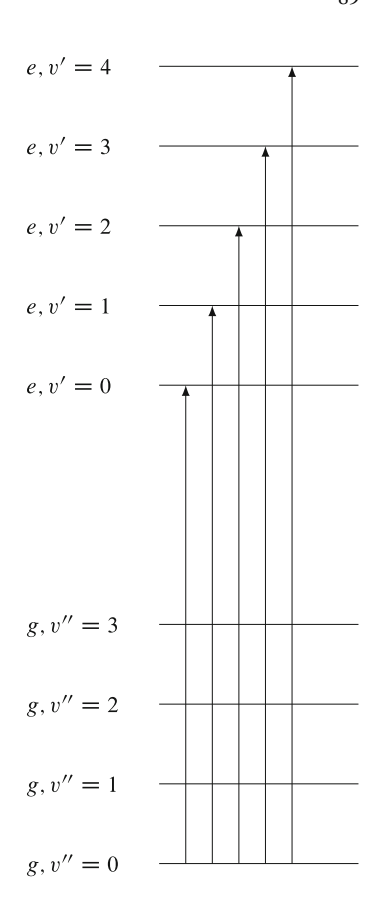
Suppose we do an experiment where the excitation pulse is so short

$$\Delta t_{\text{excitation}} > \frac{\hbar}{\Delta E_{ev'=1,ev'=0}},$$

that its Fourier transform width overlaps the energies of both the ev' = 1 and ev' = 0 levels. We prepare a coherent superposition state

$$\begin{split} \Psi(0) &= a_0 \psi_{e,v'=0} + a_1 \psi_{e,v'=1} \\ \Psi(t) &= a_0 e^{-iE_{e,v'=0}t/\hbar} \psi_{e,v'=0} + a_1 e^{-iE_{e,v'=1}t/\hbar} \psi_{e,v'=1} \\ &= e^{-iE_{e,v'=0}t/\hbar} [a_0 \psi_{e,v'=0} + a_1 e^{-i\omega_{10}t} \psi_{e,v'=1}] \end{split}$$

Fig. 6.3 A level diagram for transitions between the e and g states, which have different potential energy surfaces



The probability density, P(x,t), is

$$P(x,t) = \Psi^{\star}(t)\Psi(t) = |a_0|^2 |\psi_{ev'=0}|^2 + |a_1|^2 |\psi_{ev'=1}|^2 + a_0 a_1^{\star} \psi_{ev'=0} \psi_{ev'=1}^{\star} e^{i\omega_{10}t} + a_0^{\star} a_1 \psi_{ev'=0}^{\star} \psi_{ev'=1} e^{-i\omega_{10}t}.$$

If the wavefunctions and mixing coefficients are all real (the usual case for vibrational states), then since

$$e^{i\theta} + e^{-i\theta} = 2\cos\theta$$

$$P(x,t) = \Psi^*(t)\Psi(t) = \underbrace{a_0^2 \psi_{e,v'=0}^2 + a_1^2 \psi_{e,v'=1}^2}_{\text{time-independent and positive for all } x$$

$$+ \underbrace{2a_0 a_1 \psi_{e,v'=0} \psi_{e,v'=1} \cos \omega_{10} t}_{\text{time-dependent oscillating between + and - at each } x}.$$

90 6 Quantum Beats

Probabilities can never be negative, at any t or x. For a worst case

$$a_0 = a_1 = 2^{-1/2}$$

$$-\psi_{e,v'=0}(x_{\text{max}}) = \psi_{e,v'=1}(x_{\text{max}}) = c$$

$$\Psi^*(x_{\text{max}}, t)\Psi(x_{\text{max}}, t) = \frac{1}{2}(2c^2) - 2\frac{1}{2}c^2\cos\omega_{10}t$$

$$= c^2(1 - \cos\omega_{10}t) \ge 0 \text{ for all } t.$$

What will we observe in the undispersed fluorescence? This requires integration over x, because the emission from e, v' = 0 and e, v' = 1 comes from all values of the coordinate, x

$$\int dx \Psi^{\star}(x,t)\Psi(x,t) = a_0^2 + a_1^2.$$

The cross term with the interesting time-dependence vanishes because the e, v' = 0 and e, v' = 1 wavefunctions are orthogonal. Even if the time-dependent term could be tricked into not vanishing, the electronic bandwidth of normal photomultipliers used to monitor fluorescence would be far too small (time response ~ 1 ns) to capture oscillations at a typical vibrational frequency, $\omega \approx 1,000 \, \mathrm{cm}^{-1}$.

6.4 Dynamics

An eigenstate is a "stationary state." There is no time evolution. If a short-pulse excitation event creates a coherent superposition of eigenstates, $\Psi(\mathbf{Q}, t)$, many properties of this non-stationary state evolve with time. This evolution can be in state space (see Sect. 6.5 on Quantum Beats) or coordinate-momentum (\mathbf{Q} , \mathbf{P}) space, one Q_i , P_i pair for each vibrational normal mode. If all of the relevant time-independent eigenstates are well represented by a time-independent effective Hamiltonian, \mathbf{H}^{eff} , then all imaginable dynamics may be predictively computed from the \mathbf{H}^{eff} . All dynamics is encoded in the frequency domain spectrum, as represented by the \mathbf{H}^{eff} .

However, there are many situations in which an experimentally achievable frequency domain spectrum contains insufficient information to fully determine all relevant terms in the $\mathbf{H}^{\mathrm{eff}}$. For example, (a) when highly excited eigenstates of a small molecule are embedded in multiple continua and (b) when the shapes of the repulsive potential energy surfaces and the bound~free interaction matrix elements are unknown. It is difficult but often not impossible to obtain the information required to fully determine the $\mathbf{H}^{\mathrm{eff}}$ by frequency domain pump/probe and "action" spectroscopies. In large molecules and in condensed phase systems (the ultimate of a "large molecule") the density of eigenstates is so large that one has multiple overlapping quasi-continua. The route to a complete representation

6.4 Dynamics 91

of dynamics by frequency-domain spectroscopy via an experimentally determined \mathbf{H}^{eff} is impassable. Time-domain techniques offer exciting possibilities for direct observation of molecular dynamics.

Ahmed Zewail was awarded the 1999 Nobel Prize in Chemistry for his Femtosecond Transition State (FTS) spectroscopy experiments [16]. Using a short duration excitation pulse to excite a coherent superposition of discrete or continuum vibrational eigenstates, a particle-like wavepacket is produced that is initially localized in **Q**, **P** space. This wavepacket evolves on a single potential energy surface subject to particle-like laws of motion (Ehrenfest Theorem) [17]:

$$\langle \mathbf{H} \rangle_t = \text{constant}, \ \langle P_i \rangle_t = m \frac{d}{dt} \langle X_i \rangle_t, -\langle \nabla V(\mathbf{X}) \rangle_t = \frac{d}{dt} \langle \mathbf{P} \rangle_t.$$

In addition, if the particle were to cross from one potential surface to another, the relevant transition probability integrals accumulate in the stationary phase region (conservation of position and momentum) [18–20]. The classical mechanics of particle-like motion and the collapse of the relevant part of the transition region to the stationary phase region leads to localized mechanistic insights. The Zewail FTS experiments [20–23] are appealing because they sample dynamics directly and in a **Q.P**-localized sense.

The Zewail group used a subpicosecond pump/probe scheme to characterize the dissociation mechanisms for the

$$ICN \xrightarrow{h\nu} I(^2P_{3/2}) + CN(X^2\Sigma^+)$$

and

$$NaI \xrightarrow{h\nu} Na(3^2S) + I(^2P_{3/2})$$

photodissociation reactions.

The enormous impact and appeal of Zewail's *Femtosecond Transition State* (FTS) spectroscopy owes to the localized mechanistic picture it provides of complicated and previously experimentally unviewable intramolecular dynamics [20]. In Quantum Mechanics, we are used to calculating multidimensional integrals (for N atoms, there are 3N-6 nuclear displacement coordinates, $Q_1, Q_2, \ldots Q_{3N-6}$, denoted collectively as \mathbf{Q} , and 3N-6 conjugate momenta, $P_1, P_2, \ldots P_{3N-6}$, denoted collectively as \mathbf{P}) to describe intramolecular dynamical processes. However, intuitive dynamical pictures are generally expressed as localized (reduced-dimension), ball-and-spring, cause-and-effect mechanisms.

How do we get from delocalized multidimensional Quantum Mechanics to a simple sequence of localized events and the specific local features of potential energy surfaces that control these localized events? The answer is that the *vibrational part* of most Quantum Mechanical electronic transition integrals accumulates in an extremely localized region of coordinate space in which the classical momentum function is the same in both electronic states. This is the *stationary phase region*

92 6 Quantum Beats

and the integrals may be evaluated based on a stationary phase approximation [18, 19]. For a diatomic molecule in the ith electronic state, the classical momentum function is

$$p_i(x) = \pm [2\mu(E - V_i(x))]^{1/2},$$

and the stationary phase point, x_{sp} , for a transition between the *i*th and *j*th electronic states is defined by the requirement that

$$p_i(x_{sp}) = p_j(x_{sp}).$$

An integral over the product of two rapidly oscillating functions accumulates in the region of space where the two functions oscillate at the same spatial frequency [19]. This is the basis of the "classical Franck–Condon principle" for electronic transitions: $\Delta \mathbf{Q} = 0$ (vertical transitions) and $\Delta \mathbf{P} = 0$ (usually because $\mathbf{P} = 0$ at turning points, for a turning point to turning point transition) [24]. After the transition between electronic states occurs, the motion of the system, $\langle \mathbf{Q} \rangle_t$ and $\langle \mathbf{P} \rangle_t$, away from the stationary phase point is governed by Newton's laws (Classical Mechanics) via Ehrenfest's theorem [17].

The following discussions of two of the Zewail Group's first examples of FTS spectroscopy, (a) photodissociation of ICN [22] (Fig. 6.4) and (b) the effect of an ionic/covalent potential energy curve crossing on photodissociation of NaI [23] (Fig. 6.5), are framed in terms of localized pictures or "cartoons." It is important to remember that these are reduced-dimension, semi-quantitative pictures.

The pump pulse, with center energy hc/λ_1 , causes a vertical transition from the zero-point ($v_1=0,v_2=0,v_3=0$) vibrational level of the bound electronic ground state (surface 0) to the unbound electronic excited state (surface 1). The reaction coordinate is principally the I–CN bond-rupture.

The transition is represented by a vertical turning-point to turning-point arrow at R_0 , not at R_e . It is drawn from R_0 rather than R_e to indicate that selection of the pump pulse center wavelength permits a small tuning range of the initial (t=0) I–CN bond length. The wavepacket is born (t=0) at R_0 on potential surface 1.

It is appropriate to call this an example of **transition state spectroscopy** because the experiment samples a dynamical property in addition to the length of the breaking bond. It samples the energy of the CN $B^2\Sigma^+ - X^2\Sigma^+$ electronic transition as a function of the R_{I-CN} bond length. As the CN fragment moves away from the I atom, with increasingly positive momentum, the classical momentum of the CN fragment increases subject to a force equal to the negative gradient of the V_1 potential. As this localized motion occurs, the vertical CN B–X electronic transition energy increases. This R_{I-CN} dependent CN B–X transition energy is represented in the figure as the vertical energy separation between potential surfaces 1 and 2.

The probe pulse samples the time dependence of this B–X transition energy. Since total energy is conserved, the I–CN initial momentum at R^* on V_2 is the same as that on V_1 . This is the reason why it is customary to draw the vertical transition arrow (of length hc/λ_2^*) from $V_1(R^*)$ to $V_2(R^*)$, without cluttering the cartoon with

6.4 Dynamics 93

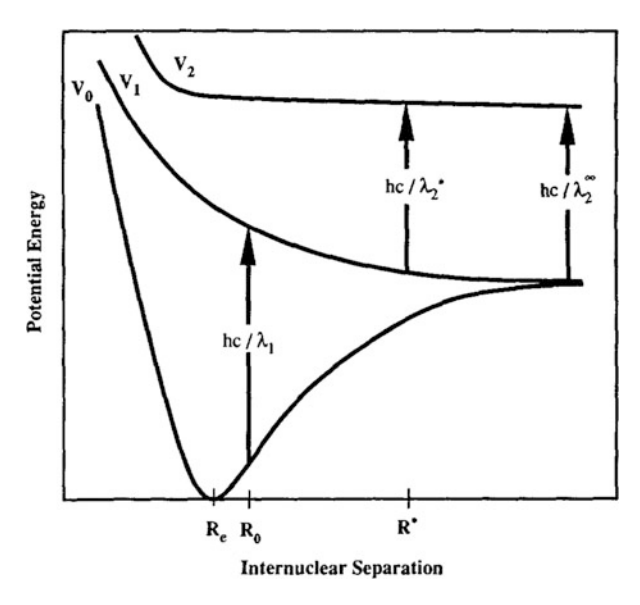


Fig. 6.4 Pump/probe scheme for photodissociation of ICN (Fig. 1 of [21]). This is a reduced dimension representation of three singlet potential energy surfaces of ICN: the bound ground electronic state, V₀ with minimum at R_e, an excited unbound state, V₁, which dissociates to $CN(X^2\Sigma^+)$ and $I(^2P_{3/2})$, and a higher energy unbound state, which dissociates to $CN(B^2\Sigma^+)$ and $I(^2P_{3/2})$. A t=0 pulse from the pump laser, with center wavelength λ_1 , excites a vertical turningpoint-to-turning-point ($P_0 = 0$, $P_1 = 0$) transition at $R = R_0 > R_e$ to the V_1 potential surface. The wavepacket on the V₁ potential surface experiences a force in the increasing R_{I-CN} direction, which causes the P_{I-CN} momentum to increase monotonically with time. At $t = \tau$, a pulse from the probe laser, with center wavelength λ_2^{\star} or λ_2^{∞} probes for the arrival of the wavepacket at $R_{I-CN} = R^*$ or R^{∞} . The energy of the vertical ($\Delta R=0$) and momentum-conserving ($\Delta P=0$) transition also increases monotonically with time as the wavepacket travels outward on V₁. This V₂-V₁ transition is essentially an excitation of the CN B-X electronic transition in the presence of the departing I atom. The $R = R_{I-CN} = R^*$ Optically Coupled Region (OCR) is interrogated by a probe pulse with center wavelength $\lambda_2^* > \lambda_2^{\infty}$, where λ_2^{∞} is the wavelength of the free CN B-X v' = 0 - v'' = 0 band. The detected signal is CN B-X spontaneous fluorescence. Reproduced with permission from Fig. 1 in M.J. Rosker, M. Dantus, and A.H. Zewail, "Femtosecond real-time probing of reactions. I. The technique," J. Chem. Phys. 89, 6113-6127 (1988). Copyright 1988, AIP Publishing LLC

the identical I–CN kinetic energies (at R^*) on the potential surfaces of electronic state-1 and state-2.

The pump pulse creates a t=0 wavepacket at $R_{I-CN}=R_0$ on state 1. When the probe pulse is chosen to have center energy hc/λ_2^* smaller than hc/λ_2^∞ , which is the free CN B–X transition energy, it vertically transfers part of the outward-moving wavepacket from state-1 to state-2 at $R_{I-CN}=R^*$. By varying the time delay between pump and probe pulses, the probe pulse "clocks" the transit of the wavepacket through $R=R^*$ (both arrival time and time-width of the wavepacket). If the pump/probe time delay is too short or too long, and none of the wavepacket is in the "Optically Coupled Region (OCR)" of the state-1 potential energy surface,

94 6 Quantum Beats

nothing happens. Thus, at $t=\infty$, all of the CN excited to state-1 by the pump pulse at t=0 ends up in the $X^2\Sigma^+$ state of free CN and is not detected. However, if part of the wavepacket is in the OCR when the probe pulse arrives, some excitation via a vertical transition to state-2 occurs. All of the ICN molecules excited to state-2 eventually decay into the $B^2\Sigma^+$ state of CN by $t=\infty$ and are detected via their B–X spontaneous fluorescence. It does not matter that the radiative lifetime of the $B^2\Sigma^+$ state of free CN is > 10 ns, the sub-picosecond clocking of the wavepacket motion is based on the pump/probe time delay. If the center energy of the probe pulse is tuned to the free CN B–X transition energy, hc/λ_2^∞ , then all of the ICN initially excited by the pump pulse to state-1 will be excited by the probe pulse to state-2 at long pump/probe time delay and detected as CN B–X spontaneous fluorescence.

More information about the photodissociation of ICN could be obtained by using, in addition to the sub-picosecond pump and probe lasers, a nanosecond tunable laser to monitor individual vibration-rotation populations of the CN photofragment. Such a scheme would provide energy resolution for product state detection without compromising the time resolution of the pump/probe scheme.

The adiabatic NaI $X^1\Sigma^+$ electronic state is Na⁺, I⁻ ionic for R < 6.93 Å and Na(3²S), I($^2P_{3/2}$) covalent for 6.93 Å< $R < \infty$ as the result of an ionic/covalent crossing of the diabatic potential curves.

The pump pulse creates a narrow- ΔR wavepacket near the inner wall of the electronically excited state by a vertical excitation from the v=0 level of the X-state. The nuclear wavepacket is born at t=0 in the covalent region of the excited state with \sim zero Na–I momentum. It experiences a very strong impulsive force in the +R direction, owing to the near-vertical inner wall and the relatively flat bottom of the electronically excited (diabatic) potential energy curve.

As the wavepacket makes its first pass outward through the curve-crossing region, it splits into two parts; one part moving on the \sim flat (unbound) lower-energy covalent potential curve and the other part on the attractive (bound) higher-energy ionic potential curve. The Landau-Zener model [25] determines how the wavepacket fractionates between the ionic and covalent potentials, based on the velocity of the wavepacket near $R=6.93\,\text{Å}$ and the size of the electronic ionic \sim covalent interaction matrix element (which is equal to one-half the vertical separation of the two adiabatic potential curves at 6.93 Å). Fast-passage and a small ionic \sim covalent interaction matrix element both favor ionic \leftrightarrow covalent interconversion. If the conversion probability is α , then after the first crossing the relative amplitudes of the ionic and covalent wavepackets are, respectively $(1-\alpha)$ and α (Figs. 6.5 and 6.6).

After the wavepacket bifurcates at its first outward passage through the curvecrossing region, the covalent part (α) irreversibly separates into ground state Na and I atoms at long-t and large-R and the ionic part $(1-\alpha)$ is reflected inward at the outer wall of the ionic curve. Its return voyage takes it though the curve-crossing region, where it can once again bifurcate, but this bifurcation gives rise to two inwardtraveling (negative momentum) wavepackets (conservation of momentum at the curve crossing): ionic $(1-\alpha)^2$, covalent $\alpha(1-\alpha)$. There is no new outward-traveling wavepacket formed on the covalent curve! The two inward-traveling wavepackets 6.4 Dynamics 95

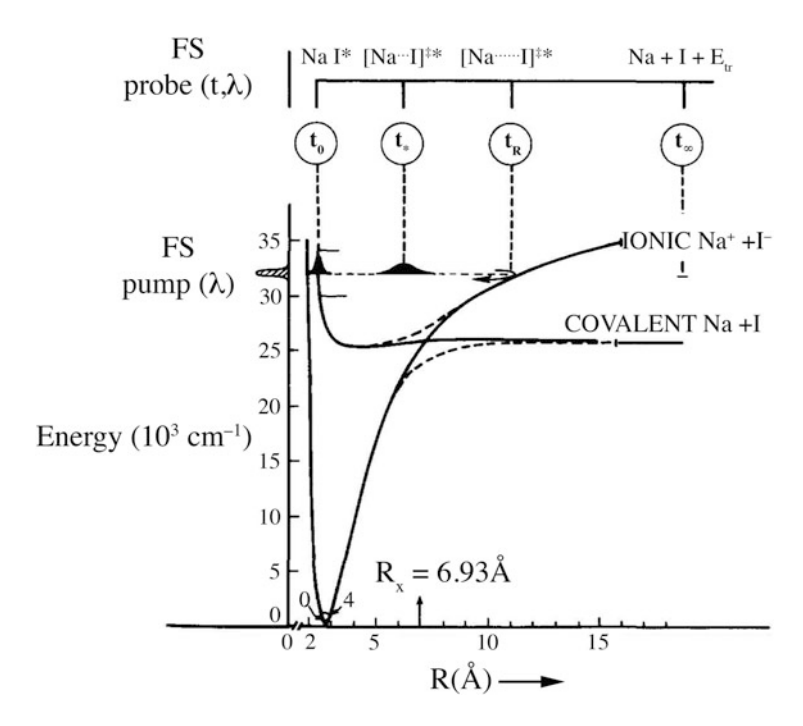


Fig. 6.5 Wavepacket transit through an ionic~covalent potential energy curve crossing in NaI (Fig. 1 of [23]). The diabatic (solid lines) Na⁺, I⁻ and Na, I potential energy curves cross at $R_x = 6.93$ Å. The avoided crossing between the adiabatic potential curves is shown as dashed lines. At $t = t_0$ the 310 nm pump pulse creates a wavepacket at the inner turning point of the covalent (Na ²S, I²P_{3/2}) potential curve at R \approx R_e(X¹ Σ ⁺) and P= 0. By adjusting the center wavelength of the pump pulse, the center total-energy (electronic plus vibrational) of the wavepacket can be adjusted between 30,000 and 34,000 cm⁻¹. The excitation energy of the ionic~covalent curve crossing is ~26,000 cm⁻¹. The wavepacket is accelerated outward, passes through the curve-crossing region at t_{\star} , and bifurcates, one part traveling on the bound ionic potential and the other part traveling irreversibly outward on the unbound covalent potential. The ionic part is reflected at t_R at the outer turning point of the ionic potential, passes with P< 0 through the R= 6.93 Å curve crossing region where it bifurcates again, and the resultant ionic and covalent parts are reflected outward at the inner turning points of the ionic and covalent potential curves, respectively. Each outward passage of a wavepacket through the curve crossing region results in a wavepacket traveling irreversibly outward on the unbound covalent potential, eventually forming free $Na(^2S)$ and $I(^2P_{3/2})$ atoms. The probe pulse (not shown) interrogates the dynamics by exciting Na(2S), I(2P_{3/2}) weakly-bound molecules to a higher energy repulsive electronic state that dissociates to $Na(^2P) + I(^2P_{3/2})$ atoms. Excitation at center-wavelength longer than 589 nm samples NaI molecules en route to full dissociation. Excitation centered at 589 nm provides what is essentially a time-integrated sample of the accumulation of the free Na(2S) atoms. Reproduced with permission from Fig. 1 in T.S. Rose, M.J. Rosker, and A.H. Zewail, "Femtosecond real-time observations of wave packet oscillations (resonance) in dissociation reactions," J. Chem. Phys. 88, 6672-6673 (1988). Copyright 1988, AIP Publishing LLC

96 Guantum Beats

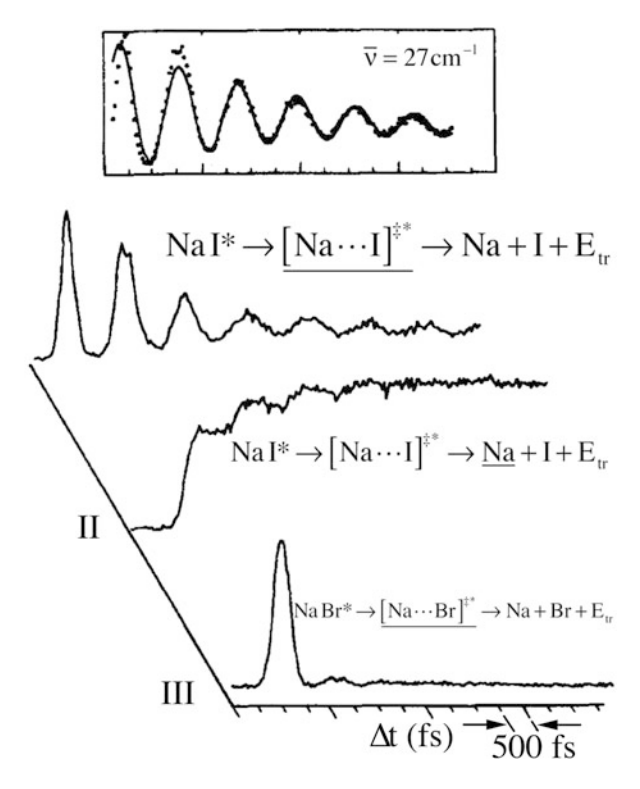


Fig. 6.6 Clocking of the photodissociation of NaI (and NaBr) as the nuclear wavepacket repeatedly traverses the ionic/covalent curve crossing (Fig. 2 of [23]). The wavepacket, illustrated in Fig. 6.5, is created at $t = t_0$ at the inner turning point on the covalent excited electronic state. At each outward-bound traversal of the curve-crossing region, part of the wavepacket follows the covalent adiabatic curve irreversibly outward to separated Na(2S) + I(2P_{3/2}) atoms. If the probe laser center-wavelength is tuned slightly to the red of the 589 nm free Na atom ${}^{2}P \leftarrow {}^{2}S$ transition, each time a wavepacket of incompletely separated Na, I molecules passes through the Optically Coupled Region, some not quite free Na atoms are excited to the ²P state, from which spontaneous fluorescence is detected. The series of Na atom fluorescence pulses shown in Spectrum I samples each outward passage of a wavepacket through the curve-crossing region. The temporal spacing of the pulses corresponds to a 36 cm⁻¹ vibrational frequency. When the center-wavelength of the probe laser is tuned to 589 nm, the arrivals of free Na atom wavepackets are displayed in Spectrum II as a periodic series of upward steps. Spectrum III shows that the (upper) adiabatic potential curve for NaBr is shallower and "leakier" than that for NaI. Reproduced with permission from Fig. 2 in T.S. Rose, M.J. Rosker, and A.H. Zewail, "Femtosecond real-time observations of wave packet oscillations (resonance) in dissociation reactions," J. Chem. Phys. 88, 6672–6673 (1988). Copyright 1988, AIP Publishing LLC

6.4 Dynamics 97

continue until each is reflected at the inner turning point of its respective potential energy curve.

Now there are two outward-traveling wavepackets, one $(1 - \alpha)^2$ with very large momentum traveling on the deeply bound diabatic ionic potential and one, $\alpha(1-\alpha)$, with much smaller momentum moving on the shallow and very nonharmonic covalent potential curve. The outward bound ionic wavepacket reaches the curve-crossing region first and bifurcates into ionic, $(1 - \alpha)^3$, and covalent, $\alpha(1-\alpha)^2$, parts. The outward bound covalent wavepacket, $\alpha(1-\alpha)$, arrives at the crossing region later and part of it, $\alpha(1-\alpha)^2$, continues on the covalent curve after this second outward passage through the crossing region. The extreme anharmonicity of the covalent curve causes the outward bound covalent wavepacket to dephase, spreading into an ignorable flux of free Na ²S atoms. This naïve analysis suggests that there will be two periodic outward traveling trains of wavepackets on the covalent potential curve, but only the covalent wavepackets generated at each outward passage of an ionic wavepacket through the curve-crossing region will form a periodic train of pulses of ground state Na atoms. The period of the pulse train should be related to the vibrational frequency of the (harmonic) diabatic ionic potential (\sim 27 cm⁻¹).

Similarly to the I–CN FTS experiment, the semi-free Na atoms are detected by Na atom $^2P \rightarrow ^2S$ spontaneous fluorescence excited by a time-delayed probe pulse. If the center energy of the probe pulse is resonant with the 589 nm Na $^2P \leftarrow ^2S$ excitation transition, then the signal intensity vs. pump/probe delay appears as a large initial step followed by a periodic sequence of smaller steps. If the center energy of the probe pulse is tuned slightly to the red of the 589 nm transition, then the fluorescence signal vs. probe delay is a periodic series of increasingly broad pulses. Each pulse reflects the leakage, at the potential energy curve-crossing, from the diabatic ionic electronic state into the diabatic covalent state. Systematic variation of the pump pulse center energy permits systematic variation of the velocity of the wavepacket in the curve-crossing region. Landau-Zener theory relates the crossing velocity to the ionic—covalent transfer probability, thereby providing a dynamical experimental measurement of the ionic—covalent electronic interaction matrix element.

It is important to remember that the impact of these revolutionary pump/probe Femtosecond Transition State experiments is based on the extreme simplicity of localized, cause-and-effect models. The concept of wavepackets is central to these experiments, because these particle-like states follow the laws of classical mechanics. This is where localization and causality come from. A wavepacket is a coherent superposition of the eigenstates and quasi-eigenstates that are familiar from the standard models of frequency-domain spectroscopy. Wavepackets are quantum beats on steroids!

98 6 Quantum Beats

6.5 Quantum Beats

6.5.1 Simple Two-Level Quantum Beats [1, 11, 12, 15]

Suppose we have two eigenstates, ψ_+ and ψ_- , that are orthogonal mixtures of the same two zero-order states, ϕ_0 and ϕ_1 ,

$$\psi_{+} = \alpha\phi_{0} + (1 - \alpha^{2})^{1/2}\phi_{1}$$

$$\psi_{-} = (1 - \alpha^{2})^{1/2}\phi_{0} - \alpha\phi_{1}$$
and
$$\phi_{0} = \alpha\psi_{+} + (1 - \alpha^{2})^{1/2}\psi_{-}$$

$$\phi_{1} = (1 - \alpha^{2})^{1/2}\psi_{+} - \alpha\psi_{-}$$
note that
$$\int |\psi_{+}|^{2}dx = \int |\psi_{-}|^{2}dx = 1 \quad \text{(normalization)}$$

$$\int \psi_{+}^{\star}\psi_{-}dx = 0 \quad \text{(orthogonality)}$$

Suppose ϕ_0 is bright and ϕ_1 is dark for the specific experimental setup. We want to express $\Psi(0) \equiv \phi_0$ as a linear combination of eigenstates, ψ_+ and ψ_- :

$$\Psi(0) \equiv \phi_0 = \alpha \psi_+ + (1 - \alpha^2)^{1/2} \psi_-$$
$$\phi_1 = (1 - \alpha^2)^{1/2} \psi_+ - \alpha \psi_-$$

thus, following the usual recipe,

$$\Psi(x,t) = \alpha \psi_{+} e^{-iE_{+}t/\hbar} + (1 - \alpha^{2})^{1/2} \psi_{-} e^{-iE_{-}t/\hbar}.$$

The time-dependent signal, S(t), from this $\Psi(x,t)$ in which only ϕ_0 is bright, is

Signal(t) =
$$S_0(t) = \left| \int dx \phi_0^* \Psi(t) \right|^2 = \left[\int dx \phi_0^* \Psi(t) \right] \left[\int dx \phi_0 \Psi(t)^* \right]$$

$$\int dx \phi_0^* \Psi(t) = \int dx \left[(\alpha^* \psi_+^*(x) + (1 - \alpha^2)^{1/2*} \psi_-^*(x)) \right]$$

$$\times (\alpha \psi_+ e^{-iE_+ t/\hbar} + (1 - \alpha^2)^{1/2} \psi_- e^{-iE_- t/\hbar} \right]$$

$$= |\alpha|^2 e^{-iE_+ t/\hbar} + |1 - \alpha^2| e^{-iE_- t/\hbar} + 0 + 0,$$

6.5 Quantum Beats 99

where ψ_+ and ψ_- are normalized and orthogonal. The $\int dx$ integrals get rid of $\psi_\pm(x)$ via orthonormality. Thus

$$\begin{split} S_0(t) &= \left[|\alpha|^2 e^{-iE_+t/\hbar} + |1 - \alpha^2| e^{-iE_-t/\hbar} \right] \left[|\alpha|^2 e^{iE_+t/\hbar} + |1 - \alpha^2| e^{iE_-t/\hbar} \right] \\ &= |\alpha|^4 + |1 - \alpha^2|^2 + |\alpha|^2 |1 - \alpha^2| \left[e^{-i(E_+ - E_-)t/\hbar} + e^{+i(E_+ - E_-)t/\hbar} \right] \\ &= |\alpha|^4 + |1 - \alpha^2|^2 + 2|\alpha|^2 |1 - \alpha^2| \cos \omega_{+-}t \\ &= \left(|\alpha|^2 + |1 - \alpha^2| \right)^2 + 2|\alpha|^2 |1 - \alpha^2| \left[\cos \omega_{+-}t - 1 \right], \end{split}$$

where $\omega_{+-}\equiv\frac{E_{+}-E_{-}}{\hbar}$ and $e^{i\omega_{+}-t}+e^{-i\omega_{+}-t}=2\cos\omega_{+}-t$. For compactness, replacing $|\alpha|^2$ by a and $|1-\alpha^2|$ by b, we have

$$S_0(t) = \underbrace{(a+b)^2}_{+1} - \underbrace{2ab[1-\cos_{+-}t]}_{>0 \text{ for all } t} \quad 0 \le a, b \le 1,$$

thus the condition for $S_0(t) > 0$ for all t is

$$4ab \le 1$$
$$4|\alpha^2| |1 - \alpha^2| \le 1.$$

The maximum value of the LHS is 1 when $\alpha^2 = \frac{1}{2}$. Note that $S_0(t) \ge 0$ for all time. The maximum modulation depth of $S_0(t)$ occurs when $\alpha = 2^{1/2}$.

$$S_{0,\text{max}}(t) = 1 + \frac{1}{2}[\cos \omega_{+-}t - 1] = \frac{1}{2} + \frac{1}{2}\cos \omega_{+-}t = \frac{1}{2}(1 + \cos \omega_{+-}t)$$

which oscillates between 1 and 0.

$$S_0(t) = \frac{1}{4} + 1 + \frac{1}{4} - 1 + \frac{1}{2}\cos\omega_{+-}t = \frac{1}{2}[1 + \cos\omega_{+-}t]$$
 Never negative!

We have considered a two-level problem that incorporates two major simplifications (Fig. 6.7):

- One basis state is perfectly dark and the other is perfectly bright. This is actually something we want to arrange in the design of the experiment. The above example gives a 100 % modulated bright/dark QB, which is bright at t=0. Sometimes we have a setup where one basis state is dark as far as excitation is concerned and bright as far as detection is concerned and the situation is reversed for the other basis state. Then we get a 100 % bright/dark QB, but dark at t=0 and bright at $t=(2n+1)\pi/\omega_{+-}$ [10].
- We have not considered decay rates. In the usual limit of two quasi-eigenstates, which may be considered narrow relative to the interaction matrix element

100 6 Quantum Beats

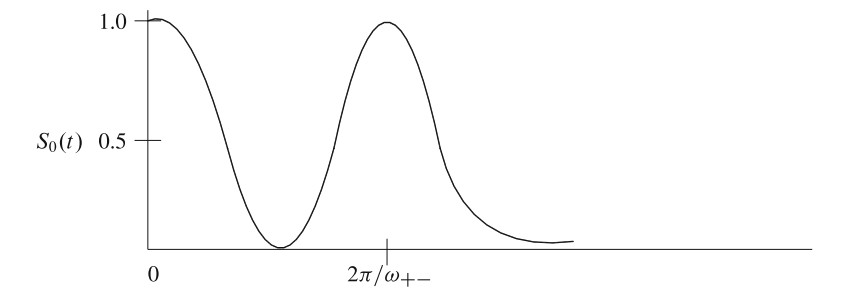


Fig. 6.7 A two-level quantum beating system with 100 % modulation depth. Maximum modulation depth occurs when the two eigenstates, ψ_+ and ψ_- , are 50,50 mixtures of the bright and dark states, ψ_0 and ψ_1 ($|\alpha| = 2^{-1/2}$)

between them (the "strong coupling" limit), we can simply use ordinary perturbation theory where the diagonal energies are treated as complex.

6.5.2 Two-Level Treatment of QB with Complex Energies [14]

Level width (FWHM) of Lorentzian, Γ (energy units)

$$\Gamma = \frac{\hbar}{\tau}$$
.

 τ is the lifetime of the level.

We redefine the energy of state j to have a real and an imaginary part

$$E_i = \varepsilon_i - i \Gamma_i / 2$$

so that an eigenstate with complex E_i decays

$$e^{-iE_{jt}/\hbar} = e^{-i\varepsilon_{jt}/\hbar} e^{-i(-i\Gamma_{jt}/2\hbar)}$$
$$= e^{-i\varepsilon_{jt}/\hbar} e^{-\Gamma_{jt}/2\hbar}.$$

The probability of finding the system in this state is

$$\int dx \Psi_j^{\star}(x,t) \Psi_j(x,t) = \left[\int dx |\psi_j|^2 \right] e^{-\Gamma_{jt}/\hbar} = e^{-t/\tau_j}$$

where the lifetime, τ_i , is

$$\tau_j = \frac{\hbar}{\Gamma_j},$$

6.5 Quantum Beats 101

thus the probability of finding the system in state j decays exponentially from 1 at t = 0 toward 0 as $t \to \infty$, with a "lifetime", τ_i .

This addition of a time decaying factor to $\Psi(x,t)$ is not entirely ad hoc. See [14] for a more complete discussion of the complex-E Hamiltonian.

For the ordinary two-level problem (no decay)

$$\mathbf{H} = \begin{pmatrix} \overline{\varepsilon} & 0 \\ 0 & \overline{\varepsilon} \end{pmatrix} + \begin{pmatrix} \delta \varepsilon & V \\ V & -\delta \varepsilon \end{pmatrix}$$
$$\overline{\varepsilon} \equiv \frac{\varepsilon_0 + \varepsilon_1}{2}$$
$$\delta \varepsilon \equiv \frac{\varepsilon_0 - \varepsilon_1}{2}.$$

The eigenvalues are

$$E_{\pm} = \overline{\varepsilon} \pm [\delta \varepsilon^2 + V^2]^{1/2}$$

and the eigenstates are

$$\begin{split} \psi_{+} &= \alpha_{-}\phi_{0} + \alpha_{+}\phi_{1} = (1 - \alpha_{+}^{2})^{1/2}\phi_{0} + \alpha_{+}\phi_{1} \\ \psi_{-} &= -\alpha_{+}\phi_{0} + (1 - \alpha_{+}^{2})^{1/2}\phi_{1} \\ \alpha_{\pm} &= \pm 2^{-1/2} \left[1 \pm \frac{\delta \varepsilon}{2|V|} \right]. \end{split}$$

Since, in order to go from $\Psi(0)$ to $\Psi(t)$, we are going to want to write $\Psi(0)$ in terms of the bright state, ϕ_0 , which in turn is expressed in the ψ_{\pm} eigenstate basis, we have

$$\phi_0 = \alpha_+ \psi_+ + \alpha_- \psi_-$$

$$\phi_1 = -\alpha_- \psi_+ + \alpha_+ \psi_-.$$

Now making the energies complex (and remaining in the "strong coupling" limit), we have

$$E_{\pm} = \left[\overline{\varepsilon} \pm \delta \varepsilon \left(1 + \frac{V^2/2}{\delta \varepsilon^2 + \delta \Gamma^2/4} \right) - i \left[\overline{\Gamma}/2 \pm \frac{\delta \Gamma}{2} \left(1 - \frac{V^2/2}{\delta \varepsilon^2 + \delta \Gamma^2/4} \right) \right] \right]$$
 real part imaginary part

where

$$\overline{\Gamma} = \frac{\Gamma_+ + \Gamma_-}{2}$$

102 6 Quantum Beats

$$\begin{split} \delta\Gamma &= \frac{\Gamma_{+} - \Gamma_{-}}{2} \\ \alpha_{\pm} &= \pm 2^{-1/2} \left(1 \pm \frac{\delta \varepsilon - i \delta \Gamma/4}{2|V|} \right) \\ \Psi_{0}(t,x) &= \phi_{0} = \alpha_{+} \psi_{+} e^{-i \varepsilon_{+} t/\hbar} e^{-\Gamma_{+} t/2\hbar} + \alpha_{-} \psi_{-} e^{-i \varepsilon_{-} t/\hbar} e^{-\Gamma_{-} t/2\hbar}. \end{split}$$

To calculate the decay of the time-evolving state we write

$$S(t) = \left| \left\langle \tilde{\Psi}_{0}(0) | \Psi_{0}(t) \right\rangle \right|^{2} = \int dx \left| \left(|\alpha_{+}^{2}| |\psi_{+}|^{2} e^{-iE_{+}t/\hbar} + |\alpha_{-}|^{2} |\psi_{-}|^{2} e^{-iE_{-}t/\hbar} \right) \right| + \left| \left(\alpha_{+}^{\star 2} |\psi_{+}|^{2} e^{+iE_{+}^{\star}t/\hbar} + \alpha_{-}^{\star 2} |\psi_{-}|^{2} e^{+iE_{-}^{\star}t/\hbar} \right) \right|,$$

the integration over x causes the wavefunction terms $|\psi_+|^2$ and $|\psi_-|^2$ to integrate to 1.

Putting in the complex E_{\pm} results in

$$S_0(t) = |\alpha_+|^4 e^{-\Gamma_+ t/\hbar} + |\alpha_-|^4 e^{-\Gamma_- t/\hbar} + \alpha_+^2 \alpha_-^{*2} e^{-i(E_+ - E_-)t/\hbar} + \alpha_-^2 \alpha_+^{*2} e^{-i(E_- - E_+)t/\hbar}.$$

With a lot more algebra (in which the complex E_{\pm} are explicitly expressed in terms of ε_{+} and Γ_{+}) we have

$$S_{0}(t) = I_{+}e^{-\Gamma_{+}t/\hbar} + I_{-}e^{-\Gamma_{-}t/\hbar} + e^{-\Gamma_{QB}t/\hbar}[2\operatorname{Re}(\alpha_{+}^{2}\alpha_{-}^{\star 2})\cos\omega_{QB}t$$
$$-2\operatorname{Im}(\alpha_{+}^{2}\alpha_{-}^{\star 2})\sin\omega_{QB}t]$$
$$= I_{+}e^{-\Gamma_{+}t/\hbar} + I_{-}e^{-\Gamma_{-}t/\hbar} + e^{-\Gamma_{QB}t/\hbar}[I_{QB}\cos(\omega_{QB}t + \phi_{QB})],$$

where

$$\begin{split} I_{QB} &= 2|\alpha_+^2 \alpha_-^{\star 2}| \\ \omega_{QB} &= \frac{\varepsilon_+ - \varepsilon_-}{\hbar} \\ \phi_{QB} &= \tan^{-1} \frac{\mathrm{Im}(\alpha_+^2 \alpha_-^{\star 2})}{\mathrm{Re}(\alpha_+^2 \alpha_-^{\star 2})} \end{split}$$

[†]The tilde on Ψ_0 is a consequence of biorthogonality required to maintain normalization and orthogonality for eigenfunctions of complex-energy effective Hamiltonian systems (see p. 676 of H. Lefebvre-Brion and R.W. Field, "The Spectra and Dynamics of Diatomic Molecules," Elsevier, 2004).

6.5 Quantum Beats 103

$$I_+ = |\alpha_+|^4$$
$$I_- = |\alpha_-|^4.$$

Now everything is expressed in terms of α_+ and α_- , which in turn are expressed in terms of

$$\overline{\varepsilon}$$
, $\delta \varepsilon$, $\overline{\Gamma}$, $\delta \Gamma$, and V .

Everything in S(t) is expressed in terms of the *five* above parameters! Yet $S_0(t)$ is expressed in terms of *eight* measurable properties: I_+ , I_- , I_{QB} , ω_{QB} , ϕ_{QB} , Γ_+ , Γ_- , and Γ_{QB} . It should be clear that we do not need to perform a least squares fit to $S_0(t)$ in which all eight parameters are allowed to vary freely. There are only five degrees of freedom, some of which can be accurately determined at t=0.

This has been a long exercise designed to show that quantum beats can have a very complicated S(t), but that much of the complexity is gratuitous. The many experimentally observable parameters that describe the appearance of S(t) are parsimoniously determined by a smaller number of physical parameters. This is always true, even for systems that involve more than two interacting states. In fact, the advantages of a fit based on *physical* parameters rather than the standard set of *empirical descriptive* parameters increases when there are more than two interacting zero-order states.

6.5.3 What Does a Quantum Beat Signal Look Like? [26]

The time-dependent fluorescence signal is

$$I(t) = \sum_{\substack{i \text{ eigenstates}}} \left[b_i e^{-t/\tau_i} + \sum_{\substack{j \neq i \text{ eigenstates}}} c_{ij} \cos(\omega_{ij}t + \delta_{ij}) e^{-t/\tau_{ij}} \right].$$

If the different emission frequencies are not spectrally resolved, we need (b_i, τ_i) , the intensity and decay rate parameters for each populated excited eigenstate and $(c_{ij}, \omega_{ij}, \delta_{ij}, \tau_{ij})$, the intensity, frequency, phase, and decay rate for each quantum-beating pair of coherently excited eigenstates. It is easy to determine $(c_{ij}, \omega_{ij}, \delta_{ij}, \alpha_{ij}, \delta_{ij})$, and τ_{ij} for every quantum-beating level-pair, precisely because each pair has a unique $\cos(\omega_{ij}t)$ signature in the fluorescence. It is quite difficult to extract all of the (b_i, τ_i) pairs, because the fluorescence for each of the i eigenstates forms a multi-exponential decay that cannot be fitted to a unique model. Each of the fit parameters is dependent on some sort of adjustable "control" parameter in the \mathbf{H}^{eff} . In fact, it is our goal to determine values of many parameters in the \mathbf{H}^{eff} , and information about these physical parameters in the \mathbf{H}^{eff} is obtained from the observed dependence on

104 6 Quantum Beats

the empirical parameters that determine the exact form of I(t). This seems to be hopelessly complicated, but it is not!

It is possible to explicitly relate all of the fit parameters $(b_i, \tau_i, c_{ii}, \omega_{ii}, \omega_{ii})$ δ_{ii} , τ_{ii} for many i and j) to the relatively small number of parameters in the \mathbf{H}^{eff} and the explicit dependence of these parameters in the \mathbf{H}^{eff} on the control parameter. This control parameter could be anything that changes the relative energies and corresponding eigenvectors of Heff. Typical control parameters are magnetic field strength (B_Z) , electric field strength (E_Z) , and rotational quantum number (J). B_Z , E_Z , and J have the effect of tuning the relative energies of the zero-order states, systematic turning off of selection rules, and modification of the magnitudes of off-diagonal matrix elements in Heff. For example, the Zeeman effect modifies the diagonal matrix elements of Heff $\left(E_i \propto B_Z \frac{M\Omega}{J(J+1)} \text{ for } \Delta M = 0, \Delta\Omega = 0, \Delta J = 0 \text{ diagonal matrix elements}\right)$ one JM level can be tuned into degeneracy with another J'M' level. The Zeeman effect has off-diagonal matrix elements following the selection rules $\Delta J = 0, \pm 1,$ $\Delta M = 0$, and parity $+ \not \rightarrow -$, which are especially important for interactions among the J-components of one N value of a case (b) $^3\Sigma$ state. The Stark effect destroys parity and J, so it might turn on an off-diagonal interaction between two neardegenerate opposite-parity levels (e.g., Λ -doublet components) that cannot perturb each other at zero field. If there are two near degenerate same-J levels that belong to two electronic-vibration states that have different B-values, then changing J serves to step-wise tune the levels of one vibronic state through degeneracy with those of the other vibronic state. All of these mechanisms can give rise to a diagnostically explicit variation of the parameters in I(t).

6.5.4 Population Quantum Beats [8]

The favorite example is a bright singlet state perturbed by an accidentally degenerate dark triplet state (Fig. 6.8).

As a function of J we often find that there is a level crossing of same-J singlet and triplet levels (Fig. 6.9).

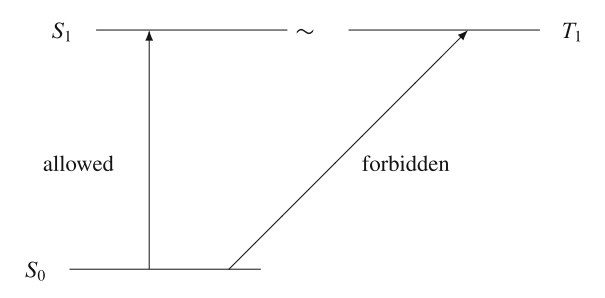


Fig. 6.8 A bright singlet state perturbed by an accidentally degenerate dark triplet state

6.5 Quantum Beats 105

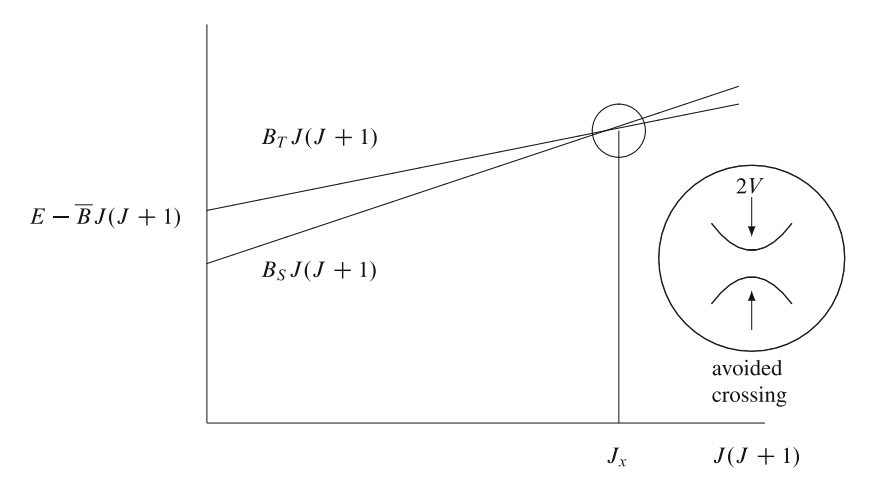


Fig. 6.9 Reduced term value plot. A bright singlet level can be crossed, at J_x , by a dark triplet level

 \overline{B} is some typical B value that provides a convenient expansion of the vertical energy scale.

Suppose the spin-orbit interaction matrix element is so small that, at closest approach of the two levels (at J_x), the $S_1(J_x)$ and $T_1(J_x)$ levels are so close together that *both* higher- and lower-energy mixed eigenstates can be "covered" by a short laser pulse. The usual intuitive picture is that the system starts out completely in the bright $(S_1(J_x))$ state and "goes" to the dark triplet $(T_1(J_x))$ and returns. This is dynamics in state space. The fluorescence seems to oscillate from full-on to full-off

$$\Psi_{J_x}(t=0) = \phi_{S_1(J_x)}.$$

If you look at the Quantum Beats at the exact point of smallest energy separation between same-J eigenstates, then

$$\Psi(0) = \phi_{S_1}$$

$$\phi_{S_1} = 2^{-1/2} [\psi_+ + \psi_-]$$

$$E_+ = \overline{E} \pm V.$$

This is a 50:50 mixed state.

Each of the two states has $50 \% S_1$ character

$$au_{+} = au_{-} = 2 au_{S_{1}}^{(0)}$$
 $au_{QB} = 2 au_{S_{1}}^{(0)}$

106 6 Quantum Beats

$$E_{+} - E_{-} = 2V, \ \omega_{+-} = \frac{2V}{\hbar}$$

$$I_{+} = I_{-} = I_{S_{1}}^{(0)} / 2$$

$$I_{QB} = I_{S_{1}}^{(0)} / 2$$

$$\phi_{QB} = 0$$

$$S(t) = \left(I_{S_{1}}^{(0)} / 2\right) e^{-t/2\tau_{S_{1}}^{(0)}} \cos(2Vt/\hbar).$$

You can detect this 100 % modulation of the fluorescence by viewing *unpolarized* fluorescence. The fractional oscillation is not affected by any choice of detection propagation direction and/or polarizer orientation.

As one tunes J (or B_Z or E_Z) away from the exact level crossing, the mixing is no longer 50:50. You see a quantum beat tuning toward higher frequency but with decreased amplitude. You also see non-modulated exponentially decaying fluorescence at τ_+ and τ_- . Everything is exactly calculable from $\tau_{S_0}^{(0)}$, \overline{E} , δE , and V.

It is also possible to observe population quantum beats between near degenerate hyperfine energy levels. The requirement that two upper-state eigenstates be populated from a common lower-level eigenstate is normally not met because of the strong $\Delta F = \Delta J$ propensity rule. However, when the angular momentum coupling cases for the upper and lower electronic states are *not* the same, then it will often be possible to excite two F' levels of the upper J' hypermultiplet from one J'', F'' hyperfine component of the lower state. Note that no quantum beats will be observable if two J', F' hyperfine components are individually excited from two J'', F'' hyperfine components. A very common case for hfs Quantum Beats is for a transition between a case (a) Π -state and a case (b) Σ -state.

The metaphor used to describe population quantum beats is that the excited molecule is born in the state that the $\Delta S = 0$ selection rule specifies and then it oscillates back and forth between the singlet and triplet state spaces. This seems easy to understand. Suppose instead we had the option of exciting from the S_0 ground state but observing fluorescence to a lower-lying triplet state (Fig. 6.10):

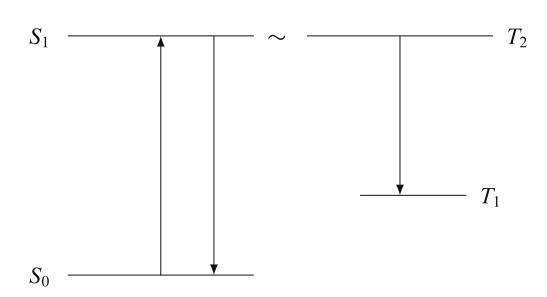


Fig. 6.10 Quantum beats detected in fluorescence to a lower-lying triplet state

6.5 Quantum Beats 107

Then the QBs will start out at their minimum intensity at t=0 and oscillate π out-of-phase with the QBs that are observed when the fluorescence is detected into S_0 rather than into T_1 . This is also easy to understand.

6.5.4.1 Polarization Quantum Beats [5]

Polarization Quantum Beats seem different from Population Quantum Beats, but they can be viewed in the same simplified way that we understand Population Quantum Beats.

Recall that the ΔM selection rule for electric dipole transitions is $\Delta M = 0$ for Z-polarized excitation and fluorescence, $\Delta M = +1$ and -1 for X or Y polarized excitation and fluorescence. This focuses on quantum numbers rather than the initial lab frame orientation of the molecule-frame electric dipole transition moment: is it along the X or the Y axis? The molecules know the difference between X and Y, but we tend to forget to think about excitation and fluorescence in this way. If you excite with linear polarization along X, then the molecules with their body frame transition moment initially along lab X are preferentially excited. So at t=0, the fluorescence is exclusively polarized along the lab-X axis. There are no excited molecules with their transition moment along lab-Y. In the presence of an electric or magnetic field along the Z-axis, the molecular body-fixed dipole rotates about the laboratory Z axis. So the transition dipole rotates too, from along X at t = 0 to along Y at $\frac{1}{4}$ of a precession period later. So if you excite X polarized and detect through a Y polarizer, the fluorescence intensity oscillates from small to large (rather than from large to small), as it would have if you had detected X polarized radiation. This seems identical to population beats. The only difference is that you need to think about optimum use of polarizers to detect polarization quantum beats.

6.5.4.2 Direction Cosine Matrix Element Based Picture of Polarization Quantum Beats

You can use an entirely matrix element-based picture to understand polarization quantum beats. If you look at a table of Direction Cosine Matrix elements (which relate the body-fixed coordinates to laboratory-fixed coordinates) [27], then you see that $\Delta M = +1$ transitions correspond to X and iY and $\Delta M = -1$ transitions correspond to X and X an

$$\frac{1}{2}(X+iY) \leftrightarrow \mathbf{R}_+, \quad \frac{1}{2}(X-iY) \leftrightarrow \mathbf{R}_-.$$

Thus

$$\mathbf{R}_+ + \mathbf{R}_- \leftrightarrow X$$
 and $\frac{1}{i}(\mathbf{R}_+ - \mathbf{R}_-) \leftrightarrow Y$.

108 6 Quantum Beats

So X polarized excitation from the $|JM\rangle$ initial state yields $|J', M+1\rangle + |J'M-1\rangle$ and Y-polarized excitation yields $|J', M+1\rangle - |J'M-1\rangle$. The molecule remembers whether it was excited along X or Y by the relative signs of the $|J'M+1\rangle$ and $|J'M-1\rangle$ states. Since, in a magnetic field, these two states do *not* have the same energy, their *relative phase* oscillates at twice the Larmor frequency, ω_L . So at $t=\frac{\pi}{2\omega_L}$, the coherent superposition state initially polarized along X is now polarized along Y and that initially polarized along Y is now polarized along Y. Several excitation and detection cases are:

• Excite X-polarized, detect X-polarized

$$I_{QB}^{XX}(t) = I^{\circ} \cos \omega_L t$$

Excite X-polarized, detect Y-polarized

$$I_{OB}^{XY}(t) = I^{\circ} \cos(\omega_L t - \pi/2)$$

• Excite X-polarized, detect unpolarized fluorescence propagating along X-axis

$$I_{QB}^{X,YZ}(t) = \frac{1}{2}I^{\circ}\cos(\omega_L t - \pi/2) + \frac{1}{2}I^{\circ}$$

Excite X-polarized, detect unpolarized fluorescence propagating along Z-axis

$$I_{OB}^{X,XY}(t) = I^{\circ}$$
 (no modulation) [WHY?]

6.5.4.3 Zeeman vs. Stark Polarization Quantum Beats [6, 7]

The basic idea is that you must create a coherent superposition of two or more M states in order to create a time-evolving $\Psi(t)$ that gives rise to quantum-beating fluorescence. The simplest case is $\Delta M = \pm 2$ coherence, which is accomplished with light polarized \perp to the external static field direction (Fig. 6.11).

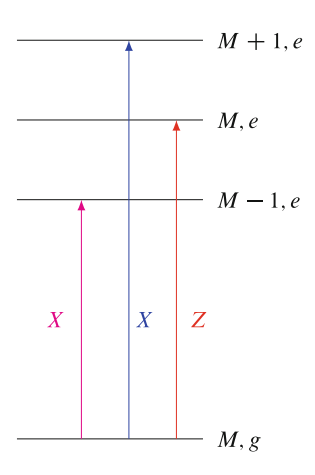
This scheme is especially simple for the case of low-field Zeeman Quantum Beats [6] because, for a given-J, the $E_{J,M-1} - E_{J,M+1}$ energy spacing is identical for all M (except at very high magnetic field strength). The frequency of the quantum beats is

$$E_{QB}/h = 2\mu_0(\Lambda + 2\Sigma)\frac{\Omega}{J(J+1)}, \quad J \ge 1/2$$

where μ_0 is the Bohr magneton (1,400 MHz/Gauss), the 2 is because the Quantum Beat is $\Delta M=2$, the factor ($\Lambda+2\Sigma$) assumes Hund's case (a), which is valid at low-J in almost all $\Lambda>0$ states (and gives zero Zeeman splitting for ${}^2\Pi_{1/2}$, ${}^3\Delta_1$ etc. states), and Ω is a reminder that there is no electronic (as opposed to nuclear) Zeeman effect for ${}^1\Sigma^{\pm}$, ${}^3\Pi_0$, ${}^5\Delta_0$ states. The $\frac{1}{I(I+1)}$ factor comes from $\Delta J=0$,

6.5 Quantum Beats 109

Fig. 6.11 Polarized excitation with linearly polarized radiation



 $\Delta M = 0$ direction cosine matrix elements and implies that low-J ($J \neq 0$) levels are best for Zeeman Quantum Beat studies.

The Stark effect is different from the Zeeman effect in two *very* important ways [7]. For the Zeeman effect, $E_{J,M} - E_{J,-M} \neq 0$, but for the Stark effect, $E_{J,M} = E_{J,-M}$. This means that the largest Stark Quantum Beat in Σ states is in J=1 for odd-multiplicity S>0 Σ states and in J=3/2 for even-multiplicity Σ states. The second difference between SQB and ZQB is that, for SQB, the $E_{J|M|} - E_{J|M+1|}$ energy differences are dependent on |M|. It is often easy to overcome this inconvenience for SQBs. All $\Lambda>0$ states have small parity splittings, with the result that, at modest electric field strength, parity is destroyed and one gets a linear Stark effect. Such SQBs behave essentially identical to ZQBs.

For ${}^1\Sigma^\pm$ and ${}^3\Sigma^\pm$ states, the best J-level for SQB is J=1 (especially the J=1, N=0 level for ${}^3\Sigma$ states). However, in J=1 there are only two energetically distinct Stark components, M=0 and |M|=1. So it is necessary to use light polarized at 45° relative to the Z-axis. This gives $2^{-1/2}$ relative transition amplitude for X- or Y-polarized $\Delta M=\pm 1$ excitation and $2^{-1/2}$ relative transition amplitude for Z-polarized $\Delta M=0$ excitation. You create an M=0, M=+1 and an M=0, M=-1 coherent superposition state. These two pairs of superposition states have the same beat frequency, so if they begin evolution in-phase, they stay in-phase for all t. If however, you were to choose an excitation and detection geometry where the two coherences start out π out-of-phase, there will be no QB unless the detection geometry is blind to either the J, M=0, +1 or the 0, -1 coherence.

If you use light propagating along the Y axis, its linear polarization must lie in the XZ plane. Polarization at $+45^{\circ}$ relative to the Z axis gives equal projections along the Z and -X axes. Detection of $|\Delta M|=1$ SQB requires collecting light propagating in the XY plane and with polarization at $\pm 45^{\circ}$ relative to the Z-axis. There is no choice of propagation direction that gives an SQB without use of a linear polarizer. The sign and amplitude of the SQB signal depend on the choice of propagation direction for the detected fluorescence and on the $+45^{\circ}$ vs. -45° orientation of the linear polarizer.

110 6 Quantum Beats

6.5.5 Level-Crossing vs. Anticrossing [2, 28]

If it is possible to cause two levels, which are excited from a common initial state, to tune through degeneracy without interaction via any non-zero off-diagonal matrix element of the $\mathbf{H}^{\mathrm{eff}}$, then the detected QB is a "level-crossing" QB. For example, two states of different J and different M will tune through degeneracy without level-repulsion and mixing. One example is: excitation from J''M'' to J' = J'' + 1, M' and J' = J'' - 1, M'. For J-tuned or Zeeman-tuned levels, any two levels of opposite parity will tune through degeneracy without interacting, but such a pair of levels can never be excited from a common initial level unless the parity of the initial level is destroyed (e.g. a $\Lambda > 0$ state) by an electric field, while the opposite parities of the final pair of crossing levels are not compromised by the electric field. What would be observed is a very weakly avoided level crossing. Two levels of opposite parity could be excited from a common level if one level is populated via a very weak magnetic dipole transition moment, μ^m , and the other via an electric dipole transition moment, μ^e . The (small) amplitude of the Quantum Beat would provide a measure of the ratio of μ^m to μ^e .

The Quantum Beats associated with level anti-crossings are most useful for measuring the off-diagonal matrix element in the effective **H** that is responsible for the level repulsion at the anti-crossing. The strength of the interaction is directly measured by 1/2 the minimum of the v_{QB} vs. the control parameter. The interaction strength is indirectly sampled by the fractional modulation depth of the QB in the vicinity of the level crossing.

References

- H. Lefebvre-Brion, R.W. Field, The Spectra and Dynamics of Diatomic Molecules (Elsevier, Amsterdam, 2004), pp. 430–434
- 2. M. Lombardi, Excited States: Rotational Effects on the Behaviour of Excited Molecules, vol. 7 (Academic, San Diego, 1988), p. 163
- 3. E. Hack, J.R. Huber, Int. Rev. Phys. Chem. 10, 287 (1991)
- 4. S. Haroche, J.A. Paisner, A.L. Schawlow, Phys. Rev. Lett. 30, 948 (1973)
- 5. H. Lefebvre-Brion, R.W. Field, *The Spectra and Dynamics of Diatomic Molecules*, Sect. 9.21 (Elsevier, Amsterdam, 2004)
- 6. G. Gouedard, J.C. Lehmann, Faraday Discuss. R. Soc. 71, 11 (1981)
- 7. H.S. Schweda, A. Renn, H. Büssener, A. Hese, Chem. Phys. 98, 157 (1985)
- 8. H. Lefebvre-Brion, R.W. Field, *The Spectra and Dynamics of Diatomic Molecules*, Sect. 9.2.2 (Elsevier, Amsterdam, 2004)
- 9. E. Abramson, C. Kittrell, J.L. Kinsey, R.W. Field, J. Chem. Phys. 76, 2293 (1982)
- 10. P.M. Felker, A.H. Zewail, Phys. Rev. Lett. 53, 501 (1984)
- 11. H. Lefebvre-Brion, R.W. Field *The Spectra and Dynamics of Diatomic Molecules*, Sect. 9.1.2 (Elsevier, Amsterdam, 2004)
- 12. H. Lefebvre-Brion, R.W. Field, *The Spectra and Dynamics of Diatomic Molecules* (Elsevier, Amsterdam, 2004), p. 635
- 13. H. Lefebvre-Brion, R.W. Field, *The Spectra and Dynamics of Diatomic Molecules* (Elsevier, Amsterdam, 2004), p. 636

References 111

14. H. Lefebvre-Brion, R.W. Field, *The Spectra and Dynamics of Diatomic Molecules*, Sect. 9.3 (Elsevier, Amsterdam, 2004)

- 15. H. Lefebvre-Brion, R.W. Field, *The Spectra and Dynamics of Diatomic Molecules*, Sect. 9.1.1 (Elsevier, Amsterdam, 2004)
- A. Zewail, Femtochemistry: Atomic-scale dynamics of the chemical bond using ultrafast lasers (Nobel lecture). Angew. Chem. Int. Ed. Engl. 39, 2586 (2000)
- C. Cohen-Tannoudj, B. Diu, F. Laloë, Quantum Mechanics, (Wiley, New York, 1977), pp. 240–244
- H. Lefebvre-Brion, R.W. Field, The Spectra and Dynamics of Diatomic Molecules, Sects. 5.1.1 and 7.6 (Elsevier, Amsterdam, 2004)
- 19. J. Tellinghuisen, J. Mol. Spectrosc. **103**, 455 (1984)
- 20. M. Dantus, M.J. Rosker, A.H. Zewail, J. Chem. Phys. 87, 2395 (1987)
- 21. M.J. Rosker, M. Dantus, A.H. Zewail, J. Chem. Phys. 89, 6113 (1988)
- 22. M. Dantus, M.J. Rosker, A.H. Zewail, J. Chem. Phys. 89, 6128 (1988)
- 23. T.S. Rose, M.J. Rosker, A.H. Zewail, J. Chem. Phys. 88, 6672 (1988)
- H. Lefebvre-Brion, R.W. Field The Spectra and Dynamics of Diatomic Molecules, Sect. 9.2.3.1 (Elsevier, Amsterdam, 2004)
- 25. R.K. Preston, C. Sloane, W.H. Miller, J. Chem. Phys. 60, 4961 (1974)
- H. Lefebvre-Brion, R.W. Field, The Spectra and Dynamics of Diatomic Molecules, Sect. 9.3.2 (Elsevier, Amsterdam, 2004)
- J.T. Hougen, The Calculation of Rotational Energy Levels and Rotational Line Intensities in Diatomic Molecules. NBS Monograph, vol. 115 (U.S. Government Printing Office, Washington, 1970)
- 28. H. Lefebvre-Brion, R.W. Field, *The Spectra and Dynamics of Diatomic Molecules*, Fig. 9.10 (Elsevier, Amsterdam, 2004)

Chapter 7 The Effective Hamiltonian for Polyatomic Molecule Vibration

7.1 The Effective Vibrational Hamiltonian for Polyatomic Molecules

The vibrational Hamiltonian may be expressed in a basis set consisting of products of harmonic oscillators, one oscillator for each of the 3N-6 normal modes, where N is the number of atoms in the molecule. The matrix elements of integer powers of momentum, P, and displacement Q, have very simple selection rules and quantum number scaling properties. The simplicity of the problem is best displayed and exploited using the properties of creation and annihilation operators, \mathbf{a}^{\dagger} and \mathbf{a} [1, 2]. Once the matrix elements for one anharmonic oscillator have been worked out, the rules for matrix elements and selection rules for matrix elements of products of harmonic oscillator basis states will be presented [2]. There is a special case where ordinary non-degenerate perturbation theory fails: when the offdiagonal matrix element is large relative to the zero-order energy difference between product basis states. This requires setting up and diagonalizing a small dimension effective Hamiltonian. Usually degeneracies are systematic, not accidental. When the harmonic oscillator frequencies for several normal modes are in near-integer multiple ratios, one gets polyads [2-4]. Polyads describe, via quantum number scaling rules for off-diagonal matrix elements, the fastestintramolecular dynamics as well as the expected frequency and intensity patterns in the frequency domain vibrational spectrum [5]. By expressing unconventional but robust patterns, polyads provide a basis for spectral assignment, a description of the mechanisms of Intramolecular Vibrational Redistribution (IVR) [5, 6], and characterization of the transition state for Unimolecular Isomerization [7, 9].

7.2 Harmonic Oscillator

For a diatomic molecule, where the atoms have masses m_1 and m_2

$$\mathbf{H} = \mathbf{T} + \mathbf{V}(\mathbf{Q}) = \frac{\mathbf{P}^2}{2\mu} + \frac{1}{2}k\mathbf{Q}^2$$

where $\mu = \frac{m_1 m_2}{m_1 + m_2}$ is the reduced mass and k is the force constant. Eigenfunctions are well known, but you only need to know some easily remembered facts about them:

- · largest amplitude near turning points
- odd/even symmetry
- there are v internal nodes, more closely spaced near Q=0 (node spacing is de Broglie $\lambda(Q)/2=\frac{h}{2P(Q)}$)

•
$$E_v = (hc) \frac{1}{2\pi c} [k/\mu]^{1/2} (v + 1/2)$$

7.2.1 Matrix Elements of P and Q[1]

Real potential energy curves are not simple parabolas. They are expressed as a sum of anharmonic terms, \mathbb{Q}^n , with integer n > 2

$$\mathbf{V}(\mathbf{Q}) = \frac{1}{2}k\mathbf{Q}^2 + \sum_{n=3}^{n_{\text{max}}} a_n \mathbf{Q}^n$$

In order to construct the effective Hamiltonian, we need to evaluate matrix elements of \mathbf{P}^2 , \mathbf{Q}^2 , \mathbf{Q}^3 , \mathbf{Q}^4 , etc. We do this very often, so it is a good idea to develop shortcuts and ways to see the universal relationships between oscillators with different values of μ and k.

7.2.2 Dimensionless Forms: \hat{H} , \hat{Q} , \hat{P} [1, 2]

The first step is to go to dimensionless **Q** and **P** operators. You probably remember that the matrix elements of **Q** and **P** are

$$\langle v + 1 | \mathbf{Q} | v \rangle = \langle v | \mathbf{Q} | v + 1 \rangle = 2^{-1/2} \left[\frac{\hbar}{2\pi c \mu \omega} \right]^{1/2} (v + 1)^{1/2}$$

 $\langle v + 1 | \mathbf{P} | v \rangle = -\langle v | \mathbf{P} | v + 1 \rangle = i 2^{-1/2} \left[\hbar 2\pi c \mu \omega \right]^{1/2} (v + 1)^{1/2},$

7.2 Harmonic Oscillator 115

where c is the speed of light, μ is the reduced mass, and ω is the harmonic frequency in cm^{-1} units. The selection rule for nonzero matrix elements of \mathbf{Q} and \mathbf{P} is $\Delta v = \pm 1$ only. This seems simple and memorable, but I am about to make a significant improvement on this simplicity.

If we take all molecule-specific dimensional information out of \mathbf{Q} , \mathbf{P} , and \mathbf{H} , we have reduced the problem to its *most fundamental* form.

$$\hat{\mathbf{Q}} = \left[\frac{2\pi c\mu\omega}{\hbar}\right]^{1/2} \mathbf{Q}$$

$$\hat{\mathbf{P}} = \left[\hbar 2\pi c\mu\omega\right]^{-1/2} \mathbf{P}$$

$$\hat{\mathbf{H}} = \frac{1}{\hbar (2\pi c\mu\omega)} \mathbf{H}.$$

7.2.2.1 Matrix Elements and Selection Rules [1, 2]

Now we have simpler expressions for *all* of the non-zero matrix elements of $\hat{\mathbf{Q}}$, $\hat{\mathbf{P}}$, and $\hat{\mathbf{H}}$ in the Harmonic Oscillator basis set.

$$\langle v+1|\hat{\mathbf{Q}}|v\rangle = \langle v|\hat{\mathbf{Q}}|v+1\rangle = 2^{-1/2}[v+1]^{1/2} \qquad (\Delta v = \pm 1)$$

$$\langle v+1|\hat{\mathbf{P}}|v\rangle = -\langle v|\hat{\mathbf{P}}|v+1\rangle = i2^{-1/2}[v+1]^{1/2} \qquad (\Delta v = \pm 1)$$

$$\langle v|\hat{\mathbf{H}}|v\rangle = v+1/2 \qquad (\Delta v = 0).$$

So we can forget about units and molecule-specific constants by factoring them out at the beginning of a calculation and then putting them back in at the end.

But there is another extremely important simplifying step. We are going to replace $\hat{\mathbf{Q}}$ and $\hat{\mathbf{P}}$ by \mathbf{a}^{\dagger} and \mathbf{a} "creation" and "annihilation" operators because $\hat{\mathbf{Q}}$ and $\hat{\mathbf{P}}$ have selection rule $\Delta v = +1$ AND $\Delta v = -1$ whereas \mathbf{a}^{\dagger} has the selection rule $\Delta v = +1$ only and \mathbf{a} has the selection rule $\Delta v = -1$ only!

$$\mathbf{a}^{\dagger} = 2^{-1/2} [\hat{\mathbf{Q}} - i\hat{\mathbf{P}}]$$

$$\mathbf{a} = 2^{-1/2} [\hat{\mathbf{Q}} + i\hat{\mathbf{P}}]$$

$$OR$$

$$\hat{\mathbf{Q}} = 2^{-1/2} (\mathbf{a}^{\dagger} + \mathbf{a})$$

$$\hat{\mathbf{P}} = 2^{-1/2} i (\mathbf{a}^{\dagger} - \mathbf{a}).$$

Then

$$\langle v + 1 | \mathbf{a}^{\dagger} | v \rangle = [v + 1]^{1/2}$$

 $\langle v | \mathbf{a} | v + 1 \rangle = [v + 1]^{1/2}$

note that the value of the non-zero matrix element is always the square root of the larger of the two vibrational quantum numbers,

$$\mathbf{a}^{\dagger}|v\rangle = (v+1)^{1/2}|v+1\rangle$$
$$\mathbf{a}|v\rangle = (v)^{1/2}|v-1\rangle.$$

 \mathbf{a}^{\dagger} is called the "creation" operator because, when \mathbf{a}^{\dagger} operates on $|v\rangle$ it creates $(v+1)^{1/2}|v+1\rangle$, which has one additional quantum of vibration.

a is called the "annihilation" operator because, when **a** operates on $|v\rangle$ it yields $v^{1/2}|v-1\rangle$, which has one fewer quantum of vibration.

There is also the "number operator", $N = a^{\dagger}a$

$$\mathbf{N}|v\rangle = \mathbf{a}^{\dagger}\mathbf{a}|v\rangle = \mathbf{a}^{\dagger}v^{1/2}|v-1\rangle = v^{1/2}v^{1/2}|v\rangle = v|v\rangle.$$

When $\mathbf{N} = \mathbf{a}^{\dagger} \mathbf{a}$ operates on $|v\rangle$ it simply tells you how many vibrational quanta there are in $|v\rangle$.

The ease of use of \mathbf{a}^{\dagger} , \mathbf{a} , and \mathbf{N} is illustrated by the following semi-robotic evaluation of matrix elements that involve a long string of operator products, for example

aaaa
$†$
aa † a † aa $|v\rangle$.

This is done in two steps:

- 1. Count the number of \mathbf{a}^{\dagger} factors and the number of \mathbf{a} factors. Here we have three \mathbf{a}^{\dagger} and six \mathbf{a} . This means that the operator product converts $|v\rangle$ uniquely into $|v+3-6\rangle = |v-3\rangle$ times a numerical factor to be determined next.
- 2. Operating in sequence outward from the operator adjacent to $|v\rangle$, the effect of each operator (or pair of operators) on what lies to its right is written by *casual inspection* (parentheses added to show the presence of $\mathbf{a}^{\dagger}\mathbf{a} = \mathbf{N}$ factors)

$$\mathbf{aaa}(\mathbf{a}^{\dagger}\mathbf{a})\mathbf{a}^{\dagger}(\mathbf{a}^{\dagger}\mathbf{a})\mathbf{a}|v\rangle = (v-2)^{1/2}(v-1)^{1/2}v^{1/2}v^{1/2}(v-1)v^{1/2}|v-3\rangle$$
$$= (v-2)^{1/2}(v-1)^{3/2}v^{5/2}|v-3\rangle.$$

The sum of exponents is always the number of \mathbf{a}^{\dagger} and \mathbf{a} factors divided by 2 $(\frac{1}{2} + \frac{3}{2} + \frac{5}{2} = \frac{9}{2})$.

7.2 Harmonic Oscillator 117

7.2.2.2 Use of Commutation Rules[1]

Commutation rules are used to rearrange the order of \mathbf{a}^{\dagger} , \mathbf{a} , and \mathbf{N} in order to yield a convenient and compact algebraic expression. Complex matrix element expressions may be simplified by operator algebra that exploits the following commutation rules:

$$[\mathbf{a}^{\dagger}, \mathbf{a}] = \mathbf{a}^{\dagger} \mathbf{a} - \mathbf{a} \mathbf{a}^{\dagger} = -1$$
$$[\mathbf{a}, \mathbf{N}] = \mathbf{a}$$
$$[\mathbf{a}^{\dagger}, \mathbf{N}] = -\mathbf{a}^{\dagger}.$$

Some operator algebra yields

$$\hat{\mathbf{Q}}^2 = \frac{1}{2}(\mathbf{a} + \mathbf{a}^{\dagger})^2 = \frac{1}{2}\left[\mathbf{a}^2 + 2\left(\mathbf{N} + \frac{1}{2}\right) + \mathbf{a}^{\dagger 2}\right]$$

$$\hat{\mathbf{P}}^2 = -\frac{1}{2}(\mathbf{a}^{\dagger} - \mathbf{a})^2 = -\frac{1}{2}\left[\mathbf{a}^2 - 2\left(\mathbf{N} + \frac{1}{2}\right) + \mathbf{a}^{\dagger 2}\right]$$

7.2.2.3 We Use this Result to Evaluate Matrix Elements of $\hat{H}^{(0)}$

$$\hat{\mathbf{H}}^{(0)} = \frac{1}{2}(\hat{\mathbf{P}}^2 + \hat{\mathbf{Q}}^2) = (\mathbf{N} + 1/2)$$

$$\hat{\mathbf{H}}^{(0)}|v\rangle = (v + 1/2)|v\rangle$$

Note that $\hat{\mathbf{Q}}^2$ and $\hat{\mathbf{P}}^2$ have nonzero $\Delta v = \pm 2$ off-diagonal matrix elements but their sum in $\hat{\mathbf{H}}$ does not.

7.2.2.4 Matrix Elements of Anharmonic V(Q)[2]

For an anharmonic oscillator (i.e. reality), we expand $V(\hat{Q})$ as a power series in \hat{Q} . This is the first important use of the \mathbf{a}^{\dagger} , \mathbf{a} , \mathbf{N} artillery. The goal is to manipulate the terms in V(Q) into simple expressions of \mathbf{a}^{\dagger} , \mathbf{a} , and \mathbf{N} , sorted according to vibrational selection rule:

$$\mathbf{V}(\mathbf{Q}) = \sum_{n=2}^{n_{\text{max}}} \frac{1}{n!} f_n \mathbf{Q}^n$$
$$f_n = \left. \frac{\partial^n \mathbf{V}(\mathbf{Q})}{\partial \mathbf{Q}^n} \right|_{\mathbf{Q}=0}.$$

Now absorb all of the units of \mathbf{Q}^n into the constant

$$F_n \equiv \left(\frac{4\pi c \mu \omega}{\hbar}\right)^{n/2} f_n$$

$$\mathbf{V}(\hat{\mathbf{Q}}) = \sum_{n=1}^{n_{\text{max}}} \frac{1}{n!} F_n (\mathbf{a}^{\dagger} + \mathbf{a})^n.$$

This means we need to simplify terms of the form $(\mathbf{a}^{\dagger} + \mathbf{a})^n$ for n = 3, 4, etc.

$$\Delta v = -2 \xrightarrow{(\mathbf{a}^{\dagger} + \mathbf{a})^2} = \mathbf{a}^2 + 2(\mathbf{N} + 1/2) + \mathbf{a}^{\dagger 2}$$

$$\Delta v = 0 \qquad \Delta v = +2$$

$$(\mathbf{a}^{\dagger} + \mathbf{a})^3 = \mathbf{a}^3 + 3\mathbf{a}\mathbf{N} + 3\mathbf{N}\mathbf{a}^{\dagger} + \mathbf{a}^{\dagger 3}$$
$$\Delta v = -3 \ \Delta v = -1 \ \Delta v = +1 \ \Delta v = +3$$

Note that the selection rules for terms in $(\mathbf{a}+\mathbf{a}^{\dagger})^n$ go from $\Delta v=-n$ to $\Delta v=+n$ in steps of 2.

$$(\mathbf{a}^{\dagger} + \mathbf{a})^4 = \mathbf{a}^{\dagger 4} + 2[2\mathbf{N} - 1]\mathbf{a}^{\dagger 2} + 3[2\mathbf{N}^2 + 2\mathbf{N} + 1] + 2\mathbf{a}^2[2\mathbf{N} + 1] + \mathbf{a}^4.$$

Now we are ready to begin dealing with the 3N-6 anharmonically-coupled anharmonic normal mode oscillators in an N-atom polyatomic molecule.

7.3 Polyatomic Molecules

7.3.1 Basis Set as Product of 3N - 6 Harmonic Oscillator Eigenstates

For an N-atom polyatomic molecule, there are 3N-6 vibrational degrees of freedom. If the molecular symmetry is not too high, there will be 3N-6 non-degenerate individual normal modes of vibration. We treat diagonal anharmonicity (within a normal mode) exactly as we treated the n>2 \mathbf{Q}^n terms for diatomic molecules. So we build on what we know. The basis functions and zero-order energies are

$$\psi_{v_1, v_2, \dots v_{3N-6}}^{(0)} = \prod_{\substack{j=1 \\ \text{(normal modes)}}}^{3N-6} \psi_{j, v_j}(\mathbf{Q}_j)$$

$$E_{v_1, v_2, \dots v_{3N-6}}^{(0)} = \sum_{\substack{j=1 \text{(normal modes)}}}^{3N-6} \omega_j(v_j + 1/2).$$

The $\left\{\psi_{v_1,v_2,...,v_{3N_6}}^{(0)}\right\}$ product functions form a complete set. Every vibrational eigenstate may be expressed as a linear combination of these zero-order product basis states. We find the mixing coefficients in front of each zero-order state by finding the eigen-energies and eigenstates of the vibrational \mathbf{H}^{eff} . As long as there are no near degeneracies between basis states connected by non-zero elements of \mathbf{H}^{eff} , we can find the eigenstates and eigenenergies using second-order non-degenerate perturbation theory. We know how to evaluate everything we need because we know how to write $\hat{\mathbf{H}}^{\text{eff}}$ in terms of $\left\{\mathbf{a}_j^{\dagger}, \mathbf{a}_j, \mathbf{N}_j\right\}$, one such set of operators for each vibrational mode (denoted by the subscript j), we know how to evaluate matrix elements of $\mathbf{a}_j^{\dagger}, \mathbf{a}_j, \mathbf{N}_j$ operators in the $\left\{\psi_{v_1, v_2, \dots, 3N-6}^{(0)}\right\}$ basis set, and we know all of the $\left\{\omega_j\right\}$ from which we get all of the $E_{(v_1, v_2, \dots, 3N-6)}^{(0)}$.

7.3.2 Matrix Elements of
$$V(\hat{Q}_1, \hat{Q}_2, \dots \hat{Q}_{3N-6})$$
 in the $\psi_{v_1, v_2, \dots, 3N-6}^{(0)}$ Basis Set [2]

The potential energy function contains anharmonic terms that operate exclusively within each normal mode as well as anharmonic interactions between normal modes,

$$\mathbf{V}(\mathbf{Q}_1, \mathbf{Q}_2, \dots \mathbf{Q}_{3N-6}) = \sum_{j=1}^{3N-6} \sum_{n=2}^{n_{\text{max}}} \frac{1}{n!} F_{jn} (\mathbf{a}_j^{\dagger} + \mathbf{a}_j)^n$$
intra-mode terms
$$+ \sum_{j=1}^{3N-6} \sum_{n=1}^{n_{\text{max}}} \sum_{k>j}^{3N-6} \sum_{m=1}^{m_{\text{max}}} \frac{1}{n!} \frac{1}{m!} F_{jn,km} (\mathbf{a}_j^{\dagger} + \mathbf{a}_j)^n (\mathbf{a}_k^{\dagger} + \mathbf{a}_k)^m$$
inter-mode terms

where the subscripts on $F_{jn,km}$ specify the $\mathbf{Q}_{i}^{n}\mathbf{Q}_{k}^{m}$ term in \mathbf{V} .

There can be simultaneous interactions between more than two normal modes (e.g. $k_{3,245}$ $\mathbf{Q}_3\mathbf{Q}_2\mathbf{Q}_4\mathbf{Q}_5$ in acetylene).

You already know how to evaluate matrix elements of this $V(\mathbf{Q}_1 \dots \mathbf{Q}_{3N-6})$ potential energy function in the $\left\{\psi_{v_1,v_2,\dots,v_{3N-6}}^{(0)}\right\}$ basis set. For example, $F_{13,22}\hat{\mathbf{Q}}_1^3\hat{\mathbf{Q}}_2^2$,

$$H_{v_1+3,v_2-2;v_1v_2} \propto F_{13,22}[(v_1+3)(v_1+2)(v_1+1)v_2(v_2-1)]^{1/2} \approx v_1^{3/2}v_2^{2/2}.$$

If you simply write down the initial and final state quantum numbers, obtained from the Δv_j and Δv_k changes in quantum number for each mode, you know the specific term in **V** that is responsible for the non-zero matrix element and the explicit v-dependence of this matrix element. You also know the value of the energy denominator for non-degeneracy perturbation theory

$$E_{v_1+3,v_2-2}^{(0)} - E_{v_1,v_2}^{(0)} = hc[3\omega_1 - 2\omega_2].$$

All is in readiness for non-degenerate perturbation theory! But, even with the operator algebra simplifications provided by the \mathbf{a}_{j}^{\dagger} , \mathbf{a}_{j} , \mathbf{N}_{j} operators, it is an algebraic nightmare best performed by a computer.

However, something evil happens.

7.3.3 Breakdown of Non-Degenerate Perturbation Theory

In order to use non-degenerate perturbation theory to obtain the energy levels and eigenstates of an effective Hamiltonian matrix, $\mathbf{H}^{\mathrm{eff}}$, it is necessary that

$$\left| \frac{H_{ij}^{\text{eff}}}{E_i^{(0)} - E_j^{(0)}} \right| \ll 1$$

for all i, j pairs.

Since the off-diagonal matrix elements of $\mathbf{H}^{\mathrm{eff}}$ scale as products of half-integer powers of vibrational quantum numbers, for example

$$H_{v_1+3,v_2-2;v_1,v_2} \propto [(v_1+1)(v_1+2)(v_1+3)(v_2)(v_2-1)]^{1/2} \approx v_1^{3/2} v_2^{2/2}.$$

The sizes of these off-diagonal matrix elements increase rapidly as v_1 and v_2 increase, leading eventually to

$$\left|H_{ij}^{\text{eff}}\right| > \left|E_i^{(0)} - E_j^{(0)}\right|.$$

The condition for the applicability of non-degenerate perturbation theory is no longer satisfied. It becomes necessary to diagonalize a large dimension \mathbf{H}^{eff} .

7.3.4 Polyads

Often H^{eff} may be factored into quasi-degenerate blocks along the diagonal [2]

Each of these blocks ① ② ③ etc. is called a *polyad*. Each block is a square matrix and the dimension varies from block to block, typically increasing as the number of vibrational quanta increases. There may be small inter-block off-diagonal matrix elements, but these are either ignored or dealt with via the Van Vleck transformation [2]. These polyads are of exceptional importance in generating the patterns of level splittings and relative intensities that make it possible to assign the spectrum [4, 8, 9] and to describe all of the fastest intramolecular dynamics rates and mechanisms [6]. These polyad patterns are more instructive and robust than the simple anharmonic progressions associated with individual normal modes.

The simplest polyad arises from an approximate 2:1 ratio between the harmonic frequencies of two normal modes,

$$\omega_1 \approx 2\omega_2$$
.

This most common form of polyad arises from what is called a *Fermi resonance*. If we denote the energy levels of modes 1 and 2 as (v_1, v_2) ,

$$E_{(v_1,v_2)}^{(0)} / hc = \omega_1(v_1 + 1/2) + \omega_2(v_2 + 1/2)$$

$$\frac{E_{(1,0)}^{(0)} - E_{(0,2)}^{(0)}}{hc} = \left(\frac{3}{2}\omega_1 + \frac{1}{2}\omega_2\right) - \left(\frac{1}{2}\omega_1 + \frac{5}{2}\omega_2\right)$$

$$= \omega_1 - 2\omega_2,$$

which is very small if $\omega_1 \approx 2\omega_2$. The non-zero off-diagonal matrix element between the (1,0) and (0,2) levels is

$$\langle v_1 + 1, v_2 - 2 | k_{122} \hat{\mathbf{Q}}_1 \hat{\mathbf{Q}}_2^2 | v_1, v_2 \rangle \propto [v_2(v_2 - 1)(v_1 + 1)]^{1/2}.$$

There are near degeneracies between levels with the following (v_1, v_2) pairs of quantum numbers

$$P = 2v_1 + v_2 = 2 \quad (1,0), (0,2)$$

$$3 \quad (1,1), (0,3)$$

$$4 \quad (2,0), (1,2), (0,4)$$
...
$$10 \quad (5,0), (4,2), (3,4), (2,6), (1,8), (0,10)$$

where *P* is called the "polyad number".

Notice that the number of near degenerate states increases as P increases. This is the *membership scaling rule*. For a 2:1 resonance the number of near degenerate states is (P+2)/2 if P is even or (P+1)/2 if P is odd. If I told you to find all of the states that belong to P=50, you could do so quickly and with confidence that you have found all of the states.

The magnitudes of the off-diagonal matrix elements (each multiplied by k_{122}) also increase as P increases.

For the P = 102:1 polyad

$$\mathbf{H}^{P=10} \propto \frac{(5,0)}{(4,2)} \begin{pmatrix} x_0 & (5 \cdot 2)^{1/2} & 0 & 0 & 0 & 0 \\ 10^{1/2} & x_1 & (4 \cdot 4 \cdot 3)^{1/2} & 0 & 0 & 0 & 0 \\ 0 & 48^{1/2} & x_2 & (3 \cdot 6 \cdot 5)^{1/2} & 0 & 0 & 0 \\ 0 & 0 & 90^{1/2} & x_3 & (2 \cdot 8 \cdot 7)^{1/2} & 0 & 0 \\ 0 & 0 & 0 & 112^{1/2} & x_4 & (1 \cdot 10 \cdot 9)^{1/2} \\ 0 & 0 & 0 & 0 & 90^{1/2} & x_5 \end{pmatrix}$$

$$x_n = \left(\frac{P}{2} - n\right) \omega_1 + 2n\omega_2 \quad \text{(when } P \text{ is even)}$$

$$\mathbf{H}^{P=2} \propto \frac{(1,0)}{(0,2)} \begin{pmatrix} x & (1 \cdot 2 \cdot 1)^{1/2} \\ 2^{1/2} & x \end{pmatrix}.$$

The remarkable feature of the polyad \mathbf{H}^{eff} is that if you observed and fitted the levels that belong to the P=2 polyad, you will be able to determine $\omega_1-2\omega_2$ and the $\mathbf{H}^{P=2}_{(1,0);(0,2)}$ off-diagonal matrix element. With these in hand you can expect to be able to generate the eigenvalues and eigenvectors of *all* P>2 polyads. This is a superbantidote to evil.

7.3.5 Patterns for Spectral Assignment and Mechanisms of Intramolecular Vibrational Redistribution (IVR) and Unimolecular Isomerization

This polyad structure provides the basis for a very powerful form of patternrecognition, which is a crucial armament in the assignment of very highly excited vibrational levels. It also enables a quantitative description of all of the fastest intramolecular vibrational energy redistribution (IVR) dynamics (rates, flow pathways, and mechanisms) for very highly excited vibrational states.

Usually a laser photon "plucks" [10] the system so that it starts, at t=0, in one of the normal mode ("zero-order") product states, for example a high-overtone state, $\phi_{(n,0,0,0,\dots)}^{(0)}=\Psi(t=0)$ (see Sect. 8.4). But we know how to express a zero-order state as a linear combination of eigenstates, recall

$$\Psi(0) = \sum_{j} a_{j} \psi_{j},$$

then

$$\Psi(t) = \sum_{j} a_{j} e^{-iE_{j}t/\hbar} \psi_{j},$$

where we get all of the $\{a_j\}$ mixing coefficients from the eigenvectors of \mathbf{H}^P . What began as a simple toy model (the polyad \mathbf{H}^P) has become a powerful tool for insight into what might appear to be an indescribably complex spectrum and ergodic rather than mechanistic dynamics. This could also provide a rational basis for the design of schemes for external control over intramolecular dynamics as well as a basis for gaining spectroscopic access to the isomerization barrier-proximal region of a potential energy surface. The amazing thing is that, at high P, large amplitude motion "isomerization states," which are localized along the minimum energy isomerization path, emerge spontaneously among the lowest-energy eigenstates of high-P polyads [7]. The molecules, even in the numerical form of very low energy polyads, seem to know what large amplitude dynamics they are destined to experience at very high excitation energies.

Some items for discussion:

- terms of the form $k_{nn,mm} \hat{\mathbf{Q}}_n^2 \hat{\mathbf{Q}}_m^2$, called Darling-Dennision, are responsible for the conversion of a symmetric and antisymmetric pair of normal modes into a pair of local modes. The emergence of local modes is *always* accompanied by the appearance of near-degenerate pairs of symmetric and antisymmetric levels [11, 12].
- HCCH S₀ has normal modes with frequency ratios $(\omega_1:\omega_2:\omega_3:\omega_4:\omega_5) = (5,3,5,1,1)$. There are many classes of polyads, and they are labeled by three polyad quantum numbers: $N_{\text{resonant}} = 5v_1 + 3v_2 + 5v_3 + v_4 + v_5$, $N_{\text{stretch}} = v_1 + v_2 + v_3$, and $\ell_{\text{total}} = \ell_4 + \ell_5$. ℓ is the vibrational angular momentum that appears for π -type vibrations of linear molecules [3, 4, 12].
- Spectral patterns associated with *bent* to *linear* [13] and *trans* to *cis* [9] isomerization.

7.4 Polyads in the Acetylene Electronic Ground State (S_0)

In its electronic ground state, HC \equiv CH is a linear four-atom molecule with 3N-2=7 vibrational degrees of freedom: five normal modes, two of which are doubly degenerate, with frequencies in the approximate integer ratios $v_1(\sigma_g^+)$: $v_2(\sigma_g^+)$: $v_3(\sigma_u^+)$: $v_4(\pi_g)$: $v_5(\pi_u)=5:3:5:1:1$. Thus, nearly every vibrational level is a member of a quasi-degenerate group of levels called a polyad [4, 11, 12]. The seven vibrational quantum numbers $(v_1, v_2, v_3, v_4^{\ell_4}, v_5^{\ell_5})$ are spoiled, even at low-J, by anharmonic resonances, of which nine are known to have an important effect on the spectrum and intramolecular dynamics of S_0 acetylene [14].

The seven vibrational quantum numbers, destroyed by the anharmonic resonances, are replaced by three good polyad quantum numbers. Each polyad is labeled by the values of the three polyad quantum numbers

$$N_{\text{resonance}} = N_{\text{res}} = 5v_1 + 3v_2 + 5v_3 + v_4 + v_5$$

 $N_{\text{stretch}} = N_s = v_1 + v_2 + v_3$
 $\ell_{\text{total}} = \ell = \ell_4 + \ell_5$.

In the special case of $N_s = 0$,

$$N_{\text{res}} = N_{\text{bend}} = v_4 + v_5.$$

It is surprising that three good quantum numbers survive despite the plague of anharmonic resonances.

It is useful to express each of the important anharmonic resonance operators in terms of creation and annihilation operators. For the two doubly degenerate bending modes, each expressed in a (v_i, ℓ_i) basis set, we need a special set of four creation and four annihilation operators, \mathbf{a}_{4g} , \mathbf{a}_{4d} , \mathbf{a}_{5g} , \mathbf{a}_{5d} , and $\mathbf{a}_{4g}^{\dagger}$, $\mathbf{a}_{4d}^{\dagger}$, $\mathbf{a}_{5g}^{\dagger}$, $\mathbf{a}_{5d}^{\dagger}$ (g = gauche, d = droite) [3]. The set of four \mathbf{a} and four \mathbf{a}^{\dagger} operators is needed because each change in v_i by +1 must be accompanied by a change of ℓ_i by +1 or -1 (for each value of v_i , the ℓ_i quantum number ranges from $+v_i$ to $-v_i$ in steps of 2). For mode 4 (the *trans*-bend)

$$\begin{aligned} \mathbf{a}_{4g} & | v_4, \ell_4 \rangle = \left(\frac{v_4 - \ell_4}{2} \right)^{1/2} | v_4 - 1, \ell_4 + 1 \rangle \\ \mathbf{a}_{4d} & | v_4, \ell_4 \rangle = \left(\frac{v_4 + \ell_4}{2} \right)^{1/2} | v_4 - 1, \ell_4 - 1 \rangle \\ \mathbf{a}_{4g}^{\dagger} & | v_4, \ell_4 \rangle = \left(\frac{v_4 - \ell_4 + 2}{2} \right)^{1/2} | v_4 + 1, \ell_4 - 1 \rangle \\ \mathbf{a}_{4d}^{\dagger} & | v_4, \ell_4 \rangle = \left(\frac{v_4 + \ell_4 + 2}{2} \right)^{1/2} | v_4 + 1, \ell_4 + 1 \rangle \,. \end{aligned}$$

For mode 5 (the *cis*-bend), the $\mathbf{a}, \mathbf{a}^{\dagger}$ operators are defined similarly. The number operators are

$$\mathbf{N}_4 = \mathbf{a}_{4d}^{\dagger} \mathbf{a}_{4d} + \mathbf{a}_{4g}^{\dagger} \mathbf{a}_{4g}, \qquad \mathbf{N}_4 | v_4 \ell_4 \rangle = v_4 | v_4 \ell_4 \rangle$$

$$\boldsymbol{\ell}_4 = \ell_4 = \mathbf{a}_{4d}^{\dagger} \mathbf{a}_{4d} - \mathbf{a}_{4g}^{\dagger} \mathbf{a}_{4g}, \qquad \boldsymbol{\ell}_4 | v_4 \ell_4 \rangle = \ell_4 | v_4 \ell_4 \rangle$$

and similarly for N_5 and ℓ_5 .

The nine important anharmonic resonances (sampled *because of* the 5:3:5:1:1 normal mode frequency ratios) are summarized in Table 7.1 [15].

The scaling of polyad matrix elements and membership illustrated here exemplify how measurements at low $E_{\rm vib}$ determine the diagonal and off-diagonal molecular constants. These molecular constants permit scaling of spectrum and dynamics to higher $E_{\rm vib}$, despite the enormous increase in the dimension of the polyad matrix and the complexity of the intramolecular dynamics. This scaling provides a template for revealing qualitative changes, such as normal mode \rightarrow local mode, emergence of new classes of regular vibrations, emergence of ergodic behavior that affects some or all members of a polyad, or the onset of the sampling of a saddle point region on the potential energy surface.

$\overline{}$
Η.
terms
resonance
Intra-polyad
7.
aple
3
æ

Name	Resonance vector	Operator (\mathbf{a}^{\dagger} , \mathbf{a} format)	Scaled matrix element
	$(\Delta v_1, \Delta v_2, \Delta v_3, \Delta v_4,$		
	$\Delta \ell_4, \Delta v_5, \Delta \ell_5)$		$(\Delta v_i, \Delta \ell_i \text{ same as for resonance vector})$
Stretch-DD	Stretch-DD (2, 0, -2, 0, 0, 0)	$ \mathbf{a}_1^* ^2 \mathbf{a}_3^2 + cc$	$\frac{1}{4}K_{11,33}\left[(v_1+1)(v_1+2)v_3(v_3-1)\right]^{1/2}$
Bend-DDI	Bend-DDI (0, 0, 0, 2, 0, -2, 0)	$\frac{1}{4} \left(\mathbf{a}_{4g}^{\dagger} \mathbf{a}_{4d}^{\dagger} + \mathbf{a}_{4d}^{\dagger} \mathbf{a}_{4g}^{\dagger} \right) \left(\mathbf{a}_{5g} \mathbf{a}_{5d} + \mathbf{a}_{5d} \mathbf{a}_{5g} \right) + cc$	$\frac{1}{4}s_{45}\left[(v_4 - \ell_4)^2(v_5 - \ell_5 + 2)\right]^{1/2}$
Bend-DDII	Bend-DDII $(0, 0, 0, 2, \pm 2, -2, \mp 2)$	$\frac{1}{2} \left(\mathbf{a}_{4d}^{\dagger 2} \mathbf{a}_{5g}^2 + \mathbf{a}_{4g}^{\dagger 2} \mathbf{a}_{5g}^2 \right) + \text{cc}$	$\frac{1}{16}d_{45}\left[(v_4 \pm \ell_4 - 2)(v_4 \pm \ell_4)\right]$
			$\times (v_5 \pm \ell_5 + 2)(v_5 \pm \ell_5 + 4)]^{1/2}$
H _{3,245}	$(0,-1,1,-1,\pm 1,-1,\mp 1)$	$(0,-1,1,-1,\pm 1,-1,\mp 1)$ $\mathbf{a}_2\mathbf{a}_3^{\dagger}\left(\mathbf{a}_{4g}\mathbf{a}_{5d}\pm\mathbf{a}_{4d}\mathbf{a}_{5g}\right)+\mathrm{cc}$	$-\frac{1}{8}K_{3,245}\left[v_2(v_3+1)(v_4\pm\ell_4)(v_5\mp\ell_5)\right]^{1/2}$
H _{1,255}	(1, -1, 0, 0, 0, -2, 0)	$\frac{1}{2}\mathbf{a}_{d}^{\dagger}\mathbf{a}_{2}\left(\mathbf{a}_{5g}\mathbf{a}_{5d}+\mathbf{a}_{5d}\mathbf{a}_{5g}^{2}\right)+cc$	$-\frac{1}{4}K_{1,244}\left[(v_1+1)v_2(v_4^2-\ell_4^2)\right]^{1/2}$
$H_{1,244}$	(1, -1, 0, -2, 0, 0, 0)	$\frac{1}{2}$ a $_{1}^{\dagger}$ a $_{2}$ (a $_{4g}$ a $_{4d}$ + a $_{4d}$ a $_{4g}$) + cc	$-\frac{1}{4}K_{1,245}\left[(v_1+1)v_2(v_5^2-\ell_5^2)\right]^{1/2}$
H _{14,35}	$(1,0,-1,1,\mp 1,-1,\pm 1)$	$\mathbf{a}^{\dagger}_{1}\mathbf{a}_{3}\left(\mathbf{a}_{4g}^{\dagger}\mathbf{a}_{5g}\mp\mathbf{a}_{4d}^{\dagger}\mathbf{a}_{5d}\right)+\mathrm{cc}$	$-\frac{1}{8}K_{14,35}[(v_1+1)v_3(v_4\pm\ell_4+2)(v_5\pm\ell_5)]^{1/2}$
H _{34,15}	$(-1,0,1,1,\mp 1,-1,\pm 1)$	$\mathbf{a}_1 \mathbf{a}_3^{\dagger} \left(\mathbf{a}_{4g}^{\dagger} \mathbf{a}_{5g} \mp \mathbf{a}_{4d}^{\dagger} \mathbf{a}_{5d} \right) + \mathrm{cc}$	$-\frac{1}{8}K_{34,15}[(v_3+1)(v_4\pm\ell_4+2)v_1(v_5\pm\ell_5)]^{1/2}$
l-resonance	ℓ -resonance $(0,0,0,0,\pm 2,0,\mp 2)$	$rac{1}{4}\left[\left(\mathbf{a}_{4d}^{\dagger}\mathbf{a}_{4g}+\mathbf{a}_{4g}\mathbf{a}_{4d}^{\dagger} ight)\left(\mathbf{a}_{5g}^{\dagger}\mathbf{a}_{5d}+\mathbf{a}_{5d}\mathbf{a}_{5g}^{\dagger} ight)$	$\frac{1}{4}r_{45}[(v_4 \pm \ell_4)(v_4 \mp \ell_4 + 2)(v_5 \mp \ell_5)(v_5 \pm \ell_5 + 2)]^{1/2}$
		$\pm \left(\mathbf{a}_{4g}^{\dagger}\mathbf{a}_{4d} + \mathbf{a}_{4d}\mathbf{a}_{4g}\right)\left(\mathbf{a}_{5d}^{\dagger}\mathbf{a}_{5g} + \mathbf{a}_{5g}\mathbf{a}_{5d}^{\dagger}\right)\right] + cc$	
DD Darling Dennison	Dannison		

DD Darling-Dennison

Notice that each of these resonance vectors conserves N_{res}, N_s, and ℓ . The three polyad quantum numbers correspond to three vectors in 7D space that are orthogonal to each other and to all nine resonance vectors,

$$N_{\text{res}} = (5, 3, 5, 1, 0, 1, 0)$$

 $N_s = (1, 1, 1, 0, 0, 0, 0)$
 $\ell = (0, 0, 0, 0, 1, 0, 1)$

References 127

References

 C. Cohen-Tannoudji, B. Diu, F. Laloë, Quantum Mechanics (Wiley, New York, 1977), pp. 488–507

- R.W. Field, J. Baraban, S.H. Lipoff, A.R. Beck, Effective Hamiltonians, in *Handbook of High-Resolution Spectroscopies*, ed. by M. Quack, F. Merkt (Wiley, Chichester, 2010)
- 3. M.P. Jacobson, R.J. Silbey, R.W. Field, J. Chem. Phys. 110, 845–859 (1999)
- S.A.B. Solina, J.P. O'Brien, R.W. Field, W.F. Polik, J. Phys. Chem. 100, 7797–7809 (1996);
 S.A.B. Solina, J.P. O'Brien, R.W. Field, W.F. Polik, Berichte der Bunsengesellschaft für Physikalishe Chemie 99, 555–560 (1995)
- 5. M.P. Jacobson, R.W. Field, Chem. Phys. Lett. **320**, 553–560 (2000)
- R.W. Field, J.P. O'Brien, M.P. Jacobson, S.A.B. Solina, W.F. Polik, H. Ishikawa, Adv. Chem. Phys. 101, 463–490 (1997) [Solvay Conference 1995]
- H. Ishikawa, R.W. Field, S.C. Farantos, M. Joyeux, J. Koput, C. Beck, R. Schinke, Ann. Rev. Phys. Chem. 50, 443–484 (1999)
- 8. M.P. Jacobson, R.W. Field, J. Phys. Chem. **104**, 3073–3086 (2000) [feature article]
- A.J. Merer, A.H. Steeves, J.H. Baraban, H.A. Bechtel, R.W. Field, J. Chem. Phys. 134(24), 244310 (2011)
- 10. E.J. Heller, W.M. Gelbart, J. Chem. Phys. **73**, 626 (1980)
- 11. L.E. Fried, G.S. Ezra, J. Chem. Phys. 86, 6270 (1987)
- 12. M.E. Kellman, J. Chem. Phys. 93, 6630 (1990)
- 13. R.N. Dixon, Trans. Faraday. Soc. 60, 1363–1368 (1964)
- 14. D.S. Perry, J. Martens, A. Amyay, M. Herman, Mol. Phys. 110, 2687 (2012)
- K. Hoshina, A. Iwasaki, K. Yamanouchi, M.P. Jacobson, R.W. Field, J. Chem. Phys. 114, 7424
 7442 (2001)

Chapter 8 Intramolecular Dynamics: Representations, Visualizations, and Mechanisms

This lecture addresses the question: Stuff moves but eigenstates are stationary. How is motion encoded in Quantum Mechanics? We are concerned with the Time Dependent Schrödinger Equation for the special case of **H** independent of time. In order to describe unimolecular dynamics we need: (a) a complete set of eigen-energies and eigenvectors $\{E_j, \psi_j\}$ of the time-independent **H**, (b) a path via perturbation theory (both non-degenerate and degenerate) between the zero-order $\{E_j^{(0)}, \psi_j^{(0)}\}$ and the eigen- $\{E_j, \psi_j\}$, which is represented by a unitary transformation

$$\mathbf{T}^{\dagger}\mathbf{H}\mathbf{T} = \begin{pmatrix} E_1 & 0 & 0 & 0 & 0 \\ 0 & \ddots & 0 & 0 & 0 \\ 0 & 0 & E_j & 0 & 0 \\ 0 & 0 & 0 & \ddots & 0 \\ 0 & 0 & 0 & 0 & E_N \end{pmatrix},$$

(c) a description of $\Psi(\mathbf{Q},t=0)$, the "pluck", as a linear combination of the eigen- $\{E_j,\psi_j\}$, and (d) the short and easy step from $\Psi(\mathbf{Q},t=0)$ to $\Psi(\mathbf{Q},t)$. The full time-dependent $\Psi(\mathbf{Q},t)$ contains so much information that reduced-information quantities are needed. These include motion in coordinate $\langle \mathbf{Q} \rangle_t$ and momentum $\langle \mathbf{P} \rangle_t$ space and state space: $\langle \mathbf{N}_1, \mathbf{N}_2, \ldots \rangle_t$, $\langle \Psi(t)\Psi(0) \rangle_t$, $|\langle \Psi(t)\Psi(0) \rangle|^2$, and the time-dependence of "resonance operators".

8.1 From the "Pluck" at t = 0 to the Time-Evolving State

The Time-Dependent Schrödinger Equation (TDSE) is

$$\mathbf{H}\Psi = i\hbar \frac{\partial \Psi}{\partial t}.$$

If **H** is time-independent and we know all $\{\psi_j, E_j\}$ of its eigenstates and eigenenergies, then we can always express the t=0 state of the system as a linear combination of eigenstates [1]:

$$\underbrace{\Psi(\mathbf{Q},t=0)}_{\text{initial state}} = \underbrace{\sum_{j} c_{j} \ \psi_{j}(\mathbf{Q})}_{\text{linear combination of eigenstates of } \mathbf{H}}$$
 then
$$\Psi(\mathbf{Q},t) = \sum_{j} c_{j} \ \psi_{j}(\mathbf{Q}) e^{-iE_{j}t/\hbar}.$$

This is a trivial step if we know $\Psi(\mathbf{Q}, 0)$ and the complete set of eigenstates and eigen-energies of $\mathbf{H}, \{\psi_i, E_i\}$.

But the difficult and necessary work is to obtain (a) a description of the t=0 state (the "pluck"), (b) the specific zero-order representation $\{\psi_j^{(0)}, E_j^{(0)}\}$ demanded by the pluck, and (c) the relationships (unitary transformation) between the zero-order states and the eigenstates.

8.2 Perturbation Theory

Summary of non-degenerate Perturbation Theory (see Sect. 3.1) [2]:

$$\begin{split} \mathbf{H} &= \mathbf{H}^{(0)} + \mathbf{H}^{(1)} \\ E_{j} &= E_{j}^{(0)} + E_{j}^{(1)} + E_{j}^{(2)} \\ &= H_{jj}^{0} + H_{jj}^{1} + \sum_{k \neq j} \frac{\left| H_{jk}^{1} \right|^{2}}{E_{j}^{(0)} - E_{k}^{(0)}} \\ \psi_{j} &= \psi_{j}^{(0)} + \psi_{j}^{(1)} \\ &= \psi_{j}^{(0)} + \sum_{k \neq j} \psi_{k}^{(0)} \frac{H_{jk}^{1}}{E_{j}^{(0)} - E_{k}^{(0)}}. \end{split}$$

Usually we try to choose $\mathbf{H}^{(0)}$ so that its eigenstates are closely related to the states that are created by an experimentally realizable pluck of the system. We embed in $\mathbf{H}^{(0)}$ an *experimentally convenient* factorization of the internal motions of the molecule. For example, it is often convenient to choose normal modes of vibration vs. bond-localized modes of vibration. More on this later.

If we define $\mathbf{H}^{(0)}$ so that we have a complete set of basis functions $\left\{\psi_{j}^{(0)}\right\}$ and zero-order energies $\left\{E_{j}^{(0)}\right\}$ that are cleverly chosen because of their appropriateness for a particular class of dynamical problem or initial excitation of the molecule, then $\mathbf{H}^{(1)}$ contains everything else beyond $\mathbf{H}^{(0)}$ in the exact \mathbf{H} . We have defined

$$\mathbf{H}^{(0)} = \begin{pmatrix} E_1^{(0)} & 0 \\ & \ddots & \\ 0 & E_n^{(0)} \end{pmatrix}$$

so that $\langle i^{(0)}|\mathbf{H}^{(0)}|j^{(0)}\rangle=\delta_{ij}E_j^{(0)}$ and, evaluated in the $\left\{\psi_j^{(0)}\right\}$ basis set, then $\mathbf{H}^{(1)}$ is

$$\mathbf{H}^{(1)} = \begin{pmatrix} H_{11}^{(1)} & H_{12}^{(1)} & \dots \\ H_{21}^{(1)} & H_{22}^{(1)} & \dots \\ \dots & \dots & \dots \\ \dots & \dots & H_{nn}^{(1)} \end{pmatrix}.$$

Usually all of the $H_{ij}^{(1)}$ matrix elements are given by simple equations rather than explicit evaluations of integrals (see Sect. 7.3). $\mathbf{H} = \mathbf{H}^{(0)} + \mathbf{H}^{(1)}$ is exactly diagonalized by the unitary transformation

$$\mathbf{T}^{\dagger}(\mathbf{H}^{(0)} + \mathbf{H}^{(1)})\mathbf{T} = \begin{pmatrix} E_1 & 0 \\ & \ddots \\ 0 & E_n \end{pmatrix}$$

and the eigenstate $|j\rangle$ is expressed in the zero-order basis set as

$$|j\rangle = \sum_{k=1}^{n} c_k^{j} |k\rangle^{(0)} = \sum_{k=1}^{n} T_{kj}^{\dagger} |k\rangle^{(0)}.$$
the j -th column of \mathbf{T}^{\dagger}

A very convenient property of a unitary matrix is

$$\mathbf{T}^{\dagger}\mathbf{T} = 1$$
.

 \mathbf{T}^{\dagger} (the conjugate transpose of \mathbf{T}) is the inverse of \mathbf{T} , $\mathbf{T}^{\dagger} = \mathbf{T}^{-1}$. The inverse of the diagonalizing transformation will come in very handy whenever we want to express $\Psi(\mathbf{Q}, t = 0)$ in terms of the eigenstates of \mathbf{H} .

When the crucial approximation of non-degenerate perturbation theory is satisfied

$$\theta_{j,k} = \left| \frac{H_{j,k}^{(1)}}{E_i^{(0)} - E_k^{(0)}} \right| \ll 1$$
 for all j, k ,

where $\theta_{j,k}$ is often called the "mixing angle", then each element of \mathbf{T}^k is obtained directly via non-degenerate perturbation theory, with one small modification, the inclusion of N_j , to ensure normalization

$$|j\rangle = N_j |j\rangle^{(0)} + \sum_{k \neq j} |k\rangle^{(0)} \underbrace{\frac{H_{j,k}^{(1)}}{E_j^{(0)} - E_k^{(0)}}}_{T_{k,j}^{\dagger}}$$

$$N_j = \left[1 - \sum_{k \neq j} \left(T_{kj}^\dagger\right)^2\right]^{1/2}.$$

This N_j normalization factor is taken as unity in the usual formulas of non-degenerate perturbation theory, which is legitimate because of the assumption that all $\theta_{ik} \ll 1$.

When the approximation of non-degeneracy is not satisfied, it is necessary to use a computer to diagonalize the "quasi-degenerate" blocks of **H** (see Fig. 4.1). The mechanics of the construction of $\Psi(\mathbf{Q},t)$ are unchanged, except that the computer provides all of the elements of \mathbf{T}^{\dagger} .

8.3 Toluene: A Hindered Rotor. A Fully Worked Out Example

A particle on a circular ring is a simple zero-order system that is ideally suited for perturbation theory,

$$\mathbf{H}^{(0)} = hcB\mathbf{J}^2/\hbar^2 + V^{(0)}(\phi)$$

where

$$V^{(0)} = 0.$$

The zero order energies and basis states are

$$E_n^{(0)} = hcBn^2$$
 $n = 0, \pm 1, \pm 2, ...$
 $\psi_n^{(0)} = \langle \phi | n \rangle = (2\pi)^{-1/2} e^{\phi}.$

Reflection in the plane of the ring, σ_v , is a rigorous symmetry

$$\sigma_v e^{in\phi} = e^{-in\phi}$$
.

The symmetrized basis set is convenient because the symmetrized states are eigenfunctions of σ_v

$$\psi_{0+}^{(0)} = \langle \phi | 0 \rangle = (2\pi)^{-1/2}$$

$$\psi_{|n|\pm}^{(0)} = 2^{-1/2} [\langle \phi | n \rangle \pm \langle \phi | - n \rangle] = (4\pi)^{-1/2} [e^{in\phi} \pm e^{-in\phi}]$$

$$\sigma_v \psi_{|n|\pm}^{(0)} = \pm \psi_{|n|\pm}.$$

Consider the example of toluene (Figs. 8.1 and 8.2). The methyl group in toluene (methyl benzene) is a hindered internal rotor in a *sixfold* symmetric potential

$$V(\phi) = V_6 \cos(6\phi)$$

where V_6 can be positive (minimum of V_6 is at the staggered geometry) or negative (minimum of V_6 is at the eclipsed geometry). Why is the hindering potential sixfold, and not threefold symmetric? It is convenient to write $V(\phi)$ in the exponential form

$$V(\phi) = (V_6/2) \left[e^{i6\phi} + e^{-i6\phi} \right].$$

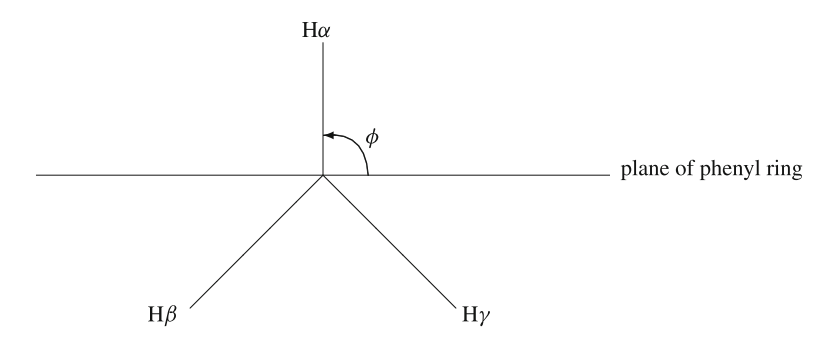


Fig. 8.1 Internal rotation of $-\text{CH}_3$ in toluene. The rotor angle, ϕ , is defined for one of the three equivalent H atoms (H α) relative to the plane of the phenyl ring. There are six equivalent eclipsed positions ($\phi = 0, \pi/3, 2\pi/3, \pi, 4\pi/3$, and 2π) and six equivalent staggered positions ($\phi = \pi/6, \pi/2, 5\pi/6, 7\pi/6, 3\pi/2$, and $11\pi/6$)

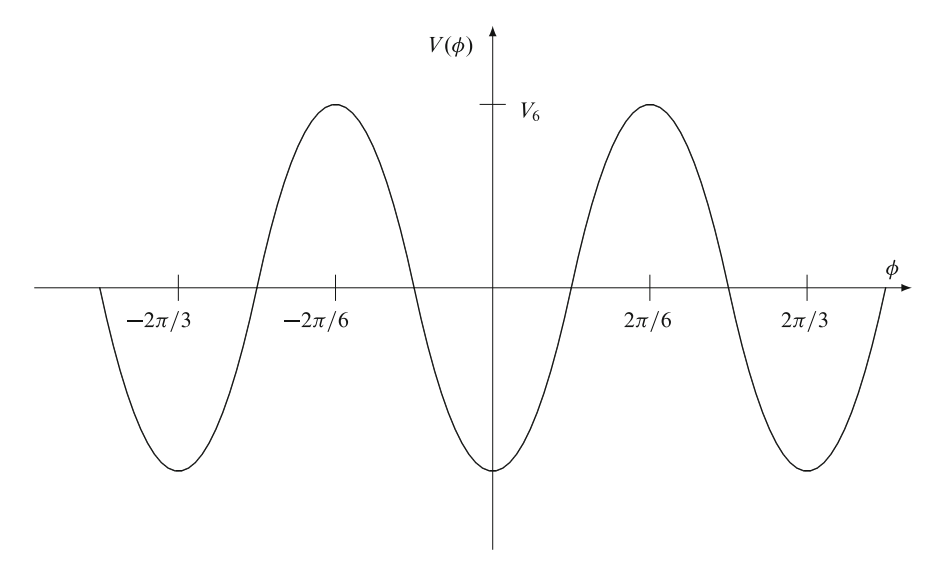


Fig. 8.2 A part of a sixfold hindered rotor potential. If $V_6 > 0$, there are six maxima corresponding to one of the three methyl hydrogen atoms in the plane of the benzene ring (eclipsed) and six minima corresponding to one of the hydrogens perpendicular to the plane of the benzene ring (staggered). ϕ specifies the rotation of the -CH₃ group relative to the plane of the benzene ring

For toluene, where the source of the perturbation of the methyl rotor is the planar phenyl ring, the hindered rotor potential *cannot* be

$$V(\phi) = V_6 \sin 6\phi = \frac{V_6}{2i} \left[e^{i6\phi} - e^{-i6\phi} \right],$$

because **H** must be symmetric with respect to σ_v .

The hindered rotor potential for an *ortho*- or *meta*-substituted halo-toluene would have the lower-symmetry sixfold plus threefold form:

$$V(\phi) = V_3 \cos 3\phi + V_6 \cos 6\phi.$$

Why?

For toluene

$$\mathbf{H}^{(1)} = (V_6/2) \left[e^{i6\phi} + e^{-i6\phi} \right].$$

 $\mathbf{H}^{(1)}$ spoils the angular momentum quantum number, n, as will be illustrated here using non-degenerate perturbation theory.

In the symmetrized free-rotor basis set, the non-zero matrix elements of $\mathbf{H}^{(1)}$ are

$$H_{n,(\pm):n'(\pm)'}^{(1)}$$
.

These matrix elements follow the selection rules

$$(\pm)' \leftrightarrow (\pm)$$
$$n' = n + 6, |n - 6|.$$

The non-zero matrix elements of $\mathbf{H}^{(1)}$ are

$$H_{n\pm;(n+6)\pm}^{(1)} = H_{n\pm;|n-6|\pm}^{(1)} = V_6/2$$

and two special cases

$$H_{3\pm;3\pm}^{(1)} = E_{3\pm}^{(1)} = \pm V_6/2$$

 $H_{0\pm;6\pm} = 2^{-1/2}V_6.$

It is possible to work out a closed-form expression for $E_{n\pm}^{(2)}$:

$$E_{n\pm}^{(2)} = \frac{(V_6/2)^2}{hcB_{\text{CH}_3}} \frac{1}{2(n^2 - 9)}.$$

Thus we have a closed-form expression for $E_{n\pm}$:

$$E_{n\pm} = E_{n\pm}^{(0)} + E_{n\pm}^{(1)} + E_{n\pm}^{(2)}$$

$$E_{n\pm} = hcB_{\text{CH}_3}n^2 \pm \delta_{n,3}(V_6/2) + \frac{(V_6/2)^2}{hcB_{\text{CH}_3}} \frac{1}{2(n^2 - 9)}$$

and also for $\langle \phi | n \pm \rangle$

$$\langle \phi | n \pm \rangle = \langle \phi | n \pm \rangle^{(0)} + \frac{V_6 / h c B_{\text{CH}_3}}{24} \left[\frac{-1}{n+3} \left\langle \phi | n+6 | \pm \right\rangle^{(0)} + \frac{1}{n-3} \left\langle \phi | | n-6 | \pm \right\rangle^{(0)} \right]$$

[with special cases for 0-, 3+, 3-, 6+ and 6- states].

The purpose of presenting all of this algebra is to illustrate two important principles:

1. for an electronic transition between two electronic states with identical potential energy surfaces, we expect *correctly* that the Franck–Condon principle permits only $\Delta n=0$ (diagonal) transitions: only one final eigenstate can be reached from each single initial eigenstate, regardless of the size of V_6 relative to hcB_{CH_3} . There will be no dynamics. When V_6 and/or B_{CH_3} is different for the initial and final electronic states, the F-C factors are no longer diagonal. The short Franck–Condon pluck of the system excites several eigenstates that belong to different eigen-energies. This satisfies the requirement for dynamics.

2. When a transition occurs between the states that are described by different coupling cases, many more transitions are allowed than when the coupling cases are identical. (This is a very useful but seldom explicitly-stated general rule.)

The coupling cases are expressed by

$$\Theta = \frac{V_6}{hcB_{\text{CH}_3}}.$$

When the upper state Θ' is identical to the lower state Θ'' , there are exclusively $\Delta n=0, \pm \leftrightarrow \pm$ transitions. In such a case, a sudden transition cannot create a time-evolving coherent superposition of two eigenstates that belong to different eigen-energies. There can be no dynamics even if $\left|\frac{V_6}{hcB_{\text{CH}_3}}\right|\gg 1$, which means that the angular momentum quantum number is utterly destroyed. However, when $\Theta'\neq\Theta''$, some non-diagonal transitions become allowed. The transition probability, $P_{n'\pm,n''\pm}$, is proportional to the square of the overlap between the wavefunction in the upper electronic state with that in the lower electronic state. This is the hindered rotor version of a one-dimensional Franck–Condon factor,

$$P_{n'\pm,n''\pm} \propto \left| \left\langle n' \pm | n'' \pm \right\rangle \right|^2$$
.

Rather than giving the general result, consider the example of the nominally forbidden transition between the n'' = 1 + level and the n' = 7 + level:

$$|n'' = 1+\rangle = (1 - \alpha_{n''=5+}^2 - \alpha_{n''=7+}^2)^{1/2} |n'' = 1+\rangle^{(0)} + \alpha_{n''=5+} |n'' = 5+\rangle^{(0)} + \alpha_{n''=7+} |n'' = 7+\rangle^{(0)}$$

where the mixing coefficients have the values

$$\alpha_{n''=5+} = -\left(V_6''/hcB_{\text{CH}_3}''\right)\frac{1}{48}$$

$$\alpha_{n''=7+} = -\left(V_6''/hcB_{\text{CH}_3}''\right)\frac{1}{96}.$$

Similarly,

$$|n' = 7+\rangle = (1 - \alpha_{n'=1+}^2 - \alpha_{n'=13+}^2)^{1/2} |n' = 7+\rangle^{(0)} + \alpha_{n'=1+} |n' = 1+\rangle^{(0)} + \alpha_{n'=13+} |n' = 13+\rangle^{(0)},$$

where

$$\alpha_{n'=1+} = + \left(V_6'/hcB_{CH_3}'\right)\frac{1}{96}$$

$$\alpha_{n'=13+} = -\left(V_6'/hcB_{CH_3}'\right)\frac{1}{120}.$$

Thus

$$\langle n' = 7 + | n'' = 1 + \rangle = \left(1 - \alpha_{n'=1+}^2 - \alpha_{n'=13+}^2 \right)^{1/2} \alpha_{n''=7+}$$

$$+ \alpha_{n'=1+} \left(1 - \alpha_{n''=5+}^2 - \alpha_{n''=7+}^2 \right)^{1/2}$$

$$\approx \alpha_{n''=7+} + \alpha_{n'=1+}$$

$$= -\left(V_6'' / hc B_{\text{CH}_3}'' \right) \frac{1}{96} + \left(V_6' / hc B_{\text{CH}_3}'' \right) \frac{1}{96}$$

$$= \frac{1}{96} \left[\frac{V_6'}{hc B_{\text{CH}_3}'} - \frac{V_6''}{hc B_{\text{CH}_3}''} \right] .$$

If $\Theta' = \Theta''$, the $n' = 7 + \leftarrow n'' = 1 +$ transition is forbidden, but whenever $\Theta' \neq \Theta''$, the transition becomes allowed. The allowedness is proportional to $[\Theta' - \Theta'']^2$. Note that, in the case where the electronic transition corresponds to a staggered \Leftrightarrow eclipsed geometry change, many $\Delta n \neq 0$ transitions are observable.

For a molecule like toluene, which contains a light rotor (e.g. $-CH_3$) attached to a heavy framework (e.g. -phenyl), the vibrational or electronic-vibrational spectrum will contain patterns of transitions, the frequencies and relative intensities of which yield unambiguous assignments of the upper- and lower-state rotor quantum numbers, n' and n''. Once the n', n'' assignments are secure, the global energy level diagram may be constructed, the details of which reveal the qualitative form of the hindered rotor potential (sixfold, sixfold plus threefold, sixfold plus twofold) and the numerical values of the rotor-relevant molecular constants.

For example, in toluene, the internal rotor levels will exhibit energy level spacings intermediate between the very fine level spacings of the full-molecule rotational levels and the much coarser structure associated with the IR-active or Franck–Condon bright normal mode vibrational fundamentals and overtones. For toluene, based on the $\Delta n=0$, $(\pm)'\leftrightarrow(\pm)''$ selection rules for transitions between rotor basis states, the n'=n''+6 and n'=|n''-6|, $(\pm)'\leftrightarrow(\pm)''$, $H_{n'(\pm)';n''(\pm)''}^{(1)}$ perturbation matrix element selection rule (weak extra transitions), and the n'=n''+12, n'=|n''-12|, and n'=|n''-6|+6, $(\pm)'\leftrightarrow(\pm)''$ two-step

perturbation selection rule (very weak extra transitions), one expects the following transitions:

$$n'' = 0+$$
 $n' = 0+$, $6+$, $12+$
 $n'' = 1\pm$
 $n' = 1\pm$, $7\pm$, $11\pm$, $13\pm$
 $n'' = 2\pm$
 $n' = 2\pm$, $4\pm$, $8\pm$, $10\pm$, $14\pm$
 $n'' = 3\pm$
 $n' = 3\pm$, $9\pm$, $15\pm$
 $n'' = 4\pm$
 $n'' = 4\pm$, $2\pm$, $8\pm$, $10\pm$, $16\pm$
 $n'' = 5\pm$
 $n'' = 5\pm$, $1\pm$, $7\pm$, $11\pm$, $17\pm$
 $n'' = 6+$
 $n'' = 6+$, $0+$, $12+$, $18+$
 $n'' = 6 n'' = 6-$, $12-$, $18-$ (note that there is no 0 -level of $-$ symmetry)

etc.

In an absorption spectrum, the lower state internal rotor $n'' > 0 \pm$ levels will be thermally populated. Thus the spectra will consist of groups of transitions (one n' series for each populated $n'' \pm$ level) approximately spaced by

$$\Delta E_{n'\pm;n''\pm} = \Delta E_0 + hc \left(B'_{\text{CH}_3} n'^2 - B''_{\text{CH}_3} n''^2 \right).$$

The zero-order transition pattern will be distorted by level shifts associated with first-order and second-order effects of the $V'_6(\phi)$ and $V''_6(\phi)$ sixfold barrier terms:

$$E_{n\pm} = \underbrace{E_0 + hcB_{\text{CH}_3}n^2}_{E_n^{(0)}} \pm \underbrace{\delta_{n,3}(V_6/2)}_{E_n^{(1)}} + \underbrace{\frac{(V_6)^2}{hcB_{\text{CH}_3}} \frac{1}{8(n^2 - 9)}}_{E_n^{(2)}}.$$

Crucial, assignment-relevant information is obtained from transitions that originate from the n''=0,3, and 6 levels (especially the 3+ and 3- levels). Five parameters are sufficient to determine all of the transition frequencies and relative intensities: $\Delta E_0 = E_0' - E_0'', B_{\text{CH}_3}', B_{\text{CH}_3}'', V_6'$, and V_6'' .

Ask an organic chemist about "resonance"-related electronic structure factors that determine the sign and magnitude of the V_6 parameter for substituted toluenes!

8.4 The Pluck: $\Psi(Q, t = 0)$

Suppose the molecule is prepared in some non-eigenstate by a short pulse applied at t = 0. This is "the pluck" [3]. We refer to what is prepared at t = 0 as "the bright state".

What is "bright" and what is "dark" is defined by the nature of the experiment. Suppose that the vibrational wavefunction of the v=0 state of the electronic ground state, \tilde{X} , $v_X=0$, is "transferred" by a short pulse to an electronically excited state, \tilde{A} . The potential energy surface of the \tilde{A} electronic state is different from that of the \tilde{X} -state. As a result, the t=0 preparation of the excited electronic state is a coherent superposition of eigenstates of the electronically excited potential energy surface

$$\psi_{\tilde{X},v_X=0}(\mathbf{Q}) = \sum_{v_A} c_{\tilde{A},v_A} \, \psi_{\tilde{A},v_A}$$

where

$$c_{\tilde{A},v_A} = \langle v_X = 0 | v_A \rangle$$

is a numerically calculable vibrational overlap integral between normal mode basis states. However, owing to intra-mode and inter-mode anharmonicity, the harmonic oscillator $\psi_{\tilde{A},v_A}$ states are not eigenstates of the $V_{\tilde{A}}(\mathbf{Q})$ potential energy surface. An additional transformation is needed to deal with these anharmonicity (and Coriolis) effects. The $\tilde{X},v_X=0$ pluck instantaneously creates amplitudes in many \tilde{A},v_A basis states that are not eigenstates. Usually, however, the pluck creates significant amplitude in only a few vibrational states (vertical transition) exclusively with excitation in the *Franck–Condon active* normal modes. These are the "bright" modes. They are the modes that express the difference in equilibrium molecular geometry between the \tilde{X} and \tilde{A} states.

Alternatively, one can imagine a "sudden" Stimulated Emission Pumping[4, 5] process where a downward stimulated emission transition from a selected highly-excited vibrational eigenstate (of one of the Franck–Condon active normal modes) of the electronically excited state creates amplitudes in several zero-order highly excited states of the Franck–Condon active normal mode in the ground state. However, at the chosen vibrational excitation energy in the electronic ground state, the normal modes have been replaced by local modes. The pluck is a superposition of local mode states [6–8].

Another scheme might be sudden excitation of a high overtone of an R-H stretch local mode vibrational level via a pure vibrational transition. The highly excited

normal mode character is distributed over many vibrational eigenstates, but the coherent superposition excited by the pluck pulse evolves initially like a local mode [8] (but the dephasing of the localized character can be very rapid: Intramolecular Vibrational Redistribution (IVR) [9]). Again, it is experimentally possible to capture the wavepacket dynamics encoded in the group of eigenstates excited by the pluck at t=0. Dynamics are encoded in the pattern of eigenstates and transition amplitudes that appear in a high resolution, eigenstate-resolved spectrum, which could in principle have been prepared as a coherent superposition state by a short excitation pulse at t=0. One does not have to perform an ultrafast time-domain experiment in order to describe, completely and accurately, the dynamics that would be observed in a time-domain experiment.

So the prescription is

- 1. The pluck is what *could have been* excited from the selected initial state by a short t = 0 pulse centered at a specified energy.
- 2. What is then seen in the experiment is determined by the nature of the detection scheme. What is made bright in a specific experiment is determined jointly by the nature of the excitation and detection schemes.

What is "bright" and what is "dark" is determined by the initial state, the excitation pulse, and most importantly by the detection scheme. Bright and dark are defined by the details of the specific experiment.

8.5 $\Psi(Q, t)$ Contains too Much Information

I have expressed $\Psi(\mathbf{Q}, t=0)$ as a linear combination of time-evolving eigenstates of \mathbf{H}

$$\Psi(\mathbf{Q},t) = \sum_{j} c_{j} \psi_{j}(\mathbf{Q}) e^{-iE_{j}t/\hbar}$$

where $\{\psi_j, E_j\}$ are eigenstates and eigen-energies and some form of perturbation theory/matrix diagonalization has been used to determine all of the mixing coefficients, $\{c_j\}$. It is necessary to reduce the information in $\Psi(\mathbf{Q},t)$ so that some sort of memorable intuitive picture may be obtained from experimental observations. The goal is "mechanism" = causality plus predictability. Alternatively, the intuitive pictures of the pluck, its free evolution, and its detection may be used to guide the design of the most mechanistically revealing experimental schemes.

8.5.1 Motion in Real Space[10]

There are several classes of reduced representations. The most familiar of these refer to the trajectory of the "center of the wavepacket" in coordinate and/or momentum space:

$$\langle x \rangle_t$$
 and $\langle p \rangle_t$

or, for a polyatomic molecule

$$\langle \vec{\mathbf{Q}} \rangle_t$$
 and $\langle \vec{\mathbf{P}} \rangle_t$

where \vec{Q} and \vec{P} consist of motions of each of the internal coordinates and their linear momenta.

$$\vec{\mathbf{Q}} = \sum_{j} q_{j}, \hat{\boldsymbol{\jmath}},$$

where \hat{j} is a unit vector associated with the jth mode. For a time-evolving wavepacket in a 1-D harmonic oscillator

$$\Psi(x,t=0) = \sum_{j=0}^{\infty} c_{v_j} \, \psi_{v_j}(q_j)$$

$$\Psi(x,t) = \sum_{j=0}^{\infty} c_{v_j} \, \psi_{v_j}(q_j) e^{-i\hbar\omega_j(v_j+1/2)t/\hbar}, \quad \omega_j = [k_j/\mu_j]^{1/2}.$$

The $\Delta v = \pm 1$ harmonic oscillator selection rules for matrix elements of **x** and **p** have some interesting consequences:

(a) If only even- v_j or only odd- v_j , c_{v_j} coefficients are non-zero, then

$$\langle x \rangle_t = 0$$
 and time-independent $\langle p \rangle_t = 0$

but

$$\langle x^2 \rangle_t \neq 0$$
 and time-dependent
 $\langle p^2 \rangle_t \neq 0$
 $\langle x^2 \rangle_t = (2/k) \langle V(x) \rangle_t$
 $\langle p^2 \rangle_t = 2\mu \langle T(p) \rangle_t$,

which means that the center of the wavepacket does not move, but the width of the wavepacket, σ_x , oscillates at an angular frequency of ω_i ,

$$\sigma_{x}(t) = \left[\langle x^{2} \rangle_{t} - \langle x \rangle_{t}^{2} \right]^{1/2} = \left[\langle x^{2} \rangle_{t} \right]^{1/2}.$$

This evolution of the wavepacket corresponds to periodic dephasing (spreading) and perfect rephasing of the wavepacket to its t=0 shape at all integer multiples of the harmonic oscillator period

$$\tau_j = \frac{2\pi}{\omega_i}.$$

(b) If the set of nonzero $\{c_{v_j}\}$ contain values for even and odd v_j , the wavepacket will move following Newton's laws

$$\mu \frac{d}{dt} \langle x \rangle_t = \langle p \rangle_t$$
$$-\left\langle \frac{d}{dx} V(x) \right\rangle_t = -k \langle x \rangle_t = \mu \frac{d}{dt} \langle p \rangle_t.$$

The motion is periodic at $\tau_j = \frac{2\pi}{\omega_j}$ regardless of the specific set of nonzero c_{v_j} , and the wavepacket periodically dephases and rephases. If the t=0 "phased up" $(\Psi(x_+,t=0)>0)$ wavepacket is located at one of the turning points

$$x_{\pm} = \pm \left(\frac{2\langle E \rangle}{k}\right)^{1/2}$$

where

$$\langle E \rangle = \hbar \omega_j \sum_j c_{v_j}^2 (v_j + 1/2),$$

then the "phased down" $(\Psi(x_-, t = \tau/2) < 0)$ wavepacket will be located at the other turning point at all odd multiples of the half period

$$t_n = (2n+1)\frac{\pi}{\omega_i}.$$

(c) When the oscillator is anharmonic, its time-dependence is more complicated, especially with respect to dephasing and partial recurrences. However, the $\langle x \rangle_t$ and $\langle p \rangle_t$ always follow Newton's laws (Ehrenfest's Theorem).

Similarly broad (but different) statements can be made about the motion of wavepackets in an infinite box potential. Periodic dephasing and perfect rephasing occur at a period

$$\tau = 2mL^2/\hbar$$
 (L is the width of the box).

(d) For a polyatomic molecule, a vibrational wavepacket has t=0 amplitude in each of 3N-6 vibrational modes. This amplitude evolves within each of the modes and also exhibits transfer between modes. This sort of evolution is most instructively viewed as evolution in *state space* rather than in coordinate space.

8.5.2 Motion in State Space

In a polyatomic molecule there are 3N-6 normal modes. Suppose the t=0 pluck creates a very large amplitude displacement of only one of these vibrational modes. This idea was the basis for the dream of laser-based "bond-specific" or "mode-specific" chemistry. Energy is inserted into the molecular vibrations non-ergodically by a short, high intensity laser pulse so that a user-selected bimolecular chemical reaction will occur at a specified site in the molecule [7]. It doesn't work [8]! The enemy is Intramolecular Vibrational Redistribution (IVR) [9]. Dynamics in state space provides a good way to visualize IVR or to infer the early time mechanism of IVR based on the transition frequencies and intensities observed in frequency domain spectra.

In a polyatomic molecule, the fastest energy flow pathways are between modes for which the frequencies are in near integer multiples [10–12]. This is called *resonance*. The most common situation is near degeneracy between pairs of symmetric and antisymmetric *stretch* [8] or *bend* [11] modes. Since the \mathbf{H}^{eff} can contain only totally symmetric operators, the lowest-order near-resonant interaction mechanism between members of a symmetric (ω_s) and antisymmetric pair of modes is

$$k_{ssaa}\mathbf{Q}_{s}^{2}\mathbf{Q}_{a}^{2} = \underbrace{k_{ssaa}\left[\frac{\hbar}{2\mu_{s}\omega_{s}}\frac{\hbar}{2\mu_{a}\omega_{a}}\right]}_{\text{this is replaced by K}} (\hat{\mathbf{a}}_{s}^{2}\mathbf{a}_{a}^{\dagger 2} + \mathbf{a}_{s}^{\dagger 2}\hat{\mathbf{a}}_{a}^{2}).$$

The near-degenerate interacting pairs of zero-order levels are $(v_s, v_a) \sim (v_s \pm 2, v_a \mp 2)$ owing to the $\Delta v_a = -\Delta v_s = \pm 2$ selection rules of the $(\hat{\mathbf{a}}_s^2 \mathbf{a}_a^{\dagger 2} + \mathbf{a}_s^{\dagger 2} \hat{\mathbf{a}}_a^2)$ operator.

We need the following

$$\begin{aligned} \hat{\mathbf{a}}_{J} & | v_{J} \rangle = (v_{J})^{1/2} | v_{J} - 1 \rangle \\ \hat{\mathbf{a}}_{J}^{\dagger} & | v_{J} \rangle = (v_{J} + 1)^{1/2} | v_{J} + 1 \rangle \\ \hat{N}_{I} & \equiv \hat{\mathbf{a}}_{J}^{\dagger} \hat{\mathbf{a}}_{J} \quad , \quad \hat{N}_{I} | v_{J} \rangle = v_{I} | v_{J} \rangle, \end{aligned}$$

where $\hat{\mathbf{a}}_J$, $\hat{\mathbf{a}}_J^{\dagger}$, and \hat{N}_J are respectively *annihilation*, *creation*, and *number* operators (see Sect. 7.3).

Consider the interaction between the $|v_s, v_a\rangle^{(0)} = |2,0\rangle^{(0)}$ and $|0,2\rangle^{(0)}$ zero-order states. Suppose, for pedagogical simplicity, that the k_{ssaa} interaction between these two zero-order states is sufficiently strong that the eigenstates are 50:50 mixtures of the zero-order states

$$|\pm\rangle = 2^{-1/2} \left[|2,0\rangle^{(0)} \pm |0,2\rangle^{(0)} \right]$$

$$E_{+} - E_{-} = 2K^{(0)} \langle 2,0 | \mathbf{a}_{s}^{\dagger 2} \hat{\mathbf{a}}_{a}^{2} | 0,2 \rangle^{(0)} = 4K.$$

Suppose $|2,0\rangle^{(0)}$ is bright and $|0,2\rangle^{(0)}$ is dark.

$$|2,0\rangle^{(0)} = 2^{-1/2}[|+\rangle + |-\rangle]$$

$$\Psi(q_{1},q_{2},t=0) = |2,0\rangle = 2^{-1/2}[|+\rangle + |-\rangle]$$

$$\Psi(q_{1},q_{2},t) = 2^{-1/2} \left[e^{-iE_{+}t/\hbar} |+\rangle + e^{-iE_{-}t/\hbar} |-\rangle \right]$$

$$\langle N_{\text{sym}} \rangle_{t} = \langle \mathbf{a}_{s}^{\dagger} \mathbf{a}_{s} \rangle_{t} = \int d\tau \Psi^{\star} \hat{N}_{s} \Psi$$

$$= \frac{1}{2} \left[\langle +|\hat{N}_{s}|+\rangle + \langle -|\hat{N}_{s}|-\rangle + (\langle +|\hat{N}_{s}|-\rangle e^{i\omega_{+}-t} + c.c.) \right]$$

$$= \frac{1}{2} \left[\frac{1}{2} 2 + \frac{1}{2} 2 + \frac{1}{2} 2 e^{i\omega_{+}-t} + \frac{1}{2} 2 e^{-i\omega_{+}-t} \right]$$

$$= 1 + \cos \omega_{+}-t \quad \text{where } \omega_{+} = \frac{4K}{\hbar}.$$

The number of quanta in the bright state $(|2,0\rangle^{(0)})$ oscillates cosinusoidally between $2\left(\operatorname{at} t=0 \text{ and } t=n\frac{2\pi}{\omega+-}\right)$ and $0\left(\operatorname{at} t=(2n+1)\frac{\pi}{\omega+-}\right)$.

At higher excitation, one has a *polyad* of near degenerate $|v_s, v_a\rangle^{(0)}$ states, e.g. for $v_s + v_a = 10$, there are six near degenerate zero-order states: $|10, 0\rangle^{(0)}$, $|8, 2\rangle^{(0)}$, $|6, 4\rangle^{(0)}$, $|4, 6\rangle^{(0)}$, $|2, 8\rangle^{(0)}$, and $|0, 10\rangle^{(0)}$. The **H**^{eff} is a 6×6 matrix controlled entirely by the values of K and $\omega = \frac{\omega_s + \omega_a}{2}$. The bright state is $|10, 0\rangle^{(0)}$ and $|N_s\rangle_t$ exhibits a much more complicated t-dependence than for the $v_s + v_a = 2$ polyad. However, all of the t-dependence of $\langle N_s \rangle_t$ for all values of $v_s + v_a > 2$ is accurately predictable from the observed behavior of the $v_s + v_a = 2$ polyad. This predictability concerns both intuitive mechanism and computational fidelity.

8.6 Mechanism

There are several other measures of dynamics that are neither real-space nor state-space quantities, but have exceptional physical significance [13]:

(a) Autocorrelation function

$$A(t) = \int_{0}^{t} d\tau \, \Psi^{\star}(\mathbf{Q}, \tau) \Psi(\mathbf{Q}, 0)$$

(b) Survival probability

$$P(t) = \left| \int_{0}^{t} d\tau \, \Psi^{\star}(\mathbf{Q}, \tau) \Psi(\mathbf{Q}, 0) \right|^{2} = |A(t)|^{2}$$

(c) Transfer probability, where $\Psi_I(\mathbf{Q},0)$ is the initial state formed by the pluck and $\Psi_F(\mathbf{Q},0)$ is the final "target" state at which the initial wavepacket is aimed

$$T_{\mathrm{I}\to\mathrm{F}}(t) = \left| \int d\, \tau \Psi_{\mathrm{I}}^{\star}(\mathbf{Q}, t) \Psi_{\mathrm{F}}(\mathbf{Q}, 0) \right|^{2}$$

and for which we want to know the values of t at which the overlaps with the target state reach their local-maximum or local-minimum values.

The frequency domain spectrum associated with the totality of electronic-vibration transitions out of an initially selected eigenstate is given by the *Fourier transform* of the *autocorrelation function* of the initial electronic-vibration state transferred by the pluck onto the potential energy surface of the final electronic state [14, 15]. Features in the spectrum are associated with how the $\Psi_I(\mathbf{Q}, 0)$ pluck, which originates from a single vibrational level of the initial electronic state, explores the final electronic state potential energy surface. The *broad spectral envelope* is determined by how $\Psi_I(\mathbf{Q},t)$ explores the final state potential surface at *early time* [16]. What $\Psi_I(\mathbf{Q},t)$ explores is determined by the initial state and the spectral content of the light pulse that creates the pluck. The finer details of the frequency domain spectrum are produced as the $\Psi_I(\mathbf{Q},t)$ explores an increasingly larger region of the final potential energy surface. An especially appealing feature of the autocorrelation function route to a spectrum is that features of the spectrum are associated with how $\Psi_I(\mathbf{Q},t)$ sequentially explores specific regions of the potential surface, especially the localized exploration that occurs at early time [14].

The *survival probability* reveals how rapidly the wavepacket initially created by the pluck departs from its birthplace. It also provides a measure of when and what fraction of the wavepacket returns. It does not specify whether the departure from its t=0 location is mainly in coordinate or momentum space. However, if the

wavepacket is initially located near a turning point, $\langle \vec{\mathbf{P}} \rangle_t$ is changing much more rapidly than $\langle \vec{\mathbf{Q}} \rangle_t$. The survival probability conveys no information about where the t=0 wavepacket goes after it departs from its t=0 location nor what term in the $\mathbf{H}^{\mathrm{eff}}$ is principally responsible for its departure. However, the survival probability does reveal the magnitudes of partial recurrences and the times at which these partial returns to the birthplace occur [15].

The *transfer probability* is valuable for displaying how well the dynamics of a specific pluck are aimed at (or away from) some target state that is expected to have useful chemical properties.

The final topic discussed here is how the dominant mechanisms responsible for intramolecular dynamics may be identified, based on the various dynamical measures discussed so far.

Suppose one sets up an \mathbf{H}^{eff} that describes very well all of the frequency-domain spectral data (intensities and transition frequencies). The \mathbf{H}^{eff} embodies many anharmonic resonance interactions. Which resonance term is responsible for each of the dynamical features prominently displayed in the survival probability, P(t)? This is a question of *why* rather than *what*. Causality and mechanism are intrinsically more interesting than numerical description. It is possible to get this mechanistic information from expectation values of "resonance operators" constructed from the various anharmonic terms in the \mathbf{H}^{eff} [17]. See Figs. 8.3 and 8.4.

In the absence of collisions, the energy and total angular momentum of a gas phase molecule are conserved. There are an infinite number of ways that a polyatomic molecule can be prepared, at t = 0, with a specified amount of energy, $\langle \mathbf{H} \rangle$, and angular momentum, $\langle \mathbf{J}^2 \rangle$.

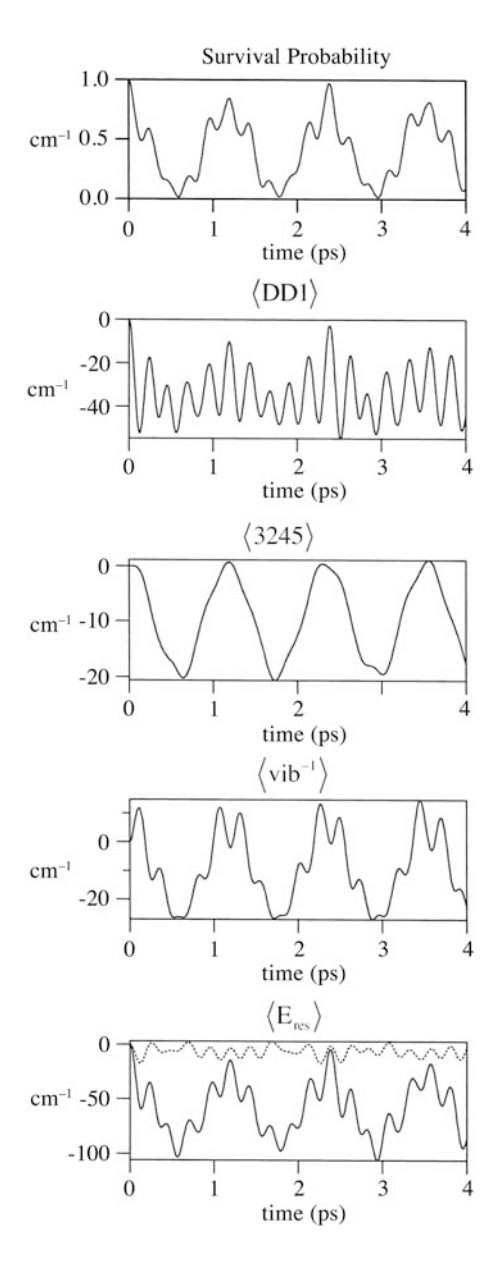
The most interesting of these ways are those that localize significant energy in a single local or normal vibrational mode. Some of these t=0 preparations are convenient to create by a simple, well-designed pluck. We want to discover which terms in the empirically determined time-independent \mathbf{H}^{eff} are responsible for the most prominent features displayed by expectation values of the descriptive dynamical quantities, such as $\langle \vec{\mathbf{Q}} \rangle_t$, $\langle \vec{\mathbf{P}} \rangle_t$, survival probability, and normal or local mode number operators, such as $\langle \mathbf{a}_i^{\dagger} \mathbf{a}_i \rangle$.

The \mathbf{H}^{eff} consists of diagonal, \mathbf{H}^{diag} , and off-diagonal (resonance) terms, \mathbf{H}^{res}

$$\mathbf{H}^{\text{eff}} = \mathbf{H}^{\text{diag}} + \mathbf{H}^{\text{res}}[17].$$

The partitioning of \mathbf{H}^{eff} between \mathbf{H}^{diag} and \mathbf{H}^{res} depends on the choice of basis set (e.g. normal modes, local modes, or basis states obtained by diagonalization of an \mathbf{H}^{eff} that contains all terms in \mathbf{H}^{eff} except one or two presumably dominant, dynamics-determining terms in \mathbf{H}^{eff}). The dynamically most important terms in \mathbf{H}^{res} are those responsible for interactions between large groups of systematically near-degenerate basis states. These groups of strongly interacting basis states are called *polyads* (see Sect. 7.3.4). The rules for basis state membership and matrix

Fig. 8.3 Various Measures of Intrapolyad Dynamics. Top: Survival probability associated with the $(0, 1, 0, 10^0, 0^0)$ zero-order state. Middle three panels: resonance energy contributions of three specific anharmonic resonances. Bottom: the total resonance energy associated with the wavepacket (solid line) and that portion of it which is not accounted for by the three resonances depicted in the middle panels (dotted line). Reproduced with permission from Fig. 1 in [17]. Copyright 2000, Elsevier B.V



element scaling in successive polyad groups are simple, based on the selection rules and quantum member scaling rules for harmonic oscillator $\mathbf{Q}_i^m \mathbf{Q}_j^n \mathbf{Q}_k^o$ matrix elements.

Consider, for example, a 2:1 bend:stretch (Fermi resonance) interaction where $2\omega_b \approx \omega_s$. There are two important interaction terms

$$\Omega = k_{sbb} \mathbf{a}_s^{\dagger} \mathbf{a}_b^2$$

and

$$\Omega = k_{sbb} \mathbf{a}_s \mathbf{a}_b^{\dagger 2},$$

which respectively follow the $(\Omega: \Delta v_s = +1, \Delta v_b = -2)$ and $(\Omega^{\dagger}: \Delta v_s = -1, \Delta v_b = +2)$ selection rules. All terms (\mathbf{O}) in the $\mathbf{H}^{\mathrm{eff}}$ must be Hermitian, but any Hermitian operator may be expressed as a sum of two non-Hermitian terms, Ω and Ω^{\dagger} ,

$$\mathbf{O} = \mathbf{\Omega} + \mathbf{\Omega}^{\dagger}.$$

Each term in \mathbf{H}^{res} may be expressed as the sum of k pairs of non-Hermitian operators

$$\mathbf{H}^{\text{res}} = \sum_{k} \mathbf{O}_{k} = \sum_{k} \left(\mathbf{\Omega}_{k} + \mathbf{\Omega}_{k}^{\dagger} \right).$$

Each term in this sum over k corresponds to a resonance of possible dynamical importance [17].

It is instructive to compute the time-dependent expectation values of $(\Omega_k + \Omega_k^{\dagger})$ and $(\Omega_k - \Omega_k^{\dagger})$ for the time-evolving form of any selected t = 0 pluck state, $\Psi(\mathbf{Q}, t)$. The Hermiticity of each \mathbf{O}_k implies that the expectation values

$$E_{\text{res},k}(t) = \langle \mathbf{O}_k \rangle_t$$
$$E = E_{\text{diag}}(t) + \sum_k \langle \mathbf{O}_k \rangle_t$$

are real and that

$$I_k(t) \equiv \frac{\langle \mathbf{O}_k \rangle_t}{E}$$

defines the time-dependent *importance* of the \mathbf{O}_k term in the time-evolution of the chosen pluck state. Each pluck state will exhibit a unique set of $\{I_k(t)\}$ importance terms. It is possible to show (see Eqs. (12)–(19) of [17]) that the expectation value of each $(\Omega_k - \Omega_k^{\dagger})$ term is pure imaginary and that it provides a measure of the *rate* of energy flow between the vibrational modes coupled by Ω_k ,

$$i\hbar\frac{d}{dt}\langle v_j\rangle_t^k = \sum_k \Delta n_{jk}\langle \mathbf{\Omega}_k - \mathbf{\Omega}_k^{\dagger}\rangle_t$$

 v_i is the number of quanta in mode j, and

$$\Delta v_j^k(t) = \langle v_j \rangle_t^k - v_j(t=0) = \int_0^t \left[\frac{d}{d\tau} \langle v_j \rangle_\tau^k \right] d\tau$$

where

$$\Delta n_{jk} \equiv \underline{n'_{jk}} - \underline{n_{jk}}$$
final n_i initial n_i

is the number of quanta in mode j exchanged by resonance k (e.g. for $\Omega_k = \left(\mathbf{a}_j^{\dagger}\right)^{n_j}$ $(\mathbf{a}_m)^{n_m}$, $\Delta n_{jk} = n_j$ and $\Delta n_{mk} = -n_m$). The quantity $\hbar \omega_j \frac{d}{dt} \langle v_j \rangle_t^k$ is the pure real rate of energy flow into or out of mode j caused by resonance k. $\Delta v_j^k(t)$ is the accumulated change in the number of quanta in mode j caused by resonance k.

Figures 8.3 and 8.4 illustrate the use of expectation values of $\Omega_k + \Omega_k^{\dagger}$ and $\Omega_k - \Omega_k^{\dagger}$, for three of the nine known important resonance operators, to gain a mechanistic understanding of the dominant dynamical mechanisms for an exemplary acetylene S_0

$$|v_1, v_2, v_3, v_4^{\ell_4}, v_5^{\ell_5}\rangle = |0, 1, 0, 10^0, 0^0\rangle$$

zero-order state (v_1 = symmetric CH stretch, v_2 = CC stretch, v_3 = antisymmetric CH stretch, v_4 = trans-bend, ℓ_4 = vibrational angular momentum of the doubly degenerate trans-bend, v_5 = cis-bend, ℓ_5 = vibrational angular momentum of the cis-bend). Three anharmonic resonances dominate the dynamics of this $[0, 1, 0, 10^0, 0^0]$ zero-order state [11, 12], which could easily be created at t = 0 by a short stimulated emission pluck pulse from any of the Franck-Condon accessible $|v_1' = 0, v_2', v_3', v_4' = 0, v_5' = 0, v_6' = 0$ vibrational levels of the trans-bent S_1 state (in S_1 v_2' is the CC stretch and v_3' is the trans-bend).

The three anharmonic resonance terms that dominate the unimolecular dynamics of the chosen pluck state, $|0, 1, 0, 10^0, 0^0\rangle$ are [11, 18]:

(a) $\langle DD1 \rangle$ (Darling–Dennison 1), $\Delta v_4 = -\Delta v_5 = 2$, $\Delta v_1 = \Delta v_2 = \Delta v_3 = \Delta \ell_4 = \Delta \ell_5 = 0$.

$$\begin{split} \left\langle v_1 v_2 v_3 v_4^{\ell_4} v_5^{\ell_5} | \mathbf{H}^{\text{DDI}} | v_1 v_2 v_3 (v_4 - 2)^{\ell_4} (v_5 + 2)^{\ell_5} \right\rangle \\ &= \frac{1}{4} K_{44,55} [(v_4^2 - \ell_4^2)(v_5 + \ell_5 + 2)(v_5 - \ell_5 + 2)]^{1/2}. \end{split}$$

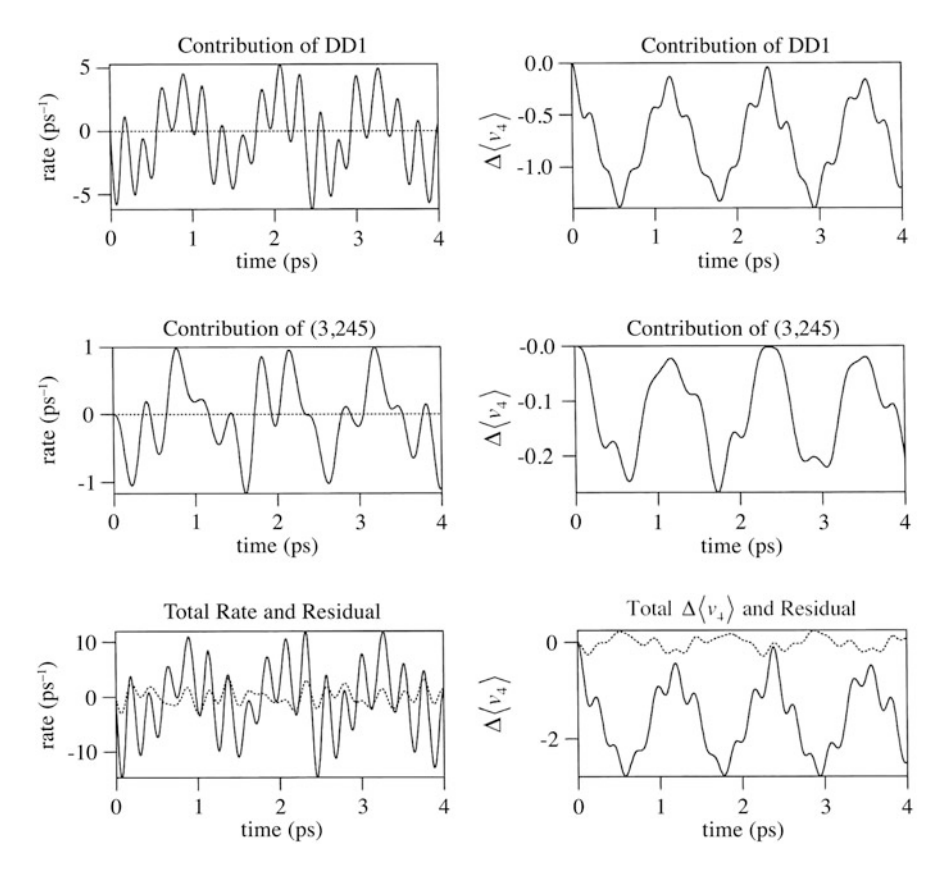


Fig. 8.4 Contributions of Specific Resonance Terms to Intrapolyad Dynamics. *Left column:* $d\langle v_4 \rangle / dt$. *Right column:* $\langle v_4 \rangle (t) - \langle v_4 \rangle (0) = \int_0^t d\langle v_4 \rangle / dt$. The Darling–Dennison 1 and (3,245) resonances account for nearly all energy transfer into and out of mode 4; the *dotted lines* in the bottom two panels represent the contributions from all of the other resonances. Reproduced with permission from Fig. 2 in [17]. Copyright 2000, Elsevier B.V

(b)
$$\langle 3,245 \rangle$$
 (quartic anharmonicity), $\Delta v_3 = -\Delta v_2 = -\Delta v_4 = -\Delta v_5 = -1$, $\Delta \ell_4 = -\Delta \ell_5 = \mp 1$, $\Delta v_1 = 0$, $\Delta \ell_{\text{tot}} = 0$

$$\left\langle v_1 v_2 v_3 v_4^{\ell_4} v_5^{\ell_5} | \mathbf{H}^{3,245} | v_1 (v_2 - 1) (v_3 + 1) (v_4 - 1)^{\ell_4 \pm 1} (v_5 - 1)^{\ell_5 \mp 1} \right\rangle$$

$$= [v_2 (v_3 + 1) (v_4 \mp \ell_4) (v_5 \pm \ell_5)]^{1/2}.$$

(c) (vib- ℓ) (vibrational ℓ -resonance), $\Delta v_1 = \Delta v_2 = \Delta v_3 = \Delta v_4 = \Delta v_5 = 0$, $\Delta \ell_4 = \mp 2$, $\Delta \ell_5 = \pm 2$

$$\langle v_1 v_2 v_3 v_4^{\ell_4} v_5^{\ell_5} | \mathbf{H}^{\text{vib-}\ell} | v_1 v_2 v_3 v_4^{\ell_4 \pm 2} v_5^{\ell_5 \mp 2} \rangle$$

$$= \frac{1}{4} r_{45} \times \left[(v_4 \mp \ell_4) (v_4 \pm \ell_4 + 2) (v_5 \pm \ell_5) (v_5 \mp \ell_5 + 2) \right]^{1/2}$$

The top panel of Fig. 8.3 shows the survival probability for the $\Psi(\mathbf{Q}, t = 0) = |01010^00^0\rangle$ pluck state,

$$P(t) = \left| \int_0^t d\tau \Psi^{\star}(\mathbf{Q}, \tau) \Psi(\mathbf{Q}, 0) \right|^2,$$

where the time-evolving pluck state, $\Psi(\mathbf{Q},t)$, is derived from $\Psi(\mathbf{Q},0)$ using the $\mathbf{H}^{\mathrm{eff}}$ that is expressed in terms of molecular constants that had been derived from fits to frequency domain spectra (IR, Raman, Dispersed Fluorescence, Stimulated Emission Pumping) [10, 11, 19, 20]. The frequency domain spectrum encodes dynamics. Our goal here is to show how the $(\Omega + \Omega^{\dagger})$ and $(\Omega - \Omega^{\dagger})$ tools are used to reveal the dominant energy flow pathways for any localized pluck state and the terms in the $\mathbf{H}^{\mathrm{eff}}$ that are responsible for each pathway [17]. This is mechanism plus causality, which is far more interesting and instructive than mere numerical description.

The survival probability describes the temporal patterns of vibrational energy flow away from and back to the t = 0 pluck state. It does not provide any information about where the energy goes and why it goes there. The survival probability plotted in the top panel of Fig. 8.3 contains nearly 100 % amplitude slow dephasings/rephasings with a period of \sim 1.2 ps. Superimposed on the large and slow modulation are shallower and faster oscillations with a period of ~ 0.24 ps. The second panel of Fig. 8.3, labeled (DD1), is the expectation value of $(\Omega_{DD1} + \Omega_{DD1}^{\dagger})$. It shows that the fast oscillations of the survival probability are "caused by" the (DD1) mechanism. The third panel, labeled (3,245), is the expectation value of $(\Omega_{3,245} + \Omega_{3,245}^{\dagger})$. It shows that the strong, slow modulations are caused by the $\langle 3,245 \rangle$ mechanism. The fourth panel, labeled $\langle \text{vib-}\ell \rangle$, is the expectation value of $(\Omega_{\text{vib-}\ell} + \Omega_{\text{vib-}\ell}^{\dagger})$. It shows both fast and slow oscillations similar to those caused respectively by the $\langle DD1 \rangle$ and $\langle 3,245 \rangle$ mechanisms. However, there is a $\pi/2$ phase difference between the fast oscillations caused by the (DD1) and (vib- ℓ) mechanisms. The fifth (bottom) panel shows the sum of the effects caused by the three resonance terms (discussed above) that apparently have the dominant effects on this specific $\Psi(\mathbf{Q}, t = 0) = [0, 1, 0, 10^0, 0^0]$ bright state. The dotted curve shows the negligibly small part of the dynamics of E_{res} that is not caused by these three dominant resonance terms (i.e. caused by the other six known resonance terms). Note that there is a strong resemblance between the survival probability and the dynamics of E_{res} shown in the top and bottom panels. Thus we have identified the primary causes of the dynamics but not yet described the dominant energy flow pathways. Information about pathways is obtained from Fig. 8.4, which is based on the expectation values of the $\Omega_k - \Omega_k^{\dagger}$ terms.

The left column of Fig. 8.4 displays the rate at which resonance k causes vibrational quanta to flow out of mode-j

$$\frac{d}{dt} \langle v_j \rangle_t^k = \left(\frac{1}{i \, \hbar} \right) \sum_k \Delta n_{jk} \left\langle \mathbf{\Omega}_k - \mathbf{\Omega}_k^{\dagger} \right\rangle_t.$$

Each resonance, k, can contribute to the rate that vibrational quanta depart from mode j. The right column of Fig. 8.4 displays the accumulated change in the number of quanta in mode-j caused by resonance k

$$\Delta v_j^k(t) = \langle v_j \rangle_t^k - v_j(t=0) = \int_0^t \left[\frac{d}{dt} \langle v_j \rangle_t^k \right] d\tau.$$

The top pair of panels shows the effect of $\langle DD1 \rangle$ on the number of vibrational quanta (v_4) in the trans-bend normal mode (v_4) for the $\begin{vmatrix} 0 & 1 & 0 & 10^0 & 0^0 \end{vmatrix}$ t=0 pluck state, in which $\langle v_4 \rangle_{t=0} = 10$. $\langle DD1 \rangle$ transfers quanta from trans-bend (v_4) to cis-bend (v_5) . The transfer rate is zero at t=0 and reaches a maximum at $t\approx \frac{0.24}{4}$ ps, which is $\frac{1}{4}$ the period of the fast oscillation of $E^{res}_{\langle DD1 \rangle}$ shown in the second panel of Fig. 8.3. The maximum value of $\langle v \rangle_4^{\langle DD1 \rangle} - \langle v_4 \rangle_{t=0} = -1.5$. The middle pair of panels shows the effect of $\langle 3,245 \rangle$. The rate of removal of mode-4 quanta from $\begin{vmatrix} 0 & 1 & 0 & 10^0 & 0^0 \end{pmatrix}$ caused by $\langle 3,245 \rangle$ is $\sim \frac{1}{5}$ that of $\langle DD1 \rangle$ and the periodic maxima in the $\Delta \langle v_4 \rangle_t$ due to $\langle 3,245 \rangle$ are $\sim \frac{1}{5}$ those due to $\langle DD1 \rangle$. $\Delta \langle v_4 \rangle_t^{\langle DD1 \rangle}$ and $\Delta \langle v_4 \rangle_t^{\langle 3,245 \rangle}$ both display fast and slow oscillations, with periods ~ 0.24 ps and ~ 1.2 ps. The bottom pair of panels show that $\langle DD1 \rangle$ and $\langle 3,245 \rangle$ have a dominant effect on $\langle \frac{d}{dt} v_4 \rangle_t$ and $\Delta \langle v_4 \rangle_t$, summed over the contributions from all nine known resonance terms. $\langle vib-\ell \rangle$ cannot have any effect on $\langle v_4 \rangle_t$ owing to the $\Delta v_4 = \Delta v_5 = 0$ selection rule for the vib- ℓ resonance term in the \mathbf{H}^{eff} . Note the unsurprising resemblance between the bottom panel of Fig. 8.3 and the bottom right panel of Fig. 8.4.

Every zero-order state will exhibit a different set of dynamic responses to the $\left(\Omega_k + \Omega_k^{\dagger}\right)$ and $\left(\Omega_k - \Omega_k^{\dagger}\right)$ resonance terms for k = 1 - 9. The dynamics will become increasingly complicated when the t = 0 pluck state contains excitation distributed over more than two normal modes. As the total vibrational energy increases, the vibrational density of states and the magnitudes of the off-diagonal elements of \mathbf{H}^{eff} both increase. This causes the dynamics to become both faster and more complex. However, since the Heff is completely determined by the frequency domain spectra observed and fitted at low E_{vib} and semi-quantitatively scalable to higher $E_{\rm vib}$ (based on harmonic oscillator matrix element selection and scaling rules), the Heff description of the free-evolution vibrational dynamics is *complete*, even if the harmonic oscillator basis set becomes inappropriate at high E_{vib} . All free evolution dynamics is quantitatively embodied in Heff. There are many useful tools for extracting energy flow pathways, rates, and causal dynamical mechanisms. The tools based on the $\left(\Omega_k + \Omega_k^{\dagger}\right)$ and $\left(\Omega_k - \Omega_k^{\dagger}\right)$ resonance operators are simple to implement, very powerful, yet rarely used [17]. Intramolecular Dynamics is encoded in frequency domain spectra, often more instructively than in time-domain spectra [21]. This might seem surprising!

References 153

References

 H. Lefebvre-Brion, R.W. Field, The Spectra and Dynamics of Diatomic Molecules (Elsevier, Amsterdam, 2004), pp. 622–626

- C. Cohen-Tannoudji, B. Diu, F. Laloë, *Quantum Mechanics* (Wiley, New York, 1977), pp. 1095–1104/1110–1119
- 3. E.J. Heller, W.M. Gelbart, J. Chem. Phys. 73, 626 (1980)
- C. Kittrell, E. Abramson, J.L. Kinsey, S. McDonald, D.E. Reisner, D. Katayama, R.W. Field, J. Chem. Phys. 75, 2056–2059 (1981)
- D.E. Reisner, P.H. Vaccaro, C. Kittrell, R.W. Field, J.L. Kinsey, H.-L. Dai, J. Chem. Phys. 77, 573–575 (1982)
- P. Jensen, Wiley interdisciplinary reviews. Comput. Mol. Sci. 2, 494–512 (2012); See also Mol. Phys. 98, 1253–1285 (2000)
- 7. R.G. Bray, M.J. Berry, J. Chem. Phys. **71**, 4909–4922 (1979)
- 8. E.L. Sibert III, J.T. Hynes, W.P. Reinhardt, J. Chem. Phys. 81, 1135-1144 (1984)
- 9. D.J. Nesbitt, R.W. Field, J. Phys. Chem. **100**, 12735–12756 (1996)
- H. Lefebvre-Brion, R.W. Field, The Spectra and Dynamics of Diatomic Molecules, Sect. 9.1.7 (Elsevier, Amsterdam, 2004)
- 11. M.P. Jacobson, R.W. Field, J. Phys. Chem. 104, 3073–3086 (2000) [feature article]
- 12. M.P. Jacobson, R.J. Silbey, R.W. Field, J. Chem. Phys. 110, 845–859 (1999)
- H. Lefebvre-Brion, R.W. Field, The Spectra and Dynamics of Diatomic Molecules, Sect. 9.1.4 (Elsevier, Amsterdam, 2004)
- 14. H. Lefebvre-Brion, R.W. Field, *The Spectra and Dynamics of Diatomic Molecules*, Sect. 9.1.3 (Elsevier, Amsterdam, 2004)
- 15. E.J. Heller, Acc. Chem. Res. 14, 368 (1981)
- 16. E.J. Heller, J. Chem. Phys. 68, 3891 (1978)
- 17. M.P. Jacobson, R.W. Field, Chem. Phys. Lett. **320**, 553–560 (2000)
- K. Hoshina, A. Iwasaki, K. Yamanouchi, M.P. Jacobson, R.W. Field, J. Chem. Phys. 114, 7424
 7442 (2001)
- 19. M.P. Jacobson, J.P. O'Brien, R.J. Silbey, R.W. Field, J. Chem. Phys. 109, 121-133 (1998)
- 20. D.S. Perry, J. Martens, A. Amyay, M. Herman, Mol. Phys. 110, 2687 (2012)
- K. Prozument, R.G. Shaver, M.A. Ciuba, J.S. Muenter, G.B. Park, J.F. Stanton, H. Guo, B.M. Wong, D.S. Perry, R.W. Field, Faraday Discuss. 163, 33–57 (2013)